# COMPUTERIZED WELL TESTING MODULES

BY:

*VIGEN GHAZARIAN AGHAN*

Thesis submitted for the degree of

**MASTER OF PHILOSOPHY**

In the Faculty of Engineering

University of London

Petroleum engineering Section
Mineral Resources Engineering
Imperial College
London SW7 2BP

April 1987

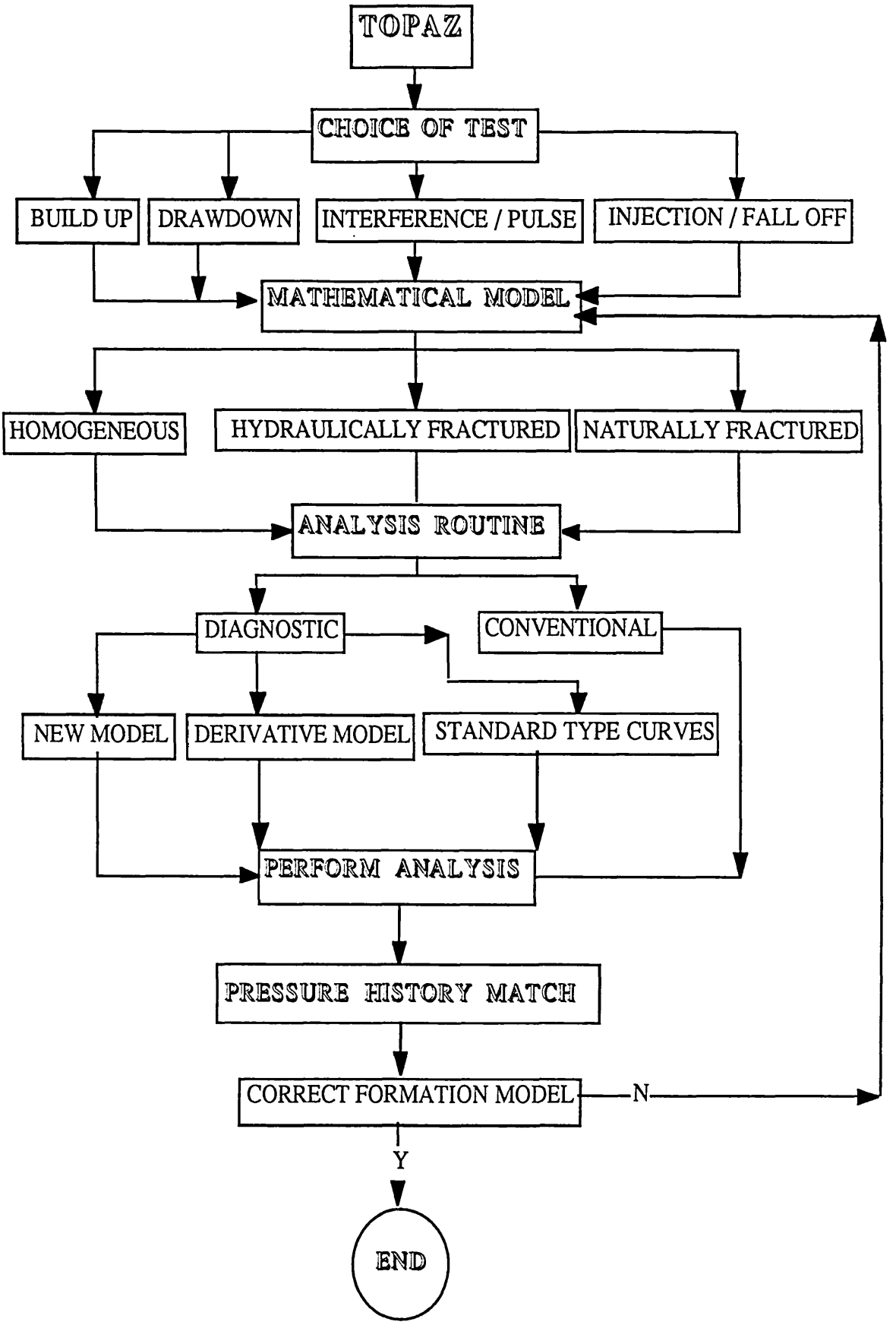
# ABSTRACT

The analysis of pressure information from well tests is vital to the estimation of reservoir properties and well performance in the appraisal stage, and in history matching and prediction for reservoir management. Recent trends in well test analysis have indeed emphasized the comprehensive analysis and matching of all test data. Attempts are made to match data to curves fitted to theoretical solutions of idealized well / reservoir models.

The present work reports the theoretical solution to all common models of well / reservoir behaviour (homogeneous, stratified, naturally fractured, hydraulically fractured, etc) through the analytical and numerical inversion of the solutions, in Laplace space, to the relevant equations. A number of new analytical solutions for the definition of the $P_D$-functions with respect to the oil bearing formations have also been developed in the literature .

These techniques have been incorporated in a fully interactive program (**TOPAZ**), enabling data to be matched to a selected theoretical solution, rather than to a standard set of type curves. The program combines the use of specialized or diagnostic plots and automated modelling techniques in order to characterize the physical nature of the formations. On average, the testing routine can be completed within about ten minutes, a time which can be reduced with improved data storage / retrieved equipment.

Whilst this work constitutes a further step towards the rapid evaluation and interpretation of well tests in real time, its main objective is to improve the conduct and interpretation of well testing by assisting the analyst to construct mathematical models whose pressure response patterns can be closely related to the actual responses observed in the fields.




FLOW CHART ASSOCIATED WITH THE TOPAZ PROGRAM

# PREFACE

I commenced my postgraduate research study in the field of pressure analysis at Imperial College in September 1984, under the joint supervision of professor C.G. Wall and professor J.S. Archer.

The first phase of my research was devoted to customizing with the HP-86B micro computer which provided the basis of constructing the fully interactive well testing program coded **[TOPAZ]**. At the end of March 1985, the second phase was accomplished through the development of the **[TOPAZ.T1]** computer program for analysing homogeneous formations. Constructive criticisms were also made by M. Baker from the Halliburton Service companies and D. Bourdet from Flopetrol Johnston plc.

In July 1985, my attention was focused on the modification of **[TOPAZ.T1]** in order to take into account fractured as well as stratified formations. The program, however, proved to be somewhat restrictive, as it only performed the analysis of field pressure data under radial flow conditions. Indeed, such restriction initiated the phase three, which commenced by implementing the most common solutions of the partial differential equation of fluid flow through porous media into **[TOPAZ.T1]**. In April 1986, the modified program **[TOPAZ.T2]** was tested successfully by means of field data which were provided by Professor C.G. Wall.

The final phase of my research program which lasted for six months and led to the development of the updated version of **[TOPAZ.T2]** well testing package, was in fact concentrated on increasing the efficiency of the existing program by reducing the computation time of the input data. The objective was achieved partially through new mathematical techniques for solving the relevant hydrodynamics problems and partially through the physical capabilities of the HP-86B micro computer.

It is remarked that although **[TOPAZ]** could be considered a powerful well test interpretation package, it will require constant modifications if it is to keep its current standards in ever changing oil industry.

# ACKNOWLEDGEMENT

The author wishes to give special recognition to Professor C.G. Wall for his technical advice and critical review of the thesis. Appreciation is extended to Professor J.S. Archer's provision of information relating to transient well test interpretation in important measures. His financial assistance in providing the HP-computer accessories for the development of **(TOPAZ)** well testing package is also greatly acknowledged.

My special thanks for technical assistance are also extended to D. Bourdet (formally from Flopetrol Johnston), M. Baker (from Halliburton Services), Dr. G. Stephenson (lecturer in mathematics at Imperial College), Dr. R. Pietlicki(research assistant) and the computer advisory staff at Imperial College.

In the course of the preparation of my thesis, I am indebted to Alex Noorbhai, primarily for his permission in making use of the Macintosh word processing facilities in the mechanical engineering department of Imperial College and secondly for his valuble suggestions in improving the presentation quality of this manuscript.

Finally the financial support of my parents and G. Theresa throughout the research program is gratefully acknowledged.

★★★★★★★★★★★

# (TABLE OF CONTENTS)

ABSTRACT 1
PREFACE 3
ACKNOWLEDGEMENTS 4
LIST OF FIGURES 9

## CHAPTER 1

1.0: INTRODUCTION 14
1.1: HISTORY 14
1.2: WELL TESTING OBJECTIVES 15
1.3: CHOICE OF EQUIPMENTS 16
1.4: CHOICE OF WELL TESTS 17
1.5: WELL TEST INTERPRETATIONS 17

## CHAPTER 2

2.0: INFINITE ACTING HOMOGENEOUS FORMATION 18
2.1: PRESSURE RESPONSES OF HOMOGENEOUS FORMATIONS 18
2.2: NUMERICAL SOLUTION OF $P_D$-FUNCTION (DAMAGED WELLS) 22
2.3: ANALYTICAL SOLUTION OF $P_D$-FUNCTION (FRACTURED WELLS) 23
2.4: APPLICATION OF DRAWDOWN TYPE CURVES TO BUILD UP TESTS 25
2.5: CHARACTERIZATION OF HOMOGENEOUS FORMATIONS ($r_{D=\infty}$) 27

## CHAPTER 3

3.0: DIFFERENTIAL MODEL OF HOMOGENEOUS FORMATIONS 28
3.1: PRESSURE DERIVATIVES WITH RESPECT TO HOMOGENEOUS MODEL 28
3.2: DIFFERENTIATION PROCEDURES ASSOCIATED WITH $P_D$-FUNCTION 30

3.3: APPLICATION OF PRESSURE DERIVATIVES TO BUILD UP TESTS 31
3.4: DIFFERENTIATION SCHEMES APPLICABLE TO PRESSURE DATA 33
3.5: MATCHING PROCEDURES ON THE DERIVATIVE TYPE CURVES 36

## CHAPTER 4

4.0: CONVENTIONAL ANALYSIS OF HOMOGENEOUS FORMATION 37
4.1: CONVENTIONAL DRAWDOWN ANALYSIS OF HOMOGENEOUS FORMATIONS 37
4.2: CONVENTIONAL BUILD UP ANALYSIS OF HOMOGENEOUS FORMATIONS 45
4.3: HORNER BUILD UP SCHEME 46
4.4: MILLER-DYES-HUTCHINSON BUILD UP TESTING MODEL 49
4.5: RUSSELL'S BUILD UP TESTING MODEL 51

## CHAPTER 5

5.0: NATURALLY FRACTURED FORMATIONS 54
5.1: PRESSURE RESPONSES ASSOCIATED WITH DUAL POROSITY FORMATIONS 54
5.2: PSEUDO STEADY STATE INTERPOROSITY FLOW MODEL (SIF) 55
5.3: PRESSURE RESPONSES OF THE SIF MODEL DURING DRAWDOWN TESTS 61
5.4: PRESSURE RESPONSES OF THE SIF MODEL DURING BUILD UP TESTS 63
5.5: DEFINITION OF THE PETROPHYSICAL PARAMETERS OF THE SIF MODEL 67
5.6: TRANSIENT INTERPOROSITY FLOW MODEL (TIF) 68
5.7: BUILD UP TESTS ASSOCIATED WITH THE TIF MODEL 73
5.8: WELL TEST INTERPRETATION PITFALLS WITH RESPECT TO THE TIF MODEL 73

## CHAPTER 6

6.0: DIFFERENTIAL MODELS OF FRACTURED FORMATIONS 76
6.1: APPLICATION OF PRESSURE DERIVATIVE TO FRACTURED FORMATIONS 76
6.2: PRESSURE DERIVATIVE RESPONSES ASSOCIATED WITH THE SIF MODEL 77
6.3: PRESSURE DERIVATIVES WITH RESPECT TO BUILD UP TESTS (SIF MODEL) 82
6.4: CHARACTERIZATION OF THE SIF MODEL VIA DERIVATIVE SCHEMES 83
6.5: PRESSURE DERIVATIVE RESPONSES ASSOCIATED WITH THE TIF MODEL 84
6.6: PRESSURE DERIVATIVES WITH RESPECT TO BUILD UP TESTS (TIF MODEL) 88

6.7: CHARACTERIZATION OF THE SIF MODEL VIA DERIVATIVE SCHEMES 90

## CHAPTER 7

7.0: CONVENTIONAL ANALYSIS OF NATURALLY FRACTURED FORMATIONS 92
7.1: CONVENTIONAL DRAWDOWN SCHEMES ASSOCIATED WITH THE SIF MODEL 92
7.2: CHARACTERIZATION OF THE SIF MODEL VIA DRAWDOWN SCHEMES 95
7.3: CONVENTIONAL BUILD UP SCHEMES ASSOCIATED WITH THE SIF MODEL 98
7.4: CHARACTERIZATION OF THE SIF MODEL VIA BUILD UP SCHEMES 99
7.5: CONVENTIONAL DRAWDOWN SCHEMES ASSOCIATED WITH THE TIF MODEL 101
7.6: CHARACTERIZATION OF THE TIF MODEL VIA DRAWDOWN SCHEMES 103
7.7: CHARACTERIZATION OF THE TIF MODEL VIA BUILD UP SCHEMES 108

## CHAPTER 8

8.0: HYDRAULICALLY FRACTURED FORMATIONS 114
8.1: PRESSURE RESPONSES OF HYDRAULICALLY FRACTURED FORMATIONS 114
8.2: PRESSURE RESPONSES ASSOCIATED WITH THE UFF MODEL 118
8.3: BUILD UP PRESSURE RESPONSES WITH RESPECT TO THE UFF MODEL 121
8.4: PRESSURE RESPONSES ASSOCIATED WITH THE ICF MODEL 122
8.5: BUILD UP PRESSURE RESPONSES WITH RESPECT TO THE ICF MODEL 125
8.6: CHARACTERIZATION OF THE UFF AND ICF FRACTURED MODELS 128

## CHAPTER 9

9.0: CONVENTIONAL ANALYSIS OF HYDRAULICALLY FRACTURED FORMATIONS 130
9.1: CONVENTIONAL DRAWDOWN SCHEMES ASSOCIATED WITH UFF/ICF MODELS 130
9.2: CONVENTIONAL BUILD UP SCHEMES ASSOCIATED WITH UFF/ICF MODELS 134

## CHAPTER 10

10.0: NUMERICAL RESULTS AND DISCUSSION 139
10.1: APPLICATION OF TOPAZ TO FIELD PRESSURE DATA 139

10.2: TRANSIENT PRESSURE ANALYSIS FOR THE EXPLORATION WELL - MX/1 139
10.3: TRANSIENT PRESSURE ANALYSIS FOR THE PRODUCTION WELL - FT/2 145
10.4: TRANSIENT PRESSURE ANALYSIS FOR THE PRODUCTION WELL - SX/O 151
10.5: CONCLUDING REMARKS 156

NOMENCLATURE 157
REFERENCES 161
APPENDIX A: DIETZ SHAPE FACTOR 165
APPENDIX B: DIMENSIONLESS PRESSURE BUILD UP RESPONSES 167
APPENDIX C: PRESSURE BUILD UP RESPONSES OF THE [TIF] MODEL ($r_D=\infty$) 168
APPENDIX D: PARTIAL PROGRAM LISTING - CODE:BU-SECTO2A 170
APPENDIX E: TOPAZ WELL TESTING NETWORK 177

**********

# LIST OF FIGURES + TABLES

## CHAPTER 1

(1.1) BOTTOMHOLE APPARATUS FOR DOWNHOLE SHUT IN
(1.2) BOTTOMHOLE APPARATUS FOR SURFACE SHUT IN

## CHAPTER 2

(2.1) DIMENSIONLESS PRESSURE RESPONSES OF INFINITE ACTING HOMOGENEOUS FORMATION WITH WELLBORE STORAGE AND SKIN
(2.2) NUMERICAL INTEGRATION WITH RESPECT TO RICHARDSON MODEL

## CHAPTER 3

(3.1) DERIVATIVE PRESSURE RESPONSES OF INFINITE ACTING HOMOGENEOUS FORMATION WITH WELLBORE STORAGE AND SKIN
(3.2) DEFINITION OF $P'_D$-FUNCTION VIA NUMERICAL INTEGRATION
(3.3) DIMENSIONLESS PRESSURE AND DERIVATIVE RESPONSES OF INFINITE ACTING HOMOGENEOUS FORMATION WITH WBS & SKIN

## CHAPTER 4

(4.1) RATE AND PRESSURE RESPONSES DURING AN IDEAL DRAWDOWN
(4.2) BHP RESPONSES DURING TRANSIENT FLOW PERIODS
(4.3) $P_D$-RESPONSES DURING WELLBORE STORAGE FLOW PERIODS
(4.4) BHP RESPONSES DURING SEMI STEADY STATE FLOW PERIODS
(4.5) RATE & PRESSURE VARIATIONS WRT MULTI-RATE DRAWDOWN TEST
(4.6) TYPICAL MULTI-RATE DRAWDOWN TEST PLOT
(4.7) VARIABLE RATE RESERVOIR LIMIT TEST (HOMOGENEOUS MODEL)
(4.8) RATE AND PRESSURE RESPONSES DURING TWO RATE TEST
(4.9) TYPICAL PRESSURE RESPONSES DURING A TWO RATE DRAWDOWN TEST
(4.10) RATE AND PRESSURE RESPONSES DURING AN IDEAL BUILD UP TESTS
(4.11) TYPICAL HORNER PLOT WITH RESPECT TO HOMOGENEOUS FORMATIONS

(4.12) PRESSURE BUILD UP RESPONSES WITH RESPECT TO PRODUCTION TIMES
(4.13) THE MDH PLOT FOR A TYPICAL BUILD UP TEST
(4.14) RATE AND PRESSURE RESPONSES DURING MULTI-RATE BUILD UP TEST
(4.15) TYPICAL MULTI-RATE PRESSURE BUILD UP PLOT
(4.16) SCHEMATIC DIAGRAM OF WELL AND FORMATION DURING BUILD UP TEST
(4.17) DETERMINATION OF WELLBORE PARAMETERS VIA RUSSELL'S MODEL

**CHAPTER 5**

(5.1) IDEALIZED MATRIX AND FISSURE REGION OF FRACTURED NETWORK
(5.2) FLOW DIRECTION THROUGH A FRACTURED FORMATION OF UNIFORMLY SPACED FRACTURES WITH DIFFERENT FRACTURE WIDTHS
(5.3) DIMENSIONLESS PRESSURE RESPONSES OF INFINITE ACTING DUAL POROSITY FORMATION WITH WBS & SKIN (SIF MODEL)
(5.4) PRESSURE BEHAVIOUR OF DUAL POROSITY FORMATION WITH PSEUDO STEADY STATE INTERPOROSITY FLOW FROM MATRIX TO FISSURE
(5.5) PRESSURE RESPONSES OF DUAL POROSITY FORMATION $[(\phi Vc_t)_f < (\phi Vc_t)_{f+m}]$
(5.6) PRESSURE RESPONSES OF DUAL POROSITY FORMATION (SMALL MATRIX BLOCKS)
(5.7) BUILD UP PRESSURE RESPONSES OF DUAL POROSITY FORMATIONS FOR FOUR DISTINCT PRODUCTION PERIODS
(5.8) PRESSURE RESPONSES OF SIF MODEL (TOTAL SYSTEM IS DEFINED-CASE A)
(5.9) PRESSURE RESPONSES OF THE SIF MODEL (CASE B)
(5.10) PRESSURE RESPONSES OF THE SIF MODEL (CASE C)
(5.11) PRESSURE RESPONSES OF THE SIF MODEL (CASE D)
(5.12) PRESSURE RESPONSES OF THE SIF MODEL (CASE E)
(5.13) PRESSURE RESPONSES OF THE SIF MODEL DURING AN IDEAL DRAWDOWN
(5.14) SCHEMATIC DIAGRAM OF THE MATRIX BLOCK GEOMETRIES ASSOCIATED WITH THE TIF MODEL (MODEL A - HORIZONTAL SLAB , MODEL B - SPHERICAL)
(5.15) DIMENSIONLESS PRESSURE RESPONSES OF INFINITE ACTING DUAL POROSITY FORMATION WITH WBS & SKIN (TIF MODEL)

**CHAPTER 6**

(6.1) DERIVATIVE PRESSURE RESPONSES OF INFINITE ACTING DUAL POROSITY FORMATION WITH WBS & SKIN (SIF MODEL)
(6.2) DIMENSIONLESS PRESSURE & DERIVATIVE RESPONSES OF INFINITE ACTING DUAL POROSITY FORMATION WITH WBS & SKIN (SIF MODEL)

(6.3) $(P_D)+(P'_D)$ RESPONSES ASSOCIATED WITH THE SIF FRACTURED MODEL

(6.4) $(P_D)+(P'_D)$ RESPONSES OF THE SIF MODEL IN THE ABSENCE OF FISSURE SLSL

(6.5) $(P_D)+(P'_D)$ RESPONSES (PRODUCTION TERMINATED DURING TRANSITION PERIOD)

(6.6) $(P_D)+(P'_D)$ RESPONSES (PRODUCTION TERMINATED DURING FISSURE FLOW)

(6.7) DERIVATIVE PRESSURE RESPONSES OF INFINITE ACTING DUAL POROSITY FORMATION WITH WBS & SKIN (TIF MODEL)

(6.8) DIMENSIONLESS PRESSURE & DERIVATIVE RESPONSES OF AN INFINITE ACTING DUAL POROSITY FORMATION WITH WBS & SKIN (TIF MODEL)

(6.9) COMPARISON OF THE $P'_D$- RESPONSES WITH RESPECT TO THE SIF&TIF MODELS

(6.10) $(P_D)$ & $(P'_D)$ RESPONSES OF THE TIF MODEL (DISTINCT MATRIX BLOCK SHAPES)

(6.11) $(P_D)$ & $(P'_D)$ RESPONSES OF TIF MODEL IN THE PRESENCE OF A SEALING FAULT

(6.12) $(P_D)_{BU} + (P'_D)_{BU}$ RESPONSES OF THE TIF MODEL (SHORT PRODUCTION)

**CHAPTER 7**

(7.1) $P_D$-RESPONSES WITH RESPECT TO THE SIF MODEL (EQUATION 7.1)

(7.2) $P_D$-RESPONSES WITH RESPECT TO THE SIF MODEL DURING DRAWDOWN

(7.3) PRESSURE DRAWDOWN RESPONSES WITH RESPECT TO THE SIF MODEL ($r_D=\infty$)

(7.4) $(P_D)_{BU}$ RESPONSES WITH RESPECT TO THE SIF MODEL ($r_D=\infty$)

(7.5) CHARACTERIZATION OF THE SIF MODEL VIA BUILD UP TESTS ($r_D=\infty$)

(7.6) IDEALIZED $P_D$ RESPONSES OF THE SIF AND TIF MODELS

(7.7) $P_D$-RESPONSES WRT THE TIF MODEL FOR SPECIFIC VALUES OF $\lambda$ & $\omega$

(7.8) PRESSURE RESPONSES OF THE TIF MODEL ($I_f$,$I_{f\leftarrow m}$,$I_{f+m}$ IDENTIFIED)

(7.9) PRESSURE RESPONSES OF THE TIF MODEL IN THE ABSENCE OF FISSURE SLSL ($I_f$)

(7.10) $\Delta P$-RESPONSES OF THE TIF MODEL (TOTAL SYSTEM NOT DEFINED)

(7.11) $(P_D)_{BU}$ RESPONSES OF TIF MODEL IN THE ABSENCE OF FISSURE FLOW SEGMENT

(7.12) BUILD UP RESPONSES OF TIF MODEL IN THE ABSENCE OF FISSURE FLOW REGION

(7.13) $(P_D)_{BU}$ RESPONSES OF TIF MODEL (TOTAL SYSTEM RESPONSES NOT DEFINED)

(7.14) $(\Delta P)_{BU}$ RESPONSES OF TIF MODEL ( $I_{f+m}$ SLSL NOT DEFINED)

**CHAPTER 8**

(8.1) SINGLE PLANE VERTICAL FRACTURE (ACROSS THE ENTIRE FORMATION)
(8.2) FLUID FLOW INTO THE FRACTURE PLANE (2N SEGMENTS)
(8.3) FRACTURED WELL IN AN INFINITE ACTING FORMATION
(8.4) FRACTURED WELL IN A CLOSED RECTANGULAR RESERVOIR
(8.5) DIMENSIONLESS PRESSURE RESPONSES OF A WELL AT THE CENTRE OF HOMOGENEOUS/RECTANGULAR FORMATION (UFF MODEL)
(8.6) DIMENSIONLESS PRESSURE RESPONSES OF A WELL AT THE CENTRE OF HOMOGENEOUS/RECTANGULAR FORMATION (ICF MODEL)
(8.7) $(P_{INT})_{DF}$ DEFINITION FOR A WELL AT THE CENTRE OF A CLOSED HOMOGENEOUS / RECTANGULAR FORMATION (UFF MODEL)
(8.8) $(P_{INT})_{DF}$ DEFINITION FOR A WELL AT THE CENTRE OF A CLOSED HOMOGENEOUS / RECTANGULAR FORMATION (ICF MODEL)
(8.9) $(P_{DF})_{BU}$ RESPONSES OF ICF MODEL (EXTRAPOLATED @ EARLY TIMES)

**CHAPTER 9**

(9.1) PRESSURE RESPONSES OF FRACTURED FORMATIONS DOMINATED BY LINEAR FLOW
(9.2) PRESSURE RESPONSES OF FRACTURED FORMATIONS DOMINATED BY RADIAL FLOW
(9.3) $(P_D)$ RESPONSES OF FRACTURED FORMATION DURING EARLY AND LATE TIMES
(9.4) BUILD UP RESPONSES OF FRACTURED FORMATIONS DOMINATED BY LINEAR FLOW
(9.5) BUILD UP RESPONSES OF FRACTURED FORMATIONS DOMINATED BY RADIAL FLOW
(9.6) BUILD UP PRESSURE RESPONSES OF BOUNDED FRACTURED FORMATIONS
(9.7) BUILD UP TESTING CORRECTION FACTOR WRT FRACTURED FORMATION
(9.8) BUILD UP TESTING FLOW CHART ASSOCIATED WITH THE FRACTURED FORMATIONS (LINEAR AND RADIAL REGIONS PREVAIL)

**CHAPTER 10**

(10.1) CHARACTERIZATION OF THE RECORDED PRESSURE DATA BY MEANS OF THE HOMOGENEOUS TYPE CURVES
(10.2) CONVENTIONAL ANALYSIS OF THE RECORDED PRESSURE DATA - HORNER BUILD UP TESTING MODEL
(10.2A) 3D HORNER PLOT OF THE PRESSURE DATA FOR THE WELL MX/1

(10.3) CHARACTERIZATION OF THE RECORDED PRESSURE DATA BY MEANS OF THE DUAL POROSITY TYPE CURVES - (SIF MODEL)

(10.4) CONVENTIONAL ANALYSIS OF THE RECORDED PRESSURE DATA VIA SINGLE RATE DRAWDOWN TEST - (SIF MODEL)

(10.4A) 3D SEMI-LOG PLOT OF THE PRESSURE DATA FOR THE WELL FT/2

(10.5) CHARACTERIZATION OF THE RECORDED PRESSURE DATA THROUGH HYDRAULICALLY FRACTURED FORMATION TYPE CURVES (ICF MODEL)

(10.6) CONVENTIONAL ANALYSIS OF THE RECORDED BUILD UP PRESSURE DATA SUBJECT TO (ICF)-FRACTURED MODEL

(10.6A) 3D HORNER PLOT OF THE PRESSURE/TIME DATA FOR THE WELL SX/O

TABLE (10.1) RECORDED PRESSURE DATA FOR THE WELL MX/1

TABLE (10.2) INTERPRETATION RESULTS FOR THE WELL MX/1 (LOG-LOG PLOT)

TABLE (10.3) INTERPRETATION RESULTS FOR THE WELL MX/1 (HORNER PLOT)

TABLE (10.4) RECORDED PRESSURE DATA FOR THE WELL FT/2

TABLE (10.5) INTERPRETATION RESULTS FOR THE WELL FT/2 (LOG-LOG PLOT)

TABLE (10.6) INTERPRETATION RESULTS FOR THE WELL FT/2 (SEMI-LOG PLOT)

TABLE (10.7) RECORDED PRESSURE DATA FOR THE PRODUCTION WELL SX/O

TABLE (10.8) INTERPRETATION RESULTS FOR THE WELL SX/O (LOG-LOG PLOT)

TABLE (10.9) INTERPRETATION RESULTS FOR THE WELL SX/O (HORNER PLOT)

TABLE (A1) DIETZ SHAPE FACTORS FOR HOMOGENEOUS/FRACTURED FORMATIONS

★★★★★★★★★★

# CHAPTER 1
# INTRODUCTION

## 1.1-HISTORY

The history of the testing of gas wells dates back to the 1920's, but modern well test analysis can be considered to date from 1935 when C.V. Theis published his original paper on the drawdown and recovery (build up) in water wells. In 1950, Miller, Dyes and Hutchinson gave an analysis for pressure build up following a long flowing period (implicitly following pseudo steady state flow), and the use of this data for evaluation of the permeability thickness production. In 1951, Horner modified the application of Theis well testing procedures for the analysis of both the initial pressure ($P^*$) in an infinite field, and the permeability thickness product. This work also introduced the method of images as a technique for the analysis of a field containing a linear boundary.

Studies on Laplace Transform applications to flow problems (Hurst and van Everdingen 1949), skin effects (van Everdingen 1953) and average pressure in bounded formations (Matthews, Brons and Hazebroek 1954) were followed by numerous papers, the status being well summarized in the texts by Matthews and Russell (Pressure Build up and flow tests in wells 1967), Polubrinov-Kochina (Theory of Ground Water Movement 1962) and Hantush (Advances in Hydroscience 1964). The work of Hantush, in particular, anticipated many later analyses of problems in well test interpretation schemes for the characterization of oil and gas bearing formations.

The earlier period of well testing practice and analysis (i.e. prior to1970) recognised the problems associated with wellbore and skin effects and sought to eliminate these through tests of relatively long duration at which such effects decay to negligible proportions. The significant difficulty in maintaining constant production rates coupled with the development of advanced surface recording gauges, however, led to the monitoring of well tests of shorter duration, which in turn emphasized the need for correct analysis of the transition regions from wellbore dominance to formation dominance, and identification of data suitable for analysis by traditional methods.

The first attempts for analysing the whole of the recorded data were made by adapting methods of the hydrologists, where the theoretical dimensionless pressure responses of idealized homogeneous reservoirs with skin and wellbore storage were solved by theoretical and numerical analysis of the appropriate equation and boundary conditions. These defined the appropriate flow regions and enabled field data to be analyzed by the theoretical pressure responses (type curve matching) of the mathematical models to characterize formations. Since the new schemes appeared to unravel more information with regard to the physical nature of the formations, type curves for more and more hypothetical well / reservoir models were developed.

Advances in well testing during the past five years which has followed the foot steps of Agarwal, Earlougher, Ramey and Raghavan have been remarkable. Introduction of pressure derivative concept, the application of Stefhest algorithm to flow problems as well as vigorous research in the field have indeed put the reservoir engineer in the position of analysing and forecasting the performance of oil and gas fields with a significant degree of confidence.

## 1.2-WELL TESTING OBJECTIVES

The fundamental objectives of well testing can be divided into three main categories.

- Determination of formation characteristics.
- Evaluation of well performance, and
- Estimation of completion/stimulation efficiency.

In field practice, these objectives are achieved from the direct measurements of bottom hole pressure responses and production rates via pressure gauges and flow meters in the tubing. These recorded data are analysed by an appropriate testing scheme and then compared with the PVT studies of downhole and surface samples in order to correlate the petrophysical characteristics of the formation. Since the precision by which the reservoir parameters are evaluated will influence the choice of most economical routine for development of oil fields, tests must be conducted properly in order to enhance the quality of recorded data during the test.

## 1.3-CHOICE OF EQUIPMENT

Whilst the choice of surface equipment is influenced by the nature of hydrocarbon and the type of test being conducted, very often the operator has the option of choosing either downhole or surface shut in equipment. Such an option, however, may be restricted to the former case when testing is performed offshore with the possibility of encountering high rate and pressures. The selection of electronic pressure gauges as opposed to their mechanical counter part are also an important part of well test design, since the ability to detect and record small pressure changes of the order of 0.01 psi permits the reservoir engineer to employ complex well testing techniques to be used efficiently.

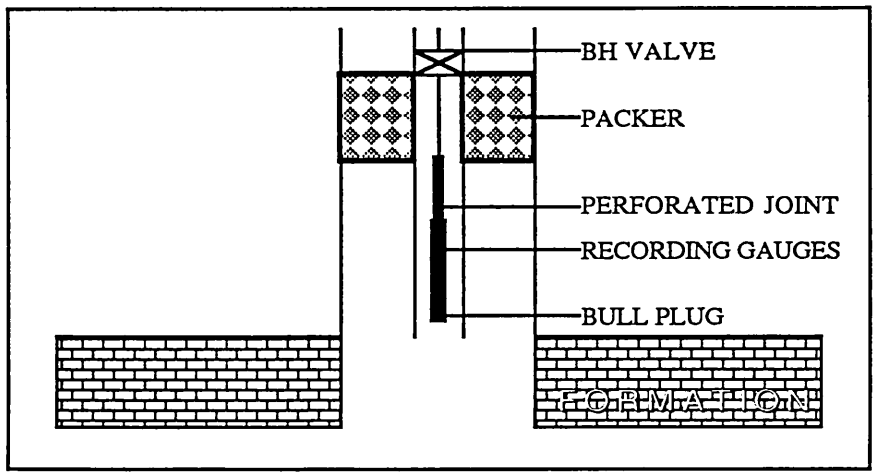



FIGURE 1.1: BOTTOMHOLE APPARATUS FOR DOWNHOLE SHUT IN.

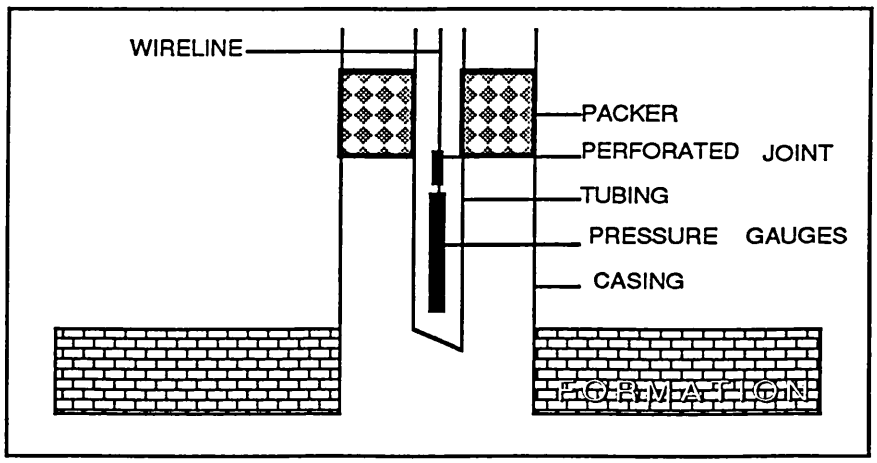



FIGURE 1.2: BOTTOMHOLE APPARATUS FOR SURFACE SHUT IN.

## 1.4-CHOICE OF WELL TESTS

In general, there are two type of flow tests which can be conducted on exploration and producing wells in order to determine the petrophysical quantities as well as any heterogeneities associated with the formation. The first category which reflects single rate, multi rate or extended draw down tests are designed primarily to estimate the basic reservoir parameters such as permeability, mechanical skin factor and drainage area, whilst the second category commonly referred to as build up tests, are designed for estimating the average reservoir pressure.

In addition to evaluating the formation mean pressure, build up tests can also be employed to determine the flow characteristics of the formation as is obtained during draw down tests. In fact, due to the difficulty in maintaining constant production rate throughout draw down schemes, preference is usually given to build up tests.

## 1.5-WELL TEST INTERPRETATIONS

Correct field interpretation of recorded pressure data is probably the most crucial part of the well testing program, since it is at this stage where the important decisions are made with regard to the development of oil and gas fields. the tedious procedures involving reservoir simulations as well as the trivial use of the conventional schemes in characterization of complex formations could indeed turn out to be costly in terms of economics. It is hence evident that the development of a new tool such as **(TOPAZ)** (An interactive well testing program) which is capable of enhancing the degree of interpretation accuracy by constructing and analysing prototype reservoir models, could prove to be a valuable asset to the well test engineer.

**(TOPAZ)** combines the preceding objectives by utilization of conventional and log-log testing as well as reservoir modelling techniques in order to assist the operator to develop theoretical models which define the physical nature of specific formations. These models once constructed, can then be updated (as more information becomes available) in order to identify the basic requirements in the future development of the producing field.

☆☆☆☆☆☆☆☆☆☆

# CHAPTER 2

# INFINITE ACTING HOMOGENEOUS FORMATION

## 2.1-PRESSURE RESPONSES OF HOMOGENEOUS FORMATIONS

Based on the following assumptions, the fundamental differential equation representing the fluid flow through a homogeneous medium can be defined by[28]:

$$\frac{\partial^2 P_D}{\partial r_D^2} + \frac{1}{r_D}\left(\frac{\partial P_D}{\partial r_D}\right) = \frac{\partial P_D}{\partial T_D} \qquad (2.1)$$

-Fluid flow is fully radial and occurs in the horizontal plane of an infinite acting isotropic medium.

-Pressure gradients of the fluid and the gravitational forces are negligible.

-Formation is fully saturated with a single phase incompressible fluid and is produced at a constant rate.

-The viscosity of the fluid as well as the porosity and the permeability of the formation are independent of pressure.

In order to generate the solutions of interest, the following initial boundary conditions are also imposed on the homogeneous model.

- $P_D=0$ @ $T_D=0$ for all values of $r_D = \frac{r}{r_w}$

- Limit $(\Delta P)_D = 0$ for all values of $T_D$

  $r_D \rightarrow \infty$

- $(\Delta P_D)_{r_D=1} = \{ \Delta P_D - S\left(\frac{\partial \Delta P_D}{\partial r_D}\right) \}_{r_D=1}$

- $C_D\left(\frac{\partial \Delta P_D}{\partial T_D}\right) = \left(\frac{\partial \Delta P_D}{\partial r_D}\right)_{r_D=1}$

Subject to the initial boundary conditions, equation (2.1) is initially evaluated in the Laplace space and the final expression is then inverted into real space solution by means

of Mellin's formula.

$$\bar{P}_D(z) = \frac{1}{z\left[ zC_D + 1/(S + \{K_0(\sqrt{z})/\sqrt{z}\,K_1(\sqrt{z})\}\right]} \tag{2.2}$$

z=Laplace operator based on the dimensionless time $T_D$.

Inversion of equation (2.2) yields:

$$\therefore P_D = \frac{4}{\pi^2}\int_0^\infty \frac{[1-\exp(-x^2T_D)]\,dx}{x^3[\{xC_DJ_o(x) - (1-C_DSx^2)J_1(x)\}^2 + \{xC_DY_o(x) - (1-C_DSx^2)Y_1(x)\}]} \tag{2.3}$$

By defining the dimensionless time and wellbore storage parameters based on effective wellbore radius[1] $r_we^{-2S}$ (ie $T_D=T_De^{2S}$ , $C_D=C_De^{2S}$) equation (2.3) can be written as:

$$P_D = \frac{4}{\pi^2}\int_0^\infty \frac{[1-\exp(-x^2\{T_D/C_D\}\,C_De^{2S})]\,dx}{x^3[\{xC_De^{2S}J_o(x) - J_1(x)\}^2 + \{xC_De^{2S}Y_o(x) - Y_1(x)\}^2]} \tag{2.4}$$

Two solutions, associated with equation (2.4), which are of particular interest, are given in the following forms;

-Short time approximation, dominated by wellbore storage flow:

$$P_D = T_D/C_D \tag{2.5}$$

-Long time approximation, dominated by radial flow:

$$P_D = 0.5[\,Ln\{4T_De^{2S}\} - 0.57722\,] \tag{2.6}$$

Introducing the dimensionless wellbore storage parameter to equation (2.6), the expression can be defined as:

$$P_D = 0.5\times[\,Ln(4) + Ln(C_De^{2S}\{\frac{T_D}{C_D}\}) - 0.57722\,] \tag{2.7}$$

$$\therefore \quad P_D = 0.5 \times [\, Ln(\frac{T_D}{C_D}) + Ln(C_D e^{2S}) + 0.80907 \,] \tag{2.8}$$

N.B. In reference {2}, equation (2.6) was defined in terms of dimensionless time $[T_D]$, whereas the definition of the dimensionless pressure in this presentation was based on the $[T_D e^{2S}]$ parameter in order to extend the applicability of equation (2.4) to non damaged and fractured wells.

With reference to equations (2.4) and (2.8) it can be seen that the dimensionless pressure is only dependent on $[T_D/C_D]$ and $[C_D e^{2S}]$ groups. This point in fact justified the generation of the type curves of figure(2.1). In order to impose time limits on the various flow regimes specific to a given value of $[C_D e^{2S}]$, the dimensionless pressure was evaluated by means of equations (2.4) and (2.8) for each incremental value of $[T_D/C_D]$ group until:

$$[\Delta P_D]_{C_D e^{2S}} = ABS\,[\{P_D\}_{EQN(2.4)} - \{P_D\}_{EQN(2.8)}] \leq \varepsilon = \{0.05\} \tag{2.9}$$

By performing the above procedure, the locus of the pressure points with respect to $[T_D/C_D]$ group which defined the start of the radial flow period, were hence determined. This enables the definition of the time range when the semilog straight line analysis could be applied to specific ranges of field pressure data.

Although equation (2.4) does represent the pressure behaviour of a homogeneous reservoir during early, intermediate and late time flow period regardless of the well condition, the actual numerical values of the dimensionless pressure were derived by both numerical and analytical schemes for two major reasons:

-The need to produce draw down type curves of varying ranges of $[C_D e^{2S}]$ that would suit a particular field data and not involve re-evaluation of Bessel functions $J_{o-1}, Y_{o-1}$.

-Even if the error involved in calculation of Bessel functions were to be considered negligible, the real time taken to evaluate equation (2.4) by means of Richardson's deferred approach[47] which was suggested in reference {2} is not acceptable, as it

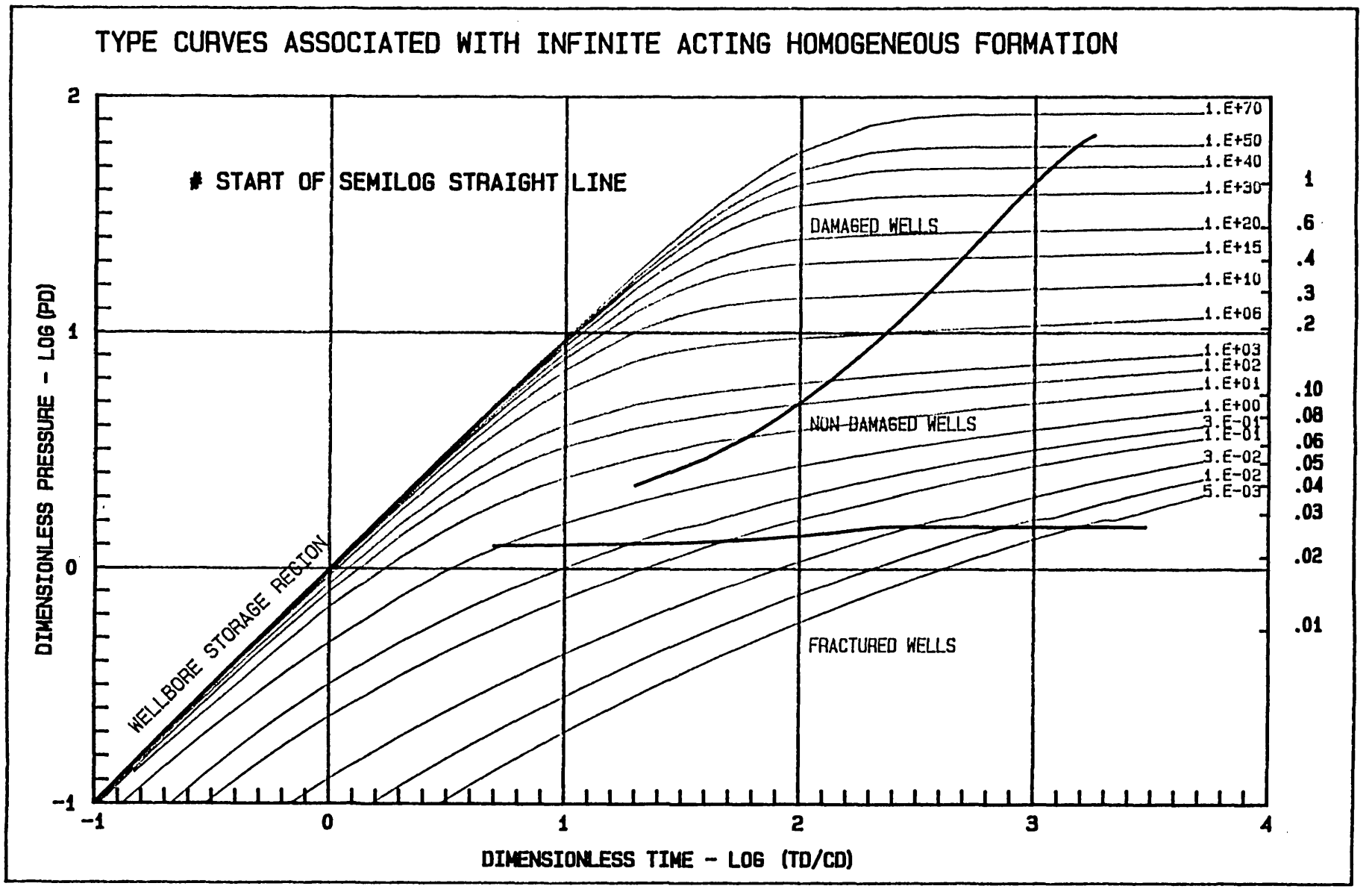



FIGURE 2.1: DIMENSIONLESS PRESSURE RESPONSES OF INFINITE ACTING HOMOGENEOUS FORMATION WITH WELLBORE STORAGE & SKIN

would take up to six hours to generate one type curve based on $[C_De^{2S}]$ value.

## 2.2-NUMERICAL SOLUTION OF PD-FUNCTION (DAMAGED WELLS)

Based on the fact that function $\{S+[K_o(\sqrt{z}) / \sqrt{z}K_1(\sqrt{z})]\}$ can be approximated by the semilog straight line $Ln(2/\gamma\sqrt{z}e^{-2S})$, equation (2.2) can be written as:

$$\overline{P}_D(g) = \frac{1}{g\left[g + Ln\left[\frac{2}{\gamma\sqrt{g/C_De^{2S}}}\right]^{-1}\right]} \qquad (2.10)$$

Where $g=\{z\times C_D\}$ is the Laplace operator based on $T_D/C_D$

Although Equation (2.10) was evaluated successfully by means of the numerical inversion scheme introduced by Stefhest[66], under negative skin condition, instabilities did arise in the flow equation. The inversion scheme in fact failed to generate logical values of the $P_D$-function. Moreover, the source program proved to be less sensitive with respect to the definition of dimensionless pressure responses for $[C_De^{2S}]$ values of less than 50 (i.e. non damaged and acidized wells). Modifications were needed to extend its applicability to non damaged wells.

The inversion scheme was performed in single precision arithmetic, by taking the number of summation term (N) with respect to equation (2.10) equal to 8. This proved to be just as effective as working in double precision with N=16, as suggested by Mavor and Cinco[46].

$$\overline{P}_D \approx u\sum_{j=1}^{N=8} V(j)\,\overline{P}_D(u\times j) \qquad \& \qquad u = Ln\{\frac{2}{T_D/C_D}\} \qquad (2.11)$$

$$V(j) = (-1)^{N/2+j}\sum_{k=INT(\frac{j+1}{2})}^{MIN(j,N/2)} \frac{k^{(N/2)}\,(2k)!}{(\frac{N}{2}-k)!\,(k-1)!\,k!\,(j-k)!\,(2k-j)!} \qquad (2.12)$$

$$\bar{P}_D(u\times j) = \frac{1}{u\times j\left[u\times j + \mathrm{Ln}\left[\frac{2}{\gamma\sqrt{u\times j/C_D e^{2S}}}\right]^{-1}\right]} \qquad (2.13)$$

For the ranges of dimensionless $[C_D e^{2S}]$ group considered, it was observed that as the value of $[C_D e^{2S}]$ increased, the approximate time to attain plane radial flow was also increased. In an infinite acting homogeneous formations,the above point emphasizes the need to flow the well for longer periods when the degree of damage to the well is considerable.

## 2.3-ANALYTICAL SOLUTION OF PD-FUNCTION (FRACTURED WELLS)

The two numerical integration schemes considered for solving equation (2.4) were Gauss-Laguarre quadrature[13] and the Richardson's defferred approach to limit. For the Following reasons, however, the preference was given to the former scheme.

-Although recommended in reference {2}, the convergence of the latter scheme was rather slow on the micro computer. This was mainly due to the halving of the integration interval until the tolerance levels were achieved.

-Whilst the Gauss-Laguarre integration model is capable of integrating functions similar to equation (2.4) over the interval of zero to infinity, the use of Richardson's numerical integration requires the specification of the upper and lower limits of the integral.

-Due to the structure of the former scheme, it was possible to create Bessel functions on a data file, thus enhancing the speed of the integration model with respect to equation (2.4). In Richardson's integration model, however, due to uncertainty of the number of stripes required for a fixed integration range, in order to reach the desired tolerance level, Bessel functions had to be implemented in the main program as subroutines which caused the computational time of $P_D$-function values to increase by 100 folds. The final point is illustrated below.

Assuming a fixed tolerance level [ε], the number of stripes between points [A] and [B] is increased until the tolerance level is reached. this is achieved by halving the value of [L], and evaluating equation (2.4) for [$X_L$] number of stripes which would also involve the determination of Bessel functions $J_{o-1}$,$Y_{o-1}$ over each incremental value of [L]. Since [$X_L$] is not fixed (i.e. For a given value of [$T_D/C_D$] and [$C_D e^{2S}$] parameters, the tolerance level may be attained when $X_L$=16 or 32 or 64,etc) the value of [L] becomes variable, making it practically impossible to create data files with respect to Bessel functions when using Richardson's numerical integration scheme for evaluation of equation (2.4).

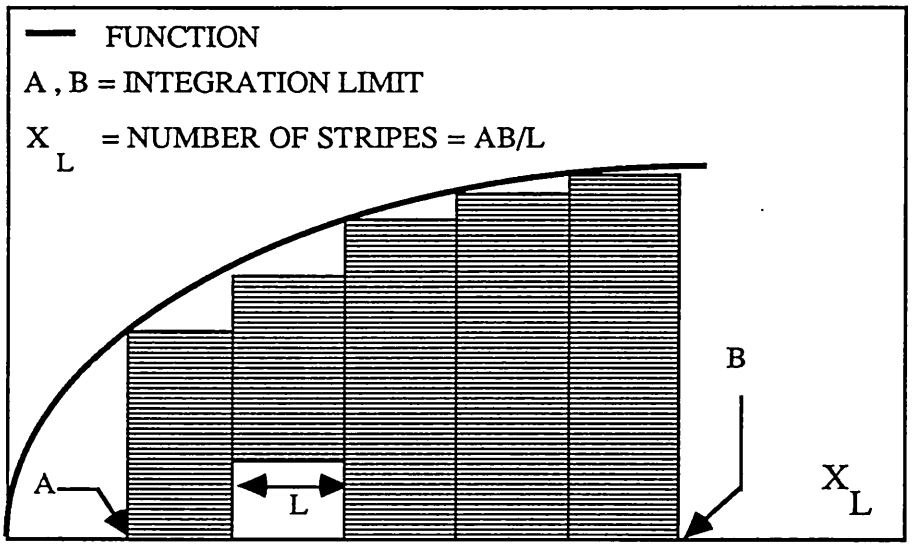



FIGURE 2.2: NUMERICAL INTEGRATION WRT RICHARDSON MODEL

Referring to the Gauss-Laguarre integration model and defining the function F(x) as:

$$F(x) = \frac{[1-\exp(-x^2\{T_D/C_D\}C_D e^{2S})]}{x^3[\{xC_D e^{2S} J_o(x) - J_1(x)\}^2 + \{xC_D e^{2S} Y_o(x) - Y_1(x)\}^2]} \qquad (2.14)$$

$$\text{Then} \quad P_D\left(\frac{T_D}{C_D}\right) = \frac{4}{\pi^2}\int_0^\infty F(x)\,dx = \frac{4}{\pi^2}\int_0^\infty e^{-x} e^{x} F(x)\,dx \qquad (2.15)$$

Equation (2.15) can hence be approximated by[13]:

$$P_D(\frac{T_D}{C_D}) \approx \frac{4}{\pi^2} \sum_{i=1}^{n} H_i e^{x_i} F(x_i) \tag{2.16}$$

$$H_i = \frac{(n!)^2 x_i}{[L_{n+1}(x_i)]^2} \tag{2.17}$$

With reference to equation (2.16), it was noted that as the value of Laguarre number [n], was increased, the accuracy of the dimensionless pressure response values were also increased. Thus, for all practical purposes, [n] was taken as 14 (i.e. Fifteen point formula) for the integration of equation (2.4). The scheme proved to be very efficient on the basis of the accuracy and the computational time of the $P_D$-function.

## 2.4-APPLICATION OF DRAWDOWN TYPE CURVES TO BUILD UP TESTS

The general equation associated with the dimensionless pressure responses of an ideal build up test is given by:

$$(P_D)_{BU} = P_D(T_D/C_D) + P_D(\{T_P\}_D/C_D] - P_D([\{T_P\}_D/C_D] + [T_D/C_D]) \tag{2.18}$$

With reference to equation (2.18), the dimensionless pressure behaviour for a build up system is dependent on;

-The $P_D$-function responses during drawdown, and

-The total production time $[T_p]$, prior to shut in.

Thus in order to analyse build up pressure data via draw down type curves, the following condition must be met:

$$P_D(\frac{\{T_P\}_D}{C_D}) \approx P_D(\frac{\{T_P\}_D}{C_D} + \frac{T_D}{C_D}) \tag{2.19}$$

The above condition is satisfied, provided:

1-The production time [$T_p$], is long enough compared to the shut in period.

2-The dimensionless pressure function over a wide range of time remains practically constant.

When condition (1) and/or (2) are achieved, equation (2.18) can be approximated by:

$$(P_D)_{BU} \approx P_D(T_D/C_D) \tag{2.20}$$

(i.e. The $P_D$-function responses for an ideal build up and drawdown systems are identical, justifying the analysis of build up pressure data via draw down type curves).

In order to implement numerical boundary conditions for the validity of equation (2.19), and establish the effects of production times on the validity of testing build up data by means of figure (2.1), values of [$\{T_p\}_D/C_D$] group were assumed and using a tolerance level of 0.05, the dimensionless pressure responses associated with $P_D(T_D/C_D)$ and $(P_D)_{BU}$, were evaluated through equations (2.4) and (2.18) respectively over a wide range of [$T_D/C_D$] parameter.

Based on the above procedures, the right hand axis of figure (2.1) was then generated , thus allowing the operator to establish the minimum duration of production period $(T_p)_{min}$ during a build up test which would indicate whether matching the test data on the draw down type curve is likely to be correct.

The general procedure in the definition of $(T_p)_{min}$ is as follows:

-Plot the build up pressure data on a 5x3 log-log scale and overlay on figure (2.1) until the best match is obtained.

-Determine $(T_p)_{min}$ using the expression;

$$(T_p)_{min} = (\Delta T)_L / T_{axis} \tag{2.21}$$

When $T_p > (T_p)_{min}$, then the match is likely to be valid, otherwise, type curves with slightly smaller values of dimensionless $[C_D e^{2S}]$ group should be used. It is emphasized, however, that if $(T_p)_{min}$ cannot be defined clearly, then specialized plots should be used in conjunction with theoretical modelling techniques of **(TOPAZ)** program in order to get a better estimate of formation characteristics.

## 2.5-CHARACTERIZATION OF HOMOGENEOUS FORMATIONS ($r_D=\infty$)

In order to use the type curves of figure (2.1), the following steps should be taken:

-Plot $P-P_{wf}$ vs $(\Delta T)$ on a 5x3 log-log grid.

-Overlay the plot on figure (2.1) and determine the best match.

-If the recorded data are taken from a build up test, determine $(T_p)_{min}$, in order to check the validity of the match.

-From the pressure match define the permeability thickness.

$$Kh = 141.2\, q\mu B_o \times \{\frac{P_D}{\Delta P}\}_{match} \tag{2.22}$$

-From the time axis match determine wellbore storage parameter.

$$C = 2.9507 \times 10^{-4} \frac{Kh}{\mu} \{\frac{\Delta T}{T_D/C_D}\}_{match} \tag{2.23}$$

$$C_D = \frac{0.8936C}{\phi c_t hr_w^2} \tag{2.24}$$

-Read the value of $[C_D e^{2S}]$ and hence determine the value of the mechanical skin factor.

$$S = 0.5 \times Ln[\,(C_D e^{2S})_{match} / C_D\,] \tag{2.25}$$

☆☆☆☆☆☆☆☆☆☆

# CHAPTER 3

# DIFFERENTIAL MODEL OF HOMOGENEOUS FORMATIONS

## 3.1-PRESSURE DERIVATIVES WITH RESPECT TO HOMOGENEOUS MODEL

The two extreme solutions associated with the diffusivity equation, were investigated via differentiation schemes in order to develop the numerical relationships with respect to the derivatives of pressure responses as a function of $T_D/C_D$ and depending upon $C_De^{2S}$ group.

-Short time approximation (wellbore storage flow)

$$P_D=\frac{T_D}{C_D} \quad \& \quad \frac{T_D}{C_D}\left[\frac{dP_D}{d(T_D/C_D)}\right]=\frac{T_D}{C_D} \tag{3.1}$$

-Long time approximation (infinite acting radial flow)

$$P_D=0.5\times\{Ln(\frac{T_D}{C_D})+0.809+Ln(C_De^{2S})\} \quad \& \quad \frac{T_D}{C_D}\left[\frac{dP_D}{d(T_D/C_D)}\right]=0.5 \tag{3.2}$$

Whilst equation (3.1) represents the behaviour of the pressure derivative responses at early times, the long time approximation emphasizes the fact that regardless of the well conditions (damaged, acidized or fractured), all the pressure derivative solutions coincide with the locus of the horizontal line whose magnitude is equal to 0.5. Furthermore, it is only during the intermediate flow periods that the dependence of the pressure derivatives on $C_De^{2S}$ group becomes significant. Therefore, for a given set of pressure data, depending on its quality and the differentiation scheme employed, a plot of $\log(\Delta T\times d\Delta P/d\Delta T)$ vs $\log(\Delta T)$ will produce the straight lines which are specific to early and late time flow regimes[11]. Such responses when overlayed on the derivative type curves (figure 3.1), can be used to identify the formation characteristics without any need for specialized plots in order to confirm the validity of the results[8].

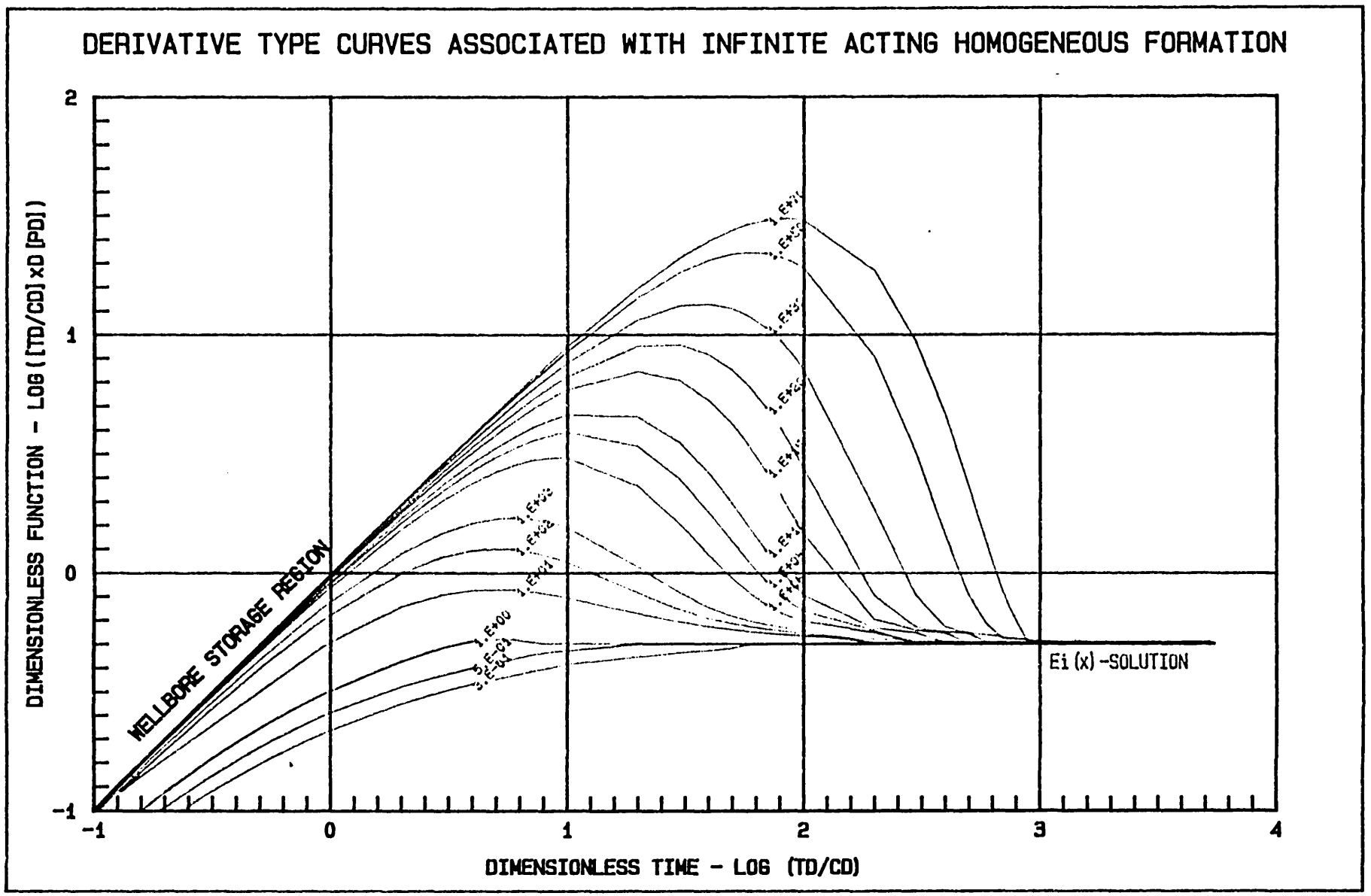



FIGURE 3.1: DERIVATIVE PRESSURE RESPONSES OF INFINITE ACTING HOMOGENEOUS FORMATION WITH WELLBORE STORAGE & SKIN

## 3.2-DIFFERENTIATION PROCEDURES ASSOCIATED WITH PD-FUNCTION

The derivatives of the dimensionless pressure with respect to $T_D/C_D$ parameter, were obtained numerically by means of the Taylor series expansion[47].

$$\left.\frac{d(P_D)}{d(T_D/C_D)}\right|_i = \frac{(P_D)_{i+1} - (P_D)_{i-1}}{2H} - ERR \qquad (3.3)$$

$$ERR = \frac{H^2}{6} \times \left.\frac{d^3P_D}{d(T_D/C_D)^3}\right|_i \quad \text{ERR = Relative error}$$

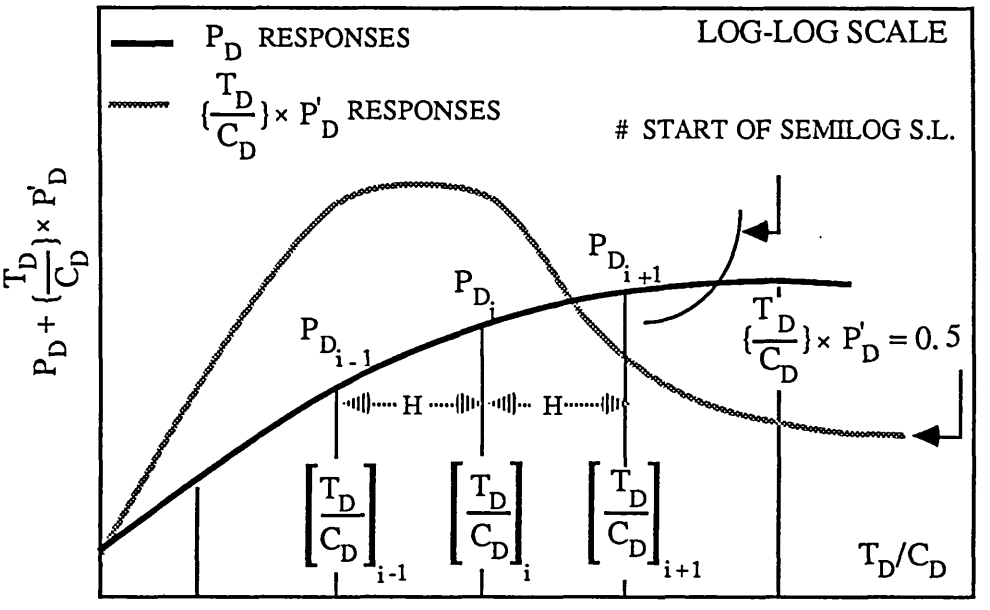



FIGURE 3.2: DEFINITION OF $P'_D$-FUNCTION VIA NUMERICAL INTEGRATION

The differentiation scheme, however, signalled the possibility of two sources of errors.

-The existence of error in the original schemes, used in generation of dimensionless pressure data.

-Errors with regard to the numerical methods employed for the differentiation of the dimensionless pressure function with respect to $T_D/C_D$ group.

Based on the assumption that the source of errors associated with the evaluation of $P_D$-function by means of numerical and analytical techniques were negligible, by taking H=0.05 (figure 3.2), the value of [ERR] in equation (3.3) was reduced considerably. This particular choice of [H] for damaged and non damaged wells provided derivative type curves (figure 3.1) which were free from noise effects and hence exhibited negligible late time distortions. Slight modifications regarding the value of [H], however, were needed in order to reduce the late time distortion effects for;

-Acidized / fractured wells, and

-Damaged wells in the range of $C_D e^{2S} \geq 10^{+5}$ @ $T_D/C_D \geq 1000$

## 3.3-APPLICATION OF PRESSURE DERIVATIVES TO BUILD UP TESTS

Although the derivative type curves of figure (3.1) were generated based on the assumption of single rate drawdown model, due to the lack of maintenance of stabilized production rates in practice, most transient well tests are performed via build up schemes.

Thus in order to extend the derivative approach to build up tests, the derivatives of $P_D$-function had to be redefined. The objective was met by considering the dimensionless pressure responses during an ideal build up test[55].

$$(P_D)_{BU} = P_D(\Delta T) + P_D(T_p) - P_D(T_p + \Delta T) \tag{3.4}$$

Differentiation of equation (3.4) with respect to $T_D/C_D$ yields:

$$\left[\frac{dP_D}{d(T_D/C_D)}\right]_{BU} = \left[\frac{dP_D}{d(T_D/C_D)}\right]_{\Delta T \equiv \frac{T_D}{C_D}} - \left[\frac{dP_D}{d(T_D/C_D)}\right]_{T_p+\Delta T \equiv (T_p)_D + \frac{T_D}{C_D}} \tag{3.5}$$

Assuming fluid flow in the infinite acting reservoir is fully radial (recall the general expression associated with late time approximation);

$$\left[\frac{dP_D}{d(T_D/C_D)}\right]_{DD} = \frac{0.5}{(T_D/C_D)} \quad \& \quad \left[\frac{dP_D}{d(T_D/C_D)}\right]_{BU} = \frac{0.5}{\{[(T_p)_D+T_D]/C_D\}} \tag{3.6}$$

Substitution of equations (3.6) into equation (3.5) thus yields:

$$\left[\frac{dP_D}{d(T_D/C_D)}\right]_{BU} = \frac{0.5}{T_D/C_D}\left[1-\frac{(T_D/C_D)}{\{(T_P)_D+T_D\}/C_D}\right] \tag{3.7}$$

$$\therefore \quad \frac{T_D}{C_D}\left[\frac{dP_D}{d(T_D/C_D)}\right]_{BU} = 0.5\left[\frac{(T_P)_D}{(T_P)_D+T_D}\right] \tag{3.8}$$

Re-arranging equation (3.8) yields:

$$\left[\frac{(T_P)_D+T_D}{(T_P)_D}\right] \times \frac{T_D}{C_D} \times \left[\frac{dP_D}{d(T_D/C_D)}\right] = 0.5 \tag{3.9}$$

With reference to equation (3.9), it was concluded that build up pressure data could be analysed by means of the derivative type curves, provided log ({($T_p$+ $\Delta$T)/$T_p$}x$\Delta$Tx [d$\Delta$P/d$\Delta$T]) is used instead of log ( $\Delta$Txd$\Delta$P/d$\Delta$T) in the plot against log( $\Delta$T) .

Based on the theory and numerical results associated with the derivative approach, the scheme proved to be advantageous in providing:

-The derivative type curves with respect to $C_De^{2S}$ group.

-The combination of global and specialized plots on the same graph, thus enhancing the degree of accuracy in the definition of formation characteristics.

-The ability to analyse build up pressure data, even for unknown values of flowing bottom hole pressure (when the pressure gauge is run in the hole after the well is shut in) and/or shut in times.

( N.B. Despite all the apparent advantages associated with the derivative approach, in field practice, figures (2.1) and (3.1) are usually used interactively in order to increase the degree of confidence in the evaluation of reservoir parameters-see figure 3.3).

## 3.4-DIFFERENTIATION SCHEMES APPLICABLE TO PRESSURE DATA

Since differentiation in general is an error amplifying process, in order to define the best derivative approach which would yield the least possible error with regard to a given set of pressure data, a number of numerical differentiation schemes such as Secant Line Approximation and Interpolating Polynomials were employed for testing purposes. However, for the reasons described previously, the preference was given to a Three Point Linear Smoothing scheme (Taylor expansion approach) in generation of the derivative type curves of figure(3.1).

### A ➳ THREE POINT SMOOTHING SCHEME

In order to employ the scheme efficiently, the incremental value between successive recorded pressure ($\Delta P=P_i - P_{i-1}$) should ideally correspond to the distance between pivotal points of the original pressure derivative responses (figure 3.1). If the same incremental value of [H] is not practical, then provided the distance from the point where the derivative is to be determined is large enough, then the noise effects will be diminished considerably. In general, the incremental value of [H] is chosen as a variable in order to;

-Compensate for early time noise effects, and

-Avoid late time over smoothing.

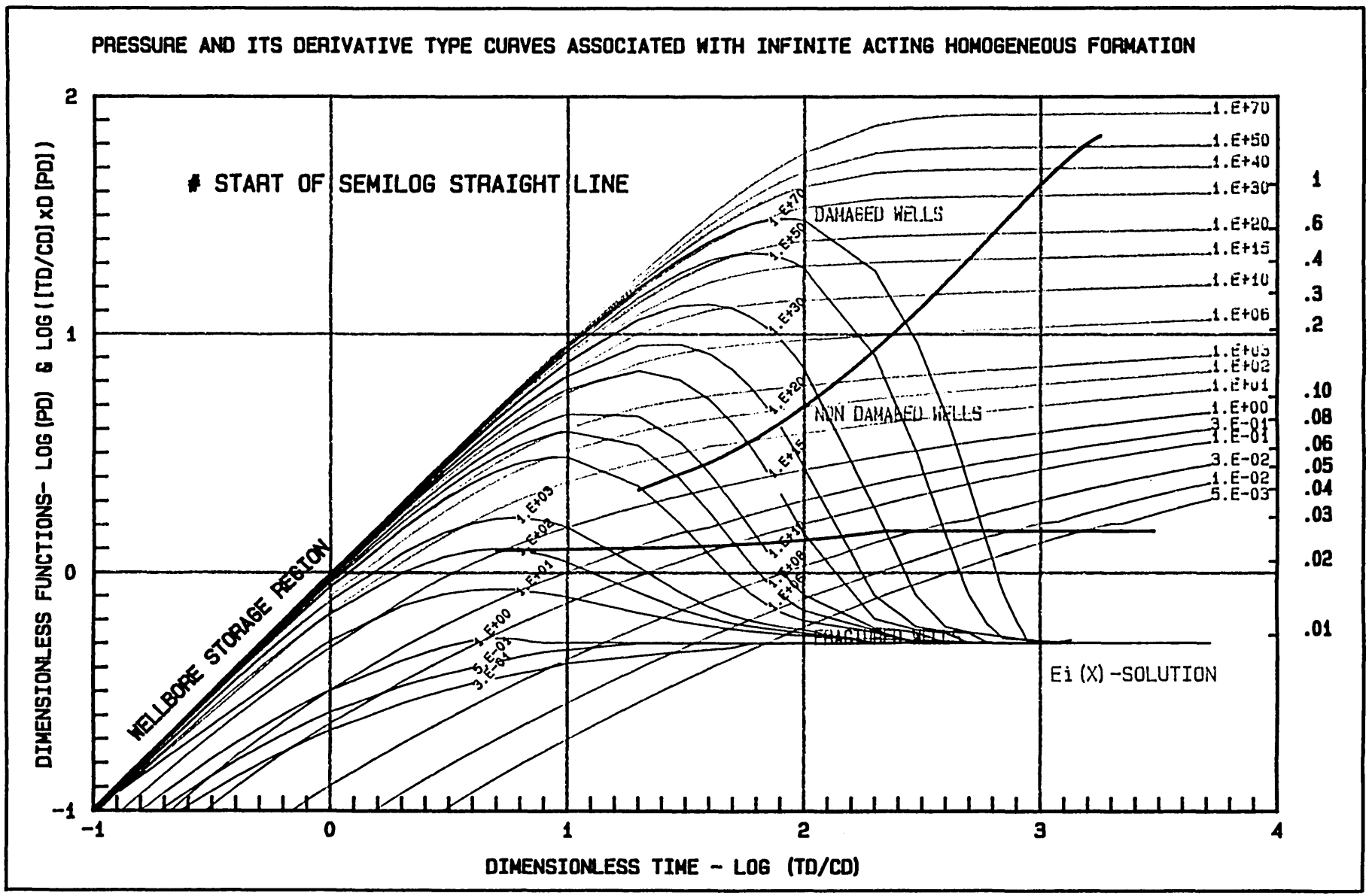



FIGURE 3.3: DIMENSIONLESS PRESSURE & DERIVATIVE RESPONSES OF INFINITE ACTING HOMOGENEOUS FORMATION WITH WBS & SKIN

B ➤ LEAST SQUARE POLYNOMIAL SCHEME

The scheme which is used to a lesser extend for the derivative plots of the recorded pressure data, has been implemented as a subroutine in the **TOPAZ** and is capable of handling four different types of polynomials. The operator specifies the desired testing model and point weighting associated with each pressure data, and the program fits up to 8th degree polynomial model through the points of interest, returning;

-The best model describing the data points.
-An indication of cumulative and average error.

. The four models used in the **(TOPAZ)** program are as follows:

-Type 1:

$$P = a+bT+cT^2+dT^3+... \quad \& \quad \frac{dP}{dT} = b+2cT+3dT^2+ ... \tag{3.10}$$

-Type 2 :

$$P = a\exp(bT+cT^2+dT^3+...) \quad \& \quad \frac{dP}{dT} = a\,(b+2cT+...)\exp(bT+cT^2+..) \tag{3.11}$$

-Type 3 :

$$Ln(P) = a+bLn(T)+c\{Ln(T)\}^2+ ... \quad \& \quad \frac{d\{Ln(P)\}}{dT} = \frac{b}{T} + \frac{2c}{T}Ln(T)+.. \tag{3.12}$$

-Type 4 :

$$P = a+bLn(T)+c\{Ln(T)\}^2+... \quad \& \quad \frac{dP}{dT} = \frac{b}{T}+\frac{2c}{T}Ln(T)+... \tag{3.13}$$

It is emphasized that the polynomial fitting technique does not always yield satisfactory results, since even a small average error generated by fitting a polynomial through the points of interest will almost certainly generate false pressure derivatives for small changes in pressure data of the order of 0.3 psi. This is particularly true during late times when noise effects are created by the derivative of the fitted polynomial model.

## 3.5-MATCHING PROCEDURES ON THE DERIVATIVE TYPE CURVES

In order to employ the pressure derivative type curves, the following steps should be taken.

-Differentiate pressure data as appropriate and plot the results as a function of time on a 5x3 log-log graph. Place the constant portion of the plot (exhibiting infinite acting radial flow) if present, on the 0.5 horizontal line and fix the pressure axis match in order to determine the permeability thickness of the formation.

$$kh = 141.2 \times q\mu B_o \left[\frac{DP_D}{\Delta P}\right]_{match} \quad \Rightarrow \quad DP_D \equiv \frac{T_D}{C_D}\left[\frac{dP_D}{d(T_D/C_D)}\right] \tag{3.14}$$

-Fix the time axis match by sliding the plot along the horizontal plane which corresponds to the scalar quantity 0.5 straight line until intermediate and possible wellbore storage pressure data are matched on one of the derivative type curves. Having obtained the best match, the value of wellbore storage can thus be determined.

$$C = 0.000295 \frac{Kh}{\mu}\left[\frac{\Delta T}{(T_D/C_D)}\right]_{match} \tag{3.15}$$

$$C_D = \frac{0.8936C}{\phi c_t h r_w^2} \tag{3.16}$$

-Identification of the specific type curve from the time axis match will then provide the value of the mechanical skin factor.

$$S = 0.5\,Ln\{\frac{C_D e^{2S}}{C_D}\} \tag{3.17}$$

★★★★★★★★★★

# CHAPTER 4

# CONVENTIONAL ANALYSIS OF HOMOGENEOUS FORMATION

## 4.1-CONVENTIONAL DRAWDOWN ANALYSIS OF HOMOGENEOUS FORMATIONS

The analysis of drawdown pressure data can be achieved from the constant terminal rate solutions of the diffusivity equation, corresponding to the rate and flowing bottom hole pressure variations during transient and pseudo steady state flow period[17,41].

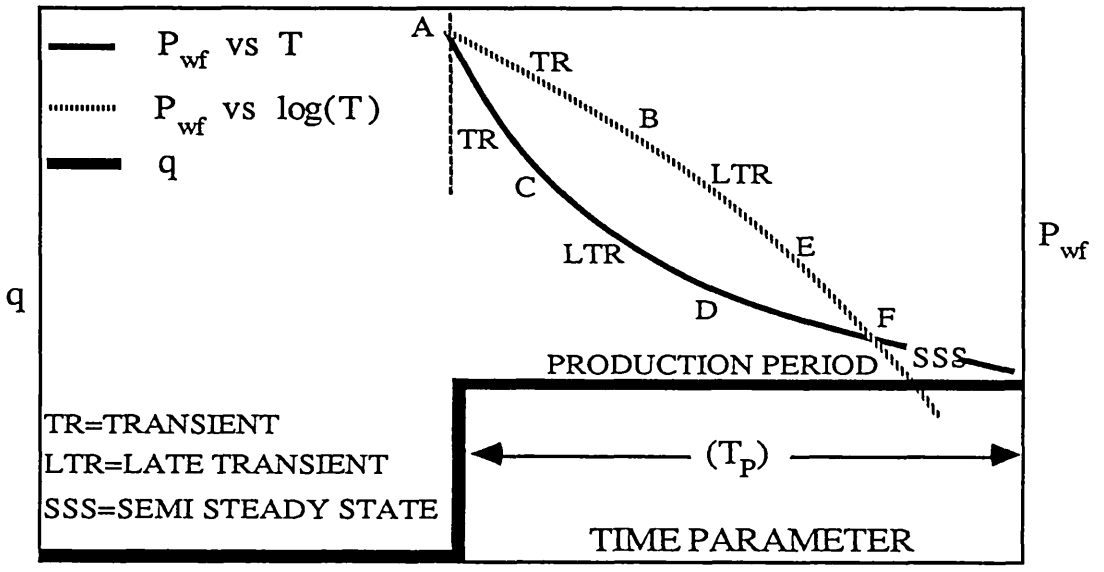



FIGURE 4.1: RATE & PRESSURE RESPONSES DURING AN IDEAL DRAWDOWN

### CASE A ➳ TRANSIENT FLOW CONDITION

The dimensionless pressure responses of homogeneous formations during transient flow periods maybe expressed by:

$$P_D(T_D) = \frac{1}{2}\,Ln\left(\frac{4T_D}{\gamma}\right) = 0.5\,Ln(T_D) + 0.4045 \qquad (4.1)$$

Definition of equation (4.1) in terms of real parameters yields:

$$P_{wf} = P_o^{TR} - m_{TR}\log(T) \quad \Rightarrow \quad m_{TR} = 162.6\,\frac{q\mu B_o}{Kh} \qquad (4.2)$$

$$P_0^{TR} = P_i - m_{TR}\left[\log\left(\frac{K}{\phi\mu c_t r_w^2}\right) - 3.23 + 0.869S\right] \quad (4.3)$$

With reference to equation (4.2), it is evident that the flowing bottom hole pressure is an inverse function of the logarithm of flowing times. Therefore, the identification of formation characteristics by means of transient flow expression necessitates the definition of the pressure and time recordings in the semilog plane (figure 4.2). Having refined the transient pressure data:

-The formation permeability is estimated from the slope of the semilog straight line defined by equation (4.2).
-The mechanical skin factor is obtained conventionally by extrapolating the semi log line to flowing times of one hour.

$$S = 1.151\left[\frac{P_i - P_{wf\text{-}1hour}}{m_{TR}} - \log\left(\frac{K}{\phi\mu c_t r_w^2}\right) + 3.23\right] \quad (4.4)$$

-The reservoir static pressure is then evaluated by implementing the estimated values of (K) and (S) into equation (4.3).

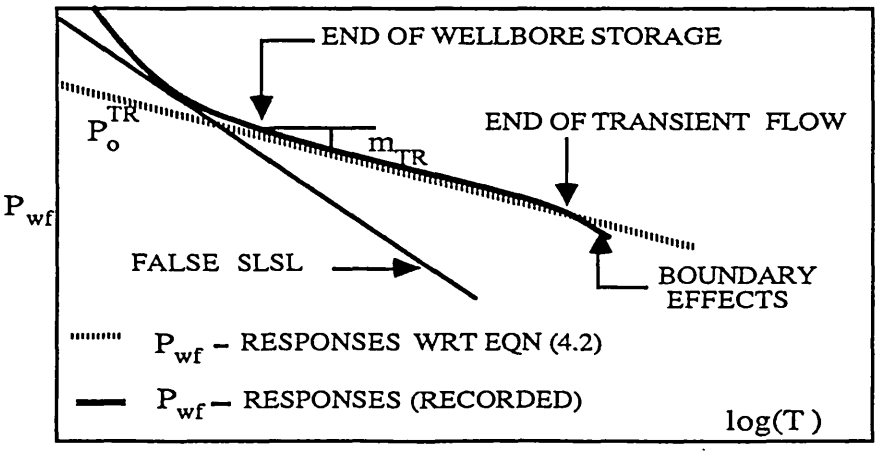



FIGURE 4.2: BHP RESPONSES DURING TRANSIENT FLOW PERIODS

A closer inspection of figure (4.2) reveals that the definition of semilog straight line through the recorded pressure data under the influence of wellbore storage is likely to lead to the incorrect determination of formation parameters. Such pressure responses,

however, can be identified and hence disregarded in the transient analysis by formulating the inner boundary condition of the homogeneous model.

$$1 - C_D \frac{dP_D}{dT_D} = \frac{q_s}{q} \tag{4.5}$$

Assuming that all production is contributed from the wellbore region (i.e. $q_s$=0), the integration solution of equation (4.5) in terms of logarithm yields:

$$\text{Log}\,(P_D) = \text{Log}(T_D) - \text{Log}(C_D) \tag{4.6}$$

Equation (4.6) indicates that as long as surface production rate is zero (i.e. wellbore storage flow), then a log-log plot of the dimensionless pressure and time functions would yield a straight line of slope unity (figure 4.3).

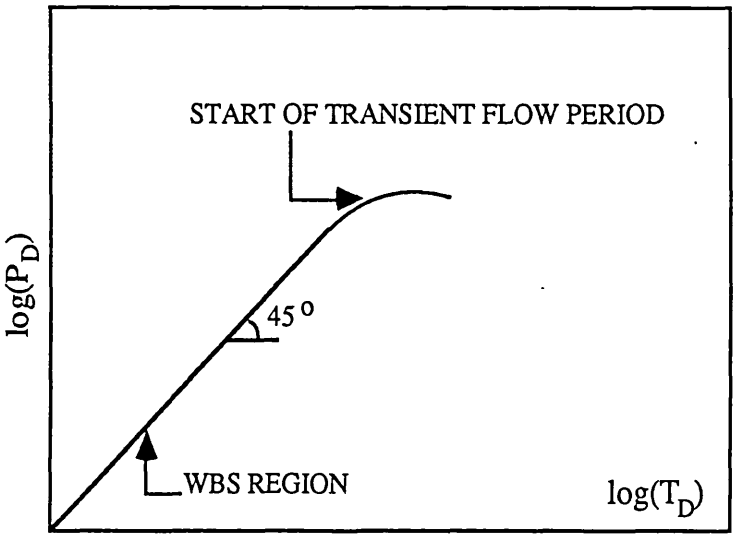



FIGURE 4.3: $P_D$ - RESPONSES DURING WELLBORE STORAGE FLOW PERIODS

From the above discussion, it is apparent that the log-log plot of recorded pressure data can be considered a powerful diagnostic well testing tool for identification of wellbore storage effects. Indeed, when used in conjunction with the conventional transient testing schemes, it provides a higher degree of confidence with regard to the definition of reservoir parameters.

CASE B ➳ SEMI STEADY STATE FLOW CONDITION

The dimensionless pressure responses during pseudo radial periods is defined by[60]:

$$P_D(T_D) = 0.5\ Ln(\frac{4A}{\gamma C_A r_w^2}) + 2\pi T_{DA} \tag{4.7}$$

Alternatively, equation (4.7) may be expressed as:

$$P_{wf} = P_o^{ss} - (\frac{0.2339qB_o}{\phi c_t hA}) \times T \tag{4.8}$$

$$\text{With} \quad P_o^{ss} = P_i - m_{TR}\left[\log(\frac{4A}{\gamma r_w^2}) - \log(C_A) + 0.869S\right] \tag{4.9}$$

Equation (4.8) implies that the flowing bottom hole pressure is a linear function of the flowing time. Thus, a cartesian plot of the recorded pressure/time data during such flow periods can provide a means of identifying formation characteristics such as drainage area, its configuration as well as the well location (figure 4.4).

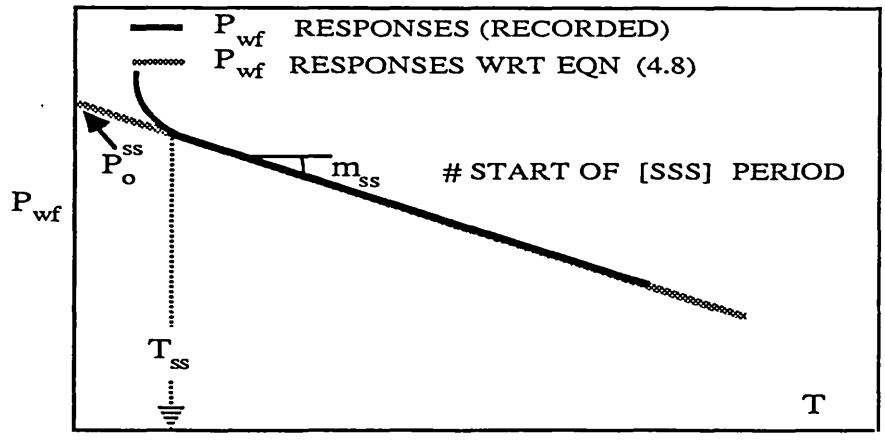



FIGURE 4.4: BHP RESPONSES DURING SEMI STEADY STATE FLOW PERIODS

-The reservoir drainage area can be determined from the slope of the cartesian straight line defined by:

$$A = -\frac{0.2339qB_o}{\phi c_t h m_{ss}} \tag{4.10}$$

-Provided the formation permeability and skin factor are pre-determined from transient flow segment of the draw down test, the Dietz shape factor can be estimated from the intercept of the straight line at flowing time of zero hour.

$$C_A = \text{Antilog}\left[\frac{P_o^{ss} - P_i}{m_{TR}} + \log\left(\frac{4A}{\gamma r_w^2}\right) + 0.869S\right] \quad (4.11)$$

-Having determined the formation shape factor, its configuration is then estimated by considering the dimensionless time parameter based on the drainage area (Appendix A):

$$T_{DA} = 0.1833 \frac{m_{ss}}{m_{TR}} T_{ss} \quad (4.12)$$

It is of prime importance to note that the basic assumption associated with the theoretical single rate draw down scheme which is rarely satisfied in practice is the maintenance of constant production rate throughout the duration of the test. Such restrictions, however, can be removed by taking into account the rate variations which may range from a series of increasing/ decreasing constant production to an uncontrolled variable rate[51].

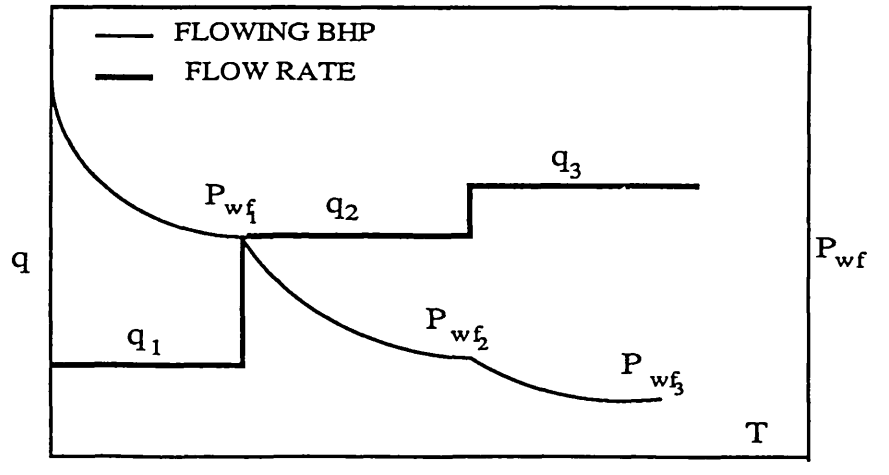



FIGURE 4.5: RATE & PRESSURE VARIATIONS WRT MULTI-RATE DRAWDOWN TEST

Assuming that the total duration of variable rate draw down scheme is short enough to ensure transient pressure responses at the testing well, then by means of superposition principle the general equation of the testing model can be expressed by:

$$\frac{P_i - P_{wf_N}}{q_N} = m_{MRD} \times MRD(q,T) + P_o^{MRD} \tag{4.13}$$

$$MRD(q,T) = \sum_{\alpha=1}^{N} \frac{\Delta q_\alpha}{q_N} \log(T_N - T_{\alpha-1}) \quad \& \quad m_{MRD} = 162.6 \frac{\mu B_o}{Kh} \tag{4.14}$$

$$P_o^{MRD} = m_{MRD} \left[ \log\left(\frac{K}{\phi \mu c_t r_w^2}\right) - 3.23 + 0.869S \right] \tag{4.15}$$

With reference to equation (4.13), the recorded pressure /time data, when plotted in terms of $(P_i-P_{wfN})/q_N$ vs MRD(q,T) in the cartesian plane, should result in a straight line whose slope and intercept are defined by equations (4.14) and (4.15) respectively. Having established the multi-rate straight line (figure 4.6), formation permeability is hence determined from equation (4.14) while the skin factor is estimated via equation (4.15).

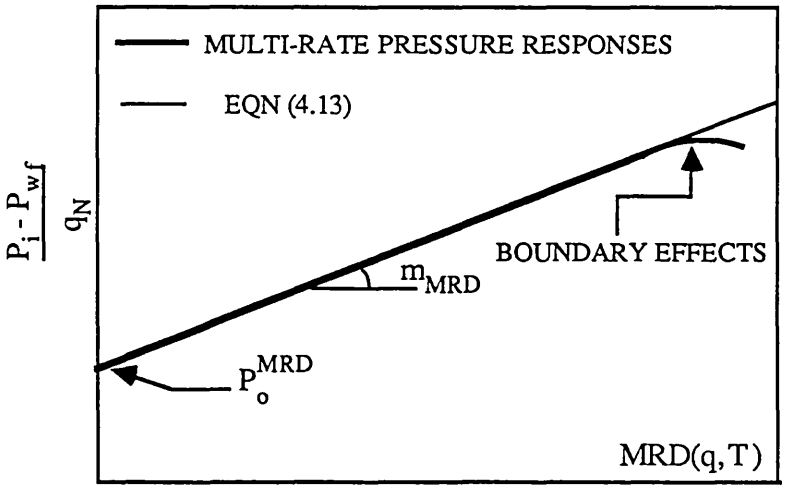



FIGURE 4.6: TYPICAL MULTI-RATE DRAWDOWN TEST PLOT

In view of the fact that the variable rate draw down is the generalized form of the single rate scheme, its application can be extended to reservoir limit testing (with less accuracy) in order to estimate the reservoir volume communicating with the well. Such an objective can be achieved by segregated plotting of the flowing bottom hole pressure and time responses which are specific to each flow periods, and then implementing the least square fitting technique to different segregated regions (figure

4.7). Having defined the best fit, the slope of the line is then used in equation (4.10) to estimate the formation drainage area.

$$A = -\frac{0.2339\,\bar{q}_N B_o}{m_{ss}\phi c_t h} \qquad (4.16)$$

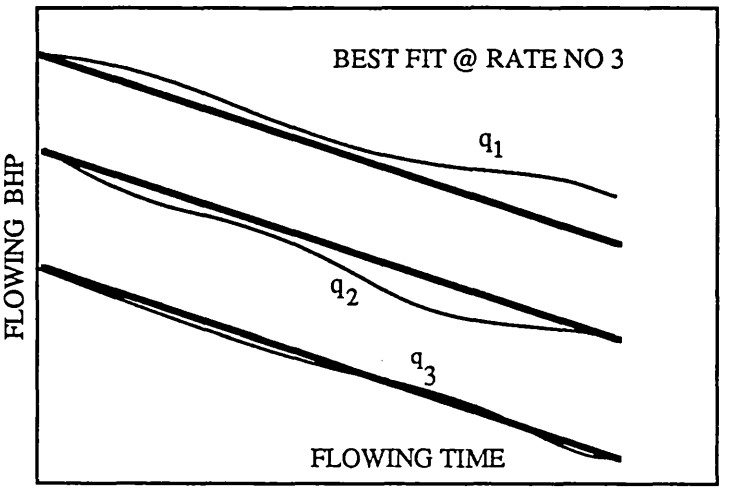



FIGURE 4.7: VARIABLE RATE RESERVOIR LIMIT TEST (HOMOGENEOUS MODEL)

The two rate test model[62] which is a simplified version of multi-rate drawdown schemes, is often used for characterization of the productive formations. In fact, the application of such a testing model to some tight formations requires transient pressure measurements periods of only 16 to 20 hours from the start of the final flow rate stabilization.

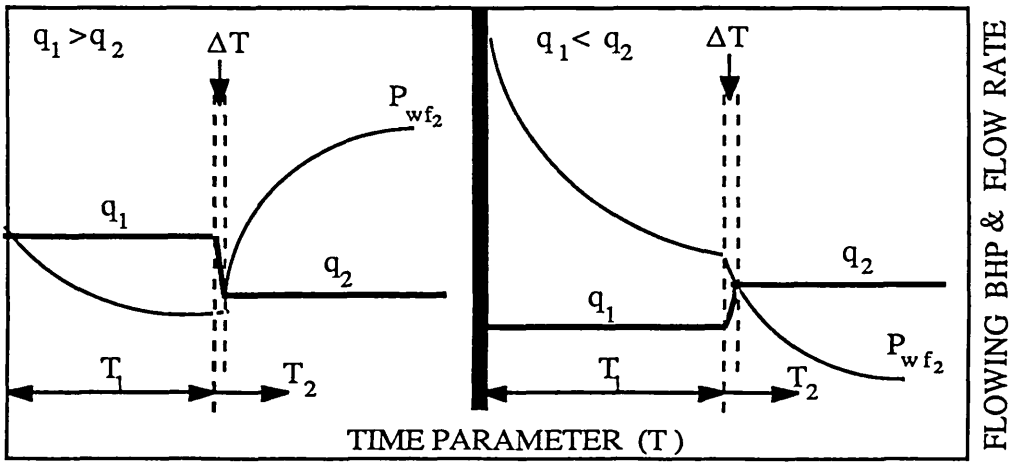



FIGURE 4.8: RATE AND PRESSURE RESPONSES DURING TWO RATE TEST

Ideally, the two rate flow test model is initiated by subjecting the testing well to a constant production for several days and then adjusting the choke at the well head in order to attain a new stabilized lower or higher rate. In mathematical terms, denoting the initial and final rate/pressure responses by subscripts (1) & (2) respectively, equation (4.14) for the case of two rate flow test is reduced to:

$$P_{wf_2} = P_o^{DR} - m_{DR} \times DR(T,q) \;\Rightarrow\; DR(T,q) = \log\left(\frac{T_1+T_2}{T_2}\right) + \frac{q_2}{q_1}\log(T_2) \qquad (4.17)$$

$$\text{With} \qquad m_{DR} = 162.6\frac{q_1 \mu B_o}{Kh} \qquad (4.18)$$

$$P_o^{DR} = P_i - m_{DR} \times \frac{q_2}{q_1}\left[\log\left(\frac{K}{\phi\mu c_t r_w^2}\right) - 3.23 + 0.869S\right] \qquad (4.19)$$

Equation (4.17) indicates that the flowing pressure responses during two rate scheme under transient flow condition is directly proportional to the Dual Rate time parameter DR(T,q), implying that a plot of observed flowing bottomhole pressure vs DR(T,q) in linear plane should yield a straight line with the slope given by equation (4.18) and the intercept defined by equation (4.19). It is hence evident that from such a plot :

-The formation permeability can be determined by considering the slope of the straight line through the transient segments of the recorded pressure data.

-The mechanical skin factor can be estimated by extrapolating the straight line to flowing times of one hour.

$$S = 1.151\left[\left(\frac{q_1}{q_1 - q_2}\right)\left\{\frac{P_{wf_{2\text{-}1\,hour}} - P_{wf(T_2=0)}}{m_{DR}}\right\} - \log\left(\frac{K}{\phi\mu c_t r_w^2}\right)\right] + 3.71 \qquad (4.20)$$

-The reservoir false pressure (P*) which is employed for estimating the average formation pressure, can hence be evaluated from the intercept of the cartesian line defined by equation (4.19).

-If desired, the magnitude of the pressure drop due to skin effects can also be determined during the initial and final flow rates.

$$\Delta P_{skin}^{q_1} = 0.869 m_{DR} \times S \quad \text{or} \quad \Delta P_{skin}^{q_2} = 0.869 m_{DR} \left(\frac{q_2}{q_1}\right) \times S \tag{4.20a}$$

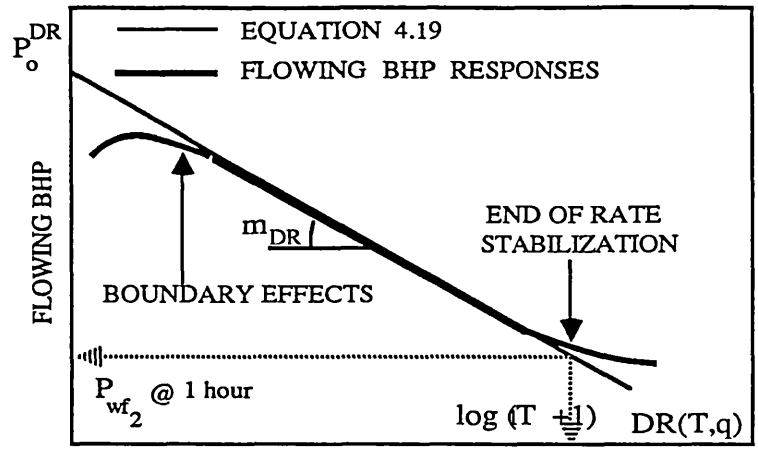



FIGURE 4.9: TYPICAL PRESSURE RESPONSES DURING A TWO RATE DRAWDOWN TEST

## 4.2-CONVENTIONAL BUILD UP ANALYSIS OF HOMOGENEOUS FORMATIONS

In view of the poor quality of flow rate measurements as well as the significant difficulty in maintaining stabilized rates throughout the duration of the draw down tests, the conventional build up schemes are often employed as an alternative tool in transient well test interpretations. Indeed such schemes when designed properly, would yield most of the required reservoir parameters.

In an ideal situation, the build up test requires the stabilization of flow rate prior to shut in and the monitoring of bottom hole pressure variations as a function of shut in time . Under such condition, the dimensionless build up pressure responses associated with the formation can be defined by means of superposition theorem (Appendix B).

$$P_i - P_{ws} = 141.2 \frac{q\mu B_o}{Kh} \{ P_D(T_p + \Delta T)_D - P_D(\Delta T_D) \} \tag{4.21}$$

Contrary to drawdown testing models, however, the absence of the mechanical skin factor from the theoretical build up expression indicates that the pressure drop due to formation damage / stimulation cannot be determined from the build up segment of the recorded pressure data. Instead, the objective is achieved by subtracting equation (4.21) from the dimensionless pressure function associated with the producing well.

$$S = 1.151\left[\frac{P_{ws} - P_{wf}}{m_{BU}} + \log\left(\frac{T_p + \Delta T}{T_p \Delta T}\right) - \log\left(\frac{K}{\phi \mu c_t r_w^2}\right) + 3.23\right] \qquad (4.22)$$

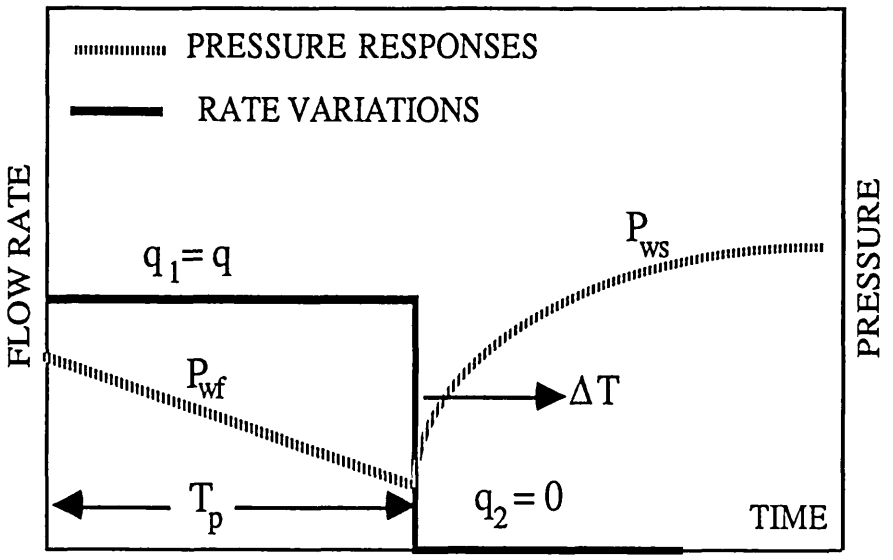



FIGURE 4.10: RATE AND PRESSURE RESPONSES DURING AN IDEAL BUILD UP TEST

## 4.3-HORNER BUILD UP SCHEME

Subject to transient flow assumption during production periods, the theoretical $(P_D)_{BU}$-function defined by equation (4.21) can be expressed by:

$$P_{ws} = P_i - m_{BU} \log\left(\frac{T_p + \Delta T}{\Delta T}\right) \quad \Rightarrow \quad m_{BU} = 162.6 \frac{q\mu B_o}{Kh} \qquad (4.23)$$

Referring to equation (4.23), the direct relationship between shut in pressure and Horner time $(T_p+\Delta T/\Delta T)$, indicates that a semilog plot of $P_{ws}$ vs $(T_p+\Delta T/\Delta T)$ should yield a semilog straight line with the slope $[m_{BU}]$ which can be solved explicitly for estimating the formation permeability. Having defined the formation permeability, the initial/average formation pressures (for short production times only) and the skin factor can then be estimated be extrapolating the semilog line to Horner time of zero and shut in time of one hour respectively.

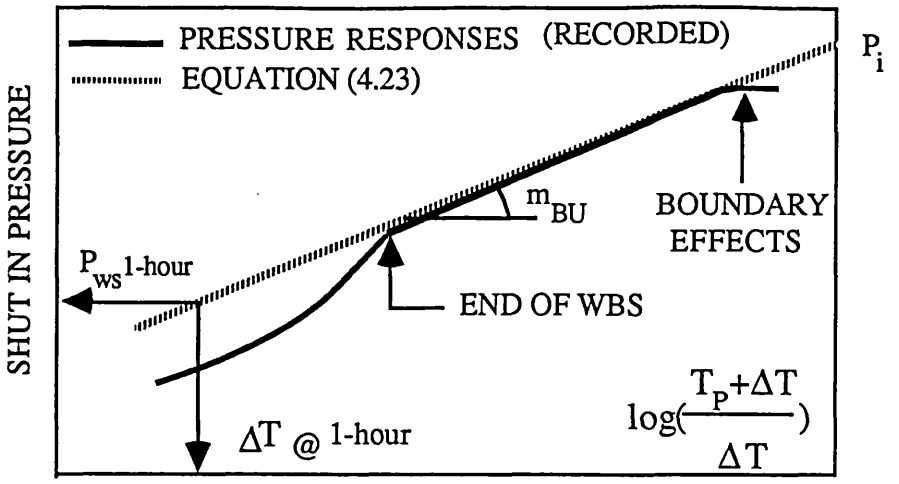



FIGURE 4.11: TYPICAL HORNER PLOT WRT HOMOGENEOUS FORMATIONS

$$S = 1.151\left[\frac{P_{ws\,(1\text{-hour})} - P_{wf}}{m_{BU}} - \log\left(\frac{K}{\phi\mu c_t r_w^2}\right) + \log\left(\frac{T_p+1}{T_p}\right) + 3.23\right] \tag{4.24}$$

At this stage, it is proper to note that the definition of [$T_p$] parameter is based on the cumulative production since the last pressure stabilization rather than on the total cumulative production form the formation (i.e. $T_p = 24 \times N_p/q$).

Strictly speaking, equation (4.23) is only valid for new wells with short production periods where the cumulative production prior to shut in could be considered negligible in comparison with the total recoverable reserves. For large producing times, the dimensionless pressure function $P_D(T_p)_D$ cannot be estimated by the transient solution, hence confining the application of build up analysis to infinite acting formations. Such restrictions, could be removed by introducing the concept of false pressure ($P^*$).

$$P_{ws} = P^* - m_{BU}\log\left(\frac{T_p+\Delta T}{\Delta T}\right) \tag{4.25}$$

$$P^* = P_i - 141.2\frac{q\mu B_o}{Kh}\left\{P_D(T_p)_D - 0.5\mathrm{Ln}\left(\frac{4(T_p)_D}{\gamma}\right)\right\} \tag{4.26}$$

$$P_D(T_p)_D = 2\pi T_{DA} + \frac{1}{2}\mathrm{Ln}\left(\frac{4(T_p)_D}{\gamma}\right) - \frac{1}{2}P_{D(MBH)}\,(T_{DA}) \tag{4.27}$$

$$P_{D(MBH)}\,(T_{DA}) = \frac{Kh}{70.6\,q\mu B_o}(P^* - \bar{P}) \tag{4.28}$$

The replacement of initial reservoir pressure by false pressure in equation(4.25) can be justified by considering the pressure build up variations of homogeneous formations during different producing times. Figure (4.12) suggests that whilst the definition of initial,average and false pressures responses during the early life of testing well can be considered to be identical, the degree of discrepancy among the three parameters, caused by the extended duration of production tend to invalidate such an equivalence. It is hence clear that the Horner equation would fail to define the average reservoir pressure which is vital in characterization of petroleum reservoirs. Fortunately, this parameter can be estimated from the MBH charts[44] which have been specifically designed for such purposes. The procedure requires:

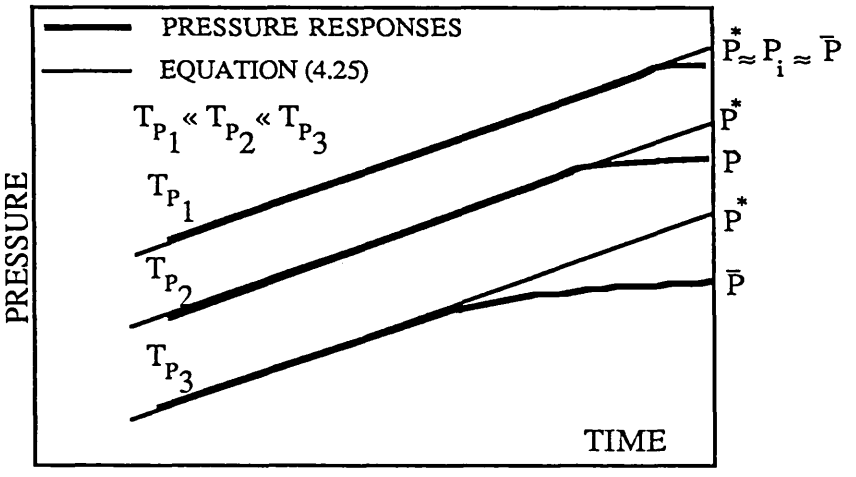



FIGURE 4.12: PRESSURE BUILD UP RESPONSES WRT PRODUCTION TIMES

-Estimation of the false reservoir pressure from equation (4.25).

-Pre-determination of the drainage area and the well location.

-Definition of the dimensionless time parameter as a function of drainage area.

$$T_{DA} = 0.000264 \frac{KT_p}{\phi \mu c_t A} \tag{4.29}$$

-Definition of $P_{DMBH}(T_{DA})$ with respect to $T_{DA}$ from available charts.

Following the preceding steps, it is hence possible to estimate the average reservoir pressure from equation (4.28).

$$\bar{P} = P^* - 70.6 \frac{q\mu B_o}{Kh} P_{D(MBH)}(T_{DA}) \qquad (4.30)$$

## 4.4-MILLER-DYES-HUTCHINSON BUILD UP TESTING MODEL

The pressure build up expression suggested by Miller,Dyes and Hutchinson[48] may be derived by implementation of the semi steady state flow assumption to equation (4.25).

$$P_{ws} = P_{(\Delta T=1)} + m_{BU} \log(\Delta T) \qquad (3.31)$$

$$\text{With} \quad P^* = P_{(\Delta T=1)} + m_{BU} \log(T_p + 1) \qquad (3.32)$$

Equation (3.31) indicates that the shut in pressure is directly related to the logarithm of the shut in time during transient flow periods. Therefore, having identified the wellbore storage and/or boundary effects, from the plot of the recorded pressure/time data in the semilog plane:

-The formation permeability thickness can be estimated from the slope of the semilog straight line defined by equation (4.23).

-The mechanical skin factor can be determined from equation (4.24).

-The extrapolated false pressure can be evaluated from the intercept of the semilog straight line at shut in time of one hour.

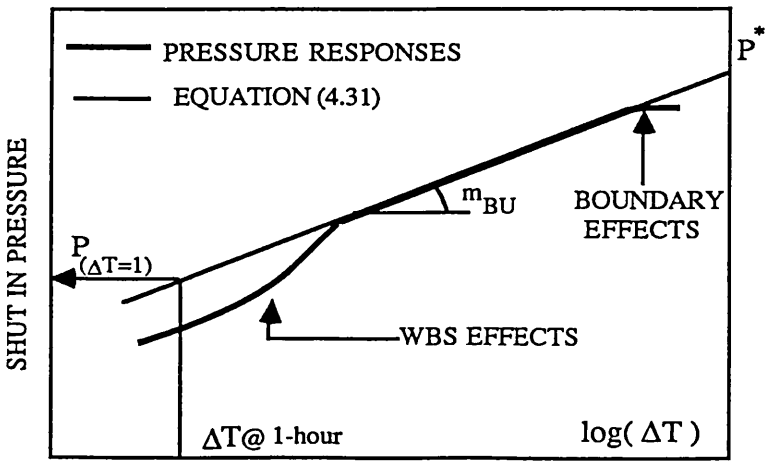



FIGURE 4.13: THE MDH PLOT FOR A TYPICAL BUILD UP TEST

-The average reservoir pressure which is a function of drainage area, can hence be established from equation (4.30).

From the direct comparison between the Horner and Miller,Dyes and Hutchinson build up plots, it can be observed that although the latter scheme requires less computation time, the definition of the semilog straight line through equation (3.32) is influenced by:

-The duration of production times, and
-The presence of wellbore storage and skin effects.

Whilst short producing times tend to reduce the possibility of reaching semi steady state flow periods prior to shut in, the presence of wellbore storage and skin tend to obscure the definition of the conventional semilog straight line. These effects which also influence the Horner testing method (to a lesser extend) must be taken into account, otherwise the implementation of build up tests to field data can lead to estimates of formation permeabilities that are too high.

As in the case of draw down methods, the application of build up tests can also be extended to wells with either short flow periods or significant rate variations prior to shut in[52]. The pressure responses of such testing schemes which are derived from the superposition principle may be expressed by:

$$P_{ws} = P_i - m_{BU} \times VR(T,q) \;\rightarrow\; VR(T,q) = \sum_{\alpha=1}^{N} \frac{q_\alpha}{q_N} \log\left(\frac{T_N - T_{\alpha-1} + \Delta T}{T_N - T_\alpha + \Delta T}\right) \qquad (4.33)$$

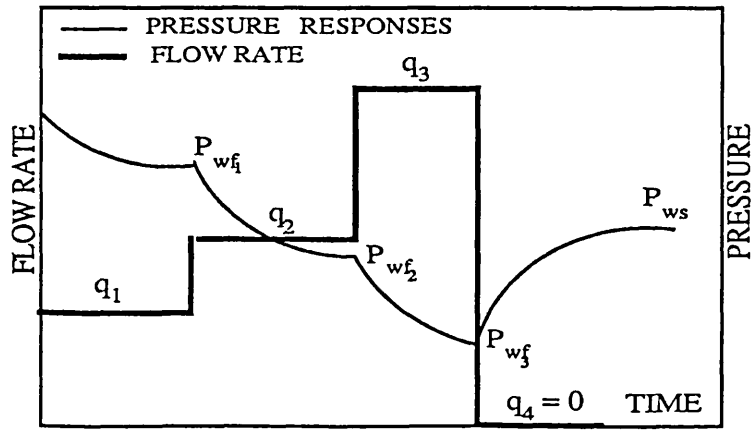



FIGURE 4.14: RATE & PRESSURE RESPONSES DURING MULTI-RATE BUILD UP TEST

Equation (4.33) indicates that the analysis of variable rate build up data requires the definition of the cartesian straight line from the linear plot of $P_{ws}$ vs VR(T,q). From such a plot (figure 4.15):

-The formation permeability can be estimated by considering the slope of the linear line defined by:

$$Kh = \frac{q_N \mu B_o}{m_{BU}} \tag{4.34}$$

-The skin factor can be determined from equation (4.24), with $[T_p]$ replaced by $(T_N - T_{N-1})$.

-The false pressure can be obtained by extrapolating the straight line to VR(T,q)=0 which is then employed for estimating the average reservoir pressure by means of equation (4.28).

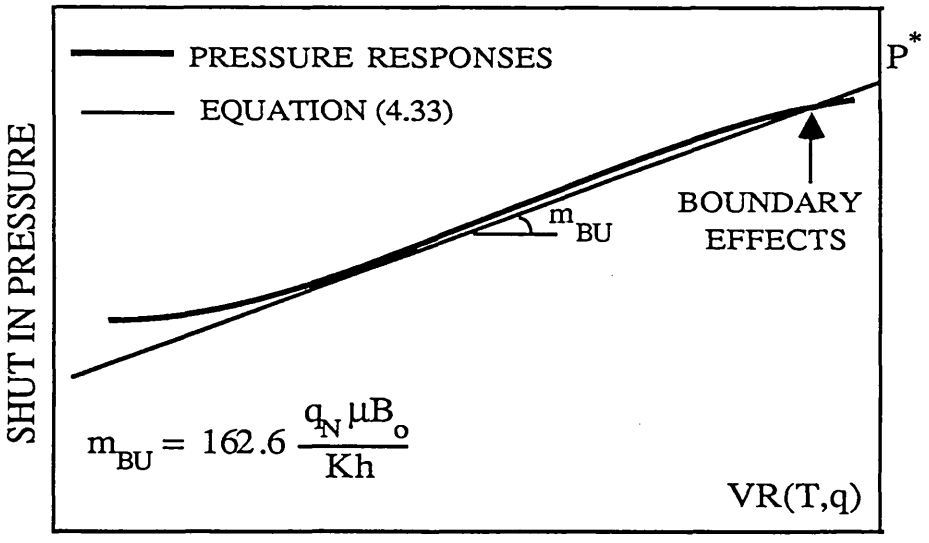



FIGURE 4.15: TYPICAL MULTI-RATE PRESSURE BUILD UP PLOT

## 4.5-RUSSELL'S BUILD UP TESTING MODEL

The basic testing model which is derived from the diffusivity equation for the case of infinite acting homogeneous formation, is mostly useful for analysing the build up pressure responses dominated by wellbore storage. The model assumes a well with stabilized production rate which is produced for a specific producing time and then shut

in at the top of the flow string while monitoring the build up pressure responses (figure 4.16). Assuming negligible phase segregation effects, the pressure responses during wellbore storage periods may be defined by:

$$P_{ws} - P_{wf} = m_{BU}\left[\frac{WB\times\Delta T-1}{WB\times\Delta T}\right]\times\left[\log(\Delta T)+\log\{\frac{5.88\times10^{-4}K}{(\phi c)_t\mu r_w^2}\}+0.869S\right] \quad (4.35)$$

$$\text{With} \quad WB = \frac{5.3\times10^{-4}Kh}{r_T^2\mu}\{\rho g+\frac{P_{wf}}{L}\} \quad (4.36)$$

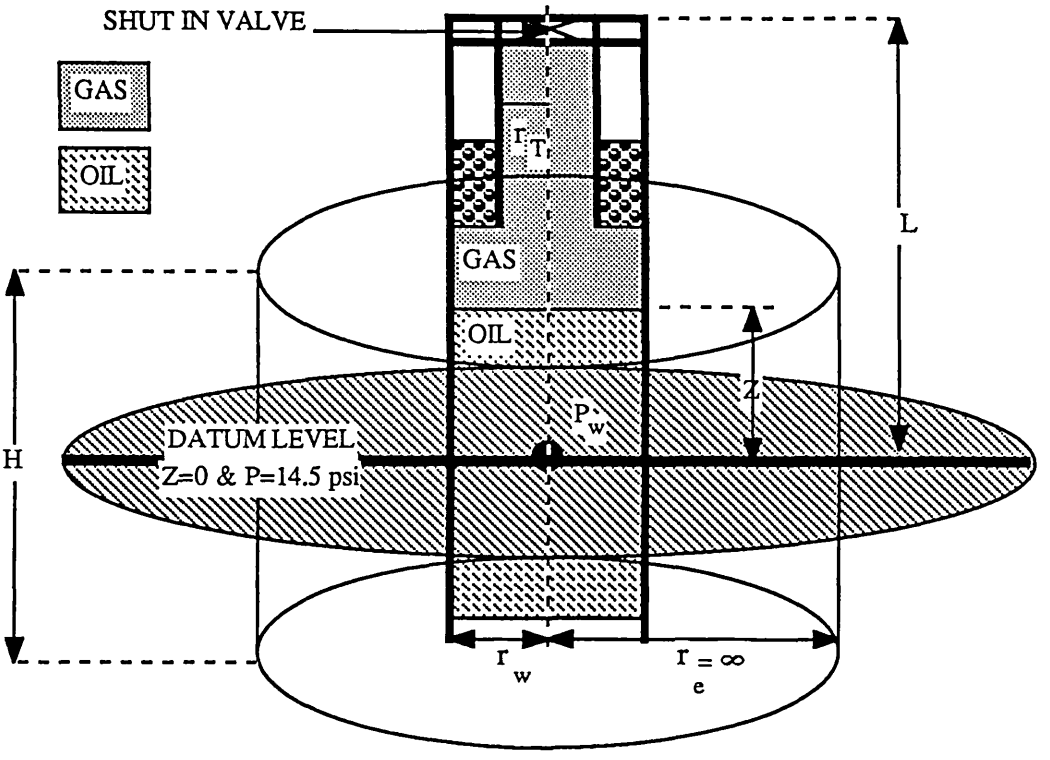



FIGURE 4.16: SCHEMATIC DIAGRAM OF WELL & FORMATION DURING BUILD UP TEST

Equation (4.35) indicates that a plot of $(P_{ws}-P_{wf})/(\{WB\Delta T-1\}/WB\Delta T)$ vs $\log(\Delta T)$ should result to the definition of the semilog straight line whose slope is a function of formation permeability and is defined by equation (4.23). In view of the dependence of wellbore parameter (WB) on permeability, however, the definition of the semilog line is performed on the trial and error basis (figure 4.17).

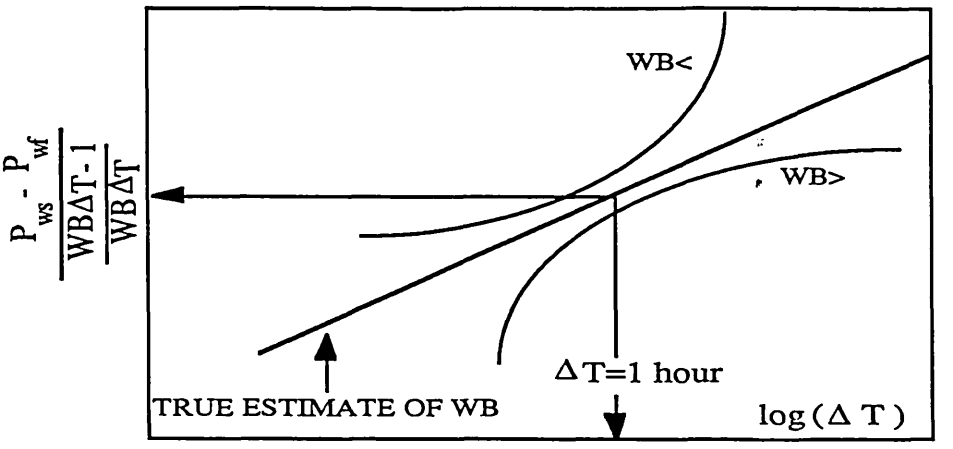



FIGURE 4.17: DETERMINATION OF WELLBORE PARAMETERS VIA RUSSELL'S MODEL

Once the correct value of wellbore parameter is determined,then:

-The permeability of the formation can be estimated from equation (4.23).

-The skin factor can be evaluated by extrapolating the correct semilog straight line to shut in time of one hour.

$$S = 1.151\left[\frac{\left[\frac{P_{ws} - P_{wf}}{(WB\Delta T-1)/WB\Delta T}\right]_{\Delta T=1}}{m_{BU}} - \log\{\frac{5.88\times10^{-4}K}{\phi c_t \mu r_w^2}\}\right] \qquad (4.37)$$

-Having defined the formation permeability and the wellbore condition, the false pressure can be obtained from:

$$P^* = P_{wf} + m_{BU}\left[\log(\frac{KT_p}{\phi\mu c_t r_w^2}) - 3.23 + 0.869S\right] \qquad (4.38)$$

-From the estimate of $P^*$, the average reservoir pressure can then be determined from equation (4.28).

★★★★★★★★★★

# CHAPTER 5

# NATURALLY FRACTURED FORMATIONS

## 5.1-PRESSURE RESPONSES ASSOCIATED WITH DUAL POROSITY FORMATIONS

Based on the following assumptions, the basic reservoir models representing the behaviour of naturally fractured medium[72] can be developed.

-The formation is radial and is bounded by two impermeable horizontal planes. Moreover, the formation is of infinite extent with uniform initial pressure and is produced at a constant rate.

-The model is made up of small rectangular cubes (i.e. matrix region, containing finer pores and high storage capacity) separated by an orthogonal network of fracture (i.e. Fissured region, possessing low storage capacity and high flowing capacity) reflecting dual porosity medium.

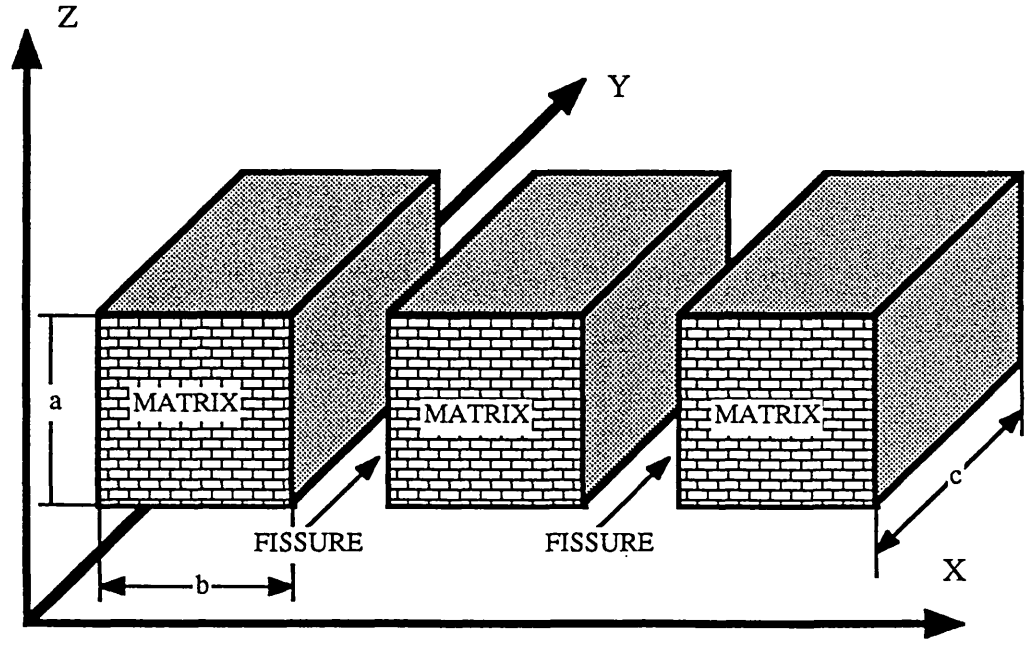



FIGURE 5.1: IDEALIZED MATRIX & FISSURE REGION OF FRACTURED NETWORK

-The pressure drop caused by fissure depletion could either be transmitted through the matrix instantaneously (i.e. semi steady state interporosity flow, SIF model), thus ensuring linear distribution of pressure within the formation or;

-may not be linearly distributed along the direction, normal to the fracture (i.e. transient interporosity flow, TIF model).

-Whilst the fissure system is the sole source of the fluid production of the well, the matrix feeds fluid into the fissure under restricted (SIF model) or unrestricted (TIF model) flow condition. Each point in the space is thus identified by two pressure points, namely pressure in the fissure region, and the pressure in the matrix region.

-The matrix and fissure permeabilities are considered constant such that $K_f > K_m$.

-The pore compressibilities in the matrix and fracture region are assumed to be independent of the local pressures (i.e. $c_m, c_f \neq F(P_m, P_f)$).

-The single phase Fluid within the formation possesses the following characteristics.

$$(\rho_{FL})_m = (\rho_{FL})_f \quad \& \quad (\mu,c)_{FL} \neq F(P_{RESERVOIR}) \tag{5.1}$$

$$u = \frac{K\rho_{FL}}{\mu_{FL}} \times \frac{d\Phi}{dr} \quad \succ \quad \frac{d\Phi}{dr} = \text{Potential gradient} \tag{5.2}$$

The general partial differential equation in the dimensionless form, describing the fluid flow through the dual porosity models in the presence of wellbore storage and skin is hence given by[10]:

$$\left(\frac{\partial^2 P_D}{\partial r_D^2}\right)_f + \frac{1}{r_D}\left(\frac{\partial P_D}{\partial r_D}\right)_f - (1-\omega)\left(\frac{\partial P_D}{\partial T_D}\right)_m = \omega\left(\frac{\partial P_D}{\partial T_D}\right)_f \tag{5.3}$$

$$\text{Where } \omega = \frac{(\phi V c_t)_f}{(\phi V c_t)_{f+m}} \quad \& \quad V = \frac{V_{(f \text{ or } m)}}{V_{f+m}} = \frac{\Sigma \text{ Fissure or matrix vol}}{\text{Bulk volume}} \tag{5.4}$$

## 5.2-PSEUDO STEADY STATE INTERPOROSITY FLOW MODEL (SIF)

With regard to the assumptions associated with the SIF model, namely uniformly spaced rectangular blocks separated by fractures and pseudo steady state interporosity flow from matrix to fissure region, The following expressions can be developed.

$$(1-\omega)\left(\frac{\partial P_D}{\partial T_D}\right)_m = \lambda\{(P_D)_f - (P_D)_m\} \tag{5.5}$$

$$\lambda = \alpha r_w^2 \frac{K_m}{K_f} \quad \succ \quad \alpha = \frac{4n\,(n+2)}{L^2} \tag{5.6}$$

| n | $\alpha$ | L | $L^2 = f(\lambda)$ | RESERVOIR CONFIGURATION |
|---|---|---|---|---|
| 1 | $12L^2$ | a | $\frac{12}{\lambda} r_w^2 K_m / K_f$ | MULTI-LAYERED |
| 2 | $32L^2$ | $2ab/(a+b)$ | $\frac{32}{\lambda} r_w^2 K_m / K_f$ | DUAL POROSITY |
| 3 | $60L^2$ | $\frac{3abc}{(ab+bc+ca)}$ | $\frac{60}{\lambda} r_w^2 K_m / K_f$ | DUAL POROSITY |

TABLE 5.2: FLOW DIRECTION THROUGH A FRACTURED FORMATION OF UNIFORMLY SPACED FRACTURES WITH DIFFERENT FRACTURE WIDTHS.

By implementing the following boundary conditions, the general solution of equation (5.3) was obtained in the Laplace space.

- $(P_D)_m = (P_D)_f = 0$ @ $T_D = 0$ for all values of $r_D = \frac{r}{r_w}$

- Limit $(P_D)_f = 0$ for $T_D > 0$

  $r_D \rightarrow \infty$

$$-C_D\left(\frac{dP_D}{dT_D}\right)_{r_D=1} = \left(\frac{d\Delta P_D}{dr_D}\right)_{r_D=1}$$

$$-(\Delta P_D)_{r_D=1} = \left\{ \Delta P_D - S\left(\frac{d\Delta P_D}{dr_D}\right) \right\}_{r_D=1}$$

$$\therefore \bar{P}_D(g) = \frac{K_o(\sqrt{gF(g)}) + S\sqrt{gF(g)}\, K_1(\sqrt{gF(g)})}{g\left[\sqrt{gF(g)}\, K_1(\sqrt{gF(g)}) + g(C_D)_{f+m}\{K_o(\sqrt{gF(g)}) + S\sqrt{gF(g)}\, K_1(\sqrt{gF(g)})\}\right]} \tag{5.7}$$

g = Laplace operator based on $(T_D)_{f+m}$ parameter

$$(T_D)_{f+m} = \frac{0.000264\, K_f T}{(\phi Vc_t)_{f+m} \mu r_w^2} \quad \succ \quad (C_D)_{f+m} = \frac{0.8936\, C}{(\phi Vc_t)_{f+m} hr_w^2} \tag{5.8}$$

By conversion of the Laplace operator [g], to $a=gx(C_D)_{f+m}$, equation (5.7) can be approximated by:

$$\bar{P}_D(a) = \frac{1}{a\left[a + \{Ln\frac{2}{\gamma\sqrt{aF(a)/(C_D e^{2S})_{f+m}}}\}^{-1}\right]} \tag{5.9}$$

With a = Laplace operator based on the parameter $(T_D/C_D)_{f+m}$

$$F(a) = \frac{\omega(1-\omega)a + \lambda(C_D)_{f+m}}{(1-\omega)a + \lambda(C_D)_{f+m}} \tag{5.10}$$

With reference to equations (5.9) and (5.10), two additional reservoir parameters are thus required to describe the dual porosity behaviour of the model (i.e. the storage capacity ratio[$\omega$], and the interporosity flow coefficient[$\lambda$]). Equation (5.9) which formed the bases of development of the type curves of figure (5.3), was evaluated via numerical models during early and late time flow periods, and analytical models during intermediate times.

-During early times, when only the fissure system contributes to the production.

$$\lim_{a \to \infty} F(a) = \frac{a[\omega(1-\omega) + \frac{\lambda(C_D)_{f+m}}{a}]}{a[(1-\omega) + \frac{\lambda(C_D)_{f+m}}{a}]} = \omega \tag{5.11}$$

Equation (5.9) can hence be defined as:

$$\bar{P}_D(a) = \frac{1}{a\left[a + \{Ln\frac{2}{\gamma\sqrt{a\omega/(C_D e^{2S})_{f+m}}}\}^{-1}\right]} \tag{5.12}$$

With reference to equations (5.4) and (5.8):

$$(C_D)_f = \frac{0.8936\ C}{(\phi Vc_t)_f\ hr_w^2} \quad \& \quad \omega = \frac{(\phi Vc_t)_f}{(\phi Vc_t)_{f+m}} = \frac{(C_D)_{f+m}}{(C_D)_f} \tag{5.13}$$

Substitution of equation (5.13) into equation (5.12) yields:

$$\overline{P}_D(a) = \frac{1}{a\left[a + \{Ln\frac{2}{\gamma\sqrt{a/(C_D e^{2S})_f}}\}^{-1}\right]} \tag{5.14}$$

a = Laplace operator based on the parameter $(T_D/C_D)_f$

-During late times, when the production comes from the total system (i.e. fissure + matrix systems):

$$F(a) = \frac{\lambda(C_D)_{f+m}}{\lambda(C_D)_{f+m}} = 1 \qquad a \rightarrow 0 \tag{5.15}$$

Equation (5.9) is hence reduced to:

$$\overline{P}_D(a) = \frac{1}{a\left[a + \{Ln\frac{2}{\gamma\sqrt{a/(C_D e^{2S})_{f+m}}}\}^{-1}\right]} \tag{5.16}$$

a = Laplace operator based on the parameter $(T_D/C_D)_{f+m}$

-During intermediate times, when matrix starts to feed fluid into the fissure:

$$F(a) = \frac{\lambda(C_D)_{f+m}}{S} \quad \text{provided} \quad \lambda \ll a \gg \omega \tag{5.17}$$

Equation (5.9) hence yields:

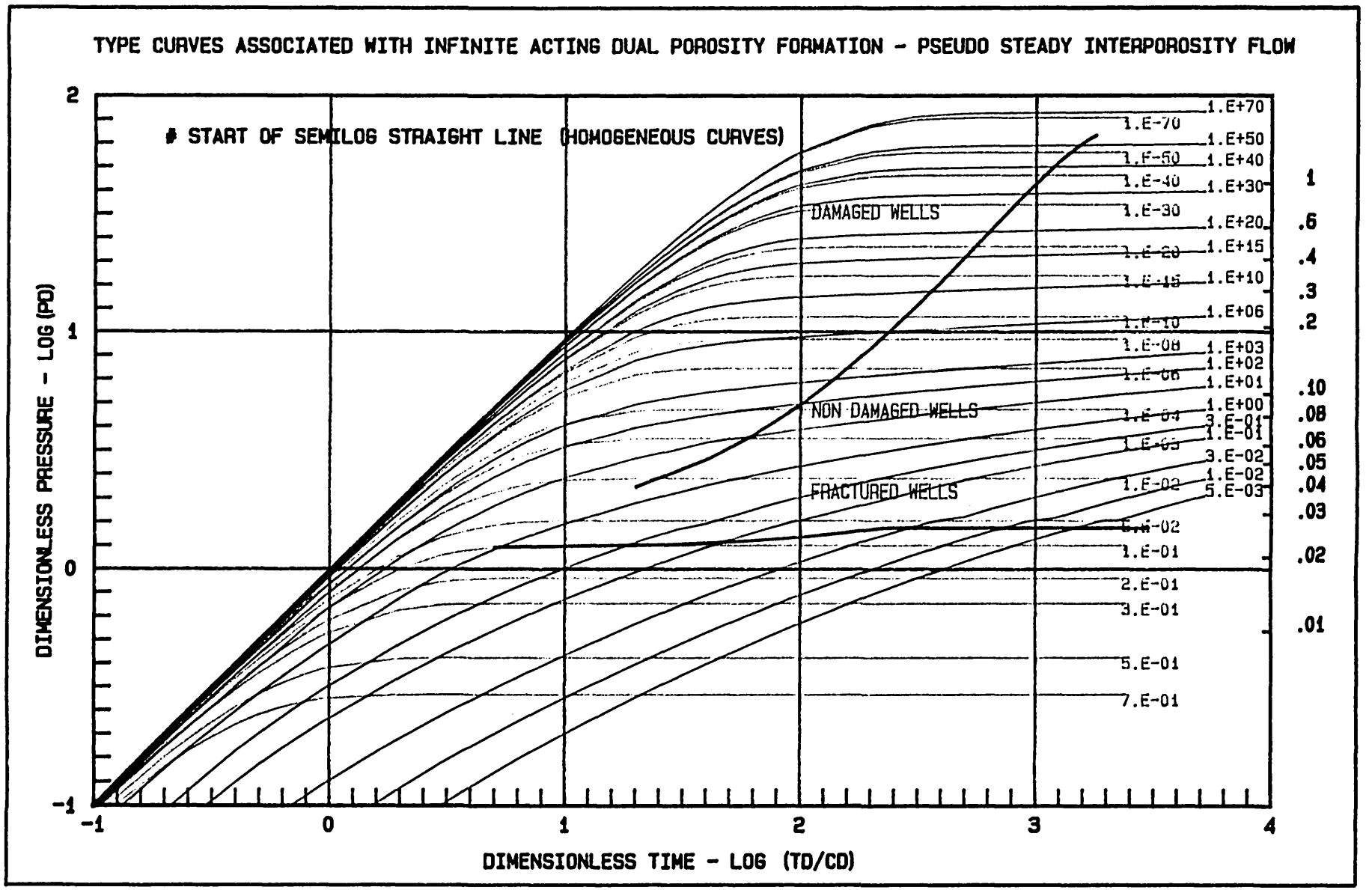



FIGURE 5.3: DIMENSIONLESS PRESSURE RESPONSES OF INFINITE ACTING DUAL POROSITY FORMATION WITH WBS & S (SIF MODEL)

$$\bar{P}_D(a) = \frac{1}{a\left[a + \left\{\ln\frac{2}{\gamma\sqrt{\lambda e^{-2S}}}\right\}^{-1}\right]} \qquad (5.18)$$

Inversion of equation (5.18) from the Laplace space to real space generates:

$$P_D\left(\frac{T_D}{C_D}\right) = LNT \times \left\{1 - \exp\left(-\frac{T_D C_D}{LNT}\right)\right\} \quad \text{with} \quad LNT = \frac{2}{\gamma\sqrt{\lambda e^{-2S}}} \qquad (5.19)$$

Based on the fact that equations (5.14) and (5.16) have the same format as the dimensionless pressure behaviour of a well with wellbore storage and skin, in an infinite acting homogeneous reservoir, type curves of figure (5.3) were generated by superimposing the draw down type curves of figure (3.1) with the set of type curves, evaluated analytically by means of the equation (5.19) which describes the responses of the dual porosity model during transition periods.

Due to the difference in the definition of dimensionless wellbore storage in equations (5.14) and (5.16), however, two distinct values of the $P_D$-functions corresponding the $(P_D)_f$ and $(P_D)_{f+m}$ were required in order to describe the full pressure variations of the system during early and late time flow periods.

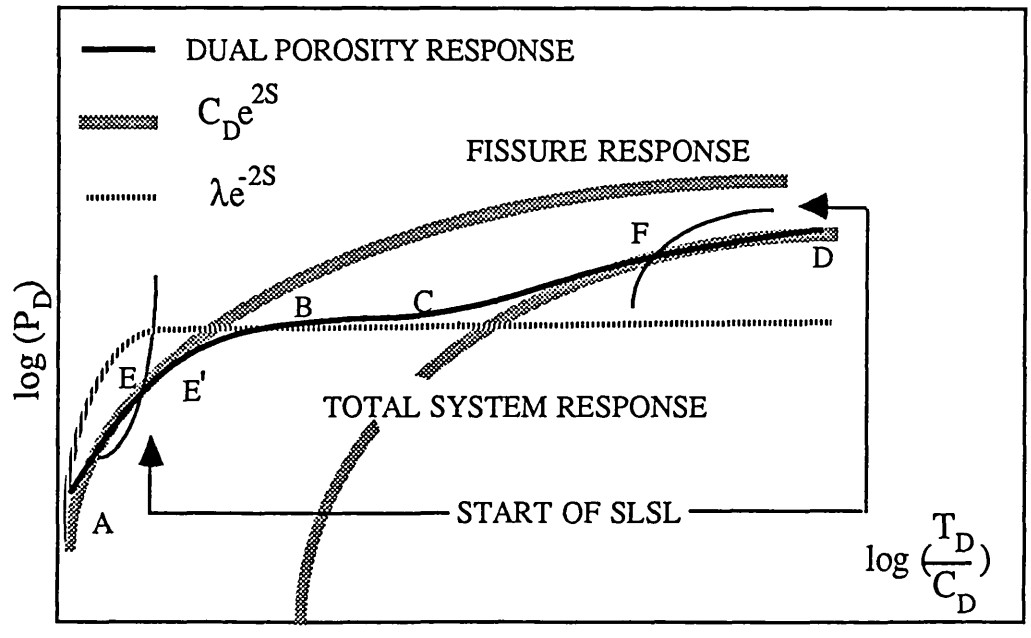



FIGURE 5.4: PRESSURE BEHAVIOUR OF A DUAL POROSITY FORMATION WITH PSEUDO STEADY STATE INTERPOROSITY FLOW FROM MATRIX TO FISSURE.

With reference to figure (5.4), during the early time flow periods (A-B), due to the high permeability contrast between fissure and matrix, only the fissure system contributes to the surface production, therefore the pressure drop in the fissure follows on of the homogeneous type curves characterized by $(C_De^{2S})_f$ group. When the pressure drop in the fissure reaches a threshold value, the matrix begins to feed fluid into the fissure, hence pressure responses stabilize and follow one of the transition related type curves labelled in terms of $[\lambda e^{-2S}]$ group (i.e. segment B-C). Eventually, the pressure drop between the matrix and the fissure stabilizes, causing the pressure responses to follow yet another homogeneous type curve (reflecting the entire system's contributions to the surface production(segment C-D), but at a lower ranges of $(C_De^{2S})_{f+m}$ group.

It is pointed out that the presence of the two semilog straight lines corresponding to $(C_De^{2S})_f$ and $(C_De^{2S})_{f+m}$ which are identified when radial flow prevails during early and late times (E-E' & F-D segments in figure 5.4), can only be observed under favourable conditions. Moreover, the first semilog straight line in general is masked by wellbore storage flow which in turn limits the use of conventional analysis, applicable to the test data. Such anomalies, emphasize the usefulness of the new set of type curves of figure (5.3) for extracting information even in the absence of the semilog line.

## 5.3-PRESSURE RESPONSES OF SIF MODEL DURING DRAWDOWN TESTS

Although an ideal draw down test associated with the dual porosity model would define the nature of the formation by considering the pressure changes during early, intermediate and late time flow periods, in practice however, two limiting cases with respect to the model, which are frequently encountered in the field, only allow certain segments of the complete dual porosity responses to be identified, thus limiting the characterizations of the formation.

Case I: When $(\phi Vc_t)_f < (\phi Vc_t)_{f+m}$, the pressure responses of the formation during early times coincide with the transition curves resulting to underestimated $(C_De^{2S})_f$.

$$\omega = \frac{(C_De^{2S})_{f+m}}{(C_De^{2S})_{f\text{-}min}} \qquad \text{where} \quad (C_De^{2S})_{f\text{-}min} = \text{minimum value of } (C_De^{2S})_f$$

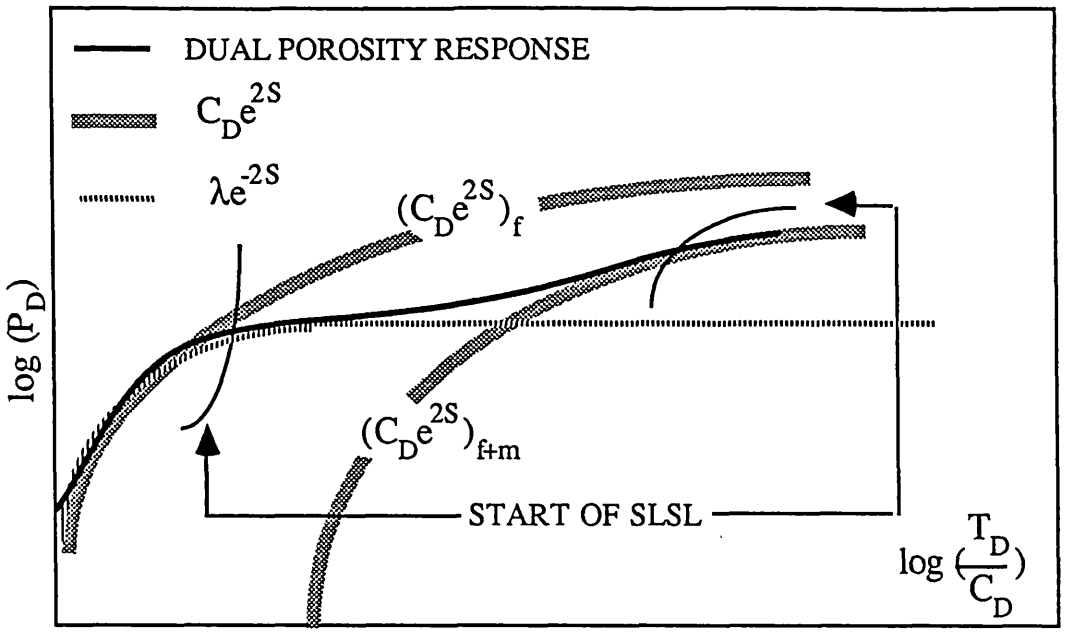



FIGURE 5.5: PRESSURE RESPONSES OF DUAL POROSITY FORMATION $[(\phi Vc_t)_f<(\phi Vc_t)_{f+m}]$

Case II: When the matrix blocks are small in size and the well is fractured, the early and intermediate flow periods are not visible and the only match available corresponds to the pressure responses during the late times. Under these conditions, when the formation acts as if it was a homogeneous model, the determination of the interporosity flow parameter becomes impossible.

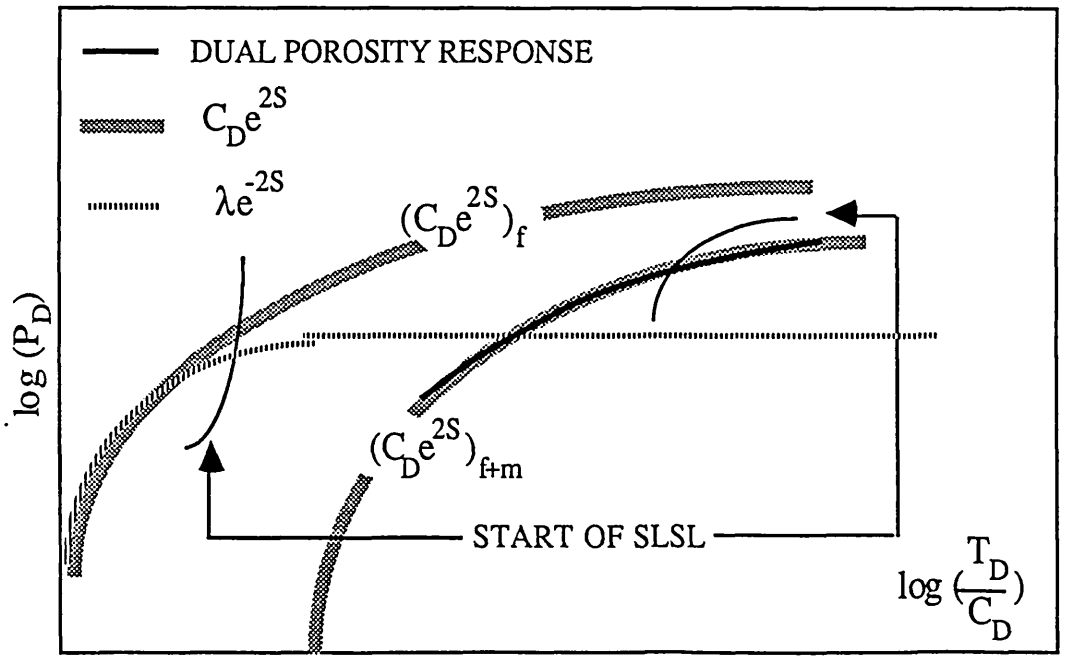



FIGURE 5.6: PRESSURE RESPONSES OF DUAL POROSITY FORMATION (SMALL MATRIX BLOCKS)

## 5.4-PRESSURE RESPONSES OF THE SIF MODEL DURING BUILD UP TESTS

As outlined in the previous sections, build up and draw down type curves become identical provided either the shut in time is small compared to production duration prior to shut in, or the $P_D(\Delta T_D)$- function exhibits small variation over long periods.

Due to the significance of producing times on the build up type curves, a tolerance level of 5% between the dimensionless pressures during drawdown and build up responses was employed in order to define the vertical time axis in figure (5.3). This scale in turn, served as an operator reference for checking the validity of testing build up pressure data by means of the type curves associated with the [SIF] fractured model.

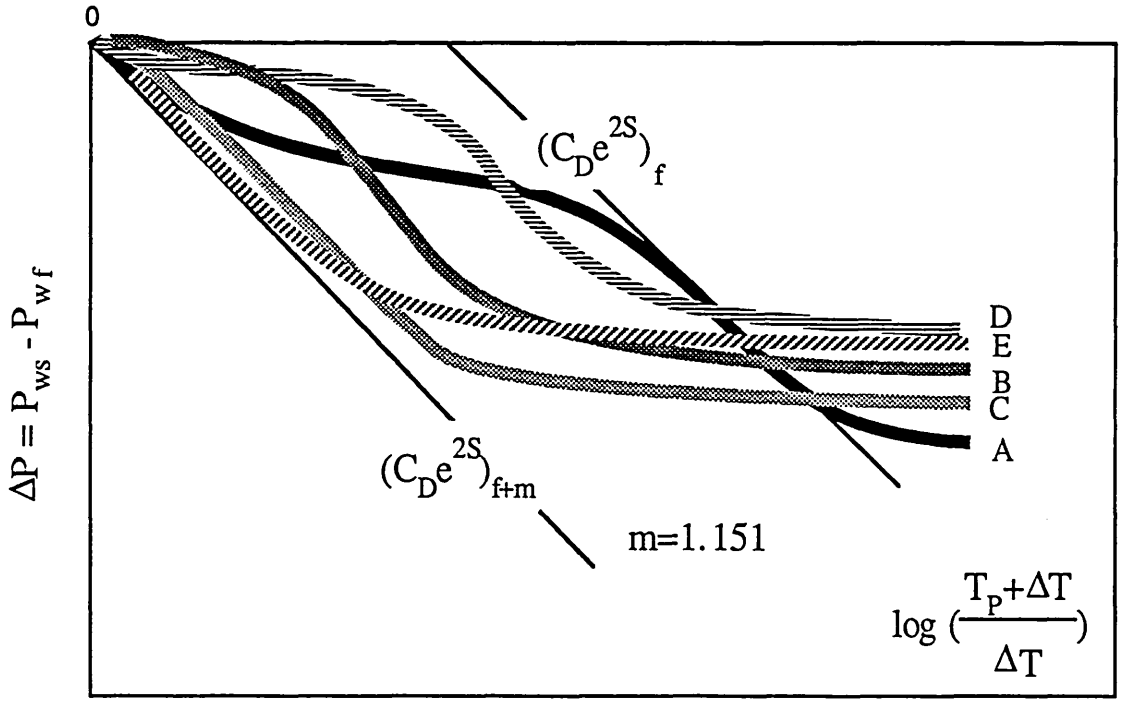



FIGURE 5.7: BUILD UP PRESSURE RESPONSE OF DUAL POROSITY FORMATION FOR FOUR DISTINCT PRODUCTION PERIODS.

Figure (5.7) which represents five typical build up pressure responses, frequently encountered in practice, indicates that the duration of the production time is even more important in the case of fractured formations since it would affect the interpretation of the formation parameters significantly (figure 5.8 to 5.12).

**Case A:** Build up section Coincides on $(C_De^{2S})_{f+m}$ type curve.

**Test duration:** Long enough to ensure the contribution of the total system to surface production.

**Description:** Using the dual porosity model type curves (figure 5.3), all reservoir and well parameters can be defined.

**specialized plot:** generates $K_fh$, S, $P^*=P_i$. The definitions of interporosity flow parameter [$\lambda$] and storage capacity ratio [$\omega$] requires the presence of the two semilog straight line (lines A-B and C-D in figure 5.8).

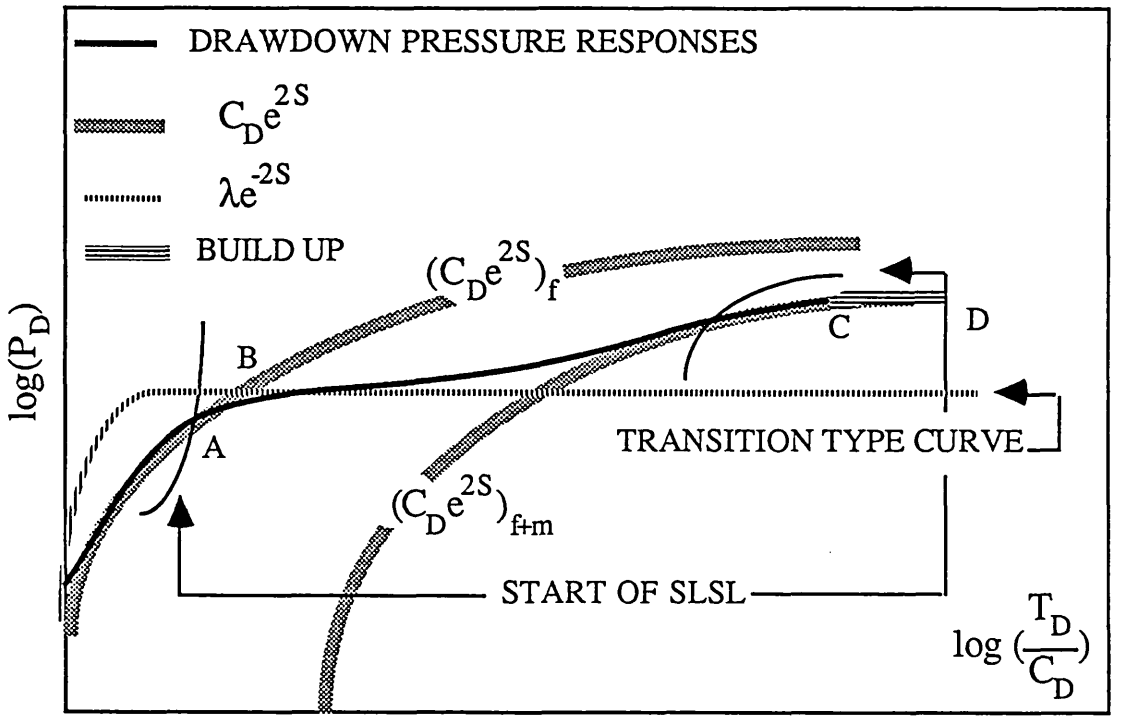



FIGURE 5.8: PRESSURE RESPONSES OF SIF MODEL (TOTAL SYSTEM IS DEFINED-CASE A)

Case B: The build up section is Parallel to [$\lambda e^{-2S}$] type curves.

**Test duration:** Draw down segment of the test only allows the production from the fissure zone.

**Description:** The transition curve is not detected which in turn prevents the detection of the dual porosity nature of the formation.

**Specialized plot:** Only applicable when the semilog straight line during fissure flow is present. Under such condition $K_fh$, S, and $P^*$ may be evaluated.

**Comment:** The numerical values of formation permeability thickness, wellbore storage

coefficient and mechanical skin factor may be obtained by employing the infinite acting homogeneous reservoir type curves of figure (5.3). Assuming the formation represents the [SIF] model, [$\lambda_{max}$] can be defined by the transition curve intersecting the $(C_De^{2S})_f$ type curve.

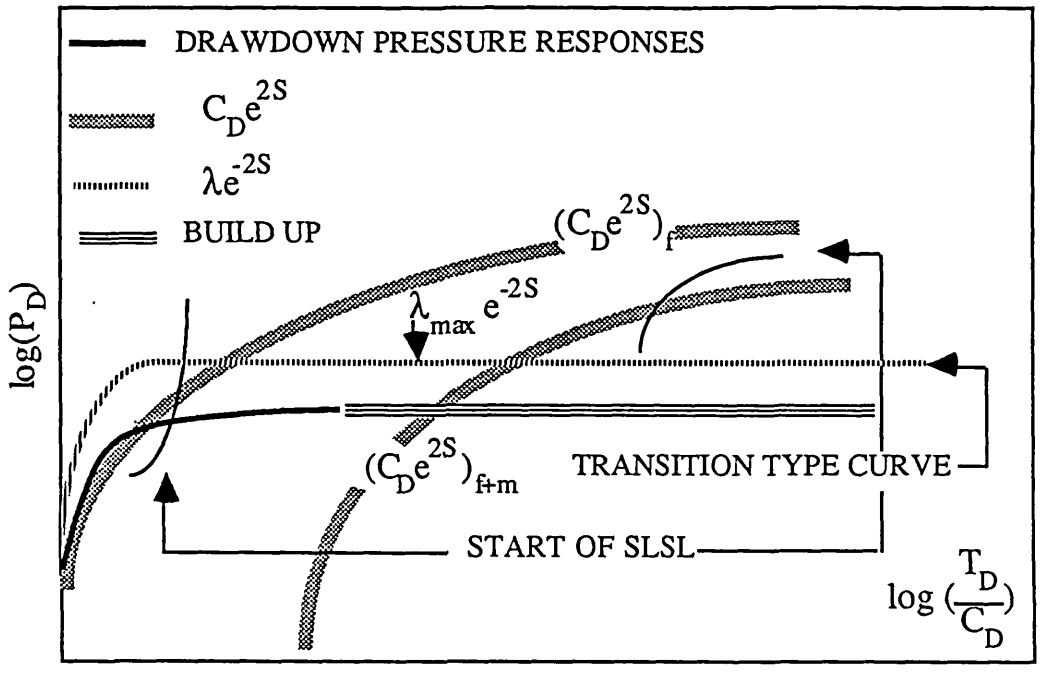



FIGURE 5.9: PRESSURE RESPONSES OF THE SIF MODEL (CASE B)

<u>Case C:</u> The Build up section Starts from the fissure region and then becomes parallel to transitional type curves(i.e. flattens like a constant pressure boundary).

**Description:** the total system responses characterized by the $(C_De^{2S})_{f+m}$ group is not detected (Regardless of the duration of build up test).Although most of the reservoir parameters can be identified, the value of [$\lambda_{max}$], corresponding to transitional type curve above the build up section, can only be estimated.

**Specialized plot:** Precautions must be taken when the slope of the build up section is considered for analysing the recorded pressure data, since due to the absence of the total system responses, the choice of incorrect straight line would yield false values of [S] and [$P^*$] parameters. On the other hand, The formation permeability and the storage capacity ratio can be estimated with a reasonable accuracy.

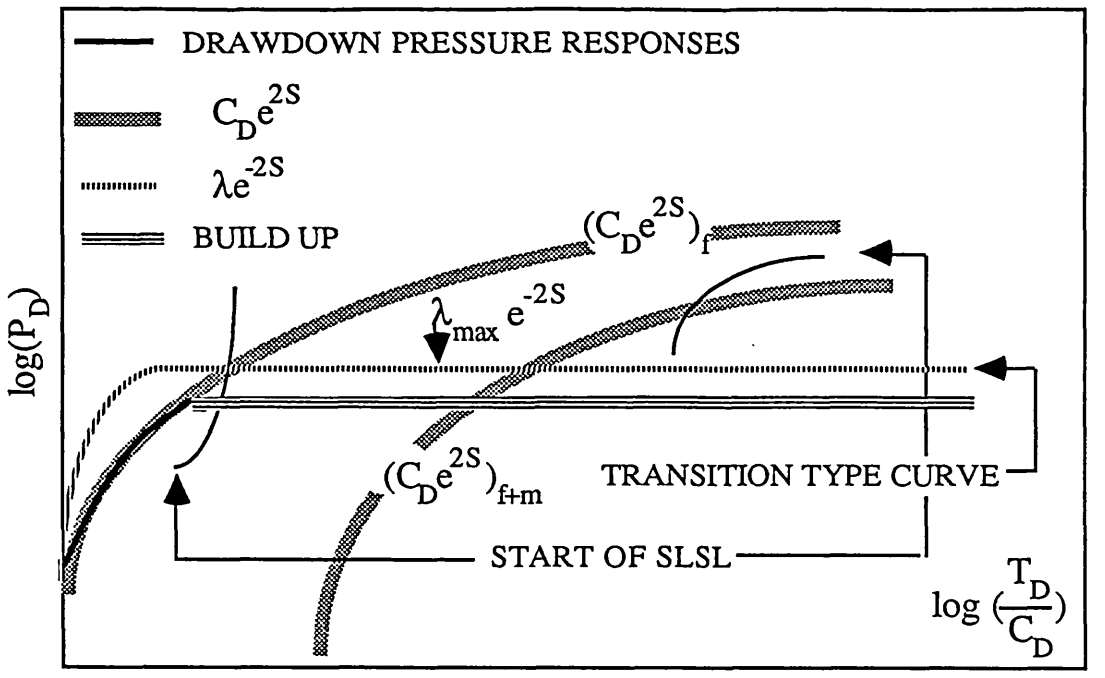



FIGURE 5.10: PRESSURE RESPONSES OF THE SIF MODEL (CASE C)

Case D: The Build up section is Coincident on the transitional type curves.

**Test duration:** Production is terminated during transition period.

**Description:** Identical procedures used for the analysis of the pressure responses in the test case C, may be employed in order to investigate the physical nature of the formation.

**Comment:** The value of $[\lambda_{max}]$ may be defined by considering the build up pressure responses corresponding to $(C_De^{2S})_{f+m}$ type curves which pass through the last recorded pressure point. $[\lambda_{max}]$ may also be obtained by means of conventional schemes, provided that fissure responses corresponding to $(C_De^{2S})_f$ type curves can be identified Under such condition:

$$\omega_{max} = \text{antilog}\left((\bar{P} - P_f^*)/m\right) \qquad (5.20)$$

(N.B. In practice, due to the short duration of build up tests, the total system responses may not be observed)

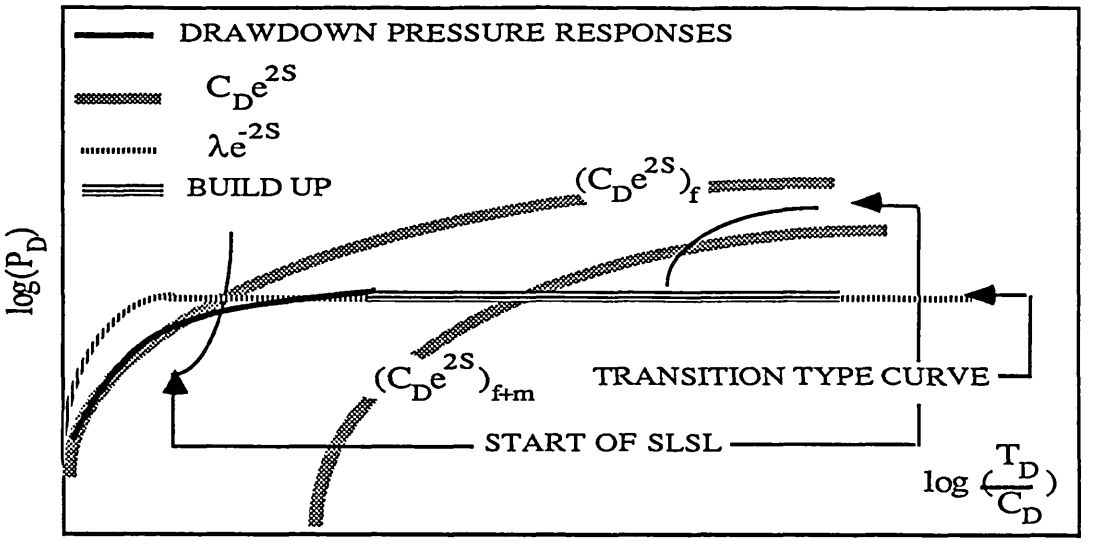



FIGURE 5.11: PRESSURE RESPONSES OF THE SIF MODEL (CASE D)

**Case E:** The Build up section is Parallel to transitional responses and starts on the $(C_De^{2S})_{f+m}$ type curves.

**Test duration:** Production is terminated just before the detection of pressure variations of the total system.

**Description:** The determination of reservoir parameters requires similar procedures as in the case D. However, Unique values of [ω] and [λ] can be obtained by considering the pressure responses during fissure/matrix and transitional periods.

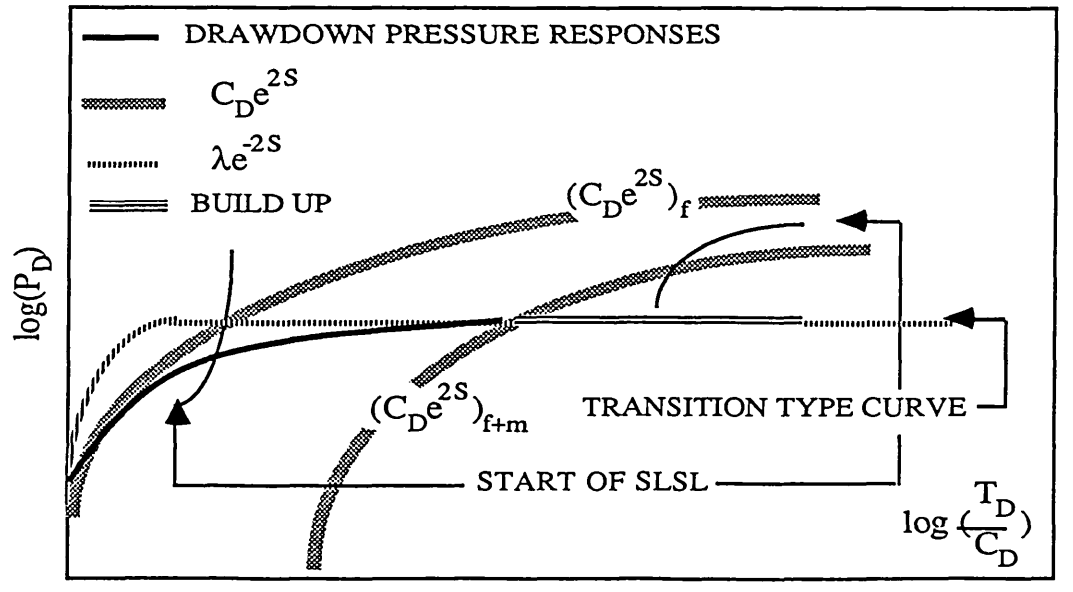



FIGURE 5.12: PRESSURE RESPONSES OF THE SIF MODEL (CASE E)

## 5.5-DEFINITION OF THE PETROPHYSICAL PARAMETERS OF THE SIF MODEL

-A plot of log(ΔP=Pressure change) vs log(ΔT=Elapsed time) is made on a 5x3 log-log paper and then overlaid on the type curves of figure (5.3) until the three regional curves corresponding to the three flow regimes (if present) are identified. Having fixed the match;

-The fissure permeability thickness and wellbore storage constant are obtained from the pressure and time axis match respectively (using identical technique employed for the case of infinite acting homogeneous model).

-Mechanical skin factor is obtained from:

$$S = 0.5\ \mathrm{Ln}\left(\frac{C_D e^{2S}}{C_D}\right)_f = 0.5\ \mathrm{Ln}\left(\frac{C_D e^{2S}}{C_D}\right)_{f+m} \qquad (5.21)$$

-The formation storage capacity ratio is determined from equation (5.13).

-Finally, the interporosity flow coefficient is evaluated from:

$$\lambda = \frac{CON}{e^{-2S}} \qquad (5.22)$$

Where [CON] represents the matched value of $[\lambda e^{-2S}]$ group and corresponds to the transitional type curves of figure (5.3).

## 5.6-TRANSIENT INTERPOROSITY FLOW MODEL (TIF)

One of the predominant features of a dual porosity system with pseudo steady state interporosity flow at the matrix/fracture interface is the presence of two parallel straight lines which are developed during radial flow state of the fissure and total system responses. Such a model, however, which disregards the matrix storage capacitance by allowing an instantaneous pressure drop throughout the matrix during the initial production period,does not account for the presence of a possible 3rd semilog straight line during transition periods. Hence it is evident that a dual porosity model which would describe the specific pressure responses during transition periods should

be developed. The gradient flow model which assumes zero interporosity skin and is commonly referred to as Transient Interporosity Flow [TIF] model is an ideal type which is capable of describing such pressure responses .

Whilst the [SIF] model is capable of describing the pressure variations of a naturally fractured reservoir, where the flow of fluid is only subjected to the gravitational forces (i.e. constant pressure gradient), due to the domination of the fluid expansion forces on the flow, the TIF model takes into account the distribution of pressure gradients via linear diffusion process by assuming:

-Matrix pressure [$P_f$] is not linearly distributed along the direction, normal to the fracture plane.

-The degree of communication between matrix and fissure is subject to the matrix permeability as well as the matrix storage capacity.

Figure (5.13) represents the pressure responses of the gradient flow model which develops the three semilog straight lines under favourable conditions.

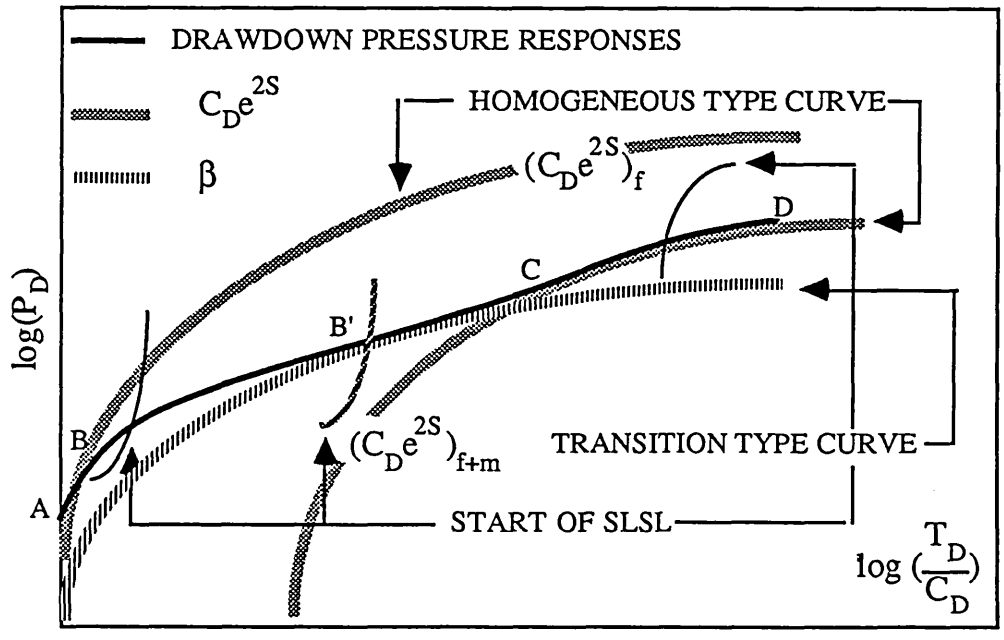



FIGURE 5.13: PRESSURE RESPONSES OF THE TIF MODEL (TRANSIENT INTERPOROSITY FLOW)

With reference to figure (5.13), the dimensionless pressure patterns represented by AB,B'C and CD segments can be summarized as follows:

-During early times, the dimensionless well pressure coincides with one of the fissure type curves, representing the compressible fracture responses to the well production (segment AB).

-At intermediate periods, the matrix region begins to feed fluid into the fracture under unrestricted flow condition and hence coincides with one of the transition type curves which are defined in terms of [β] parameter (segment B'C).

-At late times, as the pressures of the matrix and fissure regions stabilize, the pressure responses follow the appropriate fissure+matrix type curve, reflecting the total responses of the dual porosity system (segment CD).

Assuming that radial flow has been reached during fissure, transition and total system flow periods, a semilog plot of pressure vs time would then generate the three semilog straight lines with the following property (figure 5.13) :

$$\left[\frac{d(\Delta P)}{d[\log(T)]}\right]_f = \left[\frac{d(\Delta P)}{d[\log(T)]}\right]_{f+m} = 2\left[\frac{d(\Delta P)}{d[\log(T)]}\right]_\beta \qquad (5.23)$$

In order to establish the full pressure responses of the [TIF] model, the differential equations associated with the matrix and fissure regions were defined as:

$$\left(\frac{\partial^2 P_D}{\partial z_D^2}\right)_m = \xi \left(\frac{\partial P_D}{\partial T_D}\right)_m \quad \text{with} \quad \xi = \frac{3(1-\omega)}{\lambda\omega} \qquad (5.24)$$

$$\frac{1}{r_D}\frac{\partial}{\partial r_D}\left(r_D\left\{\frac{\partial P_D}{\partial r_D}\right\}_f\right) - \xi\left(\frac{\partial P_D}{\partial z_D}\right)_m = \left(\frac{\partial P_D}{\partial T_D}\right)_f \qquad (5.25)$$

Taking the effects of wellbore storage and skin into account, equation (5.25) was subjected to the following initial boundary conditions.

Fluid flow through the matrix region:

- $(P_D)_m = 0$ @ $T_D = 0$ for all values of $r_D$
- $(P_D)_m = (P_D)_f$ @ matrix / fracture interface
- $(\partial P_D/\partial r_D)_{r_D=1} = 0$ @ $T_D = 0$

Fluid flow through the fissure region:

$-(P_D)_f = 0 \quad @ \quad T_D = 0$

$-\lim_{r_D \to \infty} (P_D)_f = 0$

$-r_D (\partial P_D / \partial r_D)_f = -1 \quad @ \quad r_D = 1$

Based on the proceeding boundary status, the matrix pressure was first related to the fracture pressure via the solution of equations (5.24) and (5.25), and then the resulting expression describing the dimensionless pressure responses associated with the [TIF] model was approximated by:

$$\overline{P}_D(g) = \frac{1}{g\left[ g + \left\{ \mathrm{Ln}\left[ \frac{2}{\gamma \sqrt{gR^n(g)/(C_D e^{2S})_{f+m}}} \right] \right\}^{-1} \right]} \tag{5.26}$$

In order to produce $P_D$-functions associated with the [TIF] model which could be useful in practical terms, two simple matrix block geometries[19,65] were also investigated in conjunction with equation (5.26).

Based on the matrix block geometries(figure 5.14), the Laplace space solutions of equation (5.26) were hence generated during early, intermediate and late times.

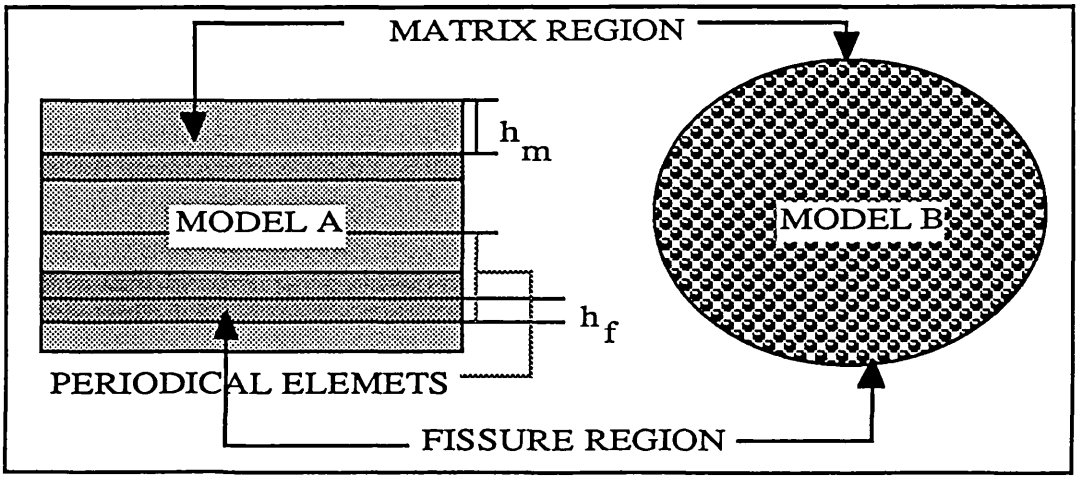



FIGURE 5.14: SCHEMATIC DIAGRAM OF THE MATRIX BLOCK GEOMETRIES ASSOCIATED WITH THE TIF MODEL (MODEL A: HORIZONTAL SLAB, MODEL B: SPHERICAL).

During early flow periods:

$$\underset{g\to\infty}{R^{a}(g)} = \omega + \sqrt{\lambda C_D\left(\frac{1-\omega}{3g}\right)}\left\{\operatorname{Tanh}\sqrt{\frac{3(1-\omega)g}{\lambda C_D}}\right\} \approx \omega \tag{5.27}$$

$$\underset{g\to\infty}{R^{b}(g)} = \omega + \frac{\lambda C_D}{5g}\left\{\sqrt{\frac{15(1-\omega)g}{\lambda C_D}}\operatorname{Tanh}\left\{\sqrt{\frac{15(1-\omega)g}{\lambda C_D}}\right\}^{-1} - 1\right\} \approx \omega \tag{5.28}$$

$$\omega = \frac{(C_D e^{2S})_{f+m}}{(C_D e^{2S})_{f}} \quad \Rightarrow \quad \bar{P}_D(g) = \frac{1}{g\left[g + \operatorname{Ln}\left\{\frac{2}{\gamma\sqrt{g/(C_D e^{2S})_f}}\right\}^{-1}\right]} \tag{5.29}$$

During intermediate flow periods:

$$R^{a}(g) = \sqrt{\frac{\lambda C_D}{3g}} \quad \& \quad R^{b}(g) = \sqrt{\frac{3\lambda C_D}{5g}} \tag{5.30}$$

$$\therefore \quad 2\bar{P}_D\left(\frac{g}{2}\right) = \frac{1}{\frac{g}{2}\left[\frac{g}{2} + \left\{\operatorname{Ln}\frac{2}{\gamma\sqrt{(\frac{g}{2})/\beta^{n}}}\right\}^{-1}\right]} \tag{5.31}$$

$$\text{With} \quad \beta^{n\to a} = \frac{6}{\gamma^2}\left\{\frac{(C_D e^{2S})_{f+m}}{\lambda e^{-2S}}\right\} \quad \& \quad \beta^{n\to b} = \frac{10}{3\gamma^2}\left\{\frac{(C_D e^{2S})_{f+m}}{\lambda e^{-2S}}\right\} \tag{5.32}$$

During late time flow periods:

$$\underset{g\to\infty}{R^{a\backslash b}(g)} \approx 1 - \left[\frac{(1-\omega)^2 g}{\lambda C_D}\right] \approx 1 \tag{5.33}$$

$$\therefore \quad \bar{P}_D(g) = \frac{1}{g\left[g + \left\{\operatorname{Ln}\frac{2}{\gamma\sqrt{g/(C_D e^{2S})_{f+m}}}\right\}^{-1}\right]} \tag{5.34}$$

The type curves of figure (5.15) were obtained by overlaying the numerical solutions of equations (5.29) and (5.34), representing the dual porosity responses during fissure and total system domination, with a set of transition type curves describing the fluid flow from matrix to fracture region and characterized by the dimensionless parameter [$\beta^n$]. These transition type curves which were displaced by a factor of [2] along the dimensionless pressure axis, accounted for the dual porosity pressure responses during intermediate flow periods.

With reference to figure (5.15) it is evident that due to the similarities between the shapes of the transition and early/late times type curves, it is possible to match the initial recorded pressure data on to the transitional type curves and thus create considerable errors in the definitions of the formation parameters. such errors tend to magnify in the absence of insufficient pressure data during early flow periods.

## 5.6-BUILD UP TESTS ASSOCIATED WITH THE TIF MODEL

Although the [TIF] model type curves were generated on the basis of single rate drawdown testing scheme, its applicability could be extended to build up pressure data analysis under the same restrictions imposed on the production times of the [SIF] model. The vertical time axis of figure (5.15) was employed in the same manner as outlined for the case of the [SIF] model in order to check the validity of the global analysis of the recorded pressure data via the theoretical pressure responses of the [TIF] model.

## 5.7-WELL TEST INTERPRETATION PITFALLS WITH RESPECT TO THE TIF MODEL

Despite the improved definitions of the reservoir parameters by means of the type curves of figure (5.15), the interpretation of the recorded pressure data through [TIF] model may sometimes create uncertainty when used as the only means of well testing tool. Typical example is the case of a sealing fault in a homogeneous reservoir, close to production well. Such faults would exhibit the doubling of the slope effect on the semilog plot (as in the case of the [TIF] model) hence creating a certain degree of confusion in choosing the correct formation configuration. Under such conditions, the recorded pressure data should be analysed through different schemes and reservoir models in

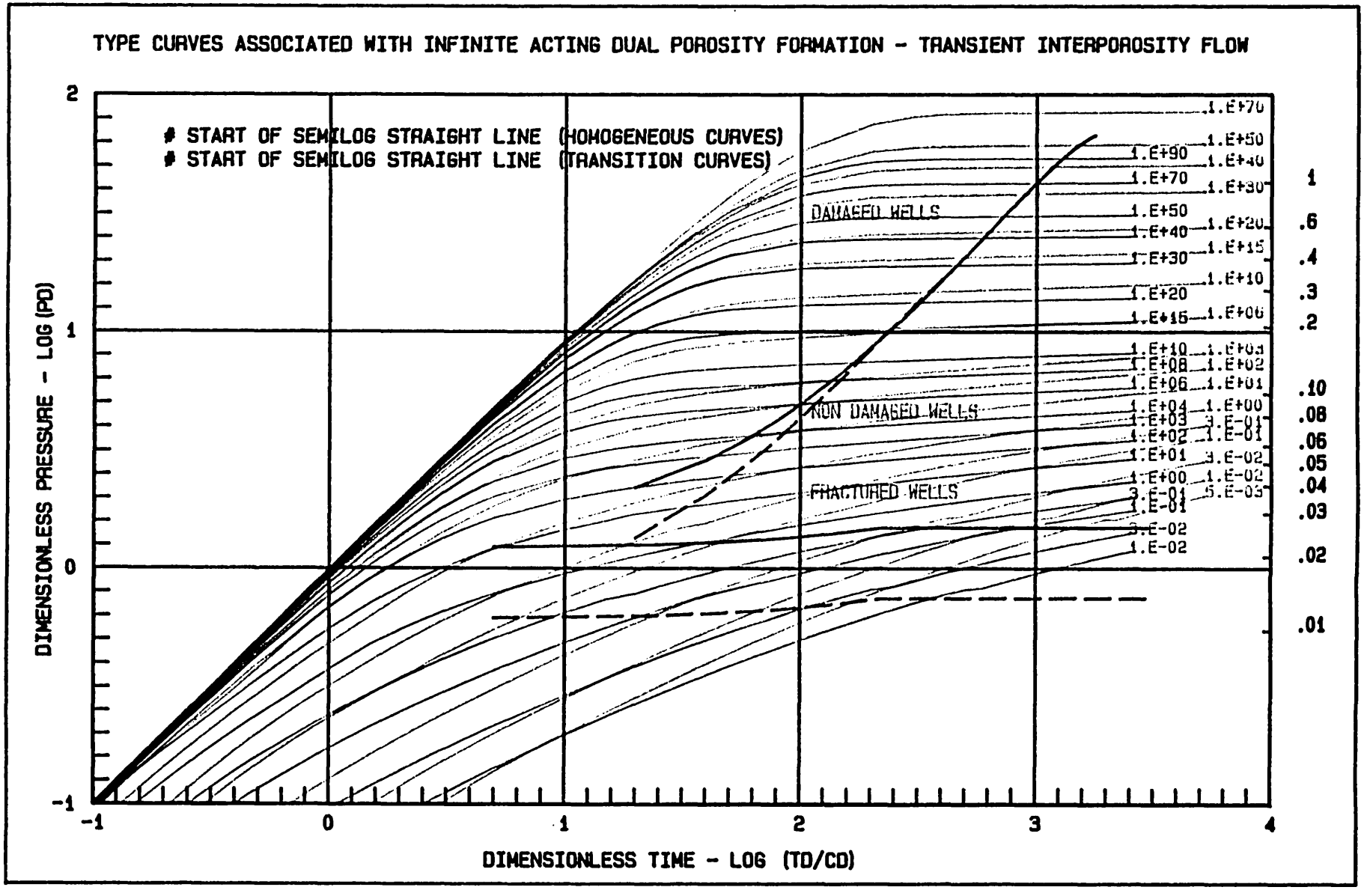



FIGURE 5.16: DIMENSIONLESS PRESSURE RESPONSES OF INFINITE ACTING DUAL POROSITY FORMATION WITH WBS & S (TIF MODEL)

order to obtain consistency with the actual geological description of the reservoir under consideration.

Assuming that the [TIF] model describes the physical nature of the formation, then using similar techniques as outlined for the the case of the [SIF] model:

-fissure permeability thickness is obtained from the pressure axis match.

-wellbore storage is determined from the time axis match.

-Interporosity flow parameter is estimated from the matched type curve, characterized by the dimensionless parameter [$\beta^{n}$].

-Storage capacity ration is obtained from equation (5.24) whilst the skin factor is estimated from either $(C_D e^{2S})_{f+m}$ or $(C_D e^{2S})_f$ match curve.

It is emphasized that if the total dual porosity behaviour is not observed, only a limited information with regard to the reservoir parameters are accessible.

☆☆☆☆☆☆☆☆☆☆

# CHAPTER 6

# DIFFERENTIAL MODELS OF FRACTURED FORMATIONS

## 6.1-APPLICATION OF PRESSURE DERIVATIVE TO FRACTURED FORMATIONS

Although the most common reservoir simulation models employed in the industry for describing the behaviour of naturally fractured reservoirs are based on the pressure responses associated with the [SIF] and [TIF] models, it is often possible to generate incorrect reservoir parameters by either choosing the wrong model or misinterpreting the recorded pressure data by means of the type curves with respect to the fracture models. Such errors may be caused by:

-The possibility of non unique solutions due to the similarities of the dimensionless pressure curves during fissure and total system responses.

-The lack of confidence in identification of pressure stabilization (in the case of SIF model) and the absence of the semilog straight line during transition periods (in the case of TIF model).

-The use of the draw down pressure curves for analysis of build up pressure data with significant production history.

In order to reduce the degree of misinterpretations of the field data, the derivative schemes associated with both the dual porosity models should be employed[3,8]. Such schemes when used in conjunction with pressure curves, tend to place a higher degree of confidence on the description of formation characteristics by:

-Identifying the appropriate model with reference to the distinct and magnified pressure derivative responses during transition periods.

-Taking into account the whole of the pressure responses (from the fist to the last recorded pressure data) for analysis purposes.

-Amplifying small pressure changes that might arise due to the specific reservoir configurations (e.g. matrix block shapes, etc).

Although the accuracy of derivative interpretation model is fully dependent on the ability to obtain good quality differentiable pressure data, recent developments of electronic pressure gauges has overcome this disadvantage. In fact, the application of the pressure derivative approach to homogeneous and especially heterogeneous formations has proved to be a powerful tool in well test interpretation techniques.

## 6.2-PRESSURE DERIVATIVE RESPONSES ASSOCIATED WITH THE SIF MODEL

With reference to the solution of dimensionless pressure function in Laplace space, corresponding to the SIF model[9], The dimensionless pressure derivatives with respect to the natural logarithm of $(T_D/C_D)$ group during early and late time flow periods were obtained by inverting the $P_D$-function defined by equation (5.9), from Laplace space to real space solution by means of the Stefhest and Gauss-Laguarre schemes:

$$P_D(\frac{T_D}{C_D}) = L^{-1}\{\bar{P}_D(a)\} \quad \rightarrow \quad \frac{d(P_D)}{d[Ln(\frac{T_D}{C_D})]} = \frac{T_D}{C_D} \times \frac{d(P_D)}{d(\frac{T_D}{C_D})} \tag{6.1}$$

During intermediate times, when the transition period prevails, equation (5.9) may be approximated by:

$$\bar{P}_D(a) = L^{-1}\left[Ln\frac{2}{\gamma\sqrt{(C_D e^{2S})_{f+m}}} - Ln(a) - Ln\left[\frac{\omega(1-\omega)a+\lambda(C_D)_{f+m}}{(1-\omega)a+\lambda(C_D)_{f+m}}\right]\right] \tag{6.2}$$

As in the case of early and late time flow periods, equation (6.2) was inverted into real space solution and the resulting expression was differentiated with respect to $Ln(T_D/C_D)$:

$$\frac{T_D}{C_D}\frac{d(P_D)}{d(\frac{T_D}{C_D})} = 0.5\left[\frac{-\lambda C_D}{1+e^{\frac{\omega(1-\omega)}{\omega(1-\omega)}\times\frac{T_D}{C_D}}} - e^{\frac{-\lambda C_D}{(1-\omega)}\times\frac{T_D}{C_D}}\right] \tag{6.3}$$

during ealry and late time transition flow periods Equation (6.3) was reduced to:

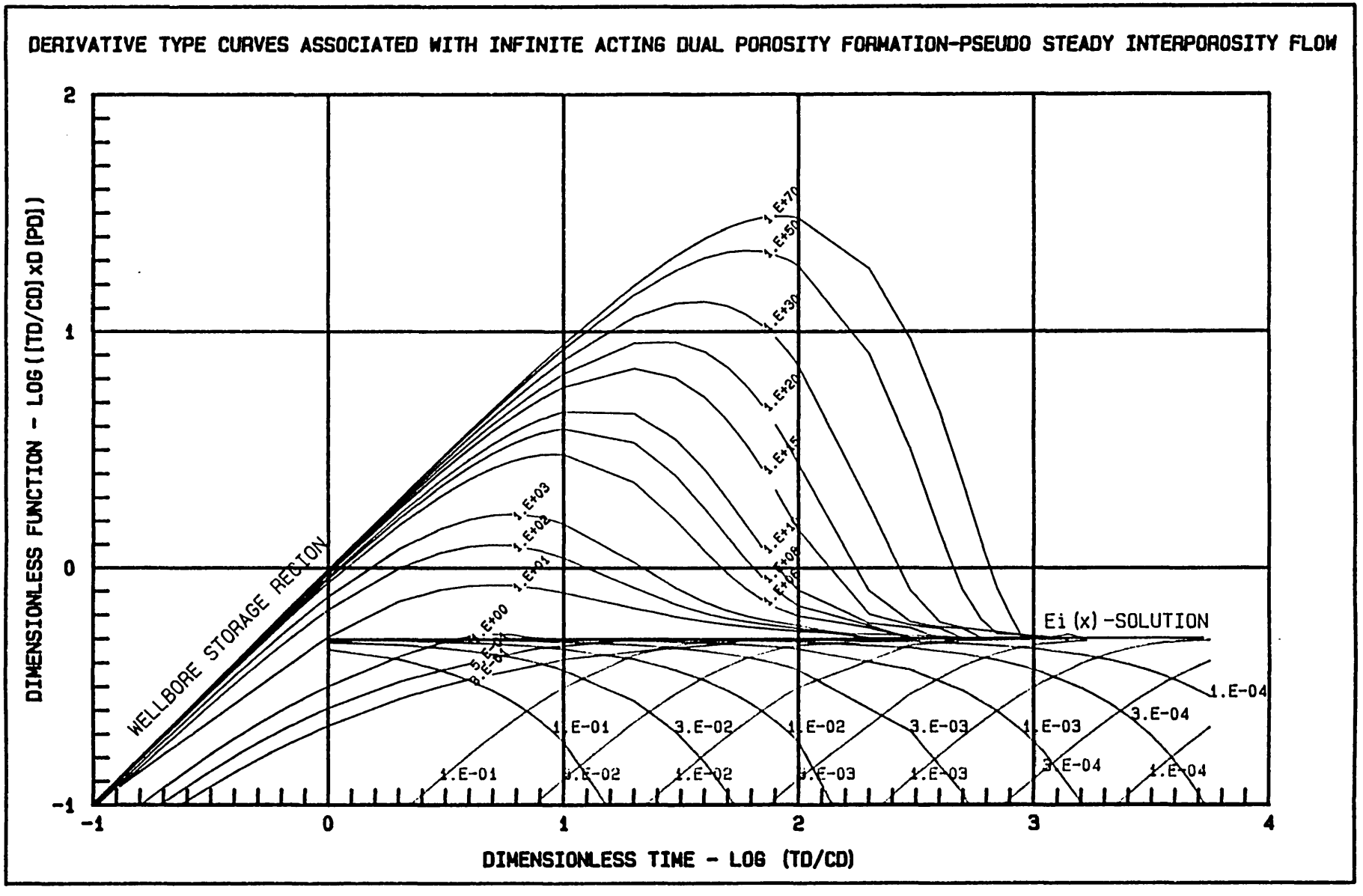



FIGURE 6.1: DERIVATIVE PRESSURE RESPONSES OF INFINITE ACTING DUAL POROSITY FORMATION WITH WBS & S (SIF MODEL)

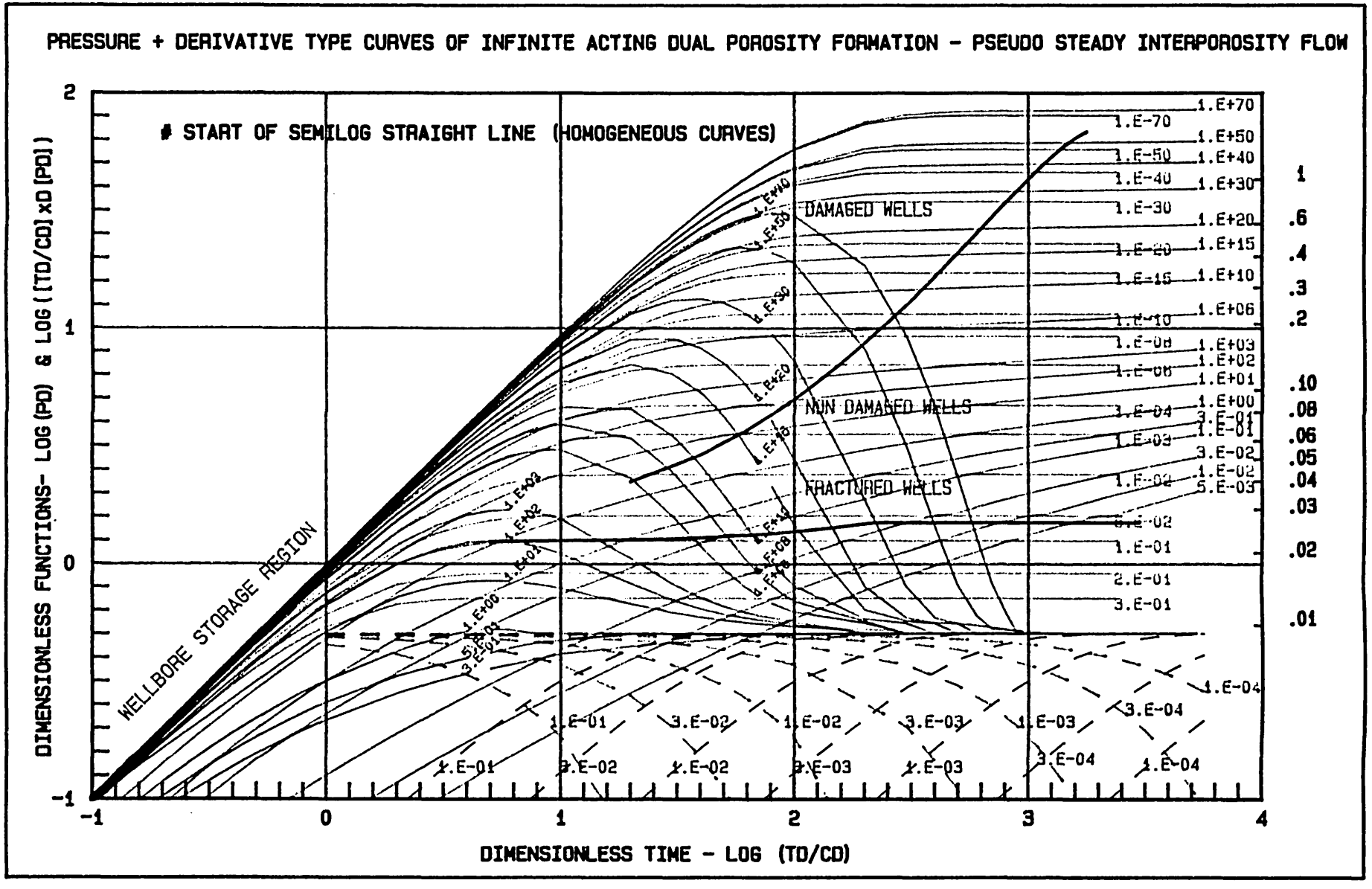



FIGURE 6.2: DIMENSIONLESS PRESSURE & DERIVATIVE RESPONSES OF AN INFINITE ACTING FRACTURED FORMATION WITH WBS & S (SIF MODEL)

$$\frac{T_D}{C_D} \times \frac{d(P_D)}{d(\frac{T_D}{C_D})} = 0.5\left[e^{\frac{-\lambda(C_D)_{f+m}}{\omega(1-\omega)} \times \frac{T_D}{C_D}}\right] \quad (6.4)$$

and

$$\frac{T_D}{C_D} \times \frac{d(P_D)}{d(\frac{T_D}{C_D})} = 0.5\left[1 - e^{\frac{-\lambda(C_D)_{f+m}}{1-\omega} \times \frac{T_D}{C_D}}\right] \quad (6.5)$$

Figure (6.1) was constructed by superimposing the derivative type curves associated with the fissure and the total system pressure responses (characterized by $(C_De^{2S})_f$ & $(C_De^{2S})_{f+m}$ group) with two sets of type curves describing the pressure responses of SIF model during transition periods and defined by equations (6.4) and (6.5).

Figure (6.3) represents an ideal pressure derivative responses under the condition of restricted flow from the matrix to the fissure zone. figure (6.3) illustrates the fact that the derivative approach provides better definitions of the limits during early, intermediate and late flow periods than the dimensionless pressure curves associated with the same model. Furthermore, by magnifying the transition periods (segment DEF) which are otherwise compressed on the conventional type curves, the scheme tends to reduce the possibility of choosing an incorrect combinations of pressure curves for the definition of formation parameters such as $K_fh$, S, $\lambda$, $\omega$.

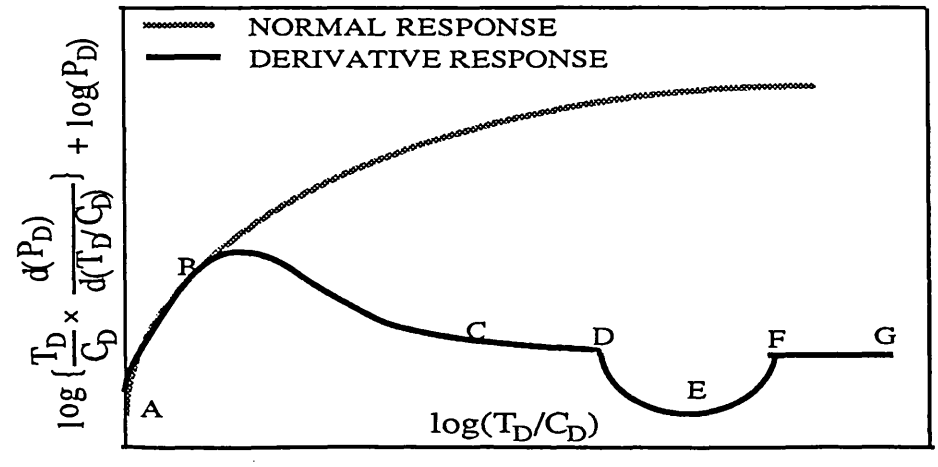



FIGURE 6.3: $(P_D) + (P'_D)$ RESPONSES ASSOCIATED WITH THE SIF FRACTURED MODEL

With reference to figure (6.3), the derivative pressure responses of the [SIF] model Initially follow the line AB, characterized by the slope of unity (in the case of damaged formations). After wellbore storage effects are over, the pressure responses in the fissure region are identified (the pressure derivative follows the curve BC). When radial flow from the fissure to the production well prevails, the pressure derivative stabilizes and thus follows the horizontal line CD, reflecting the presence of semilog straight line during fissure flow. As soon as the matrix region begins to contribute fluid to the fissure region, the pressure stabilizes and as a consequence, the derivative of the pressure drops below the line CD and follows one of the early transition period type curves defined by the equation (6.4). Eventually, the end of the transition period is signalled by the derivative responses following the late time transition curve defined by the equation (6.5) and stabilizing on the horizontal line FG. This line corresponds to the radial flow associated with the pressure responses of the total system.

Occasionally, the problem of idéntification of pressure behaviour may arise when the first semilog straight line (corresponding to radial fissure flow) is not developed. Figure (6.4) represents such pressure and its derivative responses with respect to the model. Although it may be possible to detect the absence of the first semilog straight line, by matching the pressure responses on the pressure curves of figure (6.1), the derivative testing model with its high degree of sensitivity provides a better graphical display of such anomalies (after wellbore storage periods, the derivative pressure responses goes directly into the transition zone - segment CD in figure 6.4).

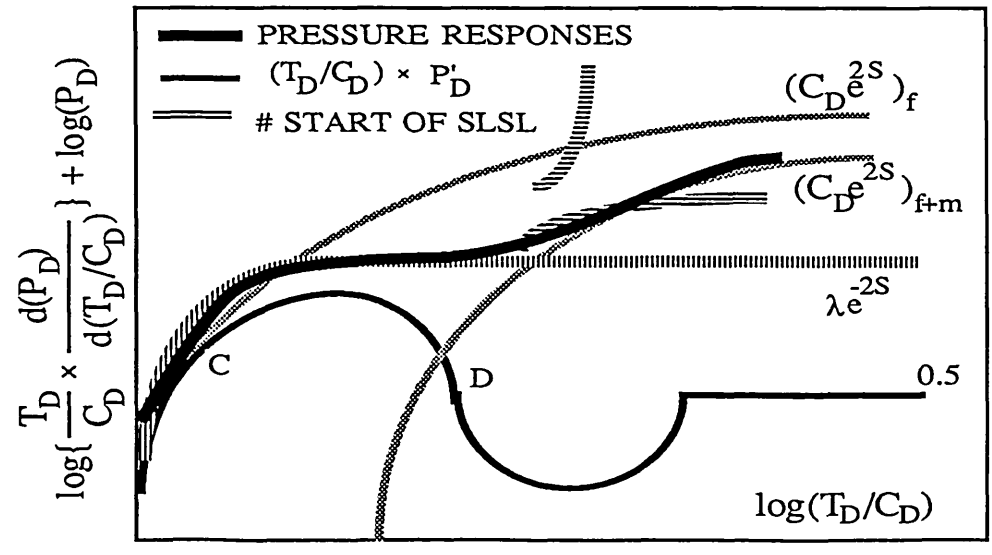



FIGURE 6.4: $(P_D)+(P'_D)$ BEHAVIOUR OF THE SIF MODEL IN THE ABSENCE OF FISSURE SLSL.

## 6.3-PRESSURE DERIVATIVES WITH RESPECT TO BUILD UP TESTS (SIF MODEL)

If the production period prior to shut in reflects transient conditions, then the build up matching may be performed by means of the type curves of figure (6.1) by differentiation of the pressure data with respect to the natural logarithm of Horner time. Frequently, however, the production prior to shut in, is terminated at times when the fissure or transition flow conditions prevail. This causes the derivative pressure response to fall below the expected minimum value, and instead of following the transition curves, it occurs at later times (figures 6.5 & 6.6).

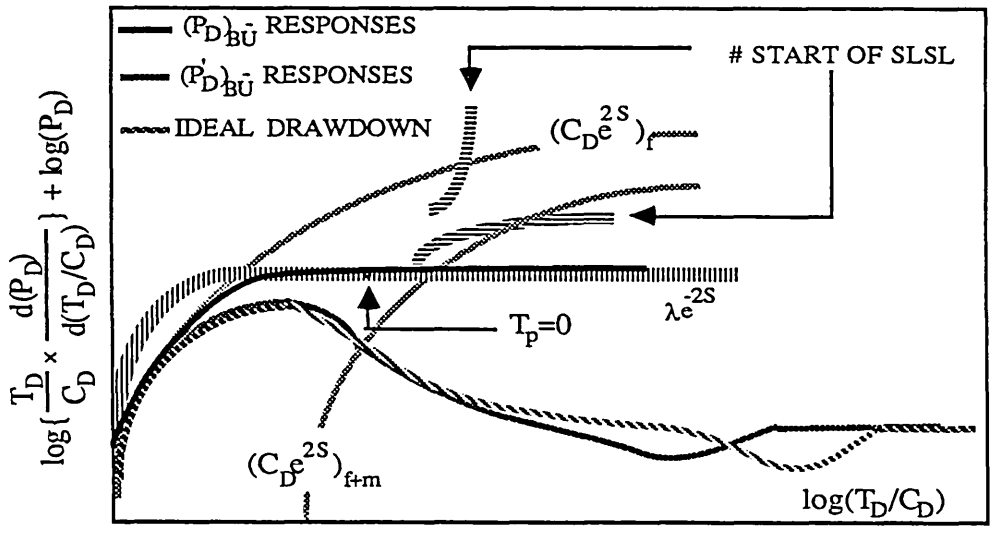



FIGURE 6.5:$(P_D)$+$(P'_D)$ RESPONSES (PRODUCTION TERMINATED DURING TRASITION PERIOD).

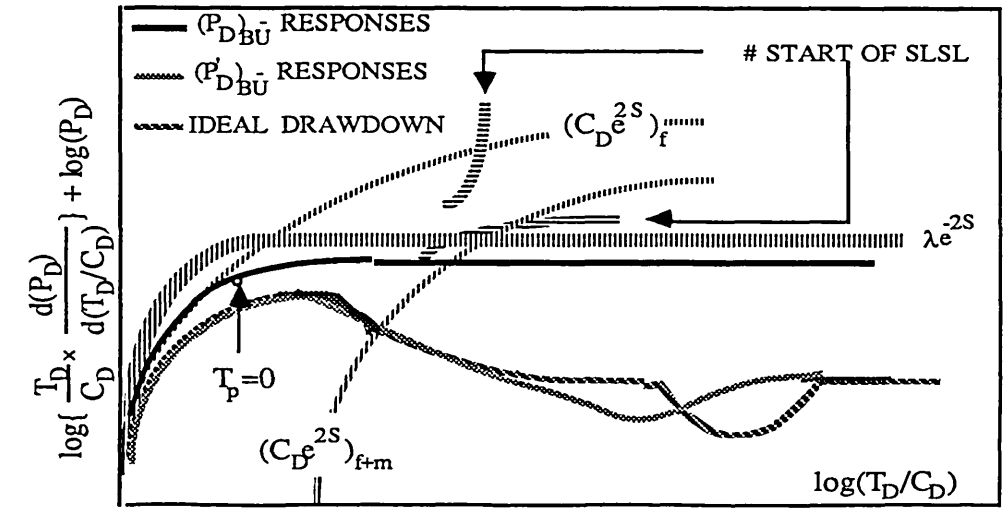



FIGURE 6.6: $(P_D)$ + $(P'_D)$ RESPONSES (PRODUCTION TERMINATED DURING FISSURE FLOW).

In order to overcome such discrepancies when matching the pressure data through figure (6.1), build up type curves, which take into account the production history of the testing well should be employed. The objective may be achieved by using :

$$(P_D)_{BU} = P_D(\frac{T_D}{C_D}) + P_D\{(T_P)_D\} - P_D\{(T_P)_D + \frac{T_D}{C_D}\} \qquad (6.7)$$

or more generally:

$$(P_D)_{BU} = \sum_{i=1}^{n} \frac{q_i - q_{i-1}}{q_{n-1} - q_n} \left[ P_D[\sum_{j=1}^{n-1} (\frac{T_D}{C_D})_j] - P_D[\sum_{j=1}^{n-1} \{(\frac{T_D}{C_D})_j + \frac{T_D}{C_D}\}] \right] + P_D(\frac{T_D}{C_D}) \qquad (6.8)$$

Since much evaluation of reservoir parameters depends on testing which is frequently of short duration, the **(TOPAZ)** program has been implemented with sub programs which generate build up curves specific to particular test conditions and durations. Although, the construction of these curves may be slightly time consuming (an approximate time of 3 minutes per type curve), once established, these curves could prove to be valuable asset in improving the definition of formation parameters.

## 6.4-CHARACTERIZATION OF THE SIF MODEL VIA DERIVATIVE SCHEMES

The procedures associated with the definition of reservoir and well parameters are identical to the case of the derivative matching technique with respect to the homogeneous model. Once the actual and theoretical pressure responses are matched, the permeability thickness is defined from the pressure axis match, wellbore storage from the time axis match, and skin factor from the theoretical pressure response match.

The values of interporosity flow parameter and storage capacity ratio, may be obtained from the early and late time transition curves.

-During early and late time transition periods:

$$\Re_1 = \frac{\lambda C_D}{1-\omega} \quad \& \quad \Re_2 = \frac{\lambda C_D}{(1-\omega)\omega} \quad \Rightarrow \quad \omega = \frac{\Re_1}{\Re_2} \quad \& \quad \lambda = \frac{\Re_1(1-\omega)}{C_D}$$

## 6.5-PRESSURE DERIVATIVE RESPONSES ASSOCIATED WITH THE TIF MODEL

Considering the dimensionless pressure responses in association with the [TIF] model:

$$\bar{P}_D(g) = \frac{1}{g\left[g + Ln\{\frac{2}{\gamma\sqrt{gR^n(g)/(C_D e^{2S})_{f+m}}}\}^{-1}\right]} \quad \& \quad R^n(g) = f(\lambda, C_D, n) \tag{5.26}$$

During early transition flow periods, equation (5.26) reduces to the case of the pressure responses with respect to the infinite acting homogeneous formation model, but displaced by a factor of [2] along the dimensionless pressure and time axis:

$$2P_D(\frac{T_D}{C_D}) = L^{-1}\left[\frac{1}{(\frac{g}{2})\left[(\frac{g}{2}) + Ln\{\frac{2}{\gamma\sqrt{(\frac{g}{2})/\beta}}\}^{-1}\right]}\right] \tag{6.9}$$

$$\therefore \left[\frac{d(P_D)}{d\{Ln(\frac{T_D}{C_D})\}}\right]_{E\&L} = \left[(\frac{T_D}{C_D}) \times \frac{d(P_D)}{d(\frac{T_D}{C_D})}\right]_{E\&L} \tag{6.10}$$

Where [E ]& [L] represent early and late time flow periods.

During late transition flow periods, equation (5.26) may be expressed as:

$$\bar{P}_D(g) = L^{-1}\left[Ln\{\frac{2}{\gamma\sqrt{g/(C_D e^{2S})_{f+m}}}\} + 0.5\, Ln\{1 + \frac{(1-\omega)^2 g}{\lambda C_D}\}\right] \tag{6.11}$$

Inversion of equation (6.11) yield:

$$P_D(\frac{T_D}{C_D}) = 0.5\ \{\ Ln(\frac{T_D}{C_D}) + Ei[\frac{\lambda C_D}{(1-\omega)^2}] \times \frac{T_D}{C_D}\ \} + CON \tag{6.12}$$

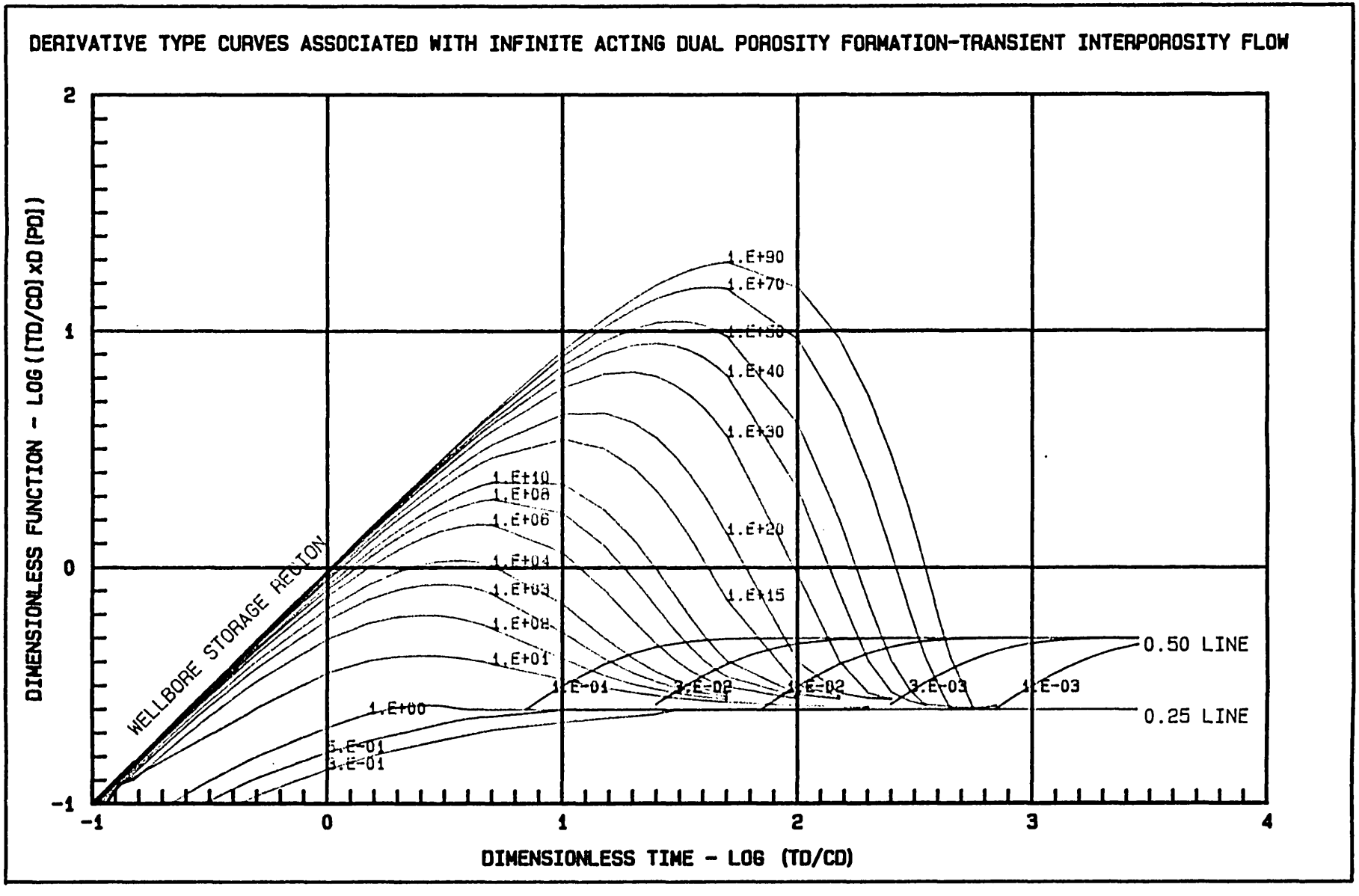



FIGURE 6.7: DERIVATIVE PRESSURE RESPONSES OF INFINITE ACTING DUAL POROSITY FORMATION WITH WBS & S (TIF MODEL)

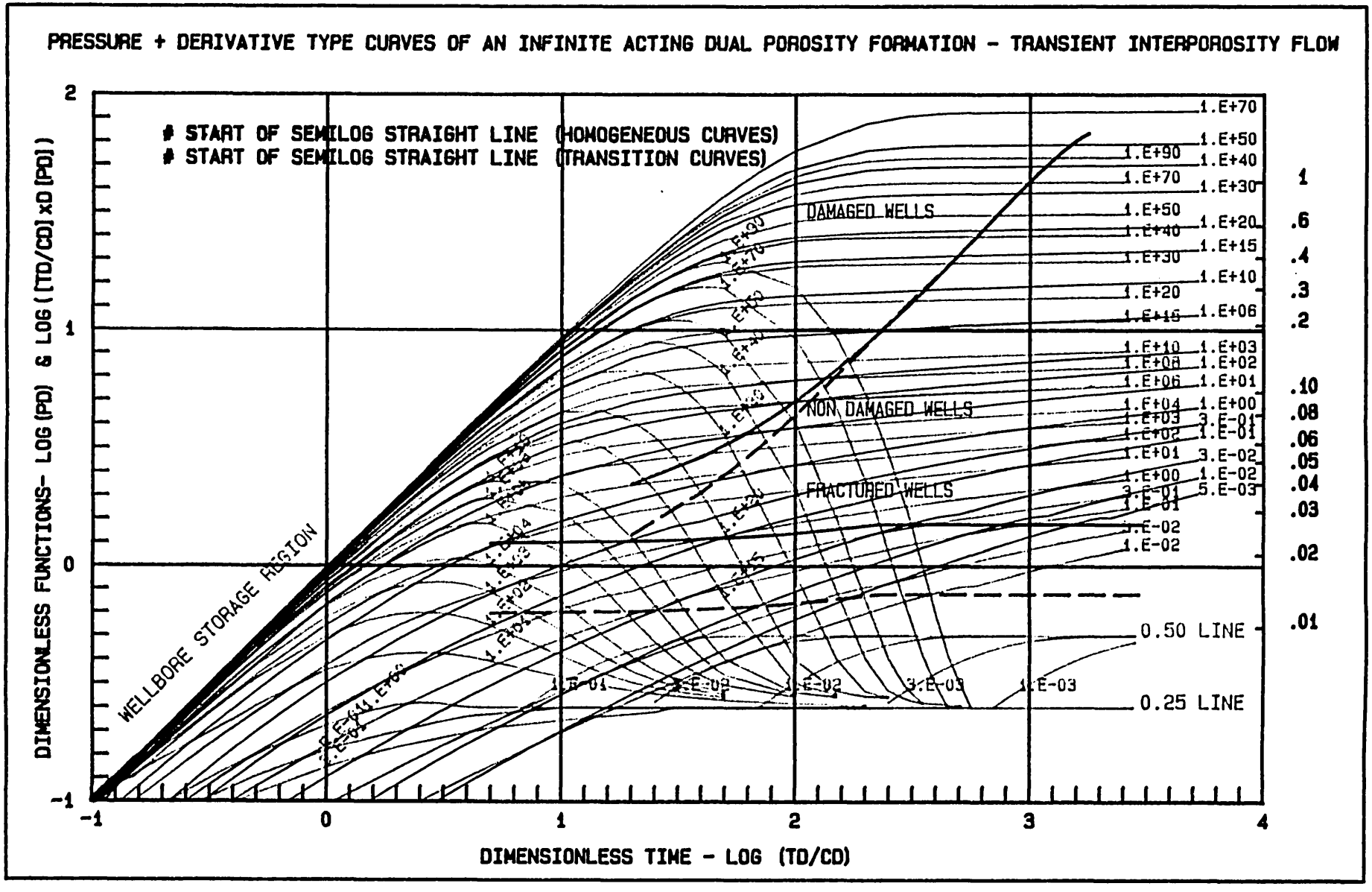



FIGURE 6.6: DIMENSIONLESS PRESSURE & DERIVATIVE RESPONSES OF AN INFINITE ACTING FRACTURED FORMATION WITH WBS & S (TIF MODEL)

$$\therefore \quad \frac{T_D}{C_D} \times \frac{d(P_D)}{d\left(\frac{T_D}{C_D}\right)} = 0.5\left[1 - e^{-\frac{\lambda C_D}{(1-\omega)^2} \times \frac{T_D}{C_D}}\right] \qquad (6.13)$$

The derivative type curves associated with the dimensionless pressure responses of the [TIF] model can hence be constructed in three stages:

-Numerical inversion of equation (6.9).
-Analytical solution of equation (6.11).
-Differentiation of the generated dimensionless pressures.

The type curves of figure (6.7) were obtained by superimposing the derivative type curves during early transient flow periods which are defined by equation (6.11), with a set of late transition type curves defined by equation (6.13) and characterized by dimensionless group $[\lambda C_D/(1-\omega)^2]$.

By considering the type curves of figures (6.1) and (6.7), it is evident that the SIF and TIF models generate different responses during intermediate times. Whilst the derivative pressure behaviour during transition periods and associated with the TIF model do not fall below the 0.25 horizontal line (corresponding to the radial flow during intermediate times), the SIF model in general, tends to produce pressure responses whose derivative values fall below this line. Indeed, Such an observation tends to provide a possible means of distinguishing between the two models.

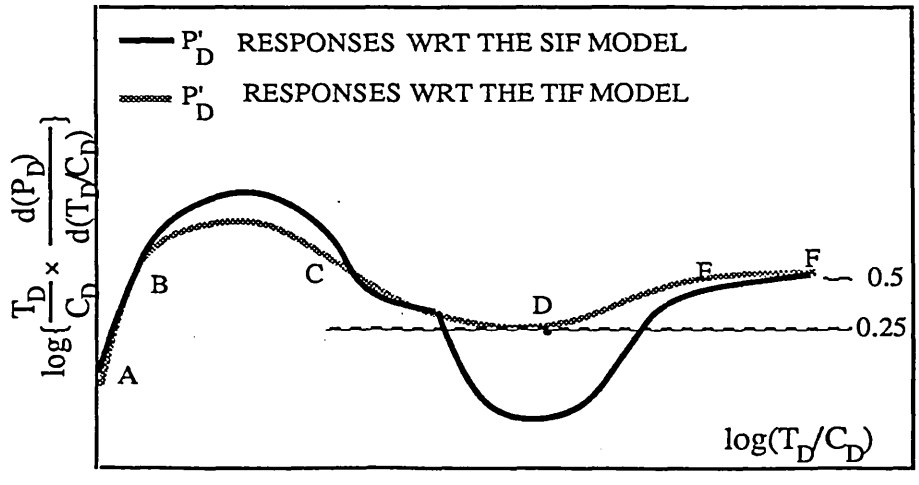



FIGURE 6.9: COMPARISON OF THE ($P'_D$) RESPONSES WRT THE SIF & TIF MODELS

One of the main advantages of the derivative application to the TIF model is the ability to identify the shapes of the matrix blocks from the raw data. Figure (6.10) indicates that although the dimensionless pressures with respect to spherical and slab shape blocks within the matrix region exhibits identical responses, their corresponding derivatives during transition periods are different. In the case of the spherical block shapes, the derivative responses do not reach the 0.25 horizontal line and as a result, radial flow during transition periods tend to define a semilog straight line whose slope is greater that 0.25. With the assumption of slab shape matrix configuration, the derivative responses during transition period become tangent to the 0.25 line and hence exhibit the doubling of slope effect.

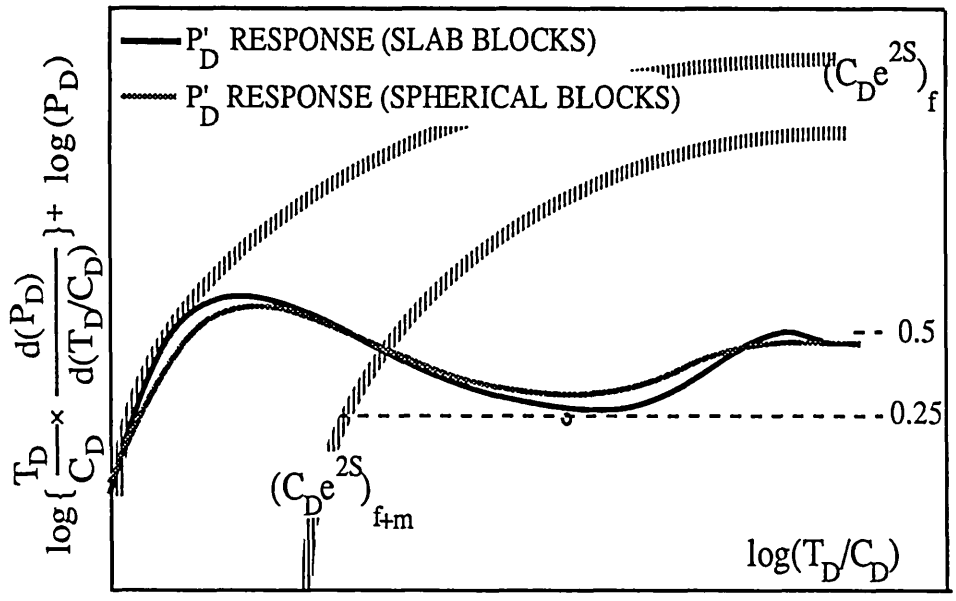



FIGURE 6.10: $P_D$ & $P'_D$ RESPONSES OF THE TIF MODEL (DISTINCT MATRIX BLOCK SHAPES).

Based on the above observations, it may be concluded that the stabilization of the derivative responses with respect to the TIF model during transition periods would only take place under favourable combinations of the formation parameters [$\lambda$] & [$\omega$] (shape of the blocks in the matrix region).

Another important aspect of the derivative technique is the distinction between a homogeneous reservoir with a sealing fault and a dual porosity formation under unrestricted interporosity flow condition (figure 6.11). Both models produce doubling of the slope phenomena (from 0.25 horizontal line to 0.5 horizontal line) and hence

exhibit identical pressure variations. By considering their derivative responses, however, small differences in the pressure responses, especially during late times transition periods are magnified. This magnification effects assist in choosing the correct reservoir model and hence reduce the possibility of misinterpretation of data. (e.g. The choice of the wrong model may result in an error of 200% in the numerical value of the formation permeability thickness).

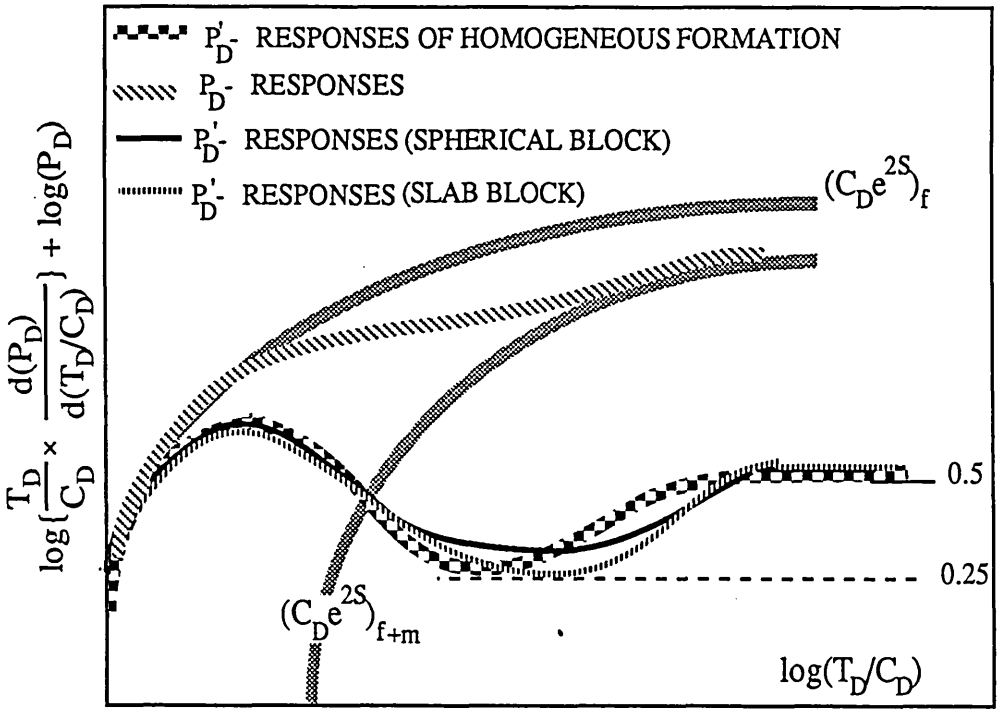



FIGURE 6.11: $(P_D)$ & $(P'_D)$ RESPONSES OF TIF MODEL IN THE PRESENCE OF A SEALING FAULT.

## 6.6-PRESSURE DERIVATIVES WITH RESPECT TO BUILD UP TESTS (TIF MODEL)

The application of the dimensionless pressure derivative associated with the TIF model (figure 6.6) could be extended to analysing the build up pressure data provided the preceding draw down prior to shut in reaches radial flow under fissure + matrix (total system) status.

As in the case of the SIF model, when the duration of the production time is too short for the total system responses to be seen, then the build up derivatives tend to deviate from the draw down type curves, thus restricting the analysis of the recorded data by means of the pressure derivative curves of figure (6.6). Under such conditions, the TIF

model for a slab (stratified) system, generates pressure derivative responses which fall below the radial flow line during transition periods(figure 6.10). Such responses which give rise to the possibility of the incorrect choice of the dual porosity model for well test interpretations and reservoir simulations, may be screened by generating build up type curves based on the production history of the formation. Having established such responses, it is then possible to match the actual data with the theoretical pressure behaviour of the mathematical model which best describes the reservoir under consideration and hence define the physical nature of the formation with a significant degree of accuracy.

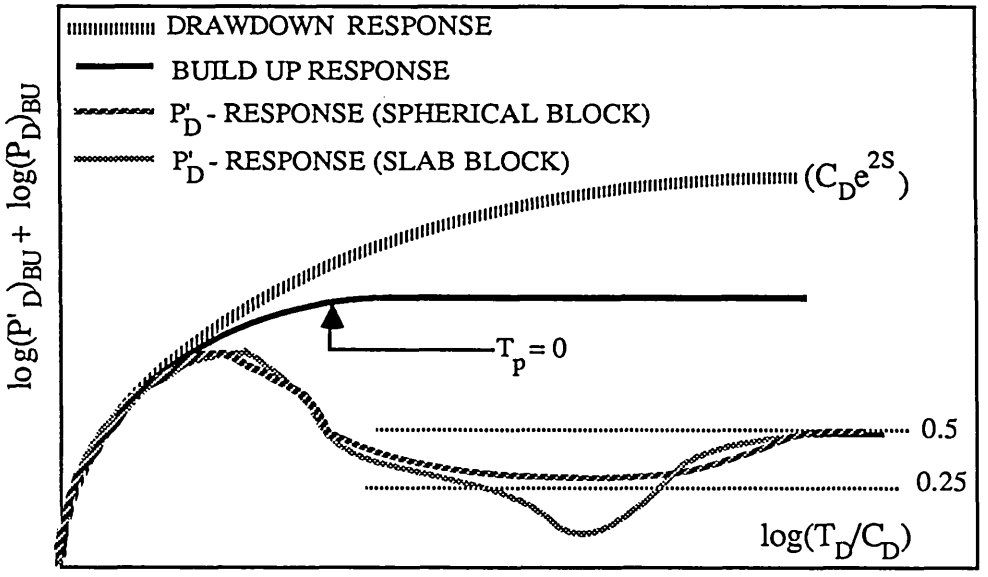



FIGURE 6.12: (P'D)BU & (PD)BU RESPONSES OF THE TIF MODEL (SHORT PRODUCTION)

## 6.7-CHARACTERIZATION OF THE TIF MODEL VIA DERIVATIVE SCHEME

Having matched the derivative pressure responses of the recorded data on to the figure (6.6), the formation parameters may be defined in the same manner associated with the [SIF] model:

$$Kh = 141.2\, q\mu B_o \left(\frac{P'_D}{\Delta P'}\right)_{match} \tag{6.14}$$

$$C = 0.000295\, \frac{Kh}{\mu} \left(\frac{\Delta T}{T_D/C_D}\right)_{match} \tag{6.15}$$

$$(C_D)_{f+m} = \frac{0.8936C}{\phi c_t h_f r_w^2} \tag{6.16}$$

$$S = 0.5\ \mathrm{Ln}\left[\frac{(C_D e^{2S})_{f+m}}{(C_D)_{f+m}}\right]_{match} \tag{6.17}$$

$$\lambda = \left[\frac{(\lambda e^{-2S})(C_D e^{2S})_{f+m}}{(C_D)_{f+m}}\right]_{match} \tag{6.18}$$

$$\omega = 1 - \sqrt{\frac{\lambda C_D}{\left[\frac{\lambda C_D}{(1-\omega)^2}\right]_{match}}} \tag{6.19}$$

(N.B.)

-For the case of build up tests:

$$\Delta P' = \frac{T_p+\Delta T}{T_p}\Delta T\frac{d(\Delta P)}{d(\Delta T)} \quad \& \quad P'_D = \left[\frac{(T_p)_D+\frac{T_D}{C_D}}{(T_p)_D}\right] \times \frac{T_D}{C_D} \times \frac{d(P_D)}{d(\frac{T_D}{C_D})} \tag{6.20}$$

-For the case of drawdown tests:

$$\Delta P' = \Delta T \times \log\{\frac{d(\Delta P)}{d(\Delta T)}\} \quad \& \quad P'_D = \frac{T_D}{C_D} \times \log\{\frac{d(P_D)}{d(\frac{T_D}{C_D})}\} \tag{6.21}$$

★★★★★★★★★★

# CHAPTER 7

# CONVENTIONAL ANALYSIS OF NATURALLY FRACTURED FORMATIONS

## 7.1-CONVENTIONAL DRAWDOWN SCHEMES ASSOCIATED WITH THE SIF MODEL

Subject to the following conditions, the fundamental pressure equation associated with the model[71] for use in conventional analysis of the recorded pressure data can be formulated by the asymptotic solution of equation (5.7) from the Laplace domain to real space.

$-T_D>100$ or

$-T_D>100\omega$ for $\lambda<<1$ or

$-T_D>(100\lambda-1)/\lambda$ for $\omega<<1$

$$P_D = 0.5\left[E_i\left(\frac{1}{4T_D}\right) + E_i\left(\frac{\lambda T_D}{1-\omega}\right) - E_i\left\{\frac{\lambda T_D}{\omega(1-\omega)}\right\}\right] + S \qquad (7.1)$$

$$\text{Where} \quad E_i(X) = \int_X^{\infty} \left(\frac{e^{-u}}{u}\right) du \qquad (7.2)$$

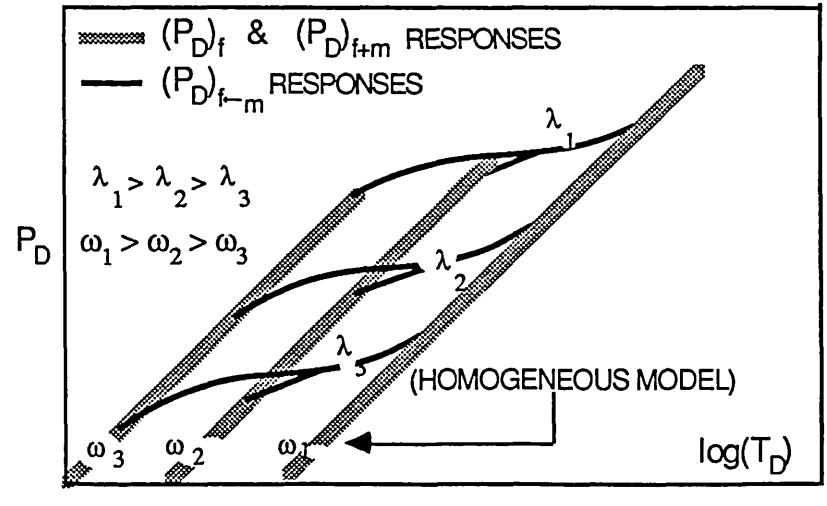



FIGURE 7.1: $P_D$ RESPONSES WRT SIF MODEL[72] (EQUATION 7.1)

With reference to equation (7.1), it is evident that the three dimensionless parameters $T_D$, $\lambda$ and $\omega$ are sufficient enough to describe the dimensionless pressure responses of the naturally fractured [SIF] model.

Figure (7.1) represents the graphical form of equation (7.1) for different ranges of interporosity flow parameter and storage capacity ratio which characterize a dual porosity system with pseudo steady state (as well as transient) interporosity flow condition during transition periods.

Following the dimensionless time variations, the limiting forms of equation (7.1), during early, intermediate and late time flow periods can be employed in order to define the dimensionless pressure responses associated with the model (figure 7.2).

-During fissure flow, when the formation is mainly produced from the fracture network (i.e. $E_i(X)=-Ln(\gamma X)$), equation (7.1) may be expressed as:

$$(P_D)_f = 0.5\,\{-Ln(\gamma) + Ln(4T_D) + Ln(\omega^{-1})\} + S \qquad (7.3)$$

Equation (7.3) when defined in terms of base 10 logarithm, is reduced to:

$$(P_D)_f = 1.151\log(T_D) + 0.4045 + 1.151\log(\omega^{-0.5}) + S \qquad (7.4)$$

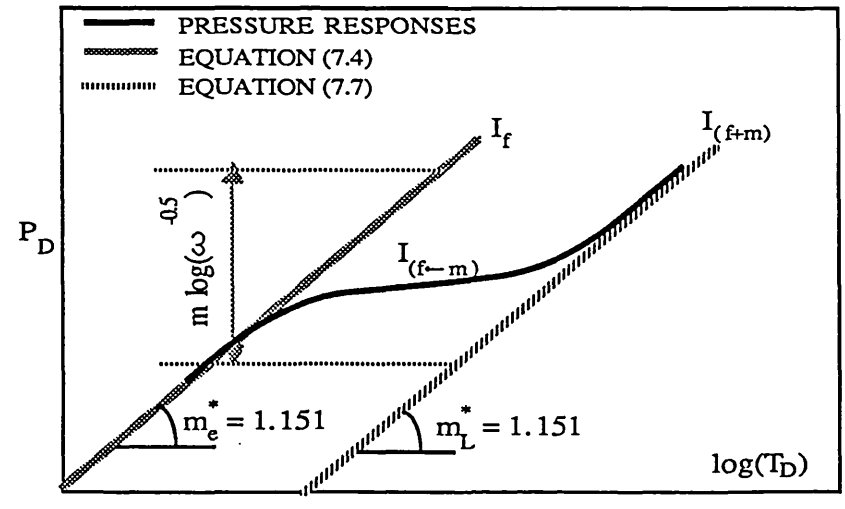



FIGURE 7.2: $P_D$- RESPONSES WRT THE SIF MODEL DURING DRAWDOWN

-During transition period, characterized by the stabilization of pressure in the fracture region, the dimensionless pressure responses are influenced by the interporosity flow parameter and the storage capacity ratio. (i.e. $E_i(X)=f(\lambda,\omega)$). During this period equation (7.1) can be written as:

$$(P_D)_{f-m} = 1.151 \log(1.26\frac{1-\omega}{\lambda}) + S \quad \text{for} \quad 10 < T_D < \infty \tag{7.5}$$

$$(P_D)_{f-m} = 0.5 \{ E_i(\frac{1}{4T_D}) - Ln(\frac{\gamma\lambda T_D}{1-\omega}) \} + S \quad \text{for} \quad 0.05 < T_D < 10 \tag{7.6}$$

-During late times ($E_i(X)\rightarrow 0$), when the matrix and fissure regions contribute to the production of the formation, equation (7.1) is reduced to:

$$(P_D)_{f+m} = 1.151 \log(T_D) + 0.4045 + S = 1.151 \log(2.246T_D) + S \tag{7.7}$$

i.e. A plot of $(P_D)_{f+m}$ vs $\log(T_D)$ should yield a straight line ($I_{f+m}$) which is parallel to the semilog straight line during fissure flow and is displaced vertically by a factor of $1.151\log(\omega^{-0.5})$.

Referring to equation (7.4),(7.5) and (7.6), the pressure responses during early and transition flow periods can be detected, provided significant permeability contrast prevails between the matrix and fissure regions of the fractured model (i.e. $\lambda<10^{-5}$ & $\omega<<1$). In fact, for large values of $\lambda$ and $\omega$, the exponential integrals $E_i(\lambda T_D/(1-\omega))$ and $E_i(\lambda T_D/\omega(1-\omega))$ tend to zero, implying that the early transient pressure responses approach the behaviour of homogeneous formation model whose dimensionless pressure function is defined by the equation (7.7).

For small values of [$\lambda$] and [$\omega$], however, the early and intermediate flow periods influence the flowing nature of the formation through the dual porosity model until the total system responses is reached. Under such conditions, it is possible to identify the three distinct flow regions which are specific to naturally fractured formations and hence determine all of the parameters associated with the model.

## 7.2-CHARACTERIZATION OF THE SIF MODEL VIA DRAWDOWN SCHEMES

From the semilog plot of $\Delta P=P_i-P_{wf}$ vs log(T=elapsed time);

-Fissure permeability may be obtained by measuring the slope of the semilog straight line during early or late time flow periods (figure 7.3).

$$K_f = 162.6 \frac{q\mu B_o}{h} \times \frac{1}{m^*} \quad \Rightarrow \quad m^* = m_e^* = m_L^* \tag{7.8}$$

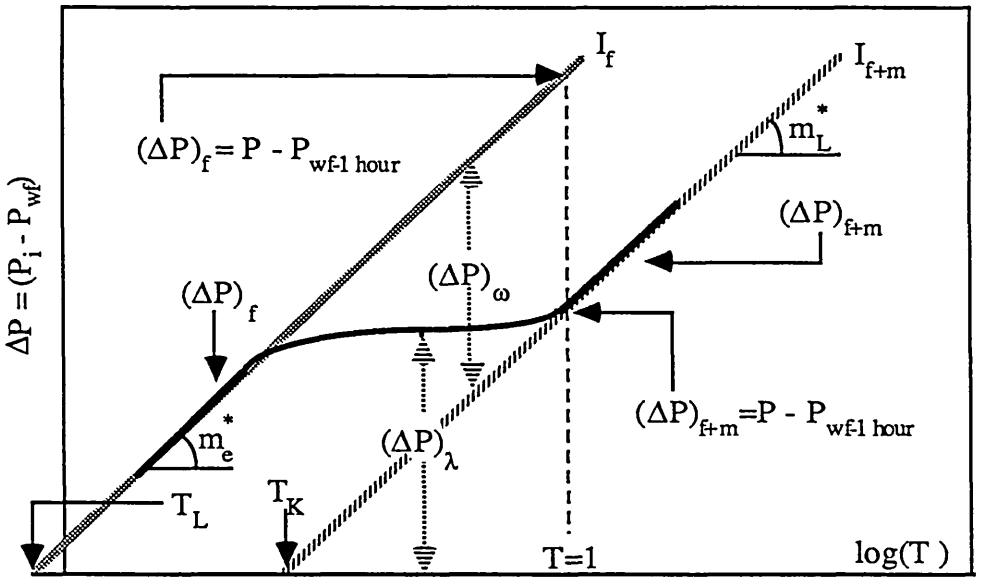



FIGURE 7.3: PRESSURE DRAWDOWN RESPONSES WRT THE SIF MODEL ($r_D=\infty$)

-Dimensionless time factor ($\Psi$), defined by equation (7.9) may be obtained by extrapolating the semilog straight line during late times to $\Delta P=0$ (figure 7.3).

$$\Psi = \frac{T_D}{T} = \frac{0.000264\, K_f}{[(\phi c)_f + (\phi c)_m]\, \mu r_w^2} \tag{7.9}$$

Substitution of equation (7.9) into equation (7.7) yields:

$$(P_D)_{f+m} = 1.151 \log(2.246 \Psi T) \tag{7.10}$$

Evaluation of equation (7.10) at $T=T_k$ corresponding to [$\Delta P=0$] would hence result to:

$$\Psi = \frac{0.445}{T_K} \tag{7.11}$$

It is important to note that when the total reservoir system is not identified (due to a large matrix and fracture region), the value of [Ψ] cannot be estimated. If on the other hand, the value of [ω] is estimated by means of the type curves specific to the model, equation (7.4) may be employed for estimating the time parameter [Ψ].

$$1.151 \log(2.246 T_D \times \omega^{-0.5}) = 0 \tag{7.12}$$

$$\therefore \quad \Psi = \frac{0.445 \sqrt{\omega}}{T_L} \tag{7.13}$$

-At small times, assuming $T_D$=0, the value of storage capacity ratio can be estimated from equation (7.4).

$$\omega = \exp\left(-2.303 \frac{\Delta P_\omega}{m^*}\right) = 10^{-\frac{\Delta P_\omega}{m^*}} \tag{7.14}$$

Where [$\Delta P_\omega$] is read directly from the plot of ΔP vs log (T) .

-Storage capacity of both the fissure and matrix regions may be obtained by considering the definitions of ω and Ψ parameters.

$$\omega = \frac{(\phi c)_f}{(\phi c)_f + (\phi c)_m} \tag{7.15}$$

By substitution of equation (7.15) into equation (7.9):

$$(\phi c)_f = \frac{\omega}{\Psi} \times \left[\frac{0.000264\, K_f}{\mu r_w^2}\right] \quad \& \quad (\phi c)_m = \frac{(\phi c)_f}{\omega} - (\phi c)_f \tag{7.16}$$

-Mechanical skin factor can be determined by extrapolating the semilog straight line during late times to flowing time of one hour. Expressing equation(7.7) in dimensional form:

$$1.151\left(\frac{P-P_{wf(1\text{-hour})}}{m_L^*}\right) = 1.151\times\log\left\{\frac{5.9294\times10^{-4}K_f\times(T=1)}{[(\phi c)_f+(\phi c)_m]\mu r_w^2}\right\}+S \qquad (7.17)$$

$$\therefore\ S = 1.151\times\left(\frac{P-P_{wf(1\text{-hour})}}{m_L^*}\right) - 1.151\times\log\left\{\frac{K_f}{[(\phi c)_f+(\phi c)_m]\mu r_w^2}\right\}+3.72 \qquad (7.18)$$

Alternatively, the value of skin factor can be estimated from the semilog straight line during fissure flow provided an estimate of the storage capacity ratio with respect to the formation is made.

-Whilst for known values of fissure and matrix compressibilities ($c_m$ & $c_f$), it is possible to estimate the porosity of the fissure system from equation (7.16), the correct estimate of the formation porosity is made by taking the water saturation of the matrix region into account.

$$\phi'_m = \frac{\phi_m}{1-\phi_f}\times\frac{1}{(1-s_{wi})} \qquad (7.19)$$

-The interporosity flow parameter can be estimated by considering the dimensional form of equation (7.6) at $T_D$=1:

$$\lambda = 0.56(1-\omega)\exp\left(-2.303\frac{\Delta P_\lambda}{m^*}\right) \qquad (7.20)$$

-Provided the matrix permeability is determined from laboratory measurements, the value of the contact surface parameter ($\alpha$) can be obtained from :

$$\alpha = \lambda\times\frac{1}{r_w^2}\times\frac{K_m}{K_f} \qquad (7.21)$$

-The block characteristic length of the formation may also be estimated for a uniformly spaced fractured network.

$$L^2 = 4n(n+2)\times\frac{r_w^2}{\lambda}\times\frac{K_m}{K_f} = \frac{4n(n+2)}{\alpha} \qquad (7.22)$$

## 7.3-CONVENTIONAL BUILD UP SCHEMES ASSOCIATED WITH THE SIF MODEL

In order to define the build up pressure equation associated with the [SIF] model, the following conditions must be implemented on equation (7.1).

$-\Delta T_D > 100\omega$ for $\lambda < 1$

$-\Delta T_D > (100\lambda - \lambda)/\lambda$ for $\omega << 1$

$$(P_D)_{BU} = 0.5\{ 2.303 \log[\frac{(T_P)_D + \Delta T_D}{\Delta T_D}] + E_i[\frac{\lambda \Delta T_D}{\omega (1-\omega)}] - E_i[\frac{\lambda \Delta T_D}{1-\omega}] \} + S \qquad (7.23)$$

Figure (7.4) represents the dimensionless build up pressure responses associated with the model and defined by equation (7.23).

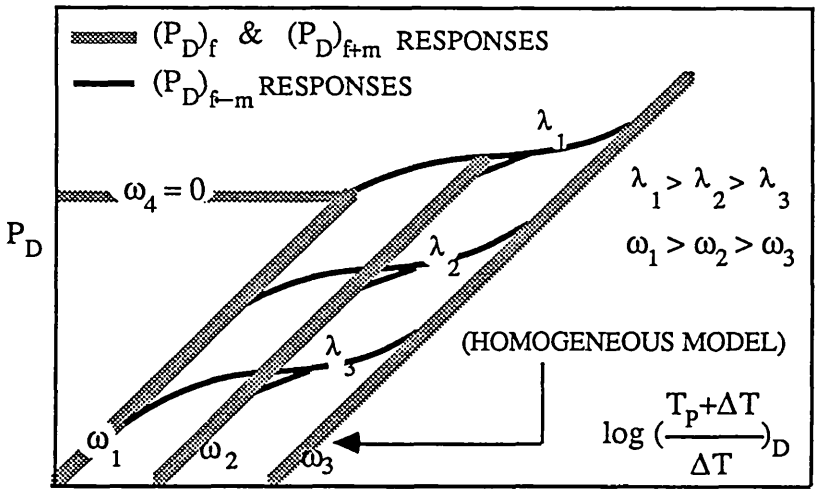



FIGURE 7.4: $(P_D)_{BU}$ RESPONSES WRT THE SIF MODEL ($r_D=\infty$)

With reference to figure (7.4), the three flow regions identifiable via draw down schemes, may be observed during a build up test.

-During early times, the build up solution is represented by the semilog line during fissure flow.

$$(P_D)_{BU\text{-}fissure} = 0.5\{ 2.303\log[\frac{(T_P)_D + \Delta T_D}{\Delta T_D}] + 2.303\log[\frac{1}{\omega}] \} + S \qquad (7.24)$$

-During transition period, the pressure drop across the matrix/fracture interface

stabilizes, representing massive fluid flow transfer from the fracture into matrix region. Provided that:

$$5 < \frac{\lambda \Delta T_D}{\omega(1-\omega)} < \infty \qquad \& \qquad 0 < \frac{\lambda \Delta T_D}{1-\omega} < 0.025 \tag{7.25}$$

Equation (7.23) may be expressed as:

$$(P_D)_{BU\text{-}(f-m)} = 0.5 \{ 2.303 \log[\frac{(T_p)_D + \Delta T_D}{\Delta T_D}] + 2.303 \log[\frac{\lambda \Delta T_D}{1-\omega}] \} + S \tag{7.26}$$

-During late times, the pressure responses within the formation become identical to the case of homogeneous system, and is characterized by the semilog straight line in the $(P_D)_{BU\text{-}f+m}$ vs $\log[\{(T_p)_D+\Delta T_D\}/\Delta T_D]$ plane, with the same slope compared to the initial flow period straight line but displaced by a factor of $Ln(\omega^{-0.5})$.

## 7.4-CHARACTERIZATION OF THE SIF MODEL VIA BUILD UP SCHEMES

From the plot of $\Delta P=(P_{ws}-P_{wf})$ vs $\log[(T_p+\Delta T)/\Delta T]$ in the two dimensional plane:

-The values of $K_f$, $\omega$, $(\phi c)_f$, $(\phi c)_m$, $[\alpha]$ and $[L^2]$ may be evaluated as outlined for the case of conventional draw down schemes, applicable to the fractured formations.

-The time parameter ($\Psi_{BU}$) which is used in estimation of the fissure and matrix storage capacities, is obtained in two stages.

1) Evaluations of $[\Psi]$ by means of equation (7.11).

2) Estimation of $[\Psi_{BU}]$ by considering the pressure drop at the end of the production period (equation 7.24).

$$\Delta P_p = m^* \log[2.246\, \Psi T_p] \tag{7.27}$$

$$\Psi_{BU} = \frac{0.445}{T_P} \times 10^{\left(\frac{\Delta P_P}{m^*}\right)} \tag{7.28}$$

-Interporosity flow parameter can be determined by considering the pressure drop measured at the inflection point during the transition period (figure 7.5).

$$\lambda = \frac{1-\omega}{\gamma \Psi_{BU}(T_P+\Delta T)} \times 10^{\left(\frac{\Delta P_\lambda}{m^*}\right)} \tag{7.29}$$

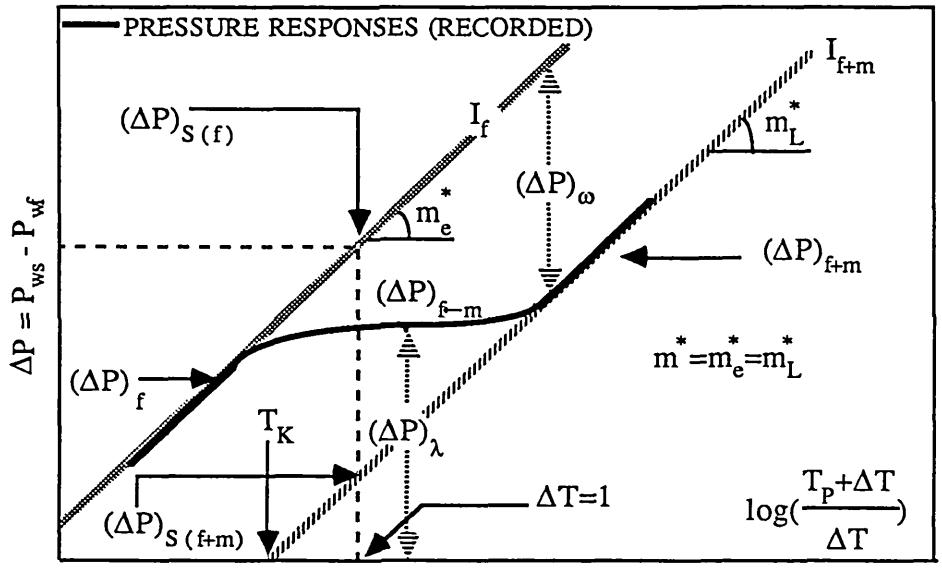



FIGURE 7.5: CHARACTERIZATION OF THE SIF MODEL VIA BUILD UP TESTS ($r_D=\infty$)

-Mechanical skin factor may be estimated by assuming that $(T_p+\Delta T)\cong T_P$ and hence extrapolating the dimensional build up pressure solution during late times (equation 7.26) to shut in time of one hour.

$$S = 1.151\left[\frac{P_{ws} - P_{wf(1\text{-hour})}}{m^*} - \log(T_p) - \log\{\frac{K_f}{[(\phi c)_f + (\phi c)_m]\mu r_w^2}\} + 3.23\right] \tag{7.30}$$

Equation (7.24) representing the dimensionless build up pressure responses during fissure flow can also be used to estimate the value of the mechanical skin factor.

## 7.5-CONVENTIONAL DRAWDOWN SCHEMES ASSOCIATED WITH THE TIF MODEL

Based on the definition of dimensionless time parameter in terms of total system storage capacity, equation (5.7) could be inverted into real space solution during early, intermediate and late times in order to establish the asymptotic expressions associated with the model.

-During early time flow periods, dominated by the fissure system, $F(g)\cong\omega$:

$$(P_D)_f = 0.5\ \{\ Ln(T_D) + 0.80907 + Ln(\frac{1}{\omega})\} + S \qquad (7.31)$$

-During transition periods, $F(g) \cong [\{\lambda(1-\omega)/3g\omega]^{0.5}$:

$$(P_D)_{f\leftarrow m} = 0.25\{\ Ln(T_D) + 1.0409 - Ln[\frac{\lambda(1-\omega)}{3}]\} + S \qquad (7.32)$$

-During late times, under the influence of the total system responses, F(g)=1:

$$(P_D)_{f+m} = 0.5\{\ Ln(T_D) + 0.80907\ \} + S \qquad (7.33)$$

With reference to equations (7.31)and (7.33), it is evident that the dimensionless pressure responses during early and late times are identical to their corresponding cases associated with the SIF model. In fact, the only difference between the two dimensionless pressure responses with regard to the two models occur during transition periods.

Figure (7.6) indicates that whilst the [SIF] model exhibits the characteristics of the pressure stabilization within the transition zone,the $P_D$-function responses with respect to the [TIF] model results in a semilog straight line with the slope defined by:

$$m_T^* = 0.5\ m_e^* = 0.5\ m_L^* = 0.5\times\ [162.5\ \frac{q\mu B_o}{K_f h}] \qquad (7.34)$$

Thus, in order to establish the time criteria with regard to the existence of the transitional semilog straight line, equation (7.32) was evaluated for different ranges

of [λ] and [ω] parameters. Using a tolerance level of ΔT=0.05, the resulting pointwise slope was compared with $m^*_T = 0.5757$ .

$$\Delta_T = | m'_T - m^*_T | \leq 0.05 \qquad (7.35)$$

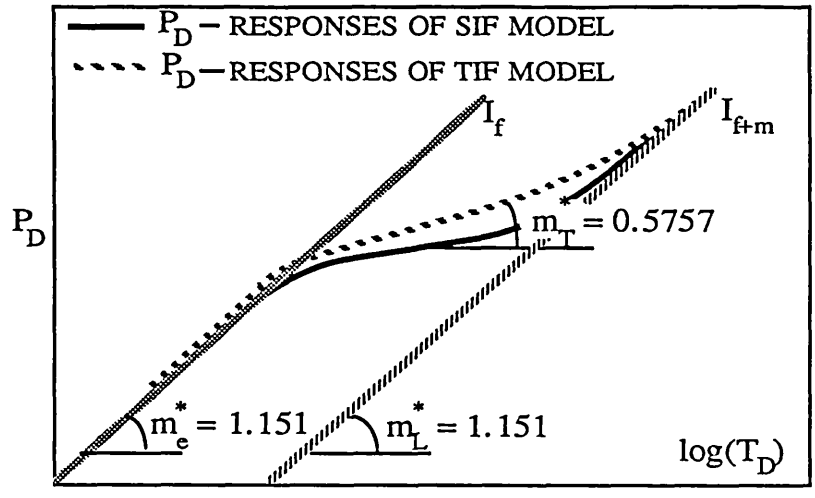



FIGURE 7.6: IDEALIZED $P_D$ RESPONSES OF THE SIF & TIF MODEL.

Based on the above procedures, it was revealed that for ω >0.01, reflecting the absence of the transitional semilog straight line, the tolerance level of 5% was never established. The assignment of ω ≤0.01, however, as well as satisfying equation (7.35), allowed the identification of the start and the end of the semilog lines (segment AB in figure 7.7).

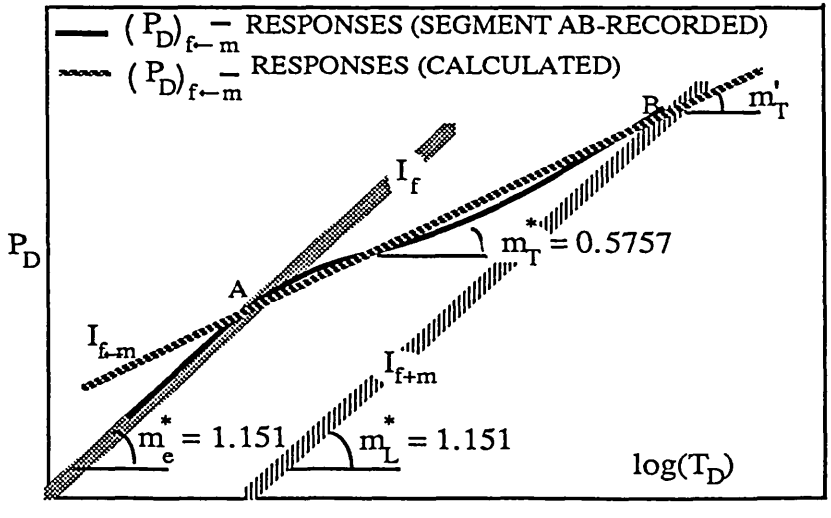



FIGURE 7.7: $(P_D)$-RESPONSES WRT THE TIF MODEL FOR SPECIFIC VALUES OF λ & ω

-Provided $\lambda(1-\omega)/\omega \leq 0.01$ then:

$$T_{Ds\,(f-m)} = \frac{380\omega^2}{\lambda(1-\omega)} \tag{7.36}$$

$$T_{De\,(f-m)} = \frac{0.63(1-\omega)}{\lambda} \tag{7.37}$$

Moreover, the analytical solution associated with the approximate start of the combined fissure and matrix responses, applicable for all ranges of [$\lambda$]and [$\omega$]parameters, were defined by considering the numerical ranges of equations (7.36) and (7.37).

$$T_{Ds\,(f+m)} = \frac{3.7(1-\omega)}{\lambda} \tag{7.38}$$

Whilst equation (7.36) implies that the time required to reach the transitional semilog straight line increases as the value of $[\lambda(1-\omega)/\omega^2]$ decreases, due to the presence of 3/4-log cycle transitional period between the definitions of $T_{De(f+m)}$ and $T_{Ds(f+m)}$ , such regions may not be apparent unless the recorded pressure data are plotted with an appropriate pressure scale.

Therefore it is evident that unless the correct segment of the recorded pressure data (during transition period) is chosen for characterization of the formation, the application of the transition related equations for the definition of the physical nature of the formation would almost certainly result in an incorrect estimation of the fissure permeability thickness by a factor of (2), which in turn would lead to the construction of an incorrect reservoir model.

## 7.6-CHARACTERIZATION OF THE TIF MODEL VIA DRAWDOWN SCHEMES

Based upon the assumption that the full reservoir pressure responses are observed during the test (figure 7.8), from a semilog plot of $\Delta P = P_i - P_{ws}$ vs log(T):

-Fissure permeability thickness may be defined from the slope of the semilog straight line during early, intermediate or late time flow periods:

$$K_f h = 162.5 \frac{q\mu B_o}{m_e^*} = 81.29 \frac{q\mu B_o}{m_T^*} = 162.5 \frac{q\mu B_o}{m_L^*} \qquad (7.39)$$

-The parameters $[\omega]$, $[\Psi]$, $[\phi c]_f$ and $[\phi c]_{f+m}$ may be obtained by means of similar procedures outlined in the case of the SIF model.

-Interporosity flow parameter can be evaluated by considering the intersection point of equations (7.32) and (7.33):

$$(T_D)_{ie} = \frac{3(1-\omega)}{e^{\gamma}\lambda} \qquad (7.40)$$

Expressing equation (7.40) in terms of dimensional form yields:

$$\lambda = 6380.2 \frac{(\phi c)_m \mu r_w^2}{K_f T_{ie}} \qquad (7.41)$$

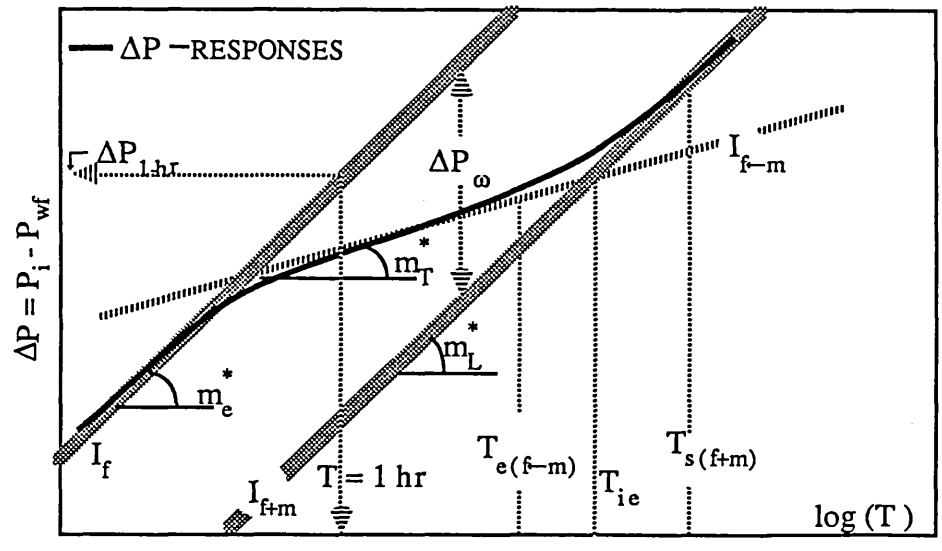



FIGURE 7.8: PRESSURE RESPONSES OF THE TIF MODEL ($I_f$, $I_{f-m}$, $I_{f+m}$ IDENTIFIED).

-Mechanical skin factor can be estimated by extrapolating the early time semilog straight line to flowing time of one hour.

$$S = 1.151 \{ \frac{\Delta P_{1\text{-hour}}}{m_e^*} - \log[\frac{K_f}{(\phi c)_f \mu r_w^2}] + 3.23 \} \quad (7.42)$$

-From the definition of the contact surface parameter ($\alpha$), the characteristic length of the matrix block can be evaluated.

$$L^2 = \frac{4n(n+2)}{\lambda K_f} r_w^2 K_m \quad (7.43)$$

-The approximate start and the end of the transition periods as well as the approximate starting time of the total system responses may be obtained from the dimensional form of equations (7.36), (7.37) and (7.38) respectively.

$$T_{s(f-m)} = 1.439 \times 10^6 \frac{(\phi c)_f^2 \mu r_w^2}{\lambda (\phi c)_m K_f} \quad (7.44)$$

$$T_{e(f-m)} = 2386.36 \times \frac{(\phi c)_m \mu r_w^2}{\lambda K_f} \quad (7.45)$$

$$T_{s(f+m)} = 14015.15 \times \frac{(\phi c)_m \mu r_w^2}{\lambda K_f} \quad (7.46)$$

It is remarked that the above procedures used in characterization of naturally fractured formations are only applicable for reservoirs with detectable full pressure responses during the three flow regimes. In practice however, due to the wellbore storage effects, the fissure semilog line corresponding to fissure flow (figure 7.9), is usually masked off. under such circumstances, having developed the semilog plot of the pressure data:

-Fissure permeability may be estimated by considering the transitional or late time semilog straight lines defined by equation (7.39).

-Provided that $\omega < 0.01$, by pre-determination of matrix storage capacity, the interporosity flow parameter can be estimated by means of equation (7.41).The condition imposed on equation (7.41) can also be removed by evaluating [$\lambda$] through equation (7.46) which is applicable for all ranges of storage capacity ratios.

-The mechanical skin factor can be determined by extrapolating the transitional semilog straight line to flowing time of one hour.

$$S = 0.5757\ \{\frac{\Delta P_{1\text{-hour}}}{m_T^*} - \log[\frac{K_f}{(\phi c)_m \mu r_w^2}] + \log[\lambda] + 2.6487\} \qquad (7.47)$$

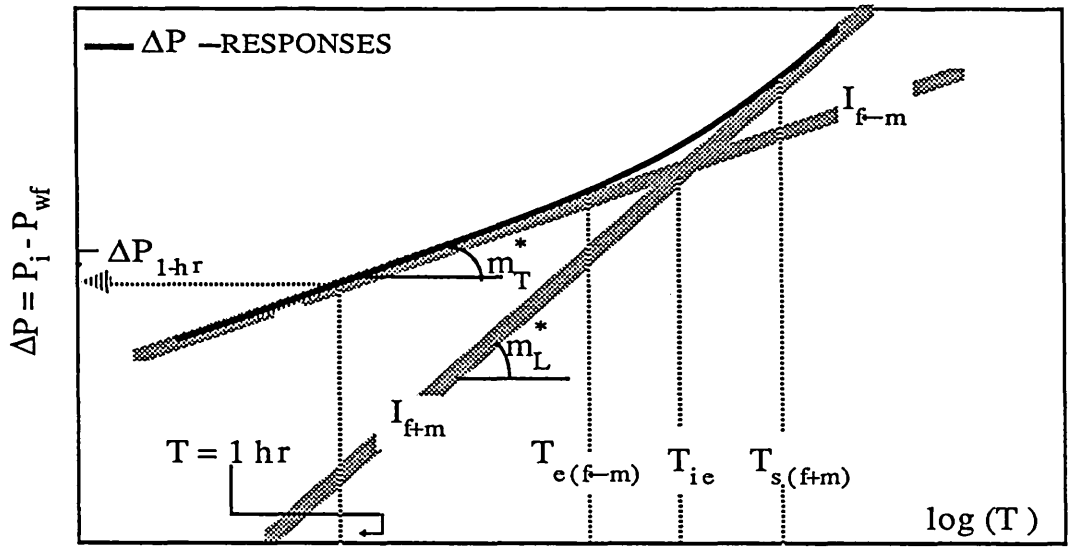



FIGURE 7.9: PRESSURE RESPONSES OF THE TIF MODEL IN THE ABSENCE OF FISSURE SLSL($I_f$)

-In view of the absence of fissure semilog straight line, the storage capacity ration may be estimated by considering the approximate start of the transitional flow period defined by equation (7.44).

$$\omega = \left[1 + \frac{(\phi c)_m \sqrt{\mu r_w^2}}{8.335 \times 10^{-4} \sqrt{K_f (\phi c)_m \lambda T_{s(f-m)}}}\right]^{-1} \qquad (7.48)$$

-From the substitution of the estimated interporosity flow parameter into equation (7.43) the characteristic length of the matrix block can be determined. For slab shape matrix blocks and one directional flow pattern, equation [7.43] can be expressed as:

$$L^2 = \frac{12}{\lambda} r_w^2 (K_m / K_f) \qquad (7.49)$$

Occasionally, only early and intermediate flow periods associated with the TIF model may be observed in the field. Such pressure responses which are not very common in practice, can be analysed by constructing the semilog plot of the recorded pressure data as depicted in figure (7.10). Form such a plot:

-Fissure permeability can be determined from either fissure or transitional semilog straight line slopes defined by equation(7.39).

-Assuming that the surface contact parameter and the matrix permeability are known, the interporosity flow parameter can be obtained from equation (7.43).

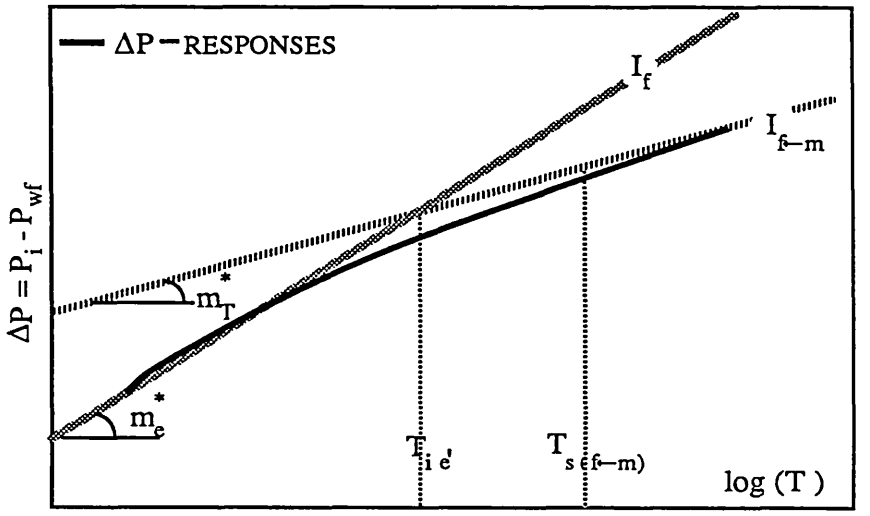



FIGURE 7.10: (ΔP)- RESPONSES OF THE TIF MODEL (TOTAL SYSTEM NOT DEFINED).

-Storage capacity ration may be estimated by considering the intersection point of fissure and transitional pressure responses defined by equations (7.31) & (7.32) respectively.

$$(T_D)_{i\cdot e} = \frac{1.6846\,\omega^2}{\lambda(1-\omega)} \tag{7.50}$$

Expressing equation (7.50) in terms of real time ($T_{ie'}$) yields:

$$\omega = \left[1 + \frac{(\phi c)_m \sqrt{\mu r_w^2}}{0.0125\sqrt{\lambda\,(\phi c)_m K_f\, T_{ie'}}}\right]^{-1} \tag{7.51}$$

-Mechanical skin factor can be evaluated through equations (7.42) and (7.47) which correspond to the extrapolated fissure and transitional semilog straight lines to flowing time of one hour.

-If desired, equations (7.44) and (7.45) can be employed in order to estimate the approximate duration of the transition period.

## 7.7-CHARACTERIZATION OF THE TIF MODEL VIA BUILD UP SCHEMES

The three basic dimensionless pressure responses during early, intermediate and late time flow periods defined by equations (7.31), (7.32) and (7.33) could be assigned to the theoretical build up equation in order to develop conventional testing schemes which are applicable to build up pressure data. In this presentation, however, in view of the unlikelihood of identifying the three flow regime during build up tests, the dimensionless build up pressure responses were derived based on the existence on only two sequential flow regimes.

Case A: $(P_D)_{BU}$-function associated with the transitional/total system responses.

Based on the assumption that the dimensionless shut in pressure reflects the pressure responses during transition periods, the dimensionless build up pressure can be expressed as:

$$(P_D)_{BU} = 1.151\{\log[\frac{(T_P+\Delta T)_D}{\sqrt{\Delta T_D}}] + 0.125 + 0.5\log[\frac{\lambda(1-\omega)}{3}]\} \qquad (7.52)$$

For large producing times, equation (7.52) is reduced to:

$$(P_D)_{BU} = 0.5757\{\log[\frac{(T_P+\Delta T)_D}{\Delta T_D}] + \log(T_P)_D + 0.25 + \log[\frac{\lambda(1-\omega)}{3}]\} \qquad (7.53)$$

With reference to equation (7.53), a plot of $(P_D)_{BU}$ vs $\log\{(T_P+\Delta T)_D/\Delta T_D\}$ would

yield a straight line (figure 7.11) of slope $m^*_T=0.5757$, and an intercept $C_{int}= 0.5757 \times \{\log(T_p)_D + \log[\lambda(1-\omega)/3]+0.25\}$.

If the dimensionless shut in pressure corresponds to the total system responses, then the associated dimensionless build up pressure will be given by:

$$(P_D)_{BU}= 1.151 \log[\frac{(T_p+\Delta T)_D}{\Delta T_D}] \qquad (7.54)$$

i.e. A semilog plot of $(P_D)_{BU}$ vs $[(T_p+\Delta T)_D/\Delta T_D]$ would yield a straight line of slope $m^*_L=1.151$ (figure 7.11).

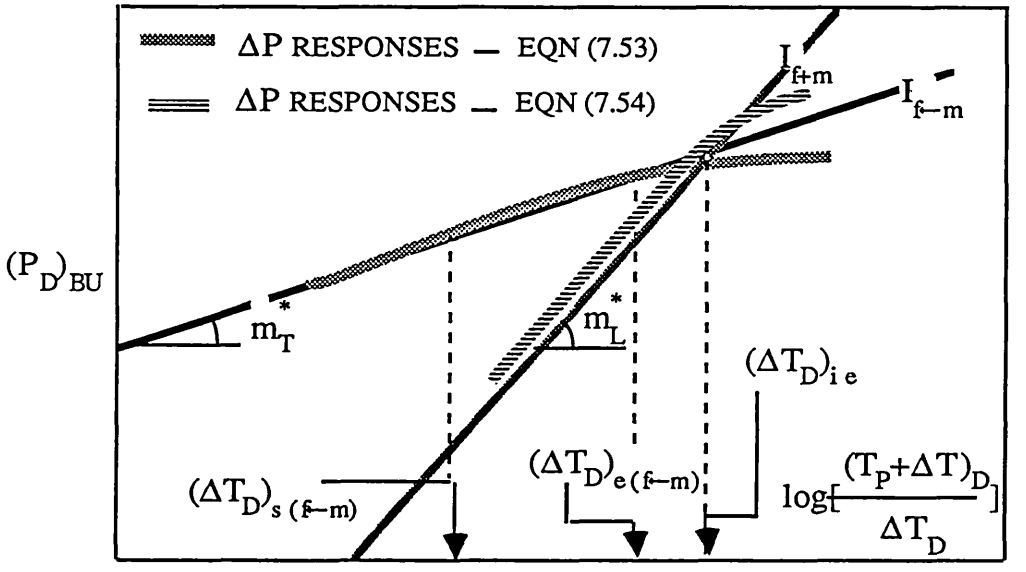



FIGURE 7.11: $(P_D)_{BU}$ RESPONSES OF TIF MODEL IN THE ABSENCE OF FISSURE FLOW SEGMENT

Based on 5% tolerance level, it was observed that the dimensionless shut in times corresponding to the end of transition and the start of late time flow periods possessed similar definitions represented by equations (7.36) and (7.37).

$$(\Delta T_D)_{e(f-m)} = \frac{380\,\omega^2}{\lambda(1-\omega)} \qquad (7.55)$$

$$(\Delta T_D)_{s(f+m)} = \frac{0.63\,(1-\omega)}{\lambda} \qquad (7.56)$$

Moreover, the intersection point between the transitional and late times semilog straight lines corresponding to $(\Delta T_D)_{ie}$ was obtained from equation (7.53) and (7.54).

$$(\Delta T_D)_{ie} = \frac{3\,(1-\omega)}{e^{\gamma}\lambda} \qquad (7.57)$$

Referring to equations (7.40) and (7.57), it is evident that the dimensionless flowing and shut in times corresponding to $(T_D)_{ie}$ and $(\Delta T_D)_{ie}$, have identical format. Thus, provided the flow times are replaced by shut in times, having constructed the Horner build up plot, the recorded pressure data can be analysed by means of draw down schemes in order to identify the physical nature of the formation . Referring to figure (7.12):

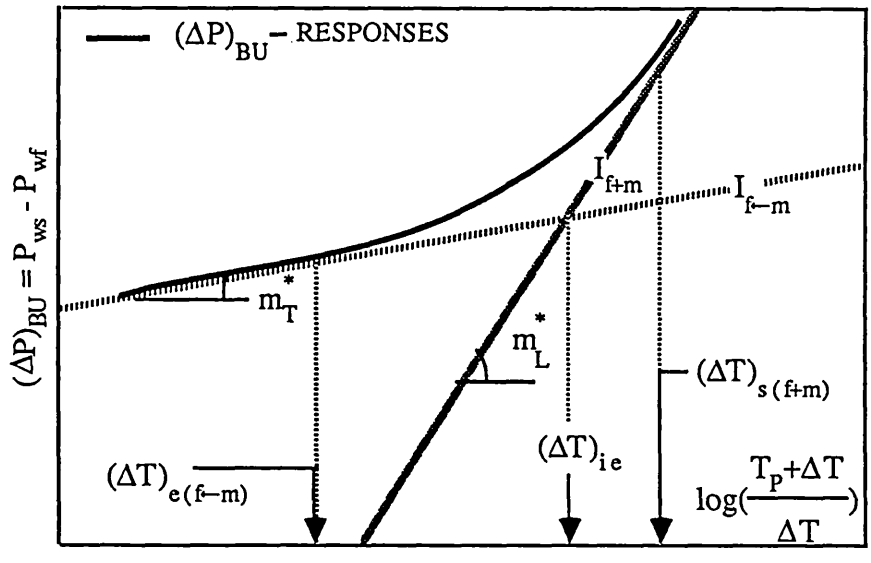



FIGURE 7.12: BUILD UP RESPONSES OF TIF MODEL IN THE ABSENCE OF FISSURE FLOW REGION

-Fissure permeability may be obtained from the slope of the semilog straight lines during transition or late time flow periods (defined by equation 7.34).

-Interporosity flow parameter and storage capacity ratio of the formation can be estimated from equations (7.46) and (7.48) respectively.

-The mechanical skin factor can be determined from equation(7.47).

-The characteristic length of the matrix block may be obtained from equation (7.49) (for the case of slab shape matrix blocks).

Case B: $(P_D)_{BU}$-function wrt fissure/transitional responses.

Assuming that $P_D(\Delta T_D)$-function corresponds to the dimensionless shut in pressure responses of the fissure system, the dimensionless build up pressure may be defined by:

$$(P_D)_{BU} = 1.151\{\log[\frac{(T_P+\Delta T)_D}{\Delta T_D}] - \log\sqrt{T_D} - 0.125 - 0.5\log[\frac{\lambda(1-\omega)}{3}]\} \qquad (7.58)$$

i.e. A Horner plot of recorded pressure data in semilog plane would result to the definition of a semilog straight line of slope $m^*_e=1.151$ and an intercept $C_{int}=-1.151\times\{\log[T_D]+[1/8]+[0.5L(1-\omega)/3]\}$.

When $P_D(\Delta T_D)_{BU}$-function represents the dimensionless shut in pressure responses during transition periods, then:

$$(P_D)_{BU} = 0.5757\{\log[\frac{(T_P+\Delta T)_D}{\Delta T_D}]\} \qquad (7.59)$$

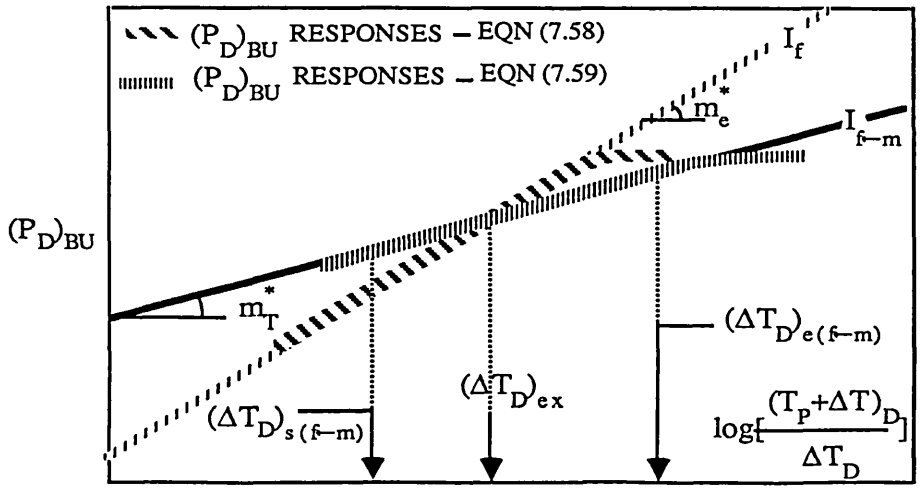



FIGURE 7.13: $(P_D)_{BU}$ RESPONSES OF TIF MODEL (TOTAL SYSTEM RESPONSES NOT DEFINED).

With reference to equation (7.59), a semilog plot of $(P_D)_{BU}$ vs $\log\{(T_p+\Delta T)_D/\Delta T_D\}$ should result in a semilog straight line during transitional pressure responses of the formation with a slope of $m^*_T=0.5757$.

Whilst the 5% slope tolerance level was employed to establish the approximate start of the transition period corresponding to the dimensionless shut in time $(\Delta T_D)_{s(f-m)}$, equations (7.58) and (7.59) allowed the definition of $(\Delta T)_{ex}$ which reflected the relationship between the intersection shut in time of fissure and transitional periods with the interporosity flow / storage capacity parameters.

$$(\Delta T_D)_{s(f-m)} = \frac{380\,\omega^2}{\lambda(1-\omega)} \tag{7.60}$$

$$(\Delta T_D)_{ex} = \frac{1.6846\,\omega^2}{\lambda(1-\omega)} \tag{7.61}$$

In view of the similarities between equations (7.50) and (7.61), in order to analyse the recorded pressure data associated with the fissure and transitional responses, a plot of $[\Delta P]$ vs $\log[(T_p+\Delta T)/\Delta T]$ is made ( figure 7.14) and hence, from the plot:

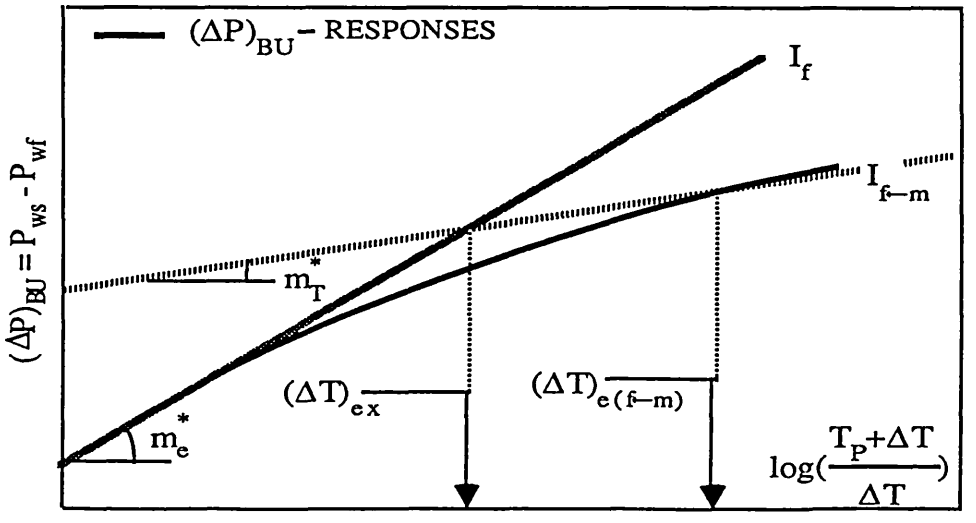



FIGURE 7.14: $(\Delta P)_{BU}$ RESPONSES OF THE TIF MODEL ($I_{f+m}$ SLSL NOT DEFINED).

-Fissure permeability is estimated from equation (7.34) by considering the slope of the fissure or transitional semilog straight lines.

-By replacing the flowing times with the shut in times, the interporosity flow parameter and storage capacity ratio are obtained from equations (7.43) and (7.51) respectively.

-The approximate start and the end of the transitional period is obtained from the dimensional forms of equation (7.55) and (7.60).

-Finally the mechanical skin factor is evaluated by means of equations (7.42) or (7.47) with $(\Delta P)_{1hour} = (P-P_{wf\text{-}1hour})$ replaced by $(\Delta P)_{1hour}=(P_{ws\text{-}1hour}-P_{wf})$.

☆☆☆☆☆☆☆☆☆☆

# CHAPTER 8

# HYDRAULICALLY FRACTURED FORMATIONS

## 8.1-PRESSURE RESPONSES OF HYDRAULICALLY FRACTURED FORMATIONS

Perhaps, the most important aspects of hydraulic fracturing operations within the oil industry are:

-Enhancing the well performance by creating deep penetrating fractures in the formation.

-Eliminating wellbore damage effects caused by the invasion of drilling fluid and filtrate into the matrix.

-Improving secondary / tertiary recovery operations by producing high capacity flow channels into the producing well.

Therefore, In order to investigate the pressure responses of such formations which are frequently encountered in field practice, the two theoretical reservoir models with distinct fracture surface boundary conditions[30,31] (i.e. uniform flux fracture-UFF and infinite conductivity vertical fracture-ICF) were subjected to the following assumptions:

-The formation is bounded by two horizontal and impermeable layers and exhibit homogeneous and isotropic behaviour.

-A single phase fluid of small compressibility flows from the porous medium into the induced fracture at a constant rate at time zero. It also satisfies the following condition.

-$c_{fl}$ , $c_{fl}$ = $f$(Formation pressure).

-Hydraulic fracturing process develops single plane vertical fracture of zero thickness which extends across the entire formation and intersects the least principal stress plane of the formation at right angle (figure 8.1).

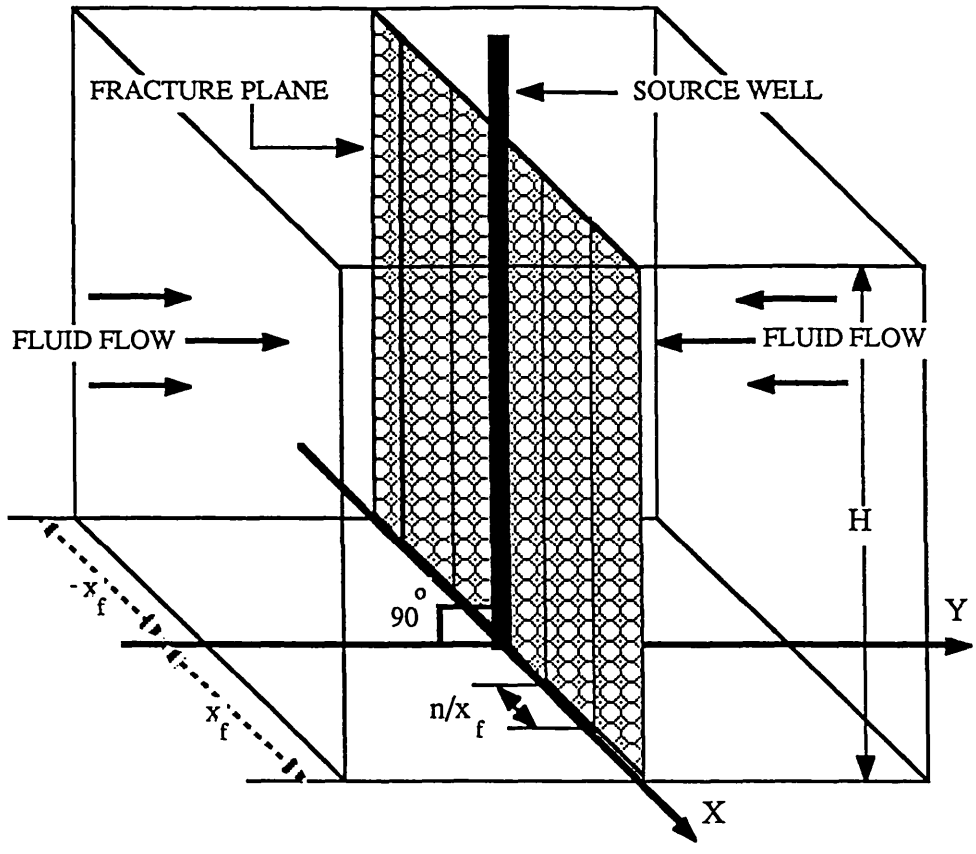



FIGURE 8.1: SINGLE PLANE VERTICAL FRACTURE (ACROSS THE ENTIRE FORMATION)

-whilst the uniform flux assumption implies little variation of pressure on the fracture surface, the infinite conductivity vertical fracture reflects zero pressure drop on the fracture plane.

-The producing pressure over the fracture plane which is the main source of production, is considered to be uniform, thus satisfying:

$$q_T = 2\sum_{n=1}^{N} q_n H\left(\frac{x_f}{N}\right) \qquad (8.1)$$

Where N=Total number of stripes associated with the fracture plane.

$q_n$=Uniform flow rate with respect to n.th stripe.

$q_T$=total flux distribution over the fracture plane.

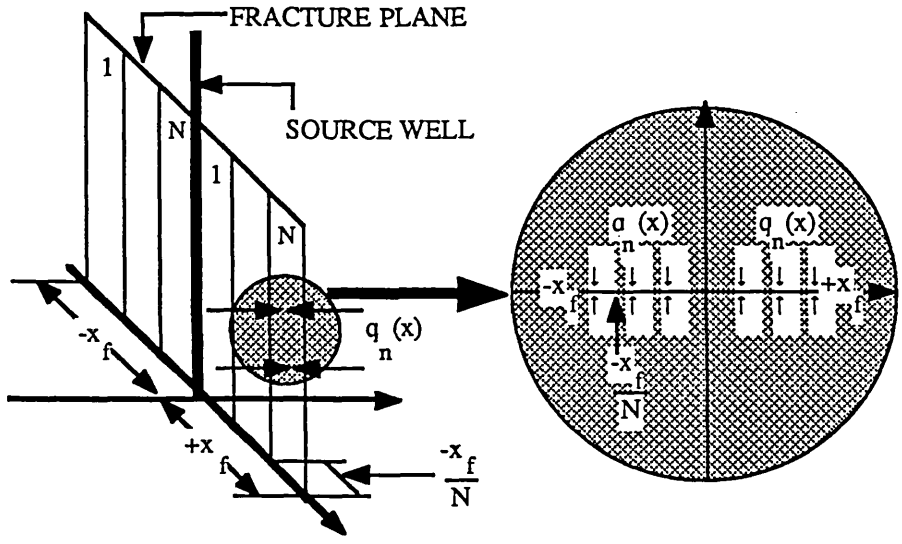



FIGURE 8.2: FLUID FLOW INTO THE FRACTURE PLANE (2N SEGMENTS)

-During the initial production period, when boundary effects are not detected.

Based on the preceding conditions, the theoretical pressure responses of both the models at the wellbore were hence defined by means of the line source and Green functions.

-Infinite external boundary status (figure8.3):

$$\Delta P = \frac{1}{\phi c}\int_0^T \left[ \sum_{n=1}^{N} q_n(u) \int_{L_1}^{L_2} e^{a}\, dx_w - \sum_{n=1}^{N} q_n(u) \int_{-L_1}^{-L_2} e^{a}\, dx_w \right] \frac{du}{4\pi\mu(T-u)} \qquad (8.2)$$

With $a = -\dfrac{(x-x_w)^2+y^2}{4\mu(T-u)}$ ♦ $L_1 = \dfrac{(n-1)}{N}x_f$ ♦ $L_2 = \dfrac{n}{N}x_f$ ♦ $x_D = \dfrac{x}{x_f}$ (Pressure point)

Considering the pressure variations on the fracture plane during early times, equation (8.2) may be expressed as:

$$P_{DF} = 0.5\sqrt{\pi T_{DF}} \left[ erf\left[\frac{(1-x_D)}{2\sqrt{T_{DF}}}\right] + erf\left[\frac{(1+x_D)}{2\sqrt{T_{DF}}}\right] \right] + \frac{(1-x_D)}{4} Ei\left[\frac{(1-x_D)^2}{4T_{DF}}\right] + \frac{(1+x_D)}{4} Ei\left[\frac{(1+x_D)^2}{4T_{DF}}\right] \qquad (8.3)$$

$$\text{With} \quad T_{DF} = \frac{0.000264\,KT}{\phi \mu c_t x_f^2} \tag{8.4}$$

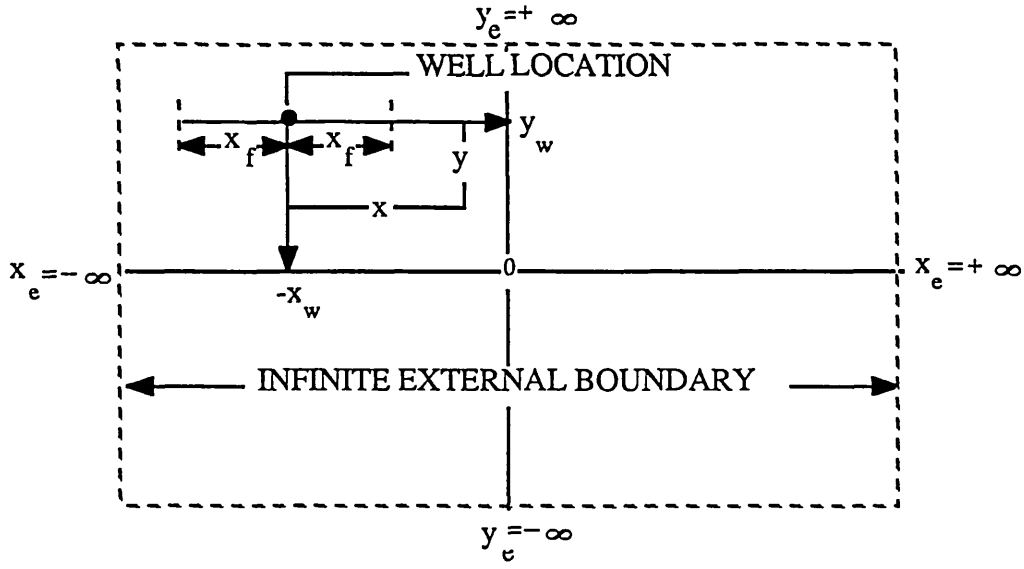



FIGURE 8.3: FRACTURED WELL IN AN INFINITE ACTING FORMATION

-Closed external boundary status (figure 8.4):

$$P_{DF} = 2\pi \int_0^{T_{DA}} \{ 1+2\sum_{n=1}^{\infty} e^{\varsigma_n x} \alpha_n \} \times \{ 1+2\sum_{n=1}^{\infty} e^{B_n x} \gamma_n \Theta_n \} dx \tag{8.5}$$

Where $$T_{DA} = T_{DF} \{ \frac{x_f}{\sqrt{A}} \}^2 \tag{8.6}$$

$$\varsigma_n = -n^2\pi^2 \frac{x_e}{y_e} = B_n (\frac{x_e}{y_e})^2 \tag{8.7}$$

$$\alpha_n = \cos[\frac{n\pi}{2}(1+\frac{y_w}{y_e})] \cos[\frac{n\pi}{2}(1+\frac{y_w}{y_e} + \frac{2y}{x_f} \times \frac{x_f}{\sqrt{A}} \sqrt{\frac{x_e}{y_e}})] \tag{8.8}$$

$$\gamma_n = \frac{\sin[n\pi \frac{x_f}{\sqrt{A}} / \sqrt{\frac{x_e}{y_e}}]}{\{n\pi \frac{x_f}{\sqrt{A}} / \sqrt{\frac{x_e}{y_e}}\}} \tag{8.9}$$

$$\Theta_n = \cos\left[\frac{n\pi}{2}\left(1+\frac{x_w}{x_e}\right)\cos\left[\frac{n\pi}{2}\left(1+\frac{x_w}{x_e}+2\frac{x}{x_f}\times\frac{x_f}{\sqrt{A}}\Big/\sqrt{\frac{x_e}{y_e}}\right)\right]\right] \quad (8.10)$$

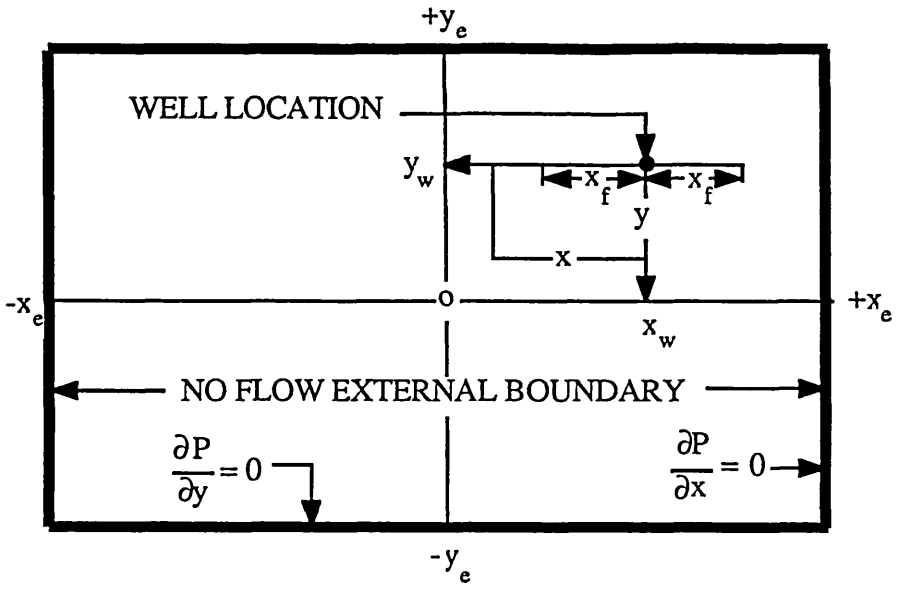



FIGURE 8.4: FRACTURED WELL IN A CLOSED RECTANGULAR RESERVOIR

## 8.2-PRESSURE RESPONSES ASSOCIATED WITH THE UFF MODEL

In order to comply with the basic assumptions of UFF model and generate useful working type curves for analysing the pressure data of such formations, the wellbore pressure responses were evaluated at the centre of the fracture plane (i.e. $x/x_f=y/x_f=0$). Based on the infinite acting external boundary assumption, equation (8.3) was approximated during:

-Early flow periods (when the fluid flow along the fracture occurs under linear system).

$$P_{DF} = \sqrt{\pi T_{DF}} \quad (8.11)$$

-And late times (when the incremental flow rates $[q_n(x)]$ are stabilized).

$$P_{DF} = 0.5\{\,\mathrm{Ln}(T_{DF}) + 2.80907\} + \mathrm{Ln}\left[\frac{|1-x_D|^{(x_D-1)}}{|1+x_D|^{(x_D+1)}}\right] \quad (8.12)$$

With closed external boundary assumption , the dimensionless pressure responses for a well at the centre of the rectangular reservoir model (figure 8.4) were defined during:

-Late transition periods.

$$P_{DF}=2\pi\left[\left[T_{DA}+\sum_{n=1}^{\infty}\frac{2\alpha_n e^{\varsigma_n T_{DA}}}{\varsigma_n}+\sum_{n=1}^{\infty}\frac{2\alpha_n\gamma_n e^{B_n T_{DA}}}{B_n}+\sum_{m=1}^{\infty}\sum_{n=1}^{\infty}\frac{4\alpha_m\gamma_m}{(\varsigma_n+B_m)}\alpha_n e^{(\varsigma_n+B_m)T_{DA}}\right]-\left[\sum_{n=1}^{\infty}\frac{2\alpha_n}{\varsigma_n}+\sum_{n=1}^{\infty}\frac{2\alpha_n\gamma_n}{B_n}+\sum_{m=1}^{\infty}\sum_{n=1}^{\infty}\frac{4\alpha_m\gamma_m}{(\varsigma_n+B_m)}\alpha_n\right]\right] \quad (8.13)$$

-And pseudo steady state flow periods.

$$P_{DF}=2\pi T_{DA}+(P_{DF})_{UFF} \quad (8.14)$$

With

$$(P_{DF})_{UFF}=\pi\sqrt{\frac{x_e}{y_e}}\left[\frac{1}{6}\sqrt{\frac{x_e}{y_e}}+\frac{1-6R_1^2}{12R_1}+\frac{R_2}{3}\left(\frac{x_f}{\sqrt{A}}\right)-\frac{1}{8\pi^2R_1}\sqrt{\frac{y_e}{x_e}}\sum_{n=1}^{\infty}U_n\right] \quad (8.15)$$

$$R_1=\frac{x_f}{\sqrt{A}}\sqrt{\frac{x_e}{y_e}}=R_2\left(\frac{x_e}{y_e}\right) \quad (8.16)$$

$$U_n=\frac{8R_2}{n^2}\left(\frac{x_e}{y_e}\right)e^{-n\pi}\times\frac{\left[1-e^{\{R_3(1-2R_2)\}}\right]}{\left[1-e^{\{R_3\}}\right]} \quad (8.17)$$

$$R_3=-2n\pi\left(\frac{x_e}{y_e}\right) \quad (8.18)$$

The type curves of figure (8.5) were generated by superimposing the dimensionless pressure responses during early and late time flow periods defined by equations (8.11) and (8.12), with a set of type curves which represent the late transition and stabilized pseudo steady flow periods associated with bounded formations and defined by equations

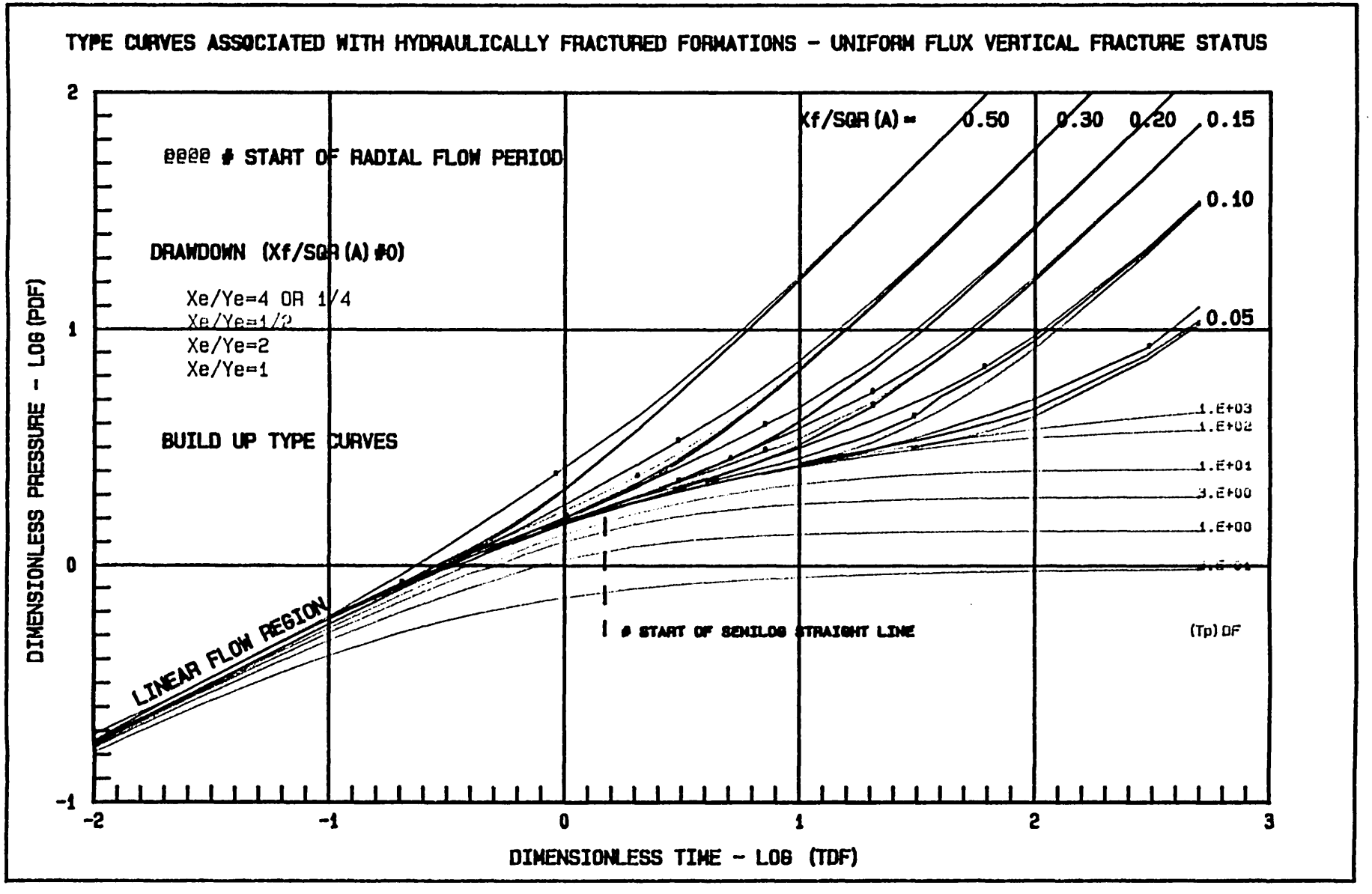



FIGURE 8.5: DIMENSIONLESS PRESSURE RESPONSES OF A WELL AT THE CENTRE OF HOMOGENEOUS/RECTANGULAR FORMATION (UFF MODEL)

(8.13) and (8.14).

With reference to equation (8.13), by assigning the summation parameter n=20, the dimensionless pressure response solutions compared favourably with those generated by Gringarten. Surprisingly however, no mention was made with regard to the actual computation time of equation (8.6).

The particular choice of the summation parameter value, in fact resulted in computational steps of over 1000+, for each incremental time function $T_{DF}$. IN terms of real time, this corresponds to approximately 45 minutes for generating just one type curve based on specific values of $[x_f/\sqrt{A}]$ and $[x_e/y_{e]}$ parameters.

However, by introducing the correction term [CTR] and assigning summation parameter to n=5, it was possible to reduce the total computational time by 10 folds. The [CTR] concept proved particularly advantageous when the recorded pressure data did not match with any of the type curves of figure (8.5), as it allowed the generation of specific pressure responses (associated with a well at an arbitrary location within the rectangular formation) within reasonable time.

$$CTR \cong \frac{0.04}{x_f/\sqrt{A}} + 0.01\left(\frac{x_e}{y_e}\right) \quad \text{for} \quad \frac{x_e}{y_e} \leq 1 \tag{8.19}$$

$$CTR \cong \frac{0.08}{x_f/\sqrt{A}} \quad \text{for} \quad \left(\frac{x_e}{y_e}\right) < 1 \tag{8.20}$$

## 8.3-BUILD UP PRESSURE RESPONSES WITH RESPECT TO THE UFF MODEL

In order to extent the application of the draw down type curves of figure (8.5) to build up pressure data, the early and late times pressure solutions represented by equations (8.11) and (8.12) were implemented into the theoretical build up responses defined by:

$$(P_{DF})_{BU} = P_{DF}\{(T_P)_{DF}\} + P_{DF}\{T_{DF}\} - P_{DF}\{(T_P)+T_{DF}\} \tag{8.21}$$

Based on a tolerance level of 5% between early and late time pressure responses, the

build up type curves, characterized by the dimensionless producing time $(T_p)_{DF}$ were hence generated via equation (8.21) and then superimposed on figure (8.5).

As expected, observation of $(P_{DF})_{BU}$ responses with respect to $(T_p)_{DF}$ revealed that for $(T_p)_{DF}$ >1000, the build up and draw down solutions become identical (i.e. For large values of draw down duration, the build up data may be analysed via draw down type curves).

## 8.4-PRESSURE RESPONSES ASSOCIATED WITH THE ICF MODEL

With the assumption of infinite conductivity vertical fracture at the centre of the formation, the dimensionless wellbore pressure responses associated with the model were computed at 73.2% of the fracture half length [$x_f$] from the centre of the fractured region ($x/x_f$=0.732 & $y/x_f$=0). The particular choice of the pressure point location ensured stabilized flow rate distribution along the vertical fracture.

Subject to the infinite boundary condition, equation (8.3) was reduced to:

$$P_{DF} = 0.5\sqrt{\pi T_{DF}}\left[\operatorname{erf}\left[\frac{0.134}{\sqrt{T_{DF}}}\right]+\operatorname{erf}\left[\frac{0.866}{\sqrt{T_{DF}}}\right]\right]+0.067\,\mathrm{Ei}\left[\frac{0.018}{T_{DF}}\right]+0.433\,\mathrm{Ei}\left[\frac{0.75}{T_{DF}}\right] \qquad (8.22)$$

during early flow periods, and:

$$P_{DF} = 0.5\,\mathrm{Ln}(T_{DF}) + 1.1 \qquad (8.23)$$

duirng late times.

Assuming closed external boundary status, the dimensionless pressure responses were determined during:

-Late transition periods.

$$P_{DF}=2\pi\left[\left[T_{DA}+\sum_{n=1}^{\infty}\frac{2\alpha_n e^{\varsigma_n T_{DA}}}{\varsigma_n}+\sum_{n=1}^{\infty}\frac{2\gamma_n\theta_n e^{B_n T_{DA}}}{B_n}+\sum_{m=1}^{\infty}\sum_{n\neq}^{\infty}\frac{4\gamma_m\theta_m}{(\varsigma_n+B_m)}\alpha_n e^{(\varsigma_n+B_m)T_{DA}}\right]-\left[\sum_{n=1}^{\infty}\frac{2\alpha_n}{\varsigma_n}+\sum_{n=1}^{\infty}\frac{2\gamma_n\theta_n}{B_n}+\sum_{m=1}^{\infty}\sum_{n=1}^{\infty}\frac{4\gamma_m\theta_m}{(\varsigma_n+B_m)}\alpha_n\right]\right] \quad (8.24)$$

-And pseudo steady state flow periods.

$$P_{DF}=2\pi T_{DA}+(P_{DF})_{ICF} \quad (8.25)$$

$$(P_{DF})_{ICF}=\pi\sqrt{\frac{x_e'}{y_e}}\times\left[\frac{1}{6}\sqrt{\frac{x_e'}{y_e}}+\frac{1-14.784R_1^2}{12R_1}+1.7973R_2-\frac{1}{8\pi^2R_1}\sqrt{\frac{y_e'}{x_e}}\sum_{n=1}^{\infty}W_n\right] \quad (8.26)$$

$$W_n=\frac{1.072R_2}{n^2}\left(\frac{x_e}{y_e}\right)e^{-n\pi}\times\left[1-e^{[R_3(1-2R_2)]}\right]\left[1+e^{[R_3(1.464R_2)]}\right] \quad (8.27)$$

The type curves of figure (8.6), representing the dimensionless pressure responses with respect to ICF model were hence generated by superimposing the early and late times pressure solutions defined by equations (8.22) and (8.23) and characterized by $x_f/\sqrt{A}=0$, with dimensionless pressure responses during late transition and infinite acting radial flow periods (under the influence of closed external boundary condition), which were characterized by the dimensionless groups $[x_f/\sqrt{A}]$, $[x_e/y_e]$, $[x_w/y_e]$, $[y_w/y_e]$ and defined by equations (8.24) and (8.25).

With reference to figures (8.5) and (8.6), it became evident the dimensionless pressures specific to $[x_f/\sqrt{A}]$ parameter, provided identical responses during semi-steady state flow periods which in turn created the possibility of choosing an incorrect value of the external boundary ratio of the formation when matching the actual recorded data. Therefore, in order to increase the degree of confidence with regard to

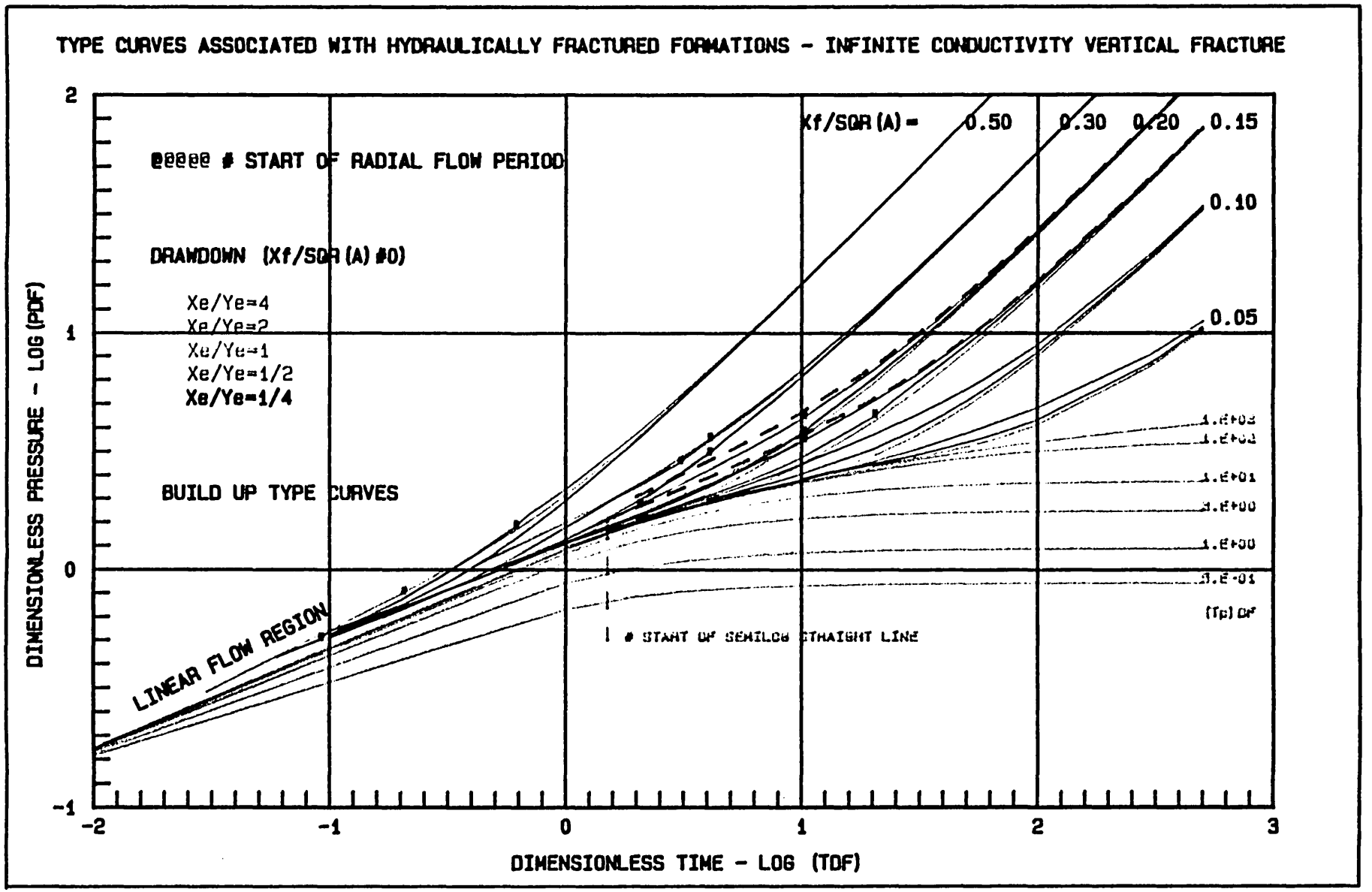



FIGURE 8.6: DIMENSIONLESS PRESSURE RESPONSES OF A WELL AT THE CENTRE OF HOMOGENEOUS/RECTANGULAR FORMATION (ICF MODEL)

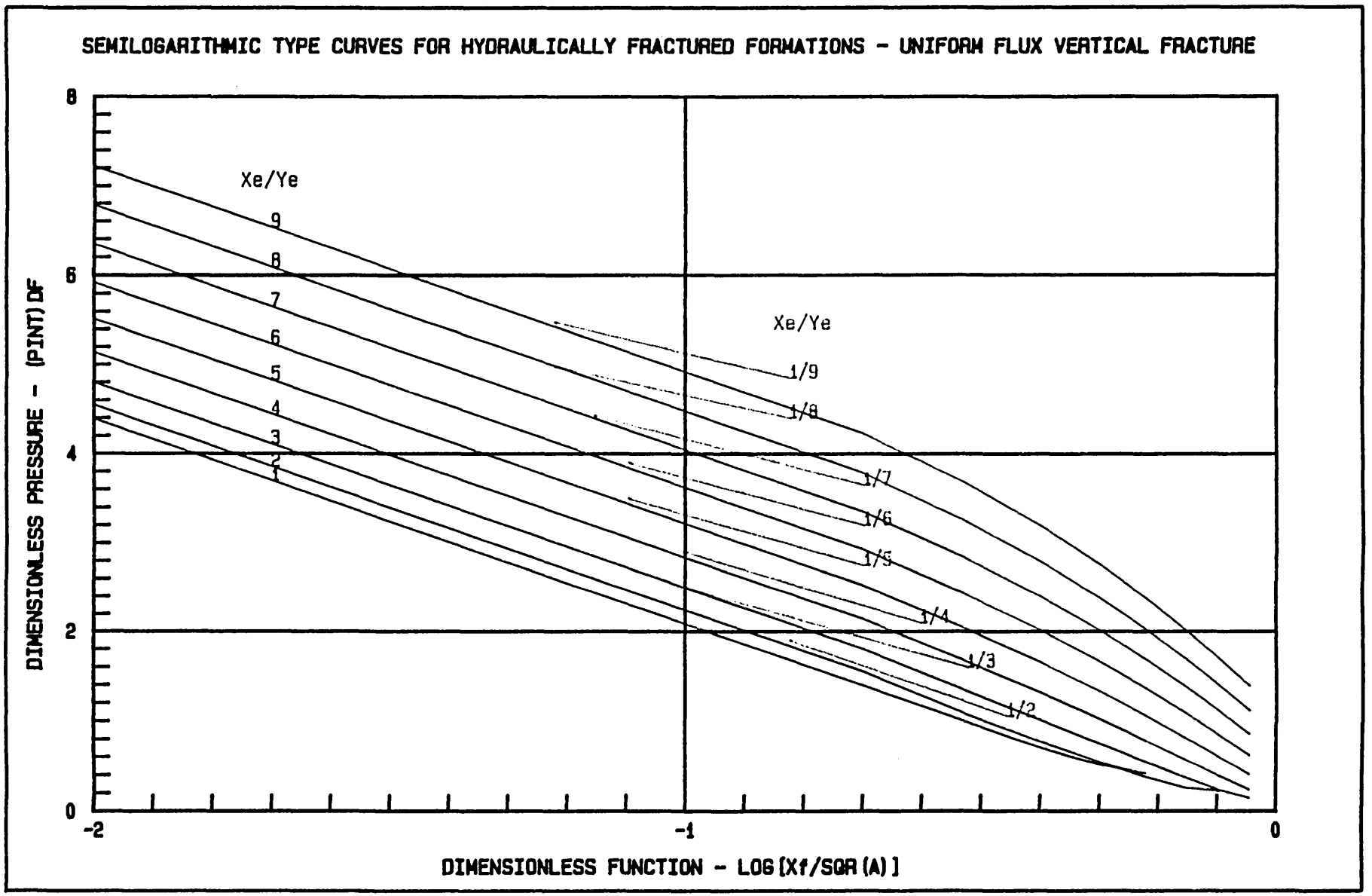



FIGURE 8.7: (PINT)DF DEFINITION FOR A WELL AT THE CENTRE OF A CLOSED HOMOGENEOUS/RECTANGULAR FORMATION (UFF MODEL)

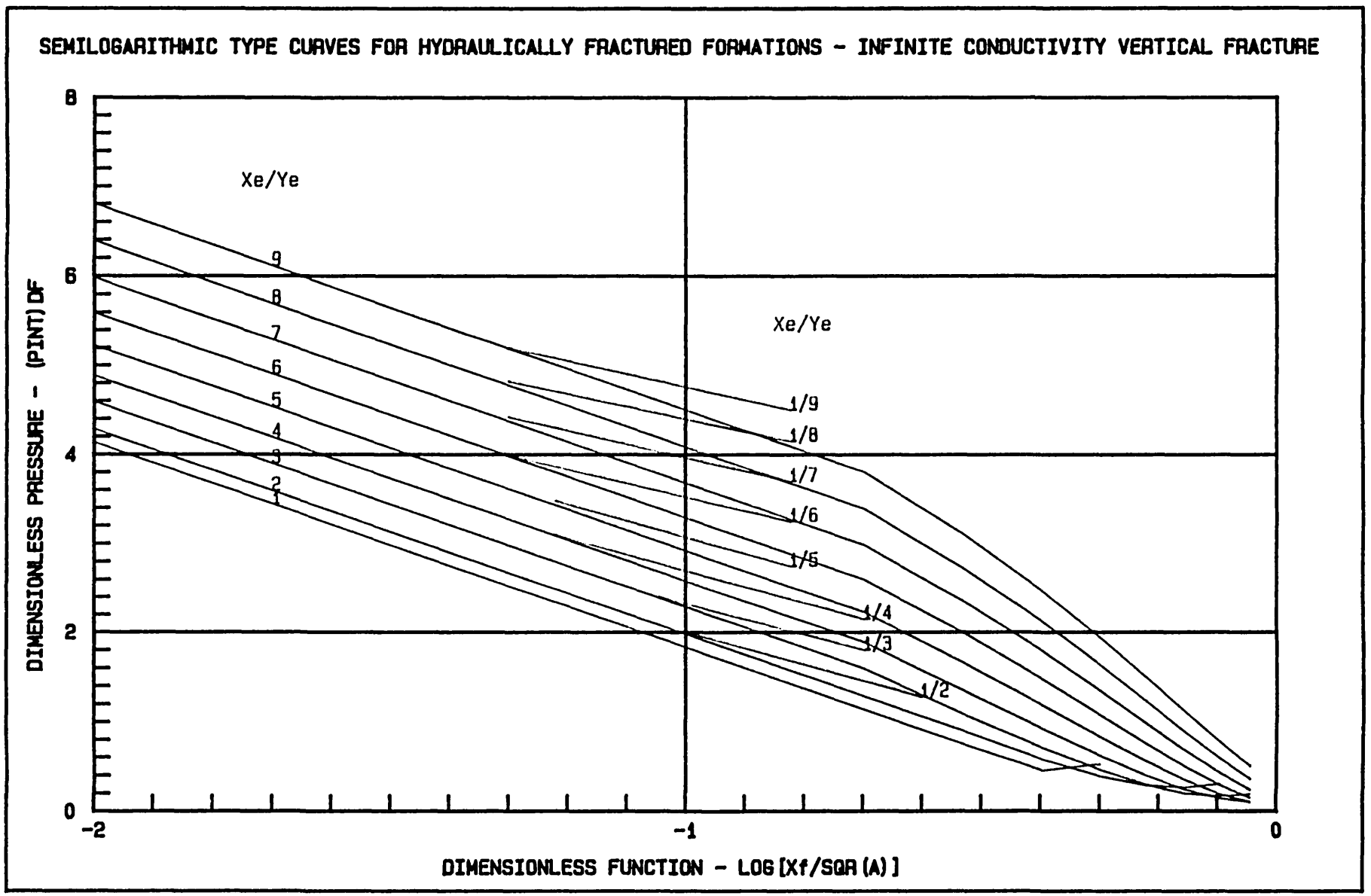



FIGURE 8.8: (PINT)DF DEFINITION FOR A WELL AT THE CENTRE OF A CLOSED HOMOGENEOUS/RECTANGULAR FORMATION (ICF MODEL)

the interpretation of the pressure data in the pseudo steady state region, the dimensionless pressures associated with both the models (defined by equations (8.15) and (8.26) respectively) were graphed as log( $x_f/\sqrt{A}$ ) vs $(P_{DF})_{UFF/ICF}$ (figures 8.7 & 8.8). These plots in turn were used to check the validity of the initial estimate of the drainage area by means of the type curves of figures (8.5) and (8.6).

## 8.5-BUILD UP PRESSURE RESPONSES WITH RESPECT TO THE ICF MODEL

Using similar procedures outlined previously, equations (8.22) and (8.23) were coupled with the general theoretical build up responses (defined by equation 8.21) in order to generate the build up type curves associated with the [ICF] model.

For small dimensionless producing times, however, it was observed that the tolerance level of 5% between early and late time build up solutions was not satisfied, and although it was possible to increase the tolerance level, such an action resulted in uneven transitional periods.

In order to develop a smooth transition period, it is suggested to :

1-Evaluate $(P_{DF})_{BU}$ at $T_{DF}$=1 through equation (8.23) and extrapolate linearly back to $(P_{DF})_{TDF}$=0.01 with the slope of the line equal to 0.5.

2-Generate $(P_{DF})_{BU}$ with respect to the ICF model for $T_{DF}$>1 using equation(8.23).

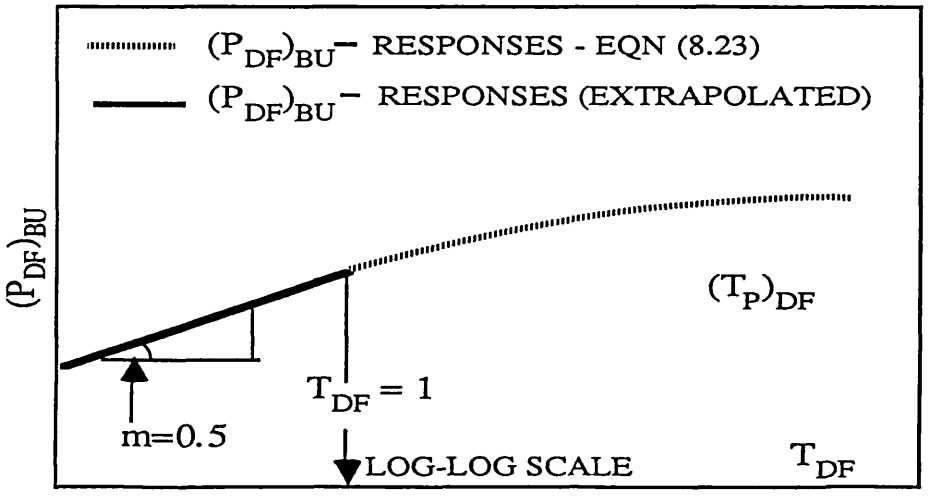



FIGURE 8.9: $(P_{DF})_{BU}$ RESPONSES OF ICF MODEL (EXTRAPOLATED @ EARLY TIMES)

The main drawback associated with the build up responses of figures (8.5) and (8.6) occurs when the draw down duration is terminated during the late transient flow periods (i.e. external boundary effects of the formation prevail) restricting the use of the buildup type curves for analysis of the recorded pressure data. Fortunately, **[TOPAZ]** has removed such a restriction by allowing the operator to generate unlimited ranges of build up type curves which are specific to each well and well testing scheme.( e.g. well location, external boundary status, test type, test duration, etc).

## 8.6-CHARACTERIZATION OF THE UFF AND ICF FRACTURED MODELS

a-A plot $\log(\Delta P=P-P_{wf})$ vs $\log(T)$ on a 5x3 log-log paper is made and then checked against the log-log straight line of slope m=0.5 which reflects fractured formation.

b-Having defined the best match on either figure (8.5) or figure (8.6), the values of the dimensionless parameters $[x_f/\sqrt{A}]$ and $[x_e/y_e]$ are read from the match.

c-Permeability thickness is then obtained from the pressure axis match and the fracture half length from the time axis match.

$$Kh = 141.2\, q\mu B_o \left(\frac{P_{DF}}{\Delta P}\right)_{match} \tag{8.28}$$

$$x_f = \left[\frac{0.000264K}{\phi \mu c_t} \times \left(\frac{T}{T_{DF}}\right)_{match}\right]^{0.5} \tag{8.29}$$

d-By refining the pseudo steady state pressure data (if present) by means of the type curves of figures (8.5) or (8.6), a cartesian plot of flowing pressure vs flowing time is next made and from the plot, the slope of the straight line and its intercept on the pressure axis (Pint) are determined.

e-Second estimate of the drainage area is made using equation (8.30) and then compared against its first estimated value from step (b).

$$A = \frac{-0.234\, qB_o}{\phi h c_t m^*} \tag{8.30}$$

f-The intercept of the pseudo steady state cartesian straight line for the fractured model is obtained using:

$$(Pint)_{DF} = \frac{Kh}{141.2q\mu B_0}(P_i - [Pint]_{ss}) \tag{8.31}$$

g-Using the values of $[x_f/\sqrt{A}]$ and $[P_{int}]_{DF}$ in steps (d)and (f), in conjunction with figures (8.7) or (8.8), a second estimate of $[x_e/y_e]$ parameter is made and then compared with its corresponding value from the type curve match.

h-Steps (b) to (g) are then repeated until consistency is obtained with regard to the dimensionless parameters $[x_f/\sqrt{A}]$ and $[x_e/y_e]$.

☆☆☆☆☆☆☆☆☆☆

# CHAPTER 9

# CONVENTIONAL ANALYSIS OF HYDRAULICALLY FRACTURED FORMATIONS

## 9.1-CONVENTIONAL DRAWDOWN SCHEMES ASSOCIATED WITH UFF/ICF MODELS

On the bases of infinite acting homogeneous model with single plane penetrating fracture, the conventional analysis of such formations may be performed by considering the dimensionless pressure responses during early and/or late times flow periods. As outlined in the previous section , the dimensionless pressure function during early times dominated by linear flow system can be expressed by:

$$P_{DF} = \sqrt{\pi T_{DF}} \tag{8.11}$$

Equation (8.11) which is valid for $T_{DF} \leq 0.2$ and $T_{DF} \leq 0.02$ with respect to the [UFF] and the [ICF] fractured models respectively, when expressed in terms of real times yields:

$$P - P_{wf} = 4.066 \frac{qB_o}{h} \sqrt{\frac{\mu}{\phi c_t K x_f^2}} \times \sqrt{T} + \Delta P_S \tag{9.1}$$

$$\text{Where} \qquad \Delta P_S = 141.2 \frac{q\mu B_o}{Kh} S \tag{9.2}$$

With reference to equation (9.1), it is evident that the pressure responses of fractured wells during linear flow periods are directly proportional to the square root of flowing times. Thus, provided the permeability of the system is estimated independently from a pre fracture testing scheme;

-The fracture half length can be determined from the slope of the straight line plot [$\Delta P=(P-P_{wf})$ vs T] defined by:

$$m_{HF} = 4.066 \frac{qB_o}{h} \sqrt{\frac{\mu}{\phi c_t K x_f^2}} \tag{9.3}$$

-The mechanical skin factor which provides an excellent method of detecting workover prospects can be estimated by extrapolation of the cartesian straight line to flowing time of zero hour (figure 9.1).

$$S = 7.082 \times 10^{-3} \frac{Kh}{q\mu B_o} \Delta P_S \tag{9.4}$$

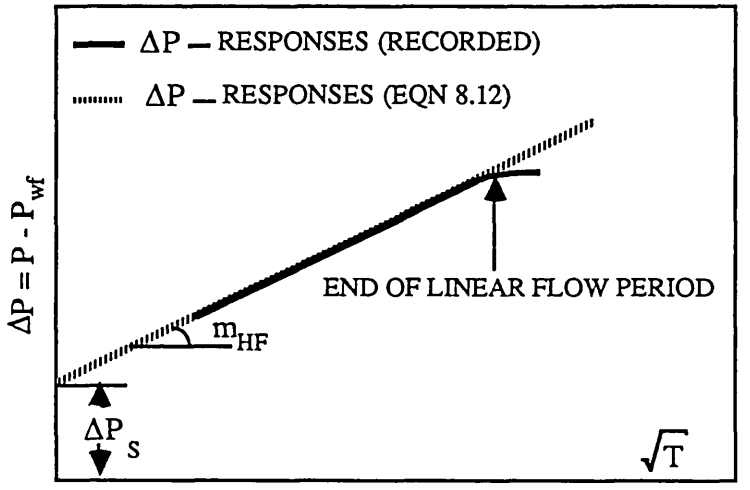



FIGURE 9.1: PRESSURE RESPONSES OF FRACTURED FORMATIONS DOMINATED BY LINEAR FLOW.

After the initial linear flow periods, the formation undergoes a transitional region until pseudo steady state of fluid into the fracture plane prevails. Under such condition, the pressure responses of both the fractured models are given by:

$$P_{DF} = 1.151 \log(T_{DF}) + \bar{x}_{U/I} \tag{9.5}$$

where $\bar{x}_{U/I} \equiv \bar{x}_U = 1.4045$ (UFF model) & $\bar{x}_{U/I} \equiv \bar{x}_I = 1.10$ (ICF model)

With reference to the definitions of dimensionless pressure and time parameters based on the fracture half length, equation (9.5) can be expressed as:

$$P - P_{wf} = m^* \{ \log[T] + \log[\frac{K}{\phi \mu c_t x_f^2}] + 0.869\bar{x}_{U/I} - 3.578 \} + \Delta P_S \tag{9.6}$$

$$\text{With} \quad m^* = 162.6 \frac{q\mu B_o}{Kh} \tag{9.7}$$

Equation (9.6) implies that at late times, provided the external boundary effects of the testing formation are not observed, then from the refined plot of pressure data

(during infinite acting radial flow period) in the semilog plane:

-The permeability of the formation is obtained from the slope of the semilog straight line defined by equation (9.7).

-Having determined the pressure drop due to skin (e.g. from drilling data), the fracture half length is then evaluated by extrapolating the semilog line during radial flow periods to flowing time of one hour.

$$\log(x_f) = 0.5 \{ \log[\frac{K}{\phi c_t \mu}] - \frac{\Delta P_{1\text{-hour}}}{m^*} + \frac{\Delta P_S}{m^*} + 0.869\bar{x}_{U/I} - 3.578 \} \qquad (9.8)$$

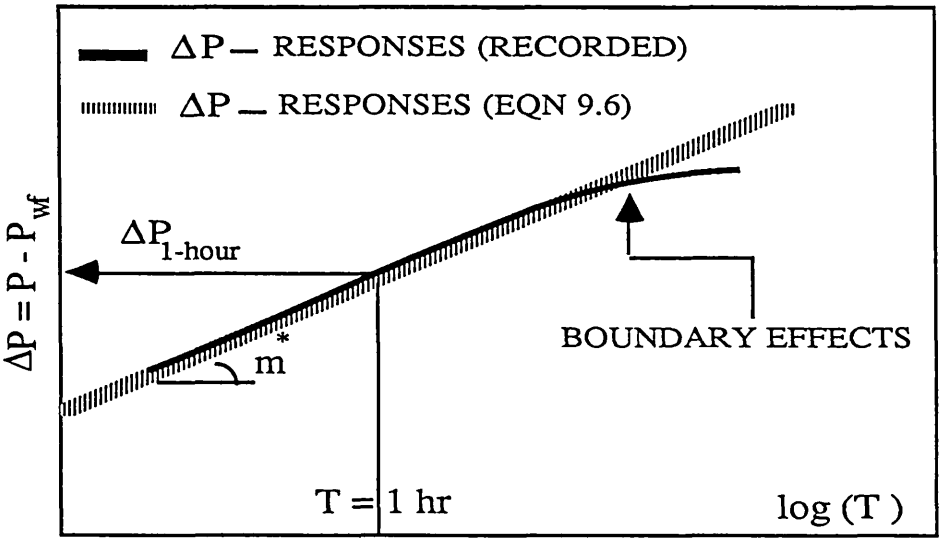



FIGURE 9.2: PRESSURE RESPONSES OF FRACTURED FORMATIONS DOMINATED BY RADIAL FLOW.

It should be noted that figures (9.1) and (9.2), representing the pressure responses of hydraulically fractured formations are based solely on ideal situations where only two straight lines corresponding to early and late times flow periods are developed. Frequently, however, due to the improper procedures with regard to the recording of pressure data, it is more than likely to identify flow regions which exhibit straight line characteristics and yet are not related to either of the flow periods. Such anomalies, which tend to make the accurate well test interpretations difficult, can be removed by estimating the approximate duration of the transition periods of fractured systems by means of the definition of the dimensionless pressure responses during early and late times.

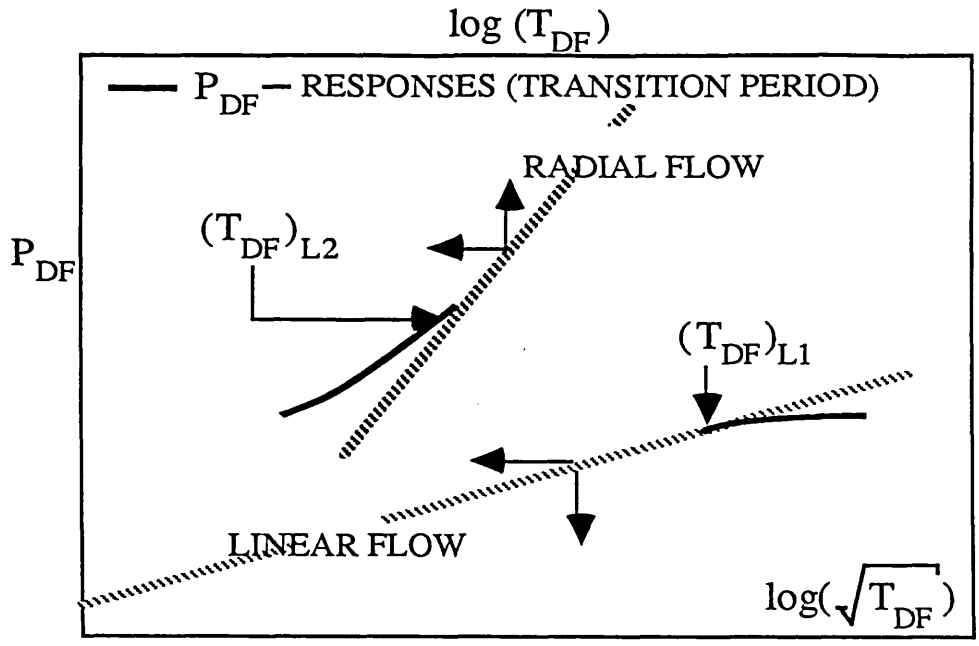



FIGURE 9.3: ($P_D$) RESPONSES OF FRACTURED FORMATION DURING EARLY & LATE TIMES

If $(T_{DF})_{L1}$ and $(T_{DF})_{L2}$ represent the lower and the upper limits of dimensionless transition time $(T_{DF})_L$, then the duration of the transition periods with respect to the fractured models can be defined as follows:

-UFF model $\quad 0.15 \leq (T_{DF})_L \leq 1.5 \quad \Rightarrow \quad 0.66 \leq (P_{DF})_L \leq 1.6$ (9.9)

-ICFmodel $\quad 0.05 \leq (T_{DF})_L \leq 1.5 \quad \Rightarrow \quad 0.20 \leq (P_{DF})_L \leq 1.4$ (9.10)

With reference to expressions (9.9) and (9.10), it is apparent that the dimensionless pressure responses at the star of the radial flow are twice the value of $P_D$-function at the end of the linear flow periods.

i.e. $\quad (P_{DF})_{EQN\text{-}9.5} \geq 2(P_{DF})_{EQN\text{-}8.11}$ (9.11)

Thus by satisfying equation (9.11), it is possible to identify specific regions of interest and hence implement the relevant testing schemes with regard to the recorded pressure data so as to define the physical nature of the formation with a greater degree of confidence.

## 9.2-CONVENTIONAL BUILD UP SCHEMES ASSOCIATED WITH THE UFF/ICF MODELS

In general, the interpretation of the build up pressure responses of such models are performed on the bases of either linear of infinite acting radial flow domination within the fracture region.

Case A: The dimensionless build up pressure responses with respect to the linear flow periods may be derived from the implementation of equation (8.11) into the theoretical build up pressure function.

$$(P_{DF})_{BU} = \sqrt{\pi(\Delta T)_{DF}} + \sqrt{\pi(T_P)_{DF}} - \sqrt{\pi(T_P+\Delta T)_{DF}} \qquad (9.12)$$

Assuming that the producing time prior to shut in is long enough for the relation $[(T_p+\Delta T) \approx T_p]$ to be valid, equation (9.12) is then reduced to:

$$(P_{DF})_{BU} = \sqrt{\pi(\Delta T)_{DF}} \qquad (9.13)$$

Equation (9.13), when expressed in terms of dimensional parameters, yields similar expression to that of equation (9.1) with the flowing time replaced by the shut in time.

$$P_{ws} - P_{wf} = m_{BU}\sqrt{\Delta T} + \Delta P_S \quad \Rightarrow \quad m_{BU} = 16.26\,\frac{qB_o}{A_f}\sqrt{\frac{\mu}{\phi c_t K}} \qquad (9.14)$$

Thus, the linear flow during build up testing would exhibit straight line characteristics on the cartesian plane, defined in terms of $(\Delta P)_{BU}=P_{ws}-P_{wf}$ vs $\sqrt{T}$.

With reference to equations (9.14), depending on the availability of petrophysical information through alternative schemes:

-The fracture surface area $[A_f]$ may be obtained from the slope of the straight line plot during linear flow periods (figure 9.4).

$$A_f = 16.26 \frac{qB_o}{m_{BU}} \left[ \frac{\mu}{\phi c_t K} \right]^{0.5} \tag{9.15}$$

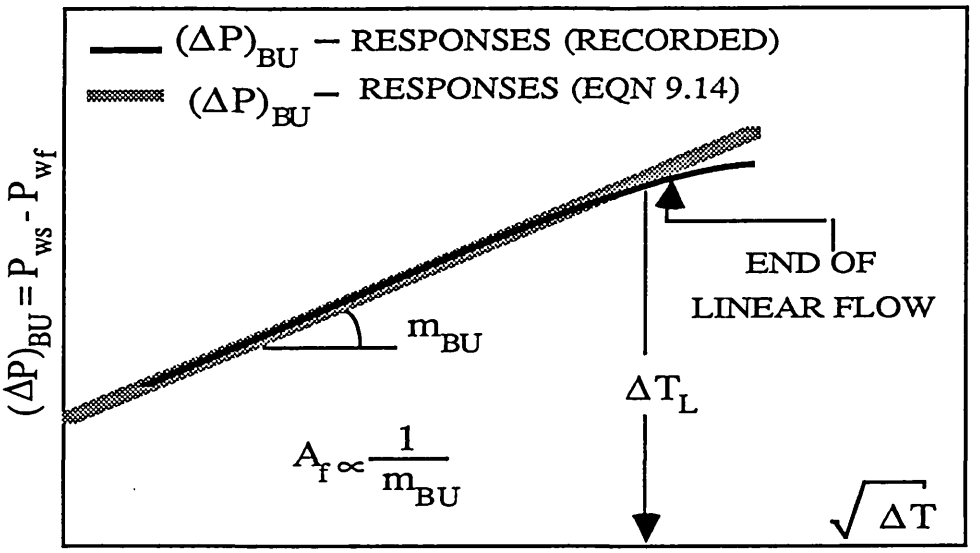



FIGURE 9.4: BUILD UP RESPONSES OF FRACTURED FORMATIONS DOMINATED BY LINEAR FLOW.

-Assuming vertically orientated fracture plane, located symmetrically about the well bore, the fracture half length can be estimated from:

$$x_f = \frac{A_f}{4h} \tag{9.16}$$

-The mechanical skin factor can be obtained by extrapolating the build up straight line to shut in time of zero hour (figure 9.5).

-The approximate start of transition period can be determined by establishing the departure point of the recorded pressure responses from the linear flow segment (figure 9.4).

Case B: Provided that the fracture penetration ratio $(x_f/x_e)<0.1$, the dimensionless build up pressure responses associated with the infinite acting radial flow during shut in periods can be defined by:

$$(P_{DF})_{BU} = Ln(T_P+\Delta T)_{DF} - Ln(\Delta T)_{DF} \qquad (9.17)$$

Alternatively, expressing equation(9.17) in terms of dimensional parameters yields:

$$P_{ws} - P_{wf} = m^*_{BU} \log[\frac{T_P+\Delta T}{\Delta T}] + \Delta P_S \quad \succ \quad m^*_{BU} = 162.6 \frac{q\mu B_o}{Kh} \qquad (9.18)$$

Hence, having developed the semilog plot of $(\Delta P)_{BU}=P_{ws}-P_{wf}$ vs Horner time (figure 9.5), the recorded pressure data with respect to the pseudo radial flow portion of the test may be analysed as follows:

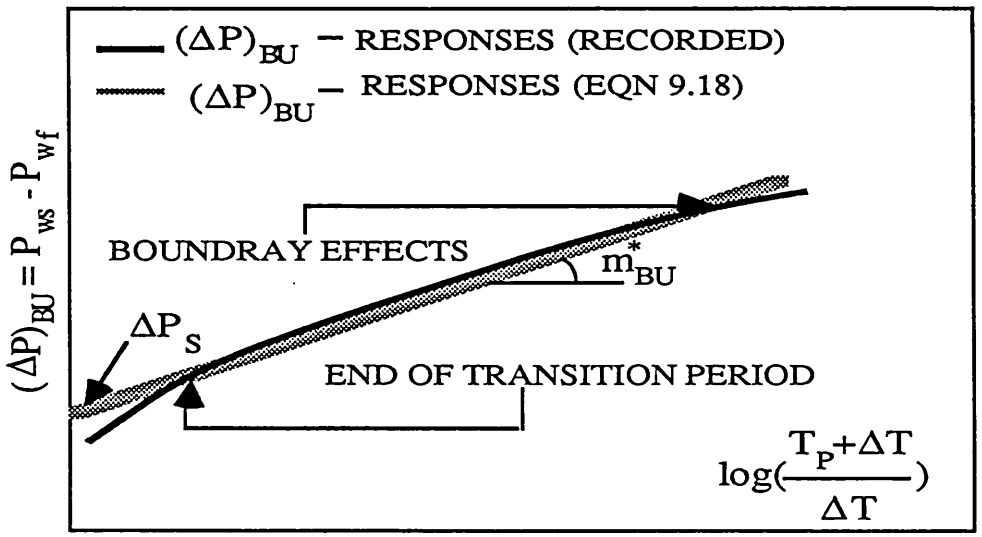



FIGURE 9.5: BUILD UP RESPONSES OF FRACTURED FORMATIONS DOMINATED BY RADIAL FLOW.

-The permeability thickness is estimated from the slope of the semilog straight line.

-The mechanical skin factor is determined from the extrapolation of the straight line to The Horner times of unity.

-Assuming infinitely conductive fractures, the fracture half length is obtained from the definition of the effective wellbore radius.

$$x_f = 2 r_w e^{-S} \qquad (9.19)$$

It is important to recognize that although analysis of the recorded pressure data based on the infinite acting radial flow concept is independent of the producing times, equation (9.17) is only valid for fracture penetration ratios of less than 0.1. Thus, in order to extend the range of the applicability associated with the build up testing of pseudo radial pressure data, equation (9.17) requires modifications.

$$(P_{DF})_{BU} = P_{DF}[(T_P+\Delta T)_{DF}, \frac{x_f}{x_e}] - P_{DF}[(\Delta T)_{DF}, \frac{x_f}{x_e}] \qquad (9.20)$$

With regard to the modified definition of the dimensionless build up pressure responses, it is evident that fro large fracture length, where the boundary effects tend to prevail before the influence of the fracture region becomes insignificant, there would be a certain degree of discrepancy between the actual slope of the build up test defined by equation (9.20) and the maximum slope of the semilog straight line during pseudo radial flow periods (figure 9.6).

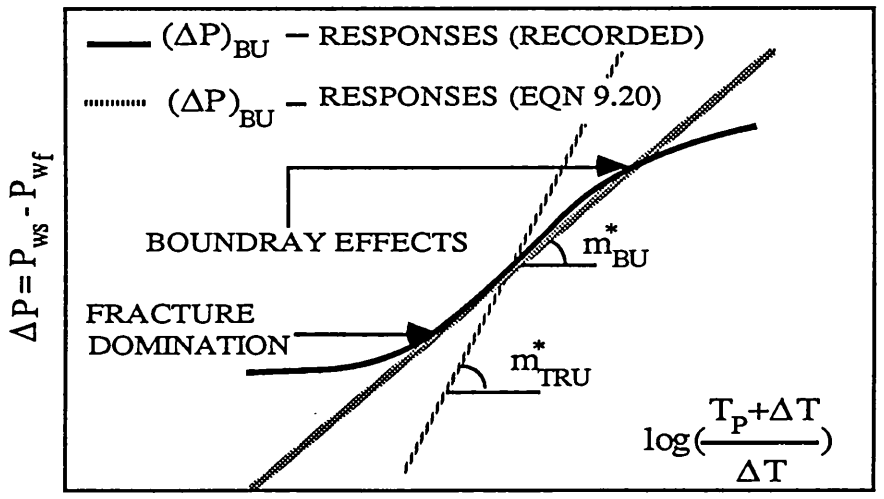



FIGURE 9.6: BUILD UP RESPONSES OF BOUNDED FRACTURED FORMATIONS

Such discrepancies which tend to yield incorrect reservoir parameters , can be eliminated by introducing the correction factor term $F_{CT}=f(x_f/x_e)$, defined by:

$$F_{CT} = \frac{m^*_{BU}}{m^*_{TRU}} = \frac{K_T}{K_{cal}} \qquad (9.21)$$

Where $K_T$ & $K_{cal}$ reflect the true and calculated values of the formation permeability.

| $x_f / x_e$ | $F_{CT}$ |
|---|---|
| 0.1 | 0.91 |
| 0.2 | 0.83 |
| 0.4 | 0.56 |
| 0.6 | 0.38 |
| 0.8 | 0.31 |
| 1.0 | 0.31 |

FIGURE 9.7: BUILD UP TESTING CORRECTION FACTOR WRT FRACTURED FORMATION

With reference to equation (9.21), in the absence of pseudo radial periods (eg. due to large fracture length), the true value of formation permeability can be estimated provided there are exclusive means of estimating the fracture penetration ratio. If, however, both the linear and the radial flow regions prevail during build up testing scheme, it is possible to use an iterative procedure in order to implement a higher degree of confidence with regard to the definition of formation parameters.

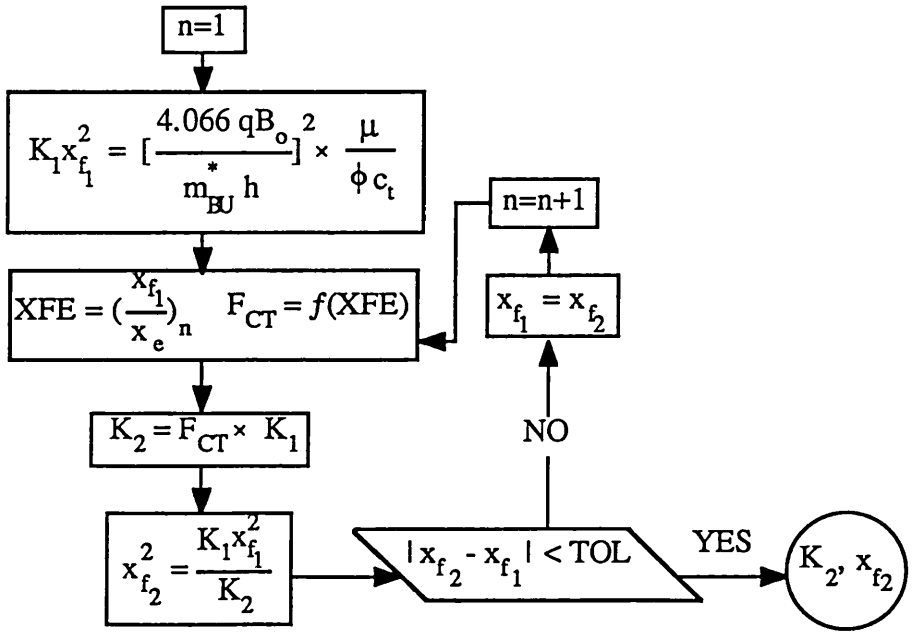



FIGURE 9.8: BUILD UP TESTING FLOW CHART ASSOCIATED WITH THE FRACTURED FORMATIONS (LINEAR & RADIAL REGIONS PREVAIL).

★★★★★★★★★★

# CHAPTER 10

# NUMERICAL RESULTS AND DISCUSSION

## 10.1-APPLICATION OF TOPAZ TO FIELD PRESSURE DATA

Whilst it seemed impractical to illustrate the analysis of the individual status of specific formations in this literature (e.g. type of test, presence of faults, no flow external boundaries, etc) three sets of pressure data corresponding to homogeneous, naturally fractured and hydraulically fractured formations were examined via mathematical models and conventional routines (incorporated in the well testing package) as a general guideline to the (TOPAZ)-applications.

The analysis was initiated by log-log plot of the recorded data which were then matched against appropriate theoretical models on the computer monitor. Having defined the best model, conventional well testing routines were implemented on the selected portion of the pressure data during infinite acting radial flow periods so as to characterize the testing formation. the generated results were then compared with the pre-defined mathematical model in order to identify the degree of confidence based on the definition of well / reservoir parameters. A Computer run time was also established throughout the duration of data interpretation as an indication of the real time required for characterizing productive formations by means of the (TOPAZ)-program.

## 10.2-TRANSIENT PRESSURE ANALYSIS FOR EXPLORATION WELL - MX/1

Test type : Pressure build up
Mathematical model: homogeneous
Input data: Formation / well / fluid properties for the well MX/1

| | | | |
|---|---|---|---|
| $P_i$ = ? | | $q_o$ = 174 | bbl/d |
| $P_{wf}$ = 3086 | psi | $T_P$ = 15.33 | hour |
| h = 107 | ft | $B_o$ = 1.06 | vol/vol |
| $r_w$ = 0.29 | ft | $\mu$ = 2.50 | cp |
| $\phi$ = 0.25 | | $c_t = 4.2 \times 10^{-6}$ | $psi^{-1}$ |

| RECORDED | | COMPUTED | | |
|---|---|---|---|---|
| $(\Delta T)$ hour | $(P_{ws})$ psig | log($\Delta$T) | log($\Delta$P) | log($\Delta T+T_p/\Delta T$) |
| 0.004 | 3091 | -2.380 | 0.699 | 3.566 |
| 0.008 | 3094 | -2.079 | 0.903 | 3.265 |
| 0.013 | 3097 | -1.903 | 1.041 | 3.089 |
| 0.017 | 3100 | -1.777 | 1.146 | 2.963 |
| 0.025 | 3107 | -1.602 | 1.322 | 2.788 |
| 0.033 | 3113 | -1.478 | 1.431 | 2.664 |
| 0.038 | 3116 | -1.426 | 1.477 | 2.613 |
| 0.050 | 3122 | -1.301 | 1.556 | 2.488 |
| 0.067 | 3136 | -1.176 | 1.699 | 2.363 |
| 0.075 | 3141 | -1.125 | 1.740 | 2.313 |
| 0.083 | 3148 | -1.079 | 1.792 | 2.267 |
| 0.121 | 3178 | -0.918 | 1.964 | 2.107 |
| 0.133 | 3187 | -0.875 | 2.004 | 2.064 |
| 0.179 | 3217 | -0.747 | 2.117 | 1.937 |
| 0.196 | 3228 | -0.708 | 2.152 | 1.899 |
| 0.213 | 3238 | -0.673 | 2.182 | 1.864 |
| 0.250 | 3262 | -0.602 | 2.246 | 1.795 |
| 0.333 | 3310 | -0.477 | 2.350 | 1.672 |
| 0.417 | 3356 | -0.380 | 2.431 | 1.577 |
| 0.500 | 3394 | -0.301 | 2.489 | 1.501 |
| 0.583 | 3434 | -0.234 | 2.542 | 1.436 |
| 0.625 | 3448 | -0.204 | 2.559 | 1.407 |
| 0.708 | 3482 | -0.150 | 2.598 | 1.355 |
| 0.750 | 3494 | -0.125 | 2.611 | 1.331 |
| 0.875 | 3537 | -0.058 | 2.654 | 1.268 |
| 1.000 | 3572 | 0.000 | 2.687 | 1.213 |
| 1.125 | 3603 | 0.051 | 2.713 | 1.165 |
| 1.250 | 3631 | 0.097 | 2.736 | 1.123 |
| 1.500 | 3674 | 0.176 | 2.769 | 1.050 |
| 1.750 | 3706 | 0.243 | 2.792 | 0.989 |
| 2.000 | 3732 | 0.301 | 2.810 | 0.938 |
| 2.500 | 3763 | 0.398 | 2.831 | 0.853 |
| 3.000 | 3785 | 0.477 | 2.844 | 0.786 |
| 3.500 | 3800 | 0.544 | 2.854 | 0.731 |
| 4.000 | 3816 | 0.602 | 2.863 | 0.684 |
| 4.500 | 3822 | 0.653 | 2.867 | 0.644 |
| 5.000 | 3826 | 0.699 | 2.869 | 0.609 |
| 6.000 | 3837 | 0.778 | 2.876 | 0.551 |
| 7.750 | 3843 | 0.889 | 2.879 | 0.474 |
| 9.750 | 3849 | 0.989 | 2.883 | 0.410 |
| 10.250 | 3850 | 1.011 | 2.883 | 0.397 |
| 12.250 | 3854 | 1.088 | 2.885 | 0.352 |
| 14.500 | 3857 | 1.161 | 2.887 | 0.313 |
| 17.500 | 3859 | 1.243 | 2.888 | 0.273 |
| 19.000 | 3861 | 1.279 | 2.863 | 0.257 |
| 22.250 | 3863 | 1.347 | 2.890 | 0.228 |
| 25.250 | 3864 | 1.402 | 2.891 | 0.206 |
| 27.250 | 3865 | 1.435 | 2.892 | 0.194 |
| 30.000 | 3866 | 1.477 | 2.892 | 0.179 |

TABLE 10.1: RECORDED PRESSURE DATA FOR THE WELL (MX/1)

Output information:

**DIAGNOSTIC ROUTINE (FIGURE 10.1)**

| | | | |
|---|---|---|---|
| $(C_D e^{2S})_{match}$ | $= 10^{10}$ | Kh | $= 1157.8$ md-ft |
| $(\frac{P_D}{\Delta P})_{match}$ | $= 0.0178$ | K | $= 10.80$ md |
| | | $C_D$ | $= 769.65$ |
| $(\frac{\Delta T}{T_D/C_D})_{match}$ | $= 0.0596$ | C | $= 0.00814$ bbl/psi |
| $\Delta P_{skin}$ | $= 552.97$ psi | S | $= +9.3$ |

Well condition: Damaged

Data analysis I/O (VDU+printer) = 1.84 min
Plotting routines (VDU+printer) = 3.08 min

TABLE 10.2: INTERPRETATION RESULTS FOR THE WELL MX/1 (LOG-LOG PLOT)

**CONVENTIONAL ROUTINE(FIGURE 10.2)**

Least square regression line:

$$P_{ws} = -63.115 \log(\frac{T_p+\Delta T}{\Delta T}) + 3877.2 \quad \& \quad \sigma = 0.997$$

| | | | |
|---|---|---|---|
| m | $= -63.115$ psi / log cycle | K | $= 11.1$ md |
| $P^*_{ws}$ | $= 3877.23$ psi | S | $= +8.42$ |
| $A_{min}$ | $= 3.93$ acre | $\bar{P}$ | $= 3887.31$ psi |
| $\Delta P_{skin}$ | $= 461.58$ psi | $E_f$ | $= 0.461$ |
| $T_{DA\,(MBH)}$ | $= 0.001$ | $P_{D\,(SSS)}$ | $= 1.80$ |
| $T_{DA\,(SSS)}$ | $= 0.1$ | $P_{D\,(MBH)}$ | $= -0.368$ |

Data analysis I/O (VDU+printer) = 2.24 min
Plotting routines (VDU+printer) = 3.17 min

TABLE 10.3: INTERPRETATION RESULTS FOR THE WELL MX/1 (HORNER PLOT)

**Diagnostic analysis:**

The recorded pressure/time data which are tabulated in table (10.1), were plotted in logarithmic domain and then overlayed on the infinite acting homogeneous type curves of

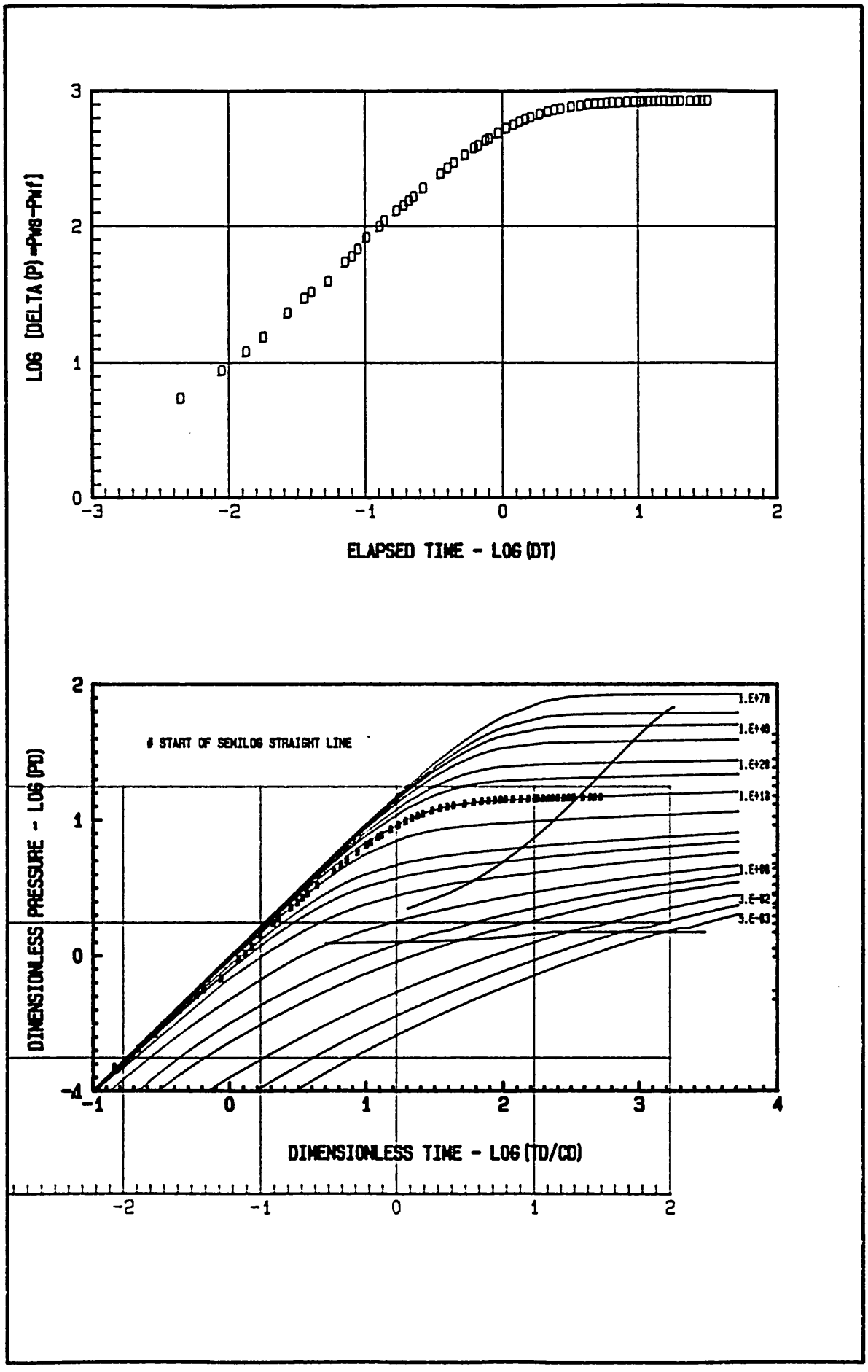



FIGURE 10.1: CHARACTERIZATION OF THE RECORDED PRESSURE DATA BY MEANS OF THE HOMOGENEOUS TYPE CURVES

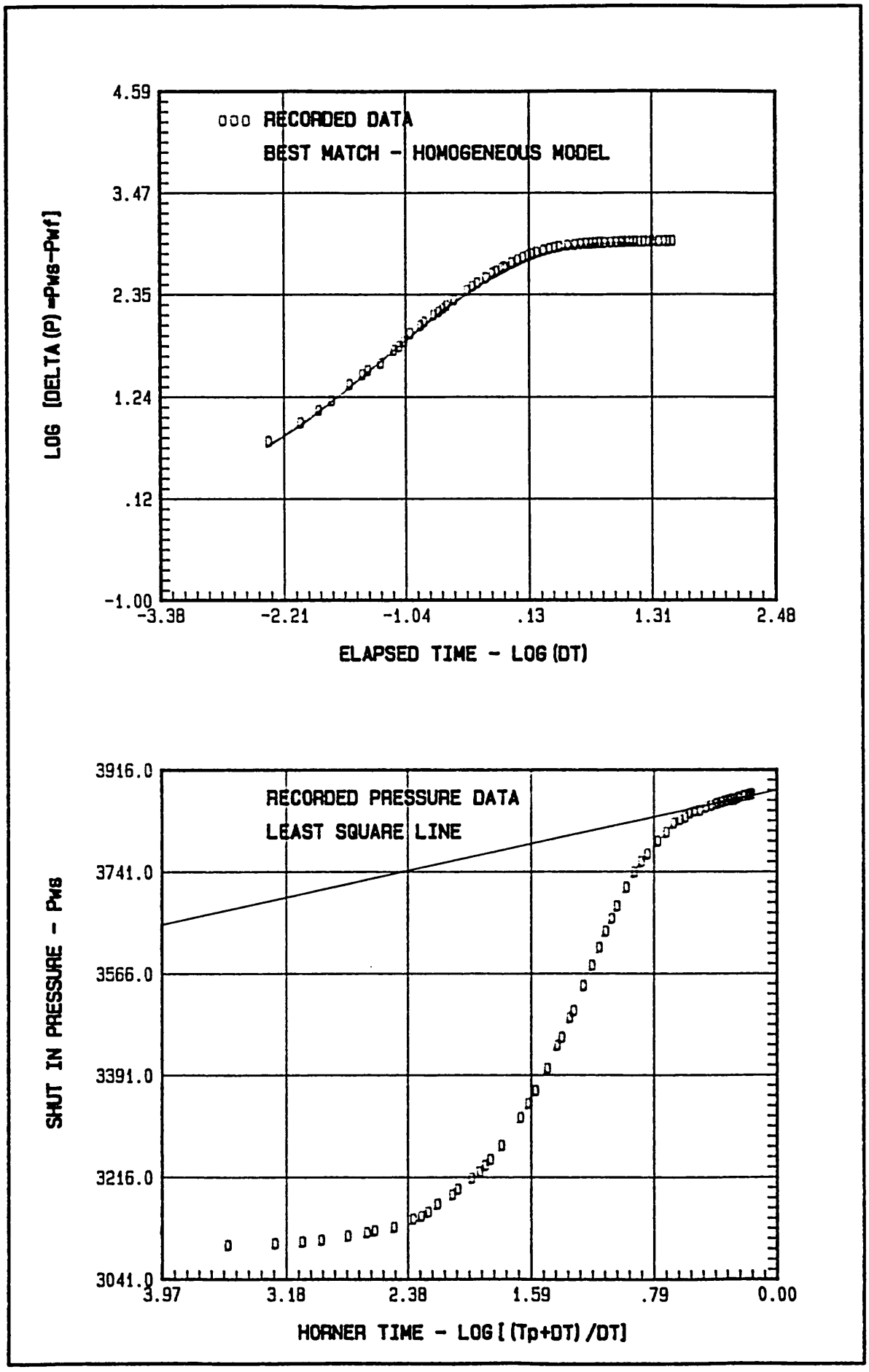



FIGURE 10.2: CONVENTIONAL ANALYSIS OF THE RECORDED PRESSURE DATA - HORNER BUILD UP TESTING MODEL

figure (2.1). Having identified the best theoretical model (characterized by the dimensionless group $C_D e^{2S}=10^{10}$), the formation permeability and wellbore storage coefficients were hence obtained from the pressure and time axes match respectively. the actual real time registered by the computer in association with the characterization of the homogeneous formation (data acquisition/interpretation + plotting routines) was just under 5 minutes.

With reference to figure (10.1), it appears that wellbore storage flow lasts for approximately 3 minutes, whilst the pressure responses during infinite acting radial flow periods prevail after 21 hours. The preceding observation allowed the refinement of the pressure data for the definition of reservoir / well parameters by means of semilog analysis. A summary of the output results are shown in table (10.2).

**Conventional analysis:**

The Horner plot of pressure data presented in figure (10.2) indicates that the application of the least square regression line for characterization of the formation is only applicable to data beyond 20 hours. This is in line with the results of the diagnostic analysis routine. In fact, the performance of semilog analysis on the selected portion of pressure data generated results which compared favourably with those shown in table (10.2). The full output results together with the computational time required for the analysis of input data are listed in table (10.3).

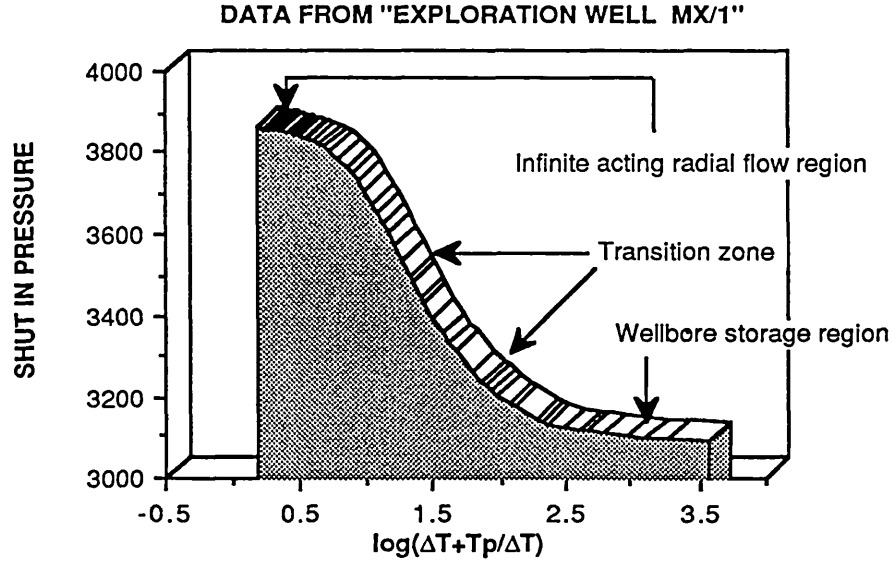



FIGURE 10.2A: 3D HORNER PLOT OF THE PRESSURE DATA FOR WELL MX/1

## 10.3: TRANSIENT PRESSURE ANALYSIS FOR THE PRODUCTION WELL FT/2

Test type: Single rate drawdown

Mathematical model: Naturally fractured (pseudo steady state interporosity flow)

Input data: Formation / well / fluid properties for the well FT/2

| | |
|---|---|
| $P_i = 11347$ psi | $q_o = 2700$ bb/d |
| h= 65 ft | $r_w = 0.292$ ft |
| $\phi = 0.048$ | $c_t = 24.5 \times 10^{-6}$ $psi^{-1}$ |
| $\mu = 0.362$ cp | $B_o = 1.8235$ vol/vol |

| RECORDED | | COMPUTED | | |
|---|---|---|---|---|
| (T) hour | ($P_{wf}$) psig | log(T) | ($P_i$-$P_{wf}$) | log($P_i$-$P_{wf}$ ) |
| 0.25 | 10989 | -0.602 | 358.000 | 2.554 |
| 0.50 | 10630 | -0.301 | 717.000 | 2.856 |
| 0.75 | 10486 | -0.125 | 861.000 | 2.935 |
| 1.00 | 10359 | 0.000 | 988.000 | 2.995 |
| 1.50 | 10271 | 0.176 | 1076.000 | 3.032 |
| 2.00 | 10183 | 0.301 | 1164.000 | 3.066 |
| 2.50 | 10136 | 0.398 | 1211.000 | 3.083 |
| 3.00 | 10112 | 0.477 | 1235.000 | 3.092 |
| 3.50 | 10080 | 0.544 | 1267.000 | 3.103 |
| 4.00 | 10056 | 0.602 | 1291.000 | 3.111 |
| 4.50 | 10048 | 0.653 | 1299.000 | 3.114 |
| 5.00 | 10040 | 0.699 | 1307.000 | 3.116 |
| 6.00 | 10016 | 0.778 | 1331.000 | 3.124 |
| 7.00 | 10000 | 0.845 | 1347.000 | 3.129 |
| 8.00 | 9984 | 0.903 | 1363.000 | 3.134 |
| 9.00 | 9968 | 0.954 | 1379.000 | 3.140 |
| 10.00 | 9960 | 1.000 | 1387.000 | 3.142 |
| 12.000 | 9936 | 1.079 | 1411.000 | 3.150 |
| 14.00 | 9920 | 1.146 | 1427.000 | 3.154 |
| 18.00 | 9880 | 1.255 | 1467.000 | 3.166 |
| 20.00 | 9864 | 1.301 | 1483.000 | 3.171 |
| 24.00 | 9832 | 1.380 | 1515.000 | 3.180 |
| 28.00 | 9816 | 1.447 | 1531.000 | 3.185 |
| 32.00 | 9792 | 1.505 | 1555.000 | 3.192 |
| 40.00 | 9735 | 1.602 | 1612.000 | 3.207 |
| 50.00 | 9679 | 1.699 | 1668.000 | 3.222 |
| 66.00 | 9487 | 1.820 | 1860.000 | 3.270 |

-Table (10.4) continued next page-

| RECORDED | | COMPUTED | | |
|---|---|---|---|---|
| (T) hour | ($P_{wf}$) psig | log(T) | ($P_i$-$P_{wf}$) | log($P_i$-$P_{wf}$ ) |
| 67.00 | 9479 | 1.826 | 1868.000 | 3.271 |
| 69.00 | 9463 | 1.839 | 1884.000 | 3.275 |
| 71.00 | 9455 | 1.851 | 1892.000 | 3.277 |
| 74.00 | 9447 | 1.869 | 1900.000 | 3.279 |
| 77.00 | 9431 | 1.886 | 1916.000 | 3.282 |
| 80.00 | 9423 | 1.903 | 1924.000 | 3.284 |
| 84.00 | 9406 | 1.924 | 1941.000 | 3.288 |
| 88.00 | 9382 | 1.944 | 1965.000 | 3.293 |
| 92.00 | 9358 | 1.964 | 1989.000 | 3.299 |
| 100.00 | 9326 | 2.000 | 2021.000 | 3.306 |
| 108.00 | 9249 | 2.033 | 2098.000 | 3.322 |
| 136.00 | 9125 | 2.134 | 2222.000 | 3.347 |
| 138.00 | 9117 | 2.140 | 2230.000 | 3.348 |
| 148.00 | 9085 | 2.170 | 2262.000 | 3.354 |
| 158.00 | 9037 | 2.199 | 2310.000 | 3.364 |
| 168.00 | 9013 | 2.225 | 2334.000 | 3.368 |
| 178.00 | 8981 | 2.250 | 2366.000 | 3.374 |

TABLE10.4: RECORDED PRESSURE DATA FOR THE WELL FT/2

Output information

| DIAGNOSTIC ROUTINE (FIGURE 10.3) | | | |
|---|---|---|---|
| $(C_De^{2S})_{f-match}$ | $= 10\times 10^{-1}$ | Kh = 282.36 | md-ft |
| | | K = 4.34 | md |
| $(C_De^{2S})_{f+m-match}$ | $= 10\times 10^{-2}$ | C = 0.05151 | bbl / psi |
| $(\frac{P_D}{\Delta P})_{match}$ | = 0.0011 | $(C_D)_{f+m}$ = 7077.4 | |
| | | S = -5.6 | |
| $(\frac{\Delta T}{T_D/C_D})_{match}$ | = 0.2239 | $\omega = 0.1$ | |
| $\lambda e^{-2S}$ | $= 5\times 10^{-2}$ | $\lambda = 7.07\times 10^{-7}$ | |

Well condition : Fractured

Data analysis I/O (VDU+printer) = 1.16 min
Plotting routines (VDU+printer) = 3.12 min

TABLE 10.5: INTERPRETATION RESULTS FOR THE WELL FT/2 (LOG-LOG PLOT)

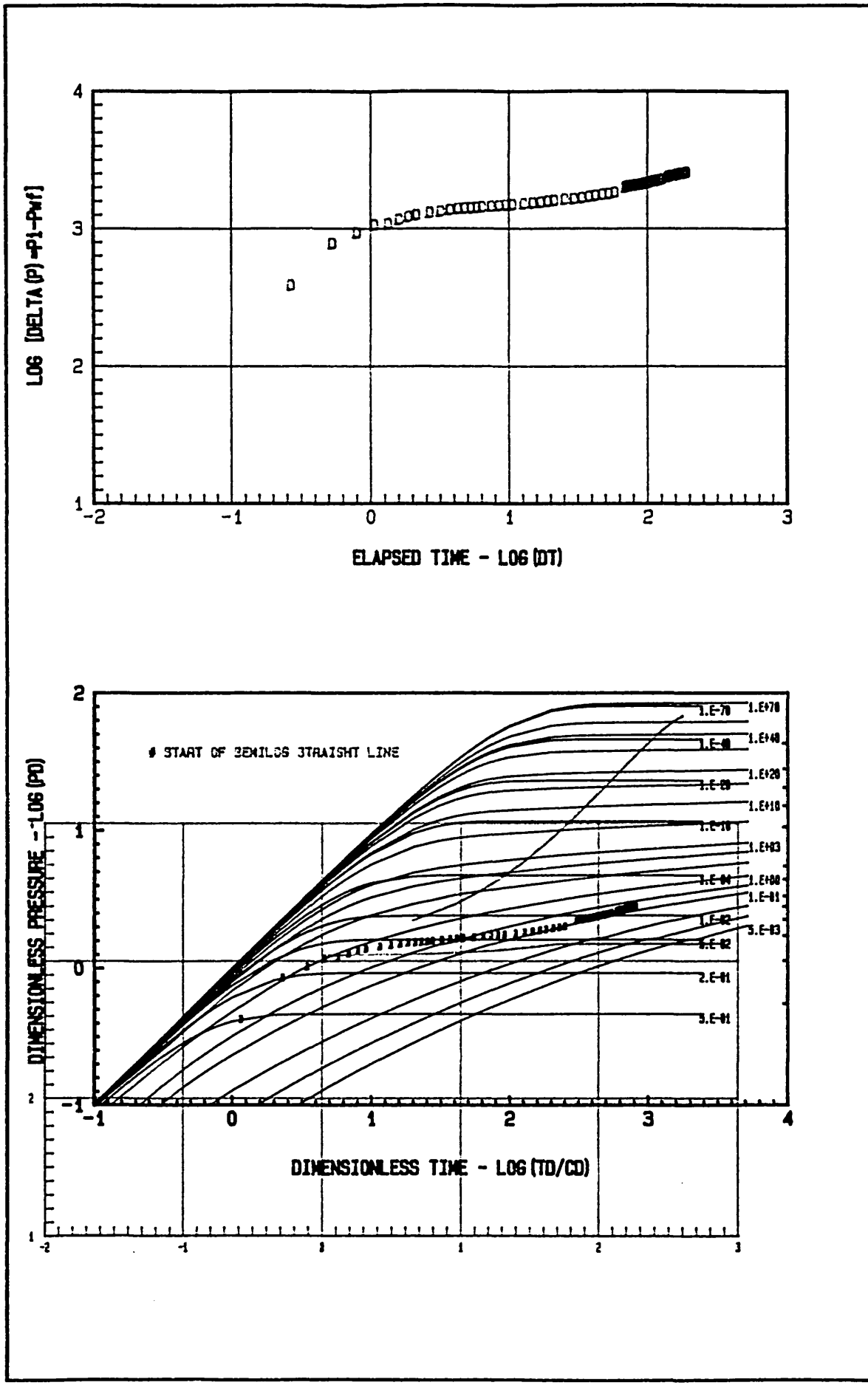



FIGURE 10.3: CHARACTERIZATION OF THE RECORDED PRESSURE DATA BY MEANS OF THE DUAL POROSITY TYPE CURVES - (SIF MODEL)

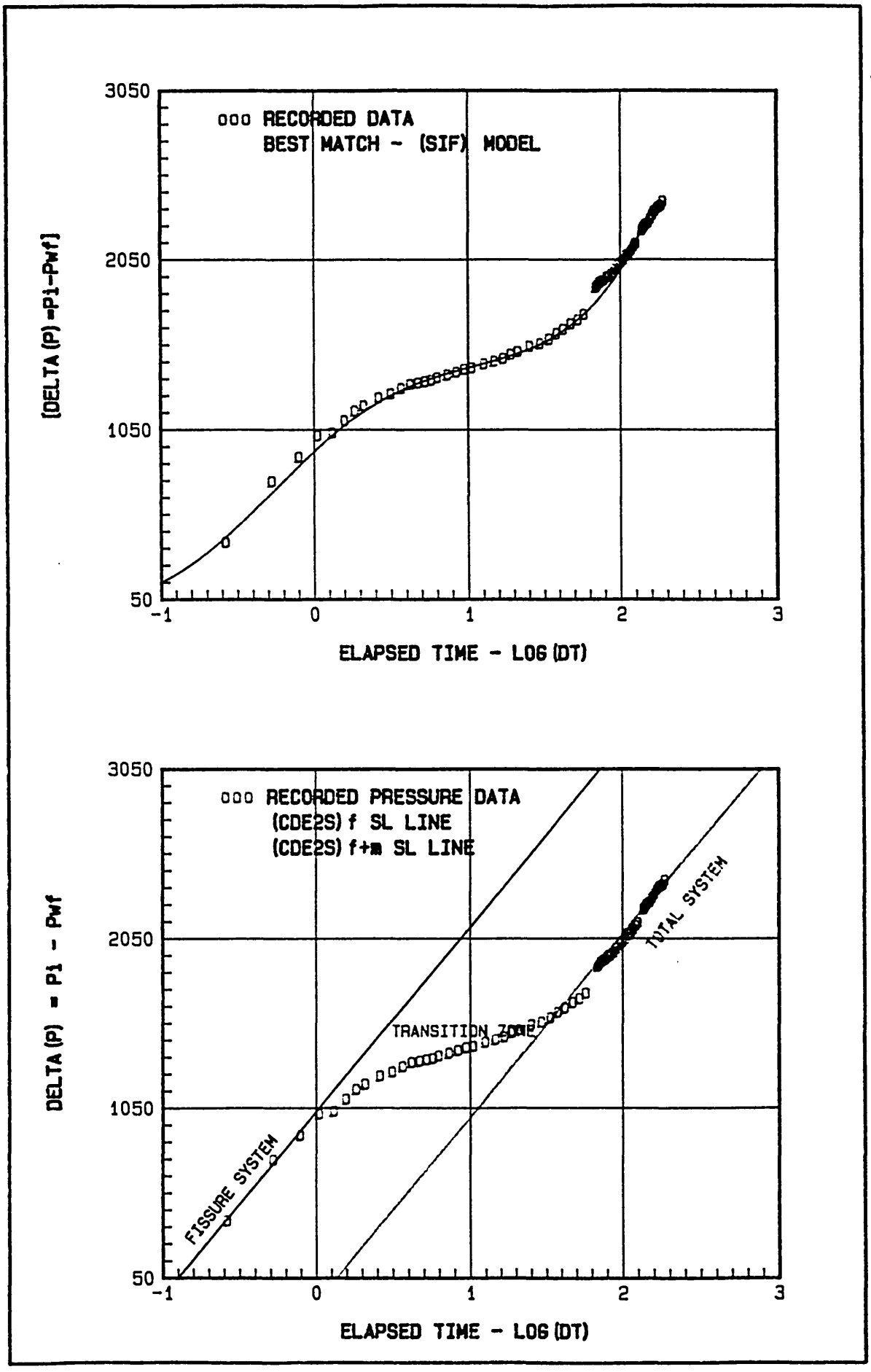



FIGURE 10.4: CONVENTIONAL ANALYSIS OF THE RECORDED PRESSURE DATA VIA SINGLE RATE DRAWDOWN TEST - (SIF MODEL)

**CONVENTIONAL ROUTINE (FIGURE 10.4)**

Fissure regression line:

$$\log(\Delta T) = 1069.1\,\Delta P + 1011.7 \quad \& \quad \sigma = 0.996$$

Fissure + matrix regression line:

$$\log(\Delta T) = 1069.1\,\Delta P - 87.94 \quad \& \quad \sigma = 0.968$$

| | | | | |
|---|---|---|---|---|
| $K_f h$ | = 271.1 | md | $\omega = 9.4 \times 10^{-2}$ | |
| $K_f$ | = 4.17 | md | $\lambda = 7.8 \times 10^{-7}$ | |
| S | = -5.65 | | $(\phi c)_f$ = $6.2 \times 10^{-4}$ | $psi^{-1}$ |
| $\Psi$ | = 5.41 | $hour^{-1}$ | | |
| $\Delta P_{skin}$ | = - 5264 | psi | $(\phi c)_m = 6.0 \times 10^{-3}$ | $psi^{-1}$ |

Data analysis I/O (VDU+printer) = 1.59 min
Plotting routines (VDU+printer) = 2.85 min

TABLE 10.6: INTERPRETATION RESULTS FOR THE WELL FT/2 (SEMI-LOG PLOT)

Diagnostic analysis:

From the examination of the recorded pressure data in association with the production well FT/2, it appeared that the naturally fractured (SIF) model, provided the best description of the testing formation. Therefore, having identified the relevant flow regions of the formation by means of the theoretical model, the log-log plot of the pressure/time data (listed in table 10.4) was matched against the type curves of figure (5.3) and then characterized using the HP computer. Table (10.5) represents a summary of the petrophysical parameters which are readily obtained through the subroutines incorporated within the (TOPAZ) program.

With reference to figure (10.3), the pressure responses during early periods which is dominated by fissure flow region and lasts for approximately one hour, follow the homogeneous model characterized by $(C_D e^{2S})_f$=0.1. Later, as the pressure stabilization is accomplished during transition flow from matrix to fissure (lasting for 14.5 hours), the recorded data follow the transition type curve characterized by $(\lambda e^{-2S})$=0.05. Eventually, the overall production is contributed by the total system of the formation and hence the pressure responses coincide with the theoretical responses of the homogeneous model corresponding to $(C_D e^{2S})_{f+m}$=0.1.

**Conventional analysis:**

Due to the absence of wellbore storage flow region (figure 10.3), the existence of two semi-log straight lines corresponding to the radial flow during fissure and total system responses, was readily verified by plotting the transient pressure data as a function of log(ΔT=elapsed time). These regression lines in turn were employed by (TOPAZ) program for quantitative interpretation of the selected portion of the recorded data. The results for the well-FT/2 via conventional and diagnostic schemes were then compared interactively In order to check the degree of accuracy with regard to the definition of the formation parameters.

With reference to figure (10.4), since the drawdown duration is long enough for the total system responses to be seen, then in addition to identifying such formation parameters as permeability thickness and mechanical skin factor, the storage capacity ratio is obtained by considering the vertical displacement between the fissure and total system responses (ω=0.094), whilst the interporosity flow parameter is estimated by considering the inflection point of the transition zone (λ=0.00000078).

Table (10.6) represents the estimated values of the reservoir parameters by means of conventional scheme together with the total computational time for characterization of the formation.

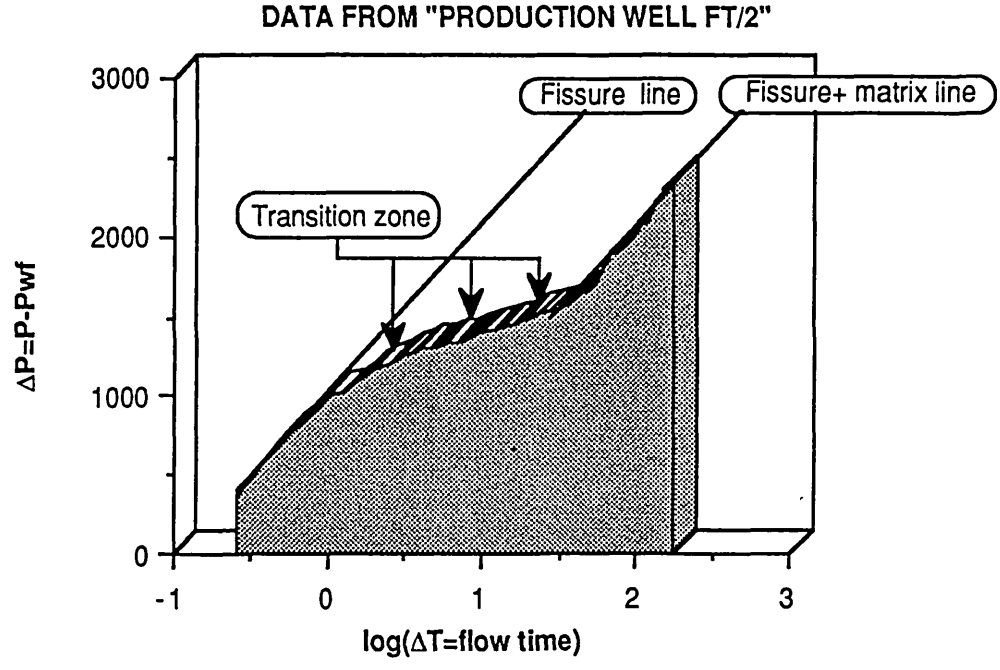



FIGURE 10.4A: 3D SEMI-LOG PLOT OF THE PRESSURE DATA FOR WELL FT/2

## 10.4: TRANSIENT PRESSURE ANALYSIS FOR THE PRODUCTION WELL-SX/O

Test type: Pressure build up

Mathematical model: vertically fractured (Infinite conductivity vertical fracture)

Input data: Formation / well / fluid properties for the well (XS/O)

| | | | |
|---|---|---|---|
| $P_i$ = 3770 | psi | $q_o$ = 419 | bbl / d |
| $P_{wf}$ = 3420 | psi | $T_P$ = 7800 | hour |
| h = 82 | ft | $r_w$ = 0.28 | ft |
| A = 1600 | acre | $\mu$ = 0.65 | cp |
| $\phi$ = 0.12 | | $B_o$ = 1.26 | vol / vol |
| $x_e / y_e = 1$ | | $c_t = 2.1 \times 10^{-5}$ | $psi^{-1}$ |

| RECORDED | | COMPUTED | | | |
|---|---|---|---|---|---|
| ($\Delta T$) hour | ($P_{ws}$) psig | ($\Delta P$) | log($\Delta T$) | log($\Delta P$) | log($\Delta T+T_P/\Delta T$) |
| 0.083 | 3431 | 11.0 | -1.079 | 1.041 | 4.971 |
| 0.167 | 3435 | 15.0 | -0.777 | 1.176 | 4.669 |
| 0.250 | 3438 | 18.0 | -0.602 | 1.255 | 4.494 |
| 0.500 | 3445 | 25.0 | -0.301 | 1.398 | 4.193 |
| 0.750 | 3449 | 29.0 | -0.125 | 1.462 | 4.017 |
| 1.000 | 3452 | 32.0 | 0.000 | 1.505 | 3.892 |
| 2.000 | 3463 | 43.0 | 0.301 | 1.633 | 3.591 |
| 3.000 | 3471 | 51.0 | 0.477 | 1.708 | 3.415 |
| 4.000 | 3477 | 57.0 | 0.602 | 1.756 | 3.290 |
| 5.000 | 3482 | 62.0 | 0.699 | 1.792 | 3.193 |
| 6.000 | 3486 | 66.0 | 0.778 | 1.820 | 3.114 |
| 8.000 | 3495 | 75.0 | 0.903 | 1.875 | 2.989 |
| 9.000 | 3498 | 78.0 | 0.954 | 1.892 | 2.938 |
| 10.000 | 3500 | 80.0 | 1.000 | 1.903 | 2.893 |
| 12.000 | 3506 | 86.0 | 1.079 | 1.934 | 2.814 |
| 24.000 | 3528 | 108.0 | 1.380 | 2.033 | 2.513 |
| 36.000 | 3544 | 124.0 | 1.556 | 2.093 | 2.338 |
| 48.000 | 3555 | 135.0 | 1.681 | 2.130 | 2.214 |
| 60.000 | 3563 | 143.0 | 1.778 | 2.155 | 2.117 |
| 72.000 | 3570 | 150.0 | 1.857 | 2.176 | 2.039 |
| 96.000 | 3582 | 162.0 | 1.982 | 2.210 | 1.915 |
| 120.000 | 3590 | 170.0 | 2.079 | 2.230 | 1.820 |
| 144.000 | 3600 | 180.0 | 2.158 | 2.255 | 1.742 |
| 192.000 | 3610 | 190.0 | 2.283 | 2.279 | 1.619 |
| 240.000 | 3620 | 200.0 | 2.380 | 2.301 | 1.525 |

TABLE 10.7: RECORDED PRESSURE DATA FOR THE PRODUCTION WELL SX/O

Output information:

| DIAGNOSTIC ROUTINE (FIGURE 10.5) | | | |
|---|---|---|---|
| $(\frac{P_D}{\Delta P})_{match}$ | = 0.0126 | $\Delta P_{skine}$ | = -430.5 psi |
| | | K | = 7.44 md |
| $(\frac{\Delta T}{T_{DF}})_{match}$ | = 13.335 | S | = -5.42 |
| Kh | = 609.99 md-ft | $x_f$ | = 126.44 ft |

Data analysis I/O (VDU+printer) = 0.17 min
Plotting routines (VDU+printer) = 1.43 min

TABLE 10.8: INTERPRETATION RESULTS FOR THE WELL SX/O (LOG-LOG PLOT)

| CONVENTIONAL ROUTINE (FIGURE 10.6) | | | |
|---|---|---|---|
| Least square regression line: $P_{ws} = -96.36 \log(\frac{T_P+\Delta T}{\Delta T}) + 3766.59$ & $\sigma = 0.999$ | | | |
| m | = -96.36 psi / log cycle | K | = 7.06 md |
| $P^*_{ws}$ | = 3767 psi | S | = - 5.5 |
| $P_{ws\,(LIN\text{-}1\,hr)}$ | = 3391.5 psi | $\bar{P}$ | = 3705.4 psi |
| $A_{min}$ | = 2038 acre | $\Delta P_{skin}$ | = -462.8 psi |
| Kh | = 578.9 md-ft | $E_f$ | = 2.622 |
| $T_{DA\,(MBH)}$ | = 0.127 | $P_{D\,(MBH)}$ | = 1.462 |
| $T_{DA(SSS)}$ | = 0.1 | $P_{D\,(SSS)}$ | = 1.18 |

Data analysis I/O (VDU+printer) = 1.735 min
Plotting routines (VDU+printer) = 1.178 min

TABLE 10.9: INTERPRETATION RESULTS FOR THE WELL SX/O (HORNER PLOT)

**Diagnostic analysis:**

The pressure response patterns of production well-SX/O were initially defined in the log-log plane and then compared with the developed theoretical models associated with

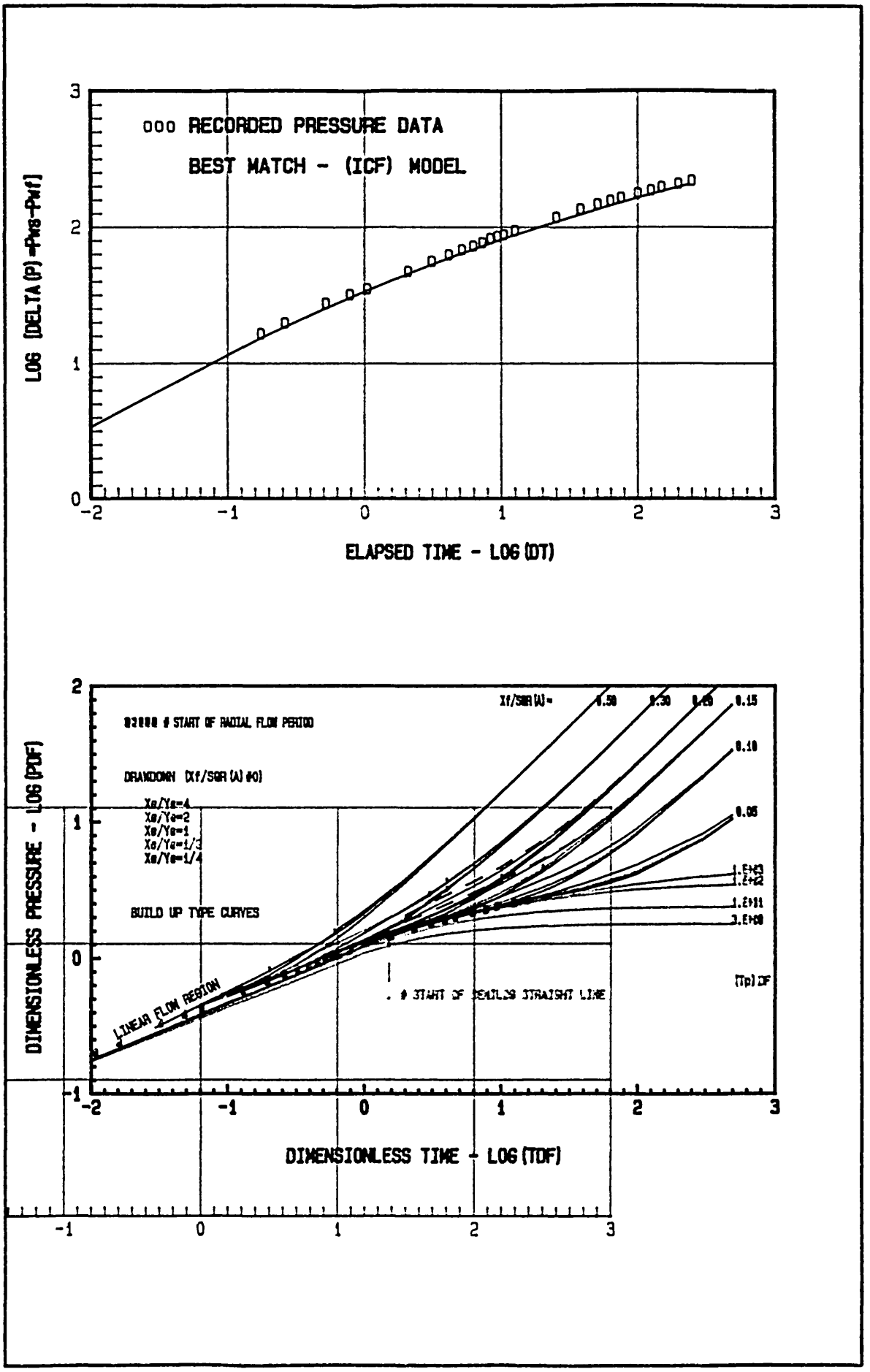
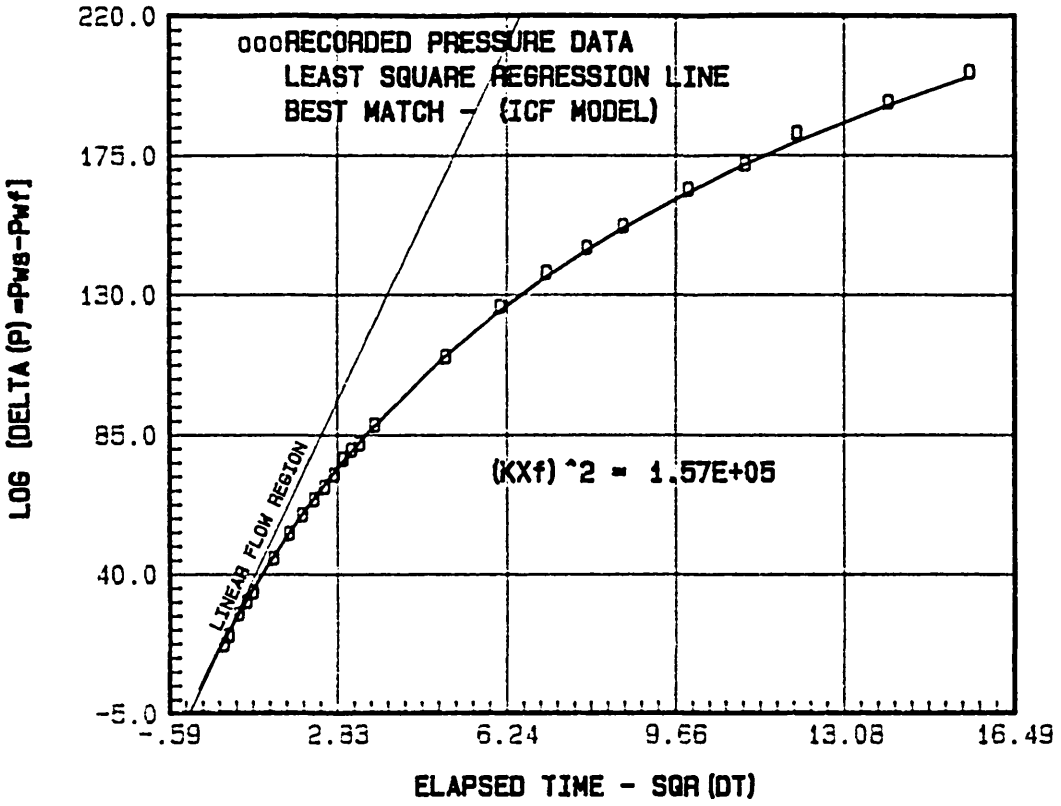



FIGURE 10.5: CHARACTERIZATION OF THE RECORDED PRESSURE DATA THROUGH HYDRAULICALLY FRACTURED TYPE CURVES (ICF MODEL)



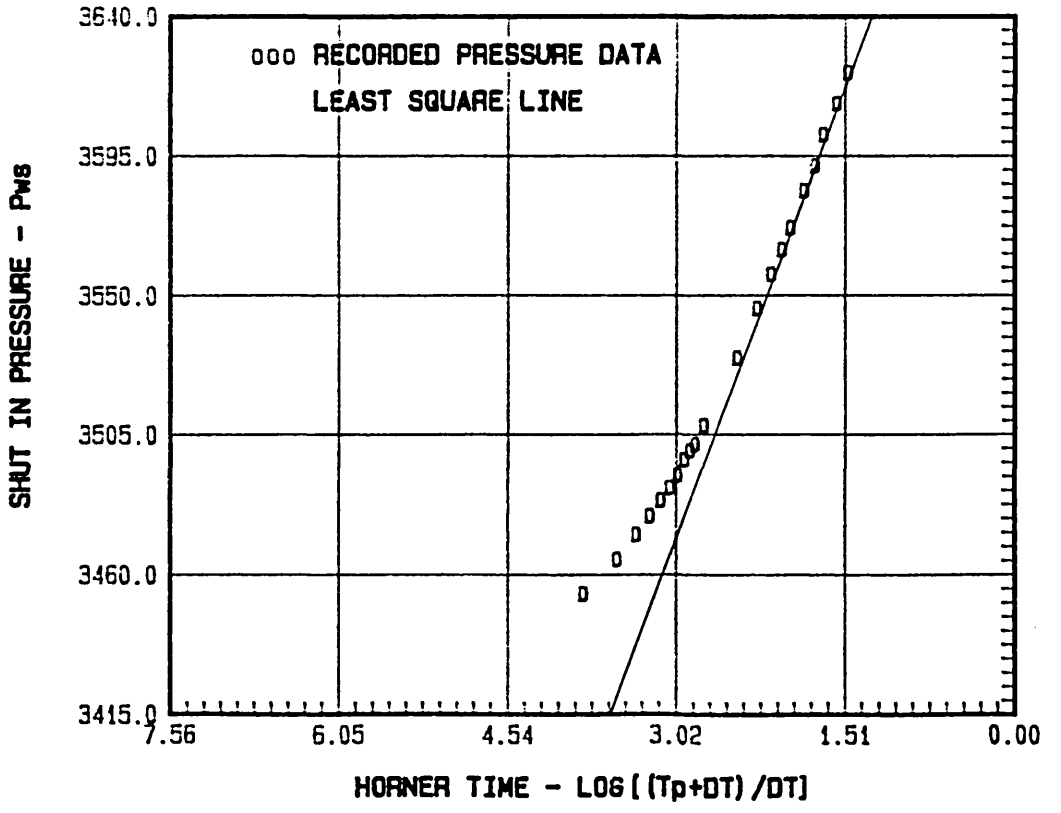




FIGURE 10.8: CONVENTIONAL ANALYSIS OF THE RECORDED BUILD UP PRESSURE DATA SUBJECT TO (ICF) - FRACTURED MODEL

the hydrualically fractured formations. As expected, The [ICF]-model provided the best description of the pressure behaviour for the well-SX/O (Figure 10.5). Due to the absence of the bend up toward outer boundary control it was further concluded that the formation was producing under infinite acting external boundary status.

The quantitative analysis of the recorded data was performed by overlaying the log-log plot of the recorded data on the type curves of figure (8.6) and then identifying the most appropriate theoretical solution in relation to the testing formation. Having obtained the best match, the formation permeability was derived from the pressure axis match whilst the half-fracture length was determined from the time axis match (table 10.8).

**Conventional analysis:**

The characterization of the fractured formation was accomplished in two stages. In the first stage, pressure data were plotted in the cartesian plane as a function of ($\sqrt{\Delta T}$) in order to define the half-fracture length from the linear portion of the figure (10.5). In the second stage, the formation parameters were computed from the analysis of the semi-log Horner plot of the refined pressure data which were identifed from the diagnostic testng schemes. The corresponding results listed in table (10.8) and (10.9) indicated reseanable agreement.

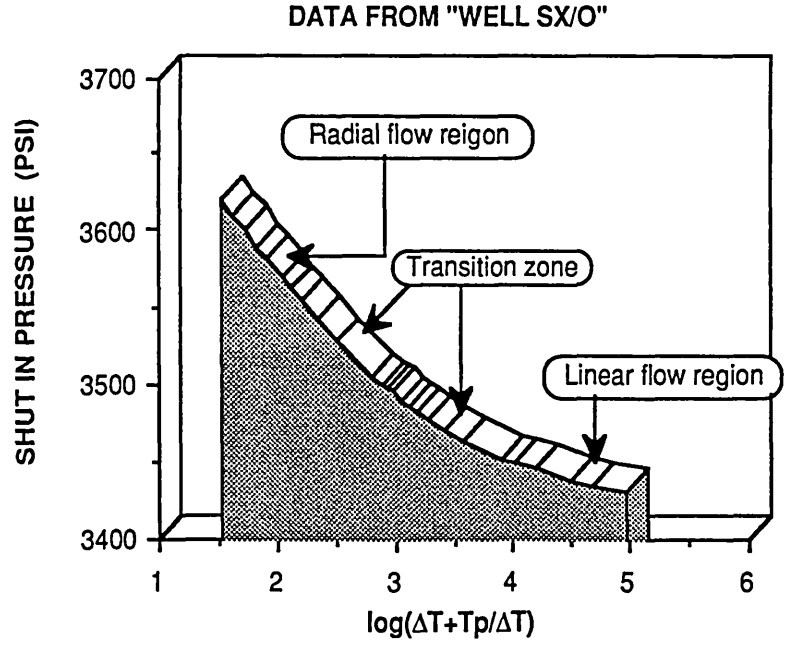



FIGURE 10.6A: 3D HORNER PLOT OF THE PRESSURE/TIME DATA FOR WELL SX/O

## 10.5-CONCLUDING REMARKS

The results of this research leads to the following conclusions.

1- Identification of the best theoretical model describing the dynamic nature of the testing formation warrants a closer examination of the transient pressure data by means of the available mathematical models (e.g. [TIF], [ICF], [UFF], etc).

2- An adequate reservoir description is only possible by means of the combined type curve matching and conventional transient well testing techniques.

3- The new sets of type curves developed in this literature are applicable for analysis of homogeneous, naturally fractured and hydraulically fractured formations. Each set also includes time limits which reflect the approximate start of the semilog straight line.

4- The application of pressure derivative to transient pressure data should enhance the degree of confidence with regard to the definition of the formation parameters. The model, however, requires accurate recording of the pressure data by means of electronic pressure gauges with high resolution.

5- The combined use of the pressure and its derivative type curves in field practice could prove to be effective in removing the basic problem of non-unique solutions associated with the type curve analysis.

6- When build up tests are performed on wells with significant production history, characterization of the formation may be achieved by constructing specific type curves which take into effect such production periods.

7- Finally, the reservoir simulators developed in this literature could prove to be a valuable asset to well test engineer, since they can characterize the testing formations at the rig site within reasonable time.

★★★★★★★★★★

# NOMENCLATURE

## LATIN LETTERS

| | | |
|---|---|---|
| a | coefficient of polynominal models. | |
| A | reservoir drainage area. | $feet^2$ |
| b | coefficient of polynomial models. | |
| $B_o$ | formation volume factor. | rb/stb |
| c | coefficient of polynomial models. | |
| $c_t$ | total system compressibility. | $psi^{-1}$ |
| C | wellbore storage coefficient. | bbl/psi |
| $C_A$ | Dietz shape factor for unfractured well. | |
| $C_D$ | dimensionless wellbore storage constant. | |
| CTR | correction term. | |
| d | coefficient of polynomial models. | |
| erf | error function. | |
| $E_f$ | flow efficiency. | |
| $E_i$ | exponential integral. | |
| g | Laplace operator based on the dimensionless parameter $T_D/C_D$. | |
| h | formation thickness. | feet |
| H | minimum abscissal distance (integration by means of Taylor series). | |
| $H_i$ | parameter defined by equation (2.17). | |
| $I_f$ | semilog straight line during fissure system domination. | |
| $I_{f\leftarrow m}$ | semilog straight line during transition flow periods. | |
| $I_{f+m}$ | semilog straight line during total system domination. | |
| $J_o$ | Bessel function of first kind and order zero. | |
| $J_1$ | Bessel function of first kind and order one. | |
| K | formation permeability | md |
| $K_o$ | modified Bessel function of second kind and zero order. | |
| $K_1$ | modified Bessel function of second kind and first order. | |
| $K_f$ | fissure permeability. | md |
| $K_m$ | matrix permeability. | md |
| L | block characteristic length | $feet^2$ |
| $L_{n+1}(x_i)$ | Laguerre polynomials. | |
| LNT | parameter defined by equation (5.19). | |
| $m_{BU}$ | slope of the semilog straight line from the Horner plot. | psi/log cycle |
| $m_e^*$ | slope of the fissure semilog straight line. | psi/log cycle |
| $m_L^*$ | slope of the total system semilog straight line. | psi/log cycle |
| $m_{ss}$ | slope of the straight line on a cartesian plot of $P_{wf}$ vs T | psi/hour |
| $m_T^*$ | slope of the semilog straight line during transition periods. | psi/log cycle |

| | | |
|---|---|---|
| $m_{TR}$ | slope of linear portion of semilog plot of the transient pressure data. | psi/hour |
| MRD(q,T) | parameter defined by equation (4.15). | |
| n | fluid flow direction through fracture network. | |
| N | number of stripes with respect to the fracture plane. | |
| $N_P$ | cumulative production. | stb |
| P | average reservoir pressure. | psi |
| $P^*$ | extrapolated false pressure from the Horner build up plot. | psi |
| $\Delta P$ | pressure drop. | psi |
| $\Delta P_s$ | pressure drop due to skin. | psi |
| $P_D$ | Laplace transformed dimensionless pressure. | |
| $P_D$ | dimensionless pressure or pressure drop. | |
| $(P_D)_{BU}$ | dimensionless build up pressure function. | |
| $P_{DF}$ | dimensionless pressure function with respect to fractured formation. | |
| $P_{D(MBH)}$ | Mathews-Borns and Hazebroek dimensionless pressure function. | |
| $P_i$ | reservoir initial pressure. | psi |
| $P_o^{MRD}$ | pressure intercept @ $(P_i-P_{wf})/q_N=0$ | psi |
| $P_o^{ss}$ | pressure intercept @ T=0 hour (semi steady state flow). | psi |
| $P_o^{TR}$ | parameter defined by equation (4.3). | psi |
| $P_{wf}$ | flowing bottomhole pressure. | psi |
| $P_{ws}$ | shut in pressure. | psi |
| q | production rate. | stb/day |
| $q_s$ | surface production rate. | stb/day |
| $q_T$ | total flux distribution over the fracture plane. | stb/day |
| $r_D$ | dimensionless radius (r/rw). | |
| $r_T$ | casing radius. | feet |
| $r_w$ | wellbore radius. | feet |
| $R^n$ | parameter defined by equations (5.27) and (5.28). | |
| S | mechanical skin factor. | |
| $S_{wc}$ | connate water saturation. | fraction |
| $\Delta T$ | shut in time (build up) , elapsed time (drawdown). | hour |
| T | flow time. | hour |
| $\Delta T_D$ | dimensionless shut in time. | |
| $T_D$ | dimensionless time based on wellbore radius. | |
| $T_{DA}$ | dimensionless time based on the drainage area. | |
| $T_{DA(MBH)}$ | MBH dimensionless time function based on drainage area. | |
| $T_{DA(sss)}$ | dimensionless time function based on drainage area (semi steady state flow). | |
| $T_{De(f\leftarrow m)}$ | dimensionless ending time of transition semilog straight line. | |
| $T_{DF}$ | dimensionless time base on half-fracture length. | |
| $(T_D)_{ie}$ | dimensionless intersection time. | |

| | | |
|---|---|---|
| $(T_D)_{ie'}$ | dimensionless intersection time. | |
| $T_{Ds(f\leftarrow m)}$ | dimensionless starting time of transition semilog straight line. | |
| $T_{Ds(f+m)}$ | dimensionless starting time of fissure+matrix semilog straight line. | |
| $T_{e(f\leftarrow m)}$ | ending time of transition semilog straight line. | |
| $T_k$ | flowing time @ $(\Delta P)_{f+m}=0$ | hour |
| $T_L$ | flowing time @ $(\Delta P)_f=0$ | hour |
| $T_{s(f\leftarrow m)}$ | starting time of transition semilog straight line. | hour |
| $T_{s(f+m)}$ | starting time of fissure+matrix semilog straight line. | hour |
| u | parameter defined by equation (2.11). | |
| V | ratio of total volume of one system to bulk volume. | |
| V(j) | parameter defined by equation (2.12). | |
| VR(T,q) | parameter defined by equation (4.33). | |
| WB | parameter defined by equation (4.36). | |
| $X_D$ | dimensionless coordinate based on half fracture length (X-direction). | |
| $X_e$ | half length of a rectangular drainage area (X-direction). | feet |
| $X_f$ | fracture half length. | feet |
| $x_i$ | roots of Laguerre polynomials. | |
| $X_w$ | X distance of the well from the centre of the UFF/ICF models. | feet |
| $Y_o$ | Bessel function of second kind and order zero. | |
| $Y_1$ | Bessel function of second kind and order one. | |
| $Y_e$ | half length of a rectangular drainage area (Y-direction). | feet |
| $Y_D$ | dimensionless coordinate based on half fracture length (Y-direction). | |
| $Y_w$ | Y distance of the well from the centre of the UFF/ICF models. | feet |
| z | Laplace operator based on the dimensionless time $T_D$. | |
| $z_D$ | dimensionless vertical coordinate. | |

## GREEK LETTERS

| | | |
|---|---|---|
| $\alpha$ | contact surface parameter. | $feet^{-2}$ |
| $\alpha_n$ | parameter defined by rquation (8.8). | |
| $\beta$ | interporosity transient flow parameter. | |
| $\gamma$ | exponential of Euler's constant = 1.781. | |
| $\gamma_n$ | parameter defined by equation (8.9). | |
| $\mu$ | fluid viscosity. | cp |
| $\phi$ | porosity. | fraction |
| $\omega$ | storage capacity ratio. | |
| $\lambda$ | interporosity pseudo steady state flow parameter. | |
| $\Psi$ | time factor. | $hour^{-1}$ |
| $\varsigma$ | parameter defined by equation (8.7). | |

## SUBSCRIPTS

| | |
|---|---|
| 1 | formation status prior to rate change |
| 2 | formation status after rate change |
| BU | build up |
| cal | calculated |
| D | dimensionless |
| e | end |
| ex | intersection |
| f | fissure |
| f+m | total system |
| i | initial |
| ie | intersection |
| j | summation index |
| m | matrix |
| min | minimum |
| o | oil |
| p | production |
| s | start |
| t | total |
| $\alpha$ | production rate index |

## SUPERSCRIPTS

| | |
|---|---|
| a | spherical shape matrix blocks |
| b | horizontal shape matrix blocks |
| DR | Dual rate |
| MRD | multi-rate drawdown |
| ss | semi steady state |
| TR | transient state |
| VR | multi-rate build up |

★★★★★★★★★★

# REFERENCES

1- **Agarwal, R.G.**, "A New Method To Account For Producing Time Effects When Draw Down Type Curves are Used to Analyse Pressure Build Up and Other Test Data", **SPE-9289 (1980)**

2- **Agarwal, R.G., Al-Hussainy, R., and Ramey, H.J. Jr.**, "An Investigation of Wellbore Storage and Skin Effect in Unsteady Liquid Flow. I: Analytical Treatment", **SPEJ (Sept 1970) P/279**

3- **Alagoa, A., Bourdet, D., and Ayoub, Y.M.**, "Pressure Derivative Simplifies Fractured Wells Analysis", **World Oil (End 1984)**

4- **Barenblatt, G.E., Zheltov, I.P., and Kochina, I.N.**, "Basic Concept in The Theory of Homogeneous Liquids in Fissured Rocks", **J. Appl. Math. Mech. (USSR) 24(5) (1960) P/1286**

5- **Barnum, R.S., and Vela, S.**, "Testing Exploration Wells Objectives", **SPE-13184 (Sept 1984)**

6- **Borns, F., and Miller, W.C.**, "A Simple Method for Correcting Spot Pressure Readings", **JPT (Aug 1961), P/803**

7- **Bourdet, D., Alagoa, A., Ayoub, J., and Pirard, Y.M.**, "New Type Curves Aid Analysis of Fissured Zone Well Tests", **World Oil (April 1984)**

8- **Bourdet, D., Ayoub, J.A., and Pirard, Y.M.**, "Use of Pressure Derivative in Well Test Interpretation", **SPE-12777 (April 1984)**

9- **Bourdet, D., Ayoub, J.A., Whittle, T.M., Pirard, Y.M., and Kniazeff, V.**, "Interpreting Well Tests in Fractured Reservoirs", **World Oil (Oct 1983)**

10- **Bourdet, D., and Gringarten, A.C.**, "Determination of Fissure Volume and Block Size in Fractured Reservoirs by Type Curve Analysis", **SPE-9293 (Sept 1980)**

11- **Bourdet, D., Whittle, T.M., Douglas, A.A., and Pirard, Y.M.**, "A New Set of Type Curves Simplifies Well Test Analysis", **World Oil (May 1983) P/95**

12- **Carlile, R., and Gillett, B.**, "Fortran and Computer Mathematics for The Engineer and Scientist", **(1973), Tulsa-USA**

13- **Carnhan, B., Luther, H.A., and Wilkes, J.O.**, "Applied Numerical Methods", John Wiley , **Son Inc., (1969)**

14- **Carslaw, H.S., and Jaeger, J.C.**, "Conduction of Heat in Solids", **1st Edition, Oxford Press, (1947)**

15- **Cinco L.H., and Samaniego V.F.**, "Transient Pressure Analysis for Fractured Well", **SPE-7490 (Oct 1978)**

16- **Cobb, W.M., and Smith, J.T.**, "An Investigation of Pressure Build Up Tests in Bounded Reservoirs", **JPT (Aug. 1975) P/991**

17- Dake, L., "Fundamentals of Reservoir Engineering", Elsevier Sci. Publication Company (1979)

18- David, P.J., and Rabinowitz, P., "Numerical Integration", Blaisdell Publishing Co., (1967) P/166

19- De Swaan, O.A., "Analytical Solutions for Determining Naturally Fractured Reservoir Properties by Well Testing", SPEJ (June 1976)

20- Dietz, D.N., "Determination of Average Reservoir Pressure from Build Up Surveys", JPT (Aug. 1965) P/955

21- Earlougher, R.C. Jr., "Estimating Drainage Shapes from Reservoir Limit Tests", JPT (Oct. 1971) P/1266

22- Earlougher, R.C. Jr., "Advances in Well Test Analysis", Monograph series, SPE of AIME, Dallas (1977)

23- Earlougher, R.C. Jr., and Kersch, K.M., "Analysis of Short Time Transient Test Data by Type Curve Matching", JPT (July 1974) P/793.

24- Earlougher, R.C. Jr., Ramey, H.J. Jr, Miller, F.G., and Muller, T.D., "Pressure Distribution in Rectangular Reservoirs", JPT (Feb 1968) P/199

25- "Gas Well Testing: Theory and Practice", 4th Edition, Calgary, Alberta

26- Gringarten, A.C., "Reservoir Limit Testing for Fractured Wells", SPE-7452 (Oct. 1979)

27- Gringarten, A.C., "Interpretation of Tests in Fissured and Multilayered Reservoirs With Double Porosity Behaviour: Theory and Practice", JPT (April 1984) P/549.

28- Gringarten, A.C., Bourdet, D.P., Landel, P.A., and Kniazeff, V., "A Comparison Between Different Skin and Wellbore Storage Type Curves for Early Time Transient Analysis", SPE-8205 (Sept 1979)

29- Gringarten, A.C., Ramey, H.J. Jr., "The Use of Source and Green's Functions in Solving Unsteady Flow Problems in Reservoirs", SPEJ (Oct 1973) P/285

30- Gringarten, A.C., Ramey, H.J. Jr., and Raghavan, R., "Unsteady Pressure Distribution Created by a Well With a Single Infinite Conductivity Vertical Fracture", SPEJ (Aug 1974) P/347

31- Gringarten, A.C., Ramey, H.J. Jr., and Raghavan, R., "Applied Pressure Analysis for Fractured Wells", JPT (JULY 1975) P/887

32- "Handbook of Mathematical Functions", 4th Printing, U.S Government Printing Office, Washington (1964)

33- Hantush, M., "Advances in Hydroscience", Ven Te Chow Edition, Academic Press, New York (1964) Vol. 1

34- "History of Petroleum Engineering", API Publication (1961)

35- Horner, D.R., "Pressure Build Up in Wells", Proc., Third World Petroleum Cong., E.J. Brill, Leiden (1951) II P/503.

36- Jaeger, J.C., "Conduction of Heat in an Infinite Region Bounded Internally by a Circular Cylinder of a Perfect Conductor", Aust. J. Phys. (1954) Vol. 25, No. 2, P/167

37- Jones, P., "Reservoir Limit Tests", Oil and Gas Journal (June 1956) No 59, P/184

38- Kazemi, H., "Pressure Transient Analysis of Naturally Fractured Reservoirs with Uniform Fracture Distribution", SPEJ (Dec 1969) P/451

39- LaFara, R., "Computer Methods for Science and Engineering", (1973), USA

40- Lai, C.H., Bodvarsson, G.S., Tsang, C.F., and Witherspoon, P.A., "A New Model for Well Test Data Analysis for Naturally Fractured Reservoirs", SPE-11688 (March 1983)

41- Larsen, L., "Limitations on The Use of Single- and Multi-rate Horner, Miller-Dyes-Hutchinson, and Matthews-Brons-Hazebroek Analysis", SPE-12135 (Oct. 1983)

42- Lee, J., "Well Testing", SPE-Book Series (1982)

43- Mackinley, R.M., "Wellbore Transmissibility from Afer Flow Dominated Pressure Build Up Data", JPT (July 1971) P/863

44- Matthews, C.S., Brons, F., and Hazebroek, P., "A Method for Determination of Average Pressure in a Bounded Reservoir", Trans. AIME (1954) Vol. 201, P/182

45- Matthews, C.S., and Russell, D.G., "Pressure Build Up and Flow Tests in Wells", Mono. series, SPE Dallas, Texas (1967)

46- Mavor, M.J., Cinco, H., "Transient Pressure Behaviour of Naturally Fractured Reservoirs", SPE-7977 (1979)

47- McCormick, J.M., and Salvadori, M.G., "Numerical Methods in FORTRAN", Prentice-Hall, Inc., (1964) P/54

48- Miller, C.C., Dyes, A.B., and Hutchinson C.A., "Estimation of Permeability and Reservoir Pressure from Bottomhole Pressure Build Up Characteristics", Trans., AIME 189 (1950) P/91

49- Muskat, M., "The Flow of Homogeneous Fluids Through Porous Media", J.W. Edwards Inc, (1946) P/273

50- Niko, H., "Well Test Interpretation in Heterogeneous Reservoirs with Skin and After Flow: Some New Theoretical Solutions and General Field Experience", SPE-11964 (Oct 1983)

51- Odeh, A.S., and Jones, L.G., "Pressure Drawdown Analysis, Variable Rate Case", JPT (Aug 1965) P/960

52- Odeh, A.S., and Selig, F., "Pressure Build Up Analysis, Variable Rate Case", JPT (July 1963) P/790

53- Perrine, R.L., "Analysis of Pressure Build Up Curves", Drill. Prod. Prac. API (1956) P/482

54- **Prats, M.**, "Effect of Vertical Fractures on Reservoir Behaviour-Incompressible Fluid Case", **SPEJ (June 1961) P/105**

55- **Raghavan, R.**, "The Effect of Producing Time on Type Curve Analysis", **JPT (June 1980) P/1053**

56- **Raghavan, R., Cady, G.V., and Ramey, H.J. Jr.**, "Well Test Analysis for Vertically Fractured Wells", **JPT (Aug 1972) P/1014**

57- **Ramey, H.J. Jr**, "Short Time Well Test Data Interpretation in The Presence of Skin Effect and Wellbore Storage", **JPT (Jan 1974) P/97**

58- **Ramey, H.J. Jr.**, "Practical Use of Modern Well Test Analysis", **SPE-5878 (April 1976)**

59- **Ramey, H.J. Jr.**, "Pressure Transient Testing", **SPE of AIME (1982)**

60- **Ramey, H.J. Jr., and Cobb, W.M.**, "A General Pressure Build Up Theory for a Well in a Closed Drainage Area", **JPT (Dec 1971) P/1493**

61- **Reynolds, A.C., Chang, W., and Raghavan, R.**, "The Wellbore Pressure Responses in Naturally Fractured Reservoirs", **SPE-12012 (Oct 1983)**

62- **Russell, D.G.**, "Determination of Formation Characteristics from Two-Rate Flow Tests" , **JPT (Dec. 1963) P/1347**

63- **Russell, D.G.**, "Extensions of Pressure Build Up Analysis Methods", **JPT (Dec. 1966) P/1624**

64- **Russell, D.G., and Truitt, N.E.**, "Transient Pressure Behaviour in Vertically Fractured Reservoirs", **JPT (Oct 1964) P/1159**

65- **Serra, K., Reynolds, A.C., and Raghavan, R.**, "New Pressure Transient Analysis Methods for Naturally Fractured Reservoirs", **JPT (Dec 1983)**

66- **Stefhest, H**, "Algorithm 368 - Numerical Inversion of Laplace Transforms", **D-5, CACM (1970), Vol. 13, No. 1,47**

67- **Streltsova, T.D.**, "Well Pressure Behaviour of a Naturally Fractured Reservoir", **SPEJ (Oct 1983) P/769**

68- **Theis, C.V.**, "The Relationship Between The Lowering of The Piezometric Surface and The Rate and Duration of Discharge Using Ground Water Storage", **Trans., AGU (1935) P/519**

69- **Uldrich, D.O., and Ershaghi, I.**, "A Method for Estimating The Interporosity Flow Parameter in Naturally Fractured Reservoirs", **SPEJ (Oct 1979) P/324**

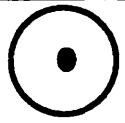
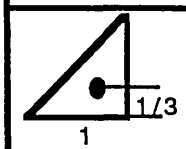
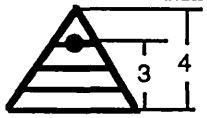
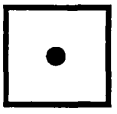
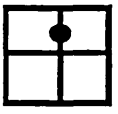
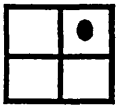
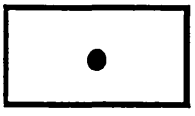
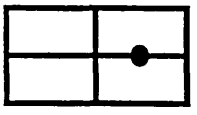
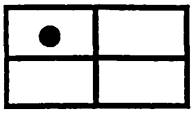
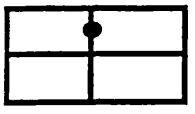
70- **van Golf-racht, T.D.**, "fundamental of fractured reservoir engineering", **Elsevier Sc., (1980) Oxford**

71- **van Everdingen, A.F., and Hurst, W.**, "The Application of Laplace Transformation to Flow Problems in Reservoirs", **Trans., AIME-186 (1949) P/305**

72- **Warren, J.E., Root, P.J.**, "The Behaviour of Naturally Fractured Reservoirs", **SPEJ (Sept 1963) P/245**

# APPENDIX A

## DIETZ SHAPE FACTORS

| BOUNDED FORMATION CONFIGURATION CODE | $C_A$ | $LN(C_A)$ | $0.5LN(\frac{2.2458}{C_A})$ | STABILIZED FOR $T_{DA}$ > |
|---|---|---|---|---|
|  H]C-1 | 31.62 | 3.4538 | -1.3224 | 0.1 |
|   H]T-1 | 21.9 | 3.0865 | -1.1387 | 0.4 |
|   H]T-2 | 0.098 | -2.3227 | 1.5659 | 0.9 |
|  H]SQ-1/1+1 | 30.88 | 3.4302 | -1.3106 | 0.1 |
|  H]SQ-2/1+1 | 12.98 | 2.5638 | -0.8774 | 0.7 |
|  H]SQ-3/1+1 | 4.51 | 1.5070 | -0.3490 | 0.6 |
|  H]SQ-4/1+1 | 3.33 | 1.2045 | -0.1977 | 0.7 |
|  H]REC-1/2+1 | 21.83 | 3.0836 | -1.1373 | 0.3 |
|  H]REC-1/2+1 | 4.51 | 1.5072 | -0.3491 | 1.5 |
|  H]REC-1/2+1 | 2.08 | 0.7309 | 0.0391 | 1.7 |
|  H]REC-1/2+1 | 10.84 | 2.3830 | -0.7870 | 0.4 |

(Continued overleaf)

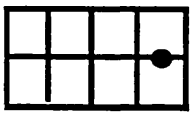
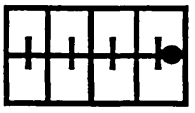
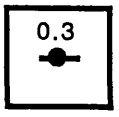
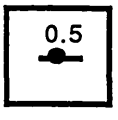
| BOUNDED FORMATION CONFIGURATION CODE | $C_A$ | $LN(C_A)$ | $0.5LN(\frac{2.2458}{C_A})$ | STABILIZED FOR $T_{DA}>$ |
|---|---|---|---|---|
|  H]REC-5/2÷1 | 3.13 | 1.1497 | -0.1703 | 0.4 |
|  H]REC-6/2÷1 | 0.58 | -0.5425 | 0.6758 | 2.0 |
|  H]REC-7/2÷1 | 0.11 | -2.1991 | 1.5041 | 3.0 |
|  H]REC-1/4÷1 | 5.38 | 1.6825 | -0.4367 | 0.8 |
|  H]REC-2/4÷1 | 0.23 | -1.4619 | 1.1355 | 4.0 |
|  H]REC-3/4÷1 | 2.69 | 0.9894 | -0.0902 | 0.8 |
|  H]REC-4/4÷1 | 0.11 | -2.1585 | 1.4838 | 4.0 |
|   F]SQ-1/1÷1 | 2.65 | 0.9761 | -0.0835 | 0.175 |
|   F]SQ-2/1÷1 | 2.03 | 0.7104 | 0.0493 | 0.175 |
|   F]SQ-3/1÷1 | 2.00 | 0.6924 | 0.0583 | 0.175 |
|   F]SQ-4/1÷1 | 1.66 | 0.5080 | 0.1505 | 0.175 |
|   F]SQ-5/1÷1 | 1.31 | 0.2721 | 0.2685 | 0.175 |

TABLE A1: DIETZ SHAPE FACTORS FOR HOMOGENEOUS/FRACTURED FORMATIONS

# APPENDIX B

## DIMENSIONLESS PRESSURE BUILD UP RESPONSES

The application of superposition theorm[22] to an ideal build up testing scheme yields:

$$\frac{2\pi Kh}{\mu}(P_i - P_{wf_2}) = \sum_{\alpha=1}^{2} \Delta q_\alpha P_D(T_{D_2} - T_{D_{\alpha-1}}) + q_2 S \qquad (B.1)$$

With reference to figure (4.NUMBR):

$$P_{wf_2} = P_{ws} \quad , \quad q_1 = q \quad , \quad q_2 = 0 \quad , \quad T_{D_1} = (T_P)_D \quad , \quad T_{D_2} = (T_P + \Delta T)_D$$

$$\therefore \frac{2\pi Kh}{\mu}(P_i - P_{ws}) = qP_D(T_P+\Delta T)_D - qP_D(\Delta T)_D \qquad (B.2)$$

In field units, equation (B.2) can be expressed as:

$$P_i - P_{ws} = 141.2 \frac{q\mu B_o}{Kh}\left(P_D(T_P+\Delta T)_D - P_D(\Delta T_D)\right) \qquad (B.3)$$

Assuming transient flow condition:

$$P_D(T_P+\Delta T)_D \cong 0.5\, Ln\left(\frac{4(T_P+\Delta T)_D}{\gamma}\right) \qquad (B.4)$$

$$P_D(\Delta T_D) \cong 0.5\, Ln\left(\frac{4\Delta T_D}{\gamma}\right) \qquad (B.5)$$

On substitution of equations (B.4) and (B.5) into equation (B.3);

$$P_i - P_{ws} = 162.6 \frac{q\mu B_o}{Kh}\left(\log(T_P+\Delta T)_D - \log(\Delta T)_D\right) \qquad (B.6)$$

$$\therefore P_{ws} = P_i - m_{BU} \times \log\left(\frac{T_P+\Delta T}{\Delta T}\right) \qquad (B.7)$$

$$\text{Where} \quad m_{BU} = 162.6 \frac{q\mu B_o}{Kh} \qquad (B.8)$$

In order to find an expression for the mechanical skin factor, the pressure responses during transient flow is introduced into equation (B.7), the result is:

$$P_{ws} = P_{wf} + m_{TR}\left(\log(T_P) + \log\left(\frac{K}{\phi\mu c_t r_w^2}\right) - 3.23\right) - m_{BU}\log\left(\frac{T_P+\Delta T}{\Delta T}\right) + \underline{0.869S} \qquad (B.9)$$

# APPENDIX C

## PRESSURE BUILD UP RESPONSES OF THE [TIF] MODEL ($r_D=\infty$)

The dimensionless build up pressure responses with respect to [TIF] fractured model can be determined by considering the definition of the theoretical build up pressure defined by equations:

$$(P_D)_{BU} = P_D(T_P+\Delta T)_D - P_D(\Delta T)_D \tag{C.1}$$

$$(P_D)_{BU} = \frac{K_f h(P_{ws} - P_{wf})}{141.2\, q\mu B_o} \tag{C.2}$$

Case A: The transitional and late time flow periods prevail during the test.

-If $P_D(\Delta T)_D$ corresponds to late times pressure responses, then:

$$(P_D)_{BU} = 0.5\left(\text{Ln}(T_P+\Delta T)_D + 0.80907\right) - 0.5\left(\text{Ln}(\Delta T_D) + 0.80907\right) \tag{C.3}$$

$$(P_D)_{BU} = 1.151\ \log\left(\frac{(T_P+\Delta T)_D}{\Delta T_D}\right) \tag{C.4}$$

-If $P_D(\Delta T)_D$ corresponds to transitional pressure responses, then:

$$(P_D)_{BU} = 0.5\left(\text{Ln}(T_P+\Delta T)_D + 0.80907\right) - 0.25\left(\text{Ln}(\Delta T)_D + 1.0409 - \text{Ln}\left(\frac{\lambda(1-\omega)}{3}\right)\right) \tag{C.5}$$

$$(P_D)_{BU} = 0.5\left(\text{Ln}(T_P+\Delta T)_D + 0.2886 - 0.5\,\text{Ln}(\Delta T)_D + 0.5\,\text{Ln}\left(\frac{\lambda(1-\omega)}{3}\right)\right) \tag{C.6}$$

$$(P_D)_{BU} = 1.151\left(\log\frac{(T_P+\Delta T)_D}{\sqrt{\Delta T_D}} + 0.125 + 0.5\log\left(\frac{\lambda(1-\omega)}{3}\right)\right) \tag{C.7}$$

For large production times (i.e. $T_p+\Delta T \approx T_p$) equation (C.7) is reduced to:

$$(P_D)_{BU} = 0.5757\left(\log(T_P)_D + \log\left(\frac{(T_P+\Delta T)_D}{\Delta T_D}\right) + 0.25 + \log\left(\frac{\lambda(1-\omega)}{3}\right)\right) \tag{C.8}$$

CaseB: The fissure and transitional pressure responses are observed.

-Subject to $P_D(\Delta T)_D$ representing the transitional pressure responses:

$$(P_D)_{BU}=0.25\left(Ln\,(T_P+\Delta T)_D - Ln\left(\frac{\lambda(1-\omega)}{3}\right)\right) - 0.25\left(Ln(\Delta T)_D - Ln\left(\frac{\lambda(1-\omega)}{3}\right)\right) \qquad (C9)$$

$$(P_D)_{BU} = 0.5757\ \log\left(\frac{(T_P+\Delta T)_D}{\Delta T_D}\right) \qquad (C.10)$$

-Subject to $P_D(\Delta T)_D$ representing the fissure pressure responses:

$$(P_D)_{BU} = 0.25\left(Ln(T_P+\Delta T)_D - Ln\left(\frac{0.26\lambda(1-\omega)}{3}\right)\right) - 0.5\left(Ln(\Delta T)_D + Ln\left(\frac{2.246}{\omega}\right)\right) \qquad (C.11)$$

$$(P_D)_{BU} = 0.25\left(Ln(T_P+\Delta T)_D - 2Ln(\Delta T)_D - 0.5772 - Ln\left(\frac{\lambda(1-\omega)}{3\omega^2}\right)\right) \qquad (C.12)$$

$$(P_D)_{BU} = 0.5\left(0.5Ln(T_P+\Delta T)_D - Ln(\Delta T)_D - 0.2886 - 0.5Ln\left(\frac{\lambda(1-\omega)}{3\omega^2}\right)\right) \qquad (C.13)$$

$$(P_D)_{BU} = 1.151\left(0.5\log(T_P+\Delta T)_D - \log(\Delta T)_D - 0.125 - 0.5\log\left(\frac{\lambda(1-\omega)}{3\omega^2}\right)\right) \qquad (C.14)$$

For large producing periods equation (C.14) can hence be defined as:

$$(P_D)_{BU} = 1.151\left(\log\frac{(T_P+\Delta T)_D}{\Delta T_D} - \log\sqrt{(T_P)_D} - 0.125 - 0.5\log\left(\frac{\lambda(1-\omega)}{3\omega^2}\right)\right) \qquad (C.15)$$

★★★★★★★★★★

# APPENDIX D

## PARTIAL PROGRAM LISTING - CODE: BU-SECTO2A

```
10  REM ------------------------------------------------------------------
20  REM PROGRAM: BU-SECTO2A (A SUBPROGRAM OF [T O P A Z] WELL TESTING PACKAGE)
30  REM ROUTINE: ANALYSIS OF BUILD UP DATA (INFINITE ACTING HOMOGENEOUS MODEL)
40  REM ////////////////////////////////////////////////////////////////////
50  REM AUTHOR : V I G E N    G H A Z A R I A N    A G H A N
60  REM ////////////////////////////////////////////////////////////////////
70  REM SUPERVISORS: PROFESSOR C.G. WALL & PROFESSOR J.S. ARCHER
80  REM LOCATION: IMPERIAL COLLEGE - LONDON UNIVERSITY
90  REM DATE: APRIL 1987
100 REM ------------------------------------------------------------------
110 REM
120 REM
130 REM
140 REM                  GENERARION OF LOG-LOG PLOT "GAREA"
150 REM ------------------------------------------------------------------
160 REM GRAPHALL @ FRAME @ LOCATE 20,161.666667,10,95 @ FRAME @ SCALE -3,2,0,3
170 REM LGRID -.1,.1,-3,0,10,10,4.5
180 REM SETGU @ CSIZE 5,.8
190 REM FAST LABEL 13.5,227,"LOG ( t=ELAPSED TIME   hr)",1 @ CSIZE 8,.5
200 REM MOVE 6,10 @ DEG @ LDIR 90 @ LABEL "LOG ( P=Pwf-Pws   psi)" @ LDIR 0
210 REM GSTORE "GAREA" @ END
220 REM ------------------------------------------------------------------
230 REM
240 REM
250 REM
260 REM            LOADING THE MULTI-APPLICATION BINARY PROGRAMS
270 REM ------------------------------------------------------------------
280 CLEAR @ AWRITE 12,13,HGL?$ ("LOADING [UTIL/1 & GDUMP] BINARY PROGRAMS - PLEASE WAIT.",1)
290 LOADBIN "UTIL/1" @ LOADBIN "GDUMP"
300 TAKE KEYBOARD @ OPTION BASE 1
310 SHORT SEG,PDmatch,TDmatch,PST,TST,CDE2S,K,WBC,WBCD,S
320 REAL INC
330 DIM Dt(100),LDt(100),DP(100),LDP(100),Ht(100),LHt(100),Pws(100),D$[50]
340 RELEASE KEYBOARD @ CLEAR @ GOTO 840
350 REM ------------------------------------------------------------------
360 REM
370 REM
380 REM
390 REM      MAIN SUBROUTINES ASSOCIATED WITH THE BU-SECTOR3 PROGRAM
400 REM ------------------------------------------------------------------
410 REM (OUTPUT1)   / HARD COPY OF THE COMPUTED PRESSURE/TIME DATA
420 REM (FUNCTION1) / COMPUTATION OF THE INPUT DATA (TIME VS PRESSURE)
430 REM (INCORRECT) / MASK OFF INPUT KEYS WHICH ARE NOT DEFINED
440 FAST LABEL 48,230,"BOUNDARY RELOCATION",1 @ RETURN
450 FAST LABEL 48,230,"                    ",0 @ RETURN
460 FAST LABEL 57,227,"          ",0 @ RETURN
470 OUTPUT1: SETTIME 0,0 @ DISP
480 DISP "            xxxxxxxxxxxxxxxxxxxxxxxxxxxxxxxxxxxxxxxxxxxxxxxxxx "
490 DISP "            x DATA ASSOCIATED WITH PRESSURE BUILD UP ANALYSIS x "
500 DISP "            xxxxxxxxxxxxxxxxxxxxxxxxxxxxxxxxxxxxxxxxxxxxxxxxxx "
510 DISP @ DISP @ AA$="xxxxxxxxxx"
```

```
520 DISP USING 530 ; Pwf
530 IMAGE "      FLOWING BHP PRIOR TO SHUT IN  = ",4Z,5X,"PSIG"
540 DISP "      x";AA$&AA$&AA$&AA$&AA$&AA$;"xxxxx"
550 DISP "      NO   Dt(HOUR)    Pws(PSIG)   Ht=(te+Dt)/Dt"
560 AWRITE 9,52,H6L?$ ("LOG(Ht)     LOG(Pws)",1) @ AWRITE 10,0,""
570 DISP "      x";AA$&AA$&AA$&AA$&AA$&AA$;"xxxxx"
580 FOR I=1 TO NDATA1
590 DISP USING 600 ; I,Dt(I),Pws(I),Ht(I),LHt(I),LDP(I)
600 IMAGE 6X,2D,3X,3Z.3D,6X,4Z.2D,7X,4Z.2D,7X,2Z.3D,8X,2Z.3D
610 NEXT I
620 DISP "      x";AA$&AA$&AA$&AA$&AA$&AA$;"xxxxx"
630 DP1T=TIME
640 TAKE KEYBOARD @ DISP "                              PRESS <C> TO CONTINUE"
650 AA=NUM (KEY$ ) @ IF NOT AA THEN 650
660 IF AA=67 OR AA=99 THEN 680
670 GOSUB INCORRECT  @ GOTO 650
680 RETURN
690 INCORRECT: BEEP 122,50 @ BEEP 149,50 @ RETURN
700 FUNCTION1: FOR I=1 TO NDATA1
710 Ht(I)=(tp+Dt(I))/Dt(I) @ LHt(I)=LGT (Ht(I))
720 DP(I)=Pws(I)-Pwf @ LDP(I)=LGT (DP(I)) @ LDt(I)=LGT (Dt(I))
730 NEXT I @ RETURN
740 FAST LABEL 50,10,"PLOTTING P/T DATA",1 @ WAIT 100 @ RETURN
750 FAST LABEL 50,10,"PLOTTING P/T DATA",0 @ WAIT 100 @ RETURN
760 FAST LABEL 50,10,"                  ",0 @ RETURN
770 FAST LABEL 13.5,227,"LOADING LOG DP - LOG Dt GRPAH-PLEASE WAIT",1 @ RETURN
780 REM ------------------------------------------------------------------------
790 REM
800 REM
810 REM
820 REM       INITIATE  PRINTER/CRT PORT AND INPUT PETROLOGICAL DATA
830 REM ------------------------------------------------------------------------
840 PRINTER IS 701 @ CRT IS 1 @ SETTIME 0,0
850 PDM1=0 @ PDM2=1 @ PDM3=2 !  P=1 LOG(10) , P=2 LOG(100),  P=3 LOG(1000)
860 TDM0=2 @ TDM1=3 @ TDM2=4 !  T=0 LOG(1)  , T=1 LOG(10) ,  T=2 LOG(100)
870 DV1T,DP1T,GPLOTV,GPLOTP,GPLOTMATCHV,FPLOTP=0
880 AWRITE 2,24,H6L?$ ("ESTIMATED RESERVOIR PROPERTIES",1)
890 AWRITE 3,12,"xxxxxxxxxxxxxxxxxxxxxxxxxxxxxxxxxxxxxxxxxxxxxxxxxxxxxxxx"
900 AWRITE 4,12,"1-Pin   RESERVOIR INITIAL PRESSURE              (PSI)"
910 AWRITE 5,12,"2-h     NET PAY THICKNESS                     (FEET)"
920 AWRITE 6,12,"3-0     RESERVOIR POROSITY                    (FRAC)"
930 AWRITE 7,12,"4-rw    WELL BORE RADIUS                      (FEET)"
940 AWRITE 8,12,"xxxxxxxxxxxxxxxxxxxxxxxxxxxxxxxxxxxxxxxxxxxxxxxxxxxxxxxx"
950 AWRITE 9,0,"  " @ INPUT Pin,h,0,rw
960 AWRITE 14,26,H6L?$ ("ESTIMATED FLUID PROPERTIES",1)
970 AWRITE 15,11,"xxxxxxxxxxxxxxxxxxxxxxxxxxxxxxxxxxxxxxxxxxxxxxxxxxxxxxxx"
980 AWRITE 16,11,"1-Bo     OIL FORMATION VOLUME FACTOR           (RB/STB)"
990 AWRITE 17,11,"2-Vo     OIL VISCOSITY                         (CPOISE)"
1000 AWRITE 18,11,"3-Ct    ROCK + FLUID COMPRESSIBILITY           (PSI-1)"
1010 AWRITE 19,11,"xxxxxxxxxxxxxxxxxxxxxxxxxxxxxxxxxxxxxxxxxxxxxxxxxxxxxxxx"
1020 AWRITE 20,0,"  " @ INPUT Bo,Vo,Ct
1030 FOR I=1 TO 23 @ DISP @ BEEP 4,I @ NEXT I
1040 AWRITE 8,30,H6L?$ ("PRODUCTION   DATA",1)
1050 AWRITE 9,12,"xxxxxxxxxxxxxxxxxxxxxxxxxxxxxxxxxxxxxxxxxxxxxxxxxxxxxxxx"
1060 AWRITE 10,12,"1-qo    PRODUCTION RATE                   (STB/DAY)"
1070 AWRITE 11,12,"2-tp    PRODUCTION TIME                     (HOUR)"
```

```
1080 AWRITE 12,12,"3-Pwf   FLOWING  B H P  PRIOR TO SHUT IN       (PSIG)"
1090 AWRITE 13,12,"4-Np   CUMULATIVE PRODUCTION PRIOR TO SHUT IN   (STB)"
1100 AWRITE 14,12,"4-NDAT  NUMBER OF SHUT IN PRESS / TIME DATA     (STB)"
1110 AWRITE 15,12,"xxxxxxxxxxxxxxxxxxxxxxxxxxxxxxxxxxxxxxxxxxxxxxxxxxxxxxxxxx"
1120 AWRITE 18,12,H6L?$ ("DATA INPUT FORMAT:  t,Pws",0)
1130 AWRITE 20,12,H6L?$ (" t= SHUT IN TIME (HOUR)",1)
1140 AWRITE 22,12,H6L?$ ("Pws=SHUT IN WELL PRESSURE (PSI)",1)
1150 AWRITE 16,0," " @ INPUT qo,tp,Pwf,Np,NDATA1
1160 AWRITE 1,13,H6L?$ ("RECORDED PRESSURE/TIME DATA ANALYSIS - PLEASE WAIT",1)
1170 REM ------------------------------------------------------------------
1180 REM
1190 REM
1200 REM
1210 REM             OPEN DATA FILE "RAW DATA" ON MEDIUM ":CS"
1220 REM ------------------------------------------------------------------
1230 ASSIGN# 1 TO  "RAW DATA:CS"
1240 FOR I=1 TO NDATA1 STEP 1
1250 READ# 1 ; DELT,PRESS@ Dt(I)=DELT @ Pws(I)=PRESS
1260 NEXT I @ ASSIGN# 1 TO  * @ TAKE KEYBOARD
1270 REM ------------------------------------------------------------------
1280 REM
1290 REM
1300 REM
1310 REM  LOG-LOG PLOT OF THE RECORDED PRESSURE DATA FOR TYPE CURVE ANALYSIS
1320 REM ------------------------------------------------------------------
1330 GOSUB FUNCTION1  @ FOR I=1 TO 22 @ DISP @ BEEP 4,I @ NEXT I @ DV1T=TIME
1340 AWRITE 1,1,"" @ GOSUB OUTPUT1
1350 GRAPHALL @ FRAME @ GOSUB 770 @ SETTIME 0,0 @ GLOAD "GAREA"
1360 LOCATE 20,161.666667,10,95
1370 FRAME @ SCALE -3,2,0,3
1380 MOVE LDt(1),LDP(1)
1390 FOR I=1 TO NDATA1 @ GOSUB 740 @ PLOT LDt(I),LDP(I) @ LABEL "o" @ GOSUB 750
1400 NEXT I
1410 GOSUB 760 @ FAST LABEL 49,8,"DATA WRT RESERVOIR",1
1420 FAST LABEL 49,20,"qo=##########",1 @ FAST LABEL 52,20,VAL$ (qo),1
1430 FAST LABEL 49,30,"tp=##########",1 @ FAST LABEL 52,30,VAL$ (tp),1
1440 FAST LABEL 49,40,"Bo=##########",1 @ FAST LABEL 52,40,VAL$ (Bo),1
1450 FAST LABEL 49,50,"Ct=##########",1 @ FAST LABEL 52,50,VAL$ (Ct),1
1460 FAST LABEL 49,60,"h =##########",1 @ FAST LABEL 52,60,VAL$ (h),1
1470 FAST LABEL 49,70,"rw=##########",1 @ FAST LABEL 52,70,VAL$ (rw),1
1480 FAST LABEL 49,80,"Vo=##########",1 @ FAST LABEL 52,80,VAL$ (Vo),1
1490 FAST LABEL 49,90,"O =##########",1 @ FAST LABEL 52,90,VAL$ (O),1
1500 FAST LABEL 63,20,"RB/B",1
1510 FAST LABEL 63,30,"HOUR",1
1520 FAST LABEL 63,40,"V/V ",1
1530 FAST LABEL 63,50,"/PSI",1
1540 FAST LABEL 63,60,"FEET",1
1550 FAST LABEL 63,70,"FEET",1
1560 FAST LABEL 63,80,"CPOI",1
1570 FAST LABEL 63,90,"FRAC",1
1580 GPLOTV=TIME  @ TAKE KEYBOARD
1590 ON TIMER# 1,20000000 GOTO 300 @ AA=NUM (KEY$ )
1600 IF AA=89 OR AA=121 THEN 1650
1610 IF AA=78 OR AA=110 THEN 1740
1620 FAST LABEL 52,227,"HARD COPY  Y/N",1 @ WAIT 300
1630 FAST LABEL 52,227,"HRAD COPY  Y/N",0 @ WAIT 300
```

```
1640 GOTO 1590
1650 GRAPHALL @ SETTIME 0,0
1660 DUMP GRAPHICS 0,0,0,1 @ GPLOTP=TIME
1670 REM ------------------------------------------------------------------
1680 REM
1690 REM
1700 REM
1710 REM  GRAPH CODED "GHOM" - HOMOGENEOUS MODEL (INFINITE ACTING)
1720 REM  REQUIREMENTS FOR CONSTRUCTION - PROGRAM (IHOM/SECTOR1B)
1730 REM ------------------------------------------------------------------
1740 GRAPHALL @ GLOAD "GHOM"
1750 SETTIME 0,0 @ FAST LABEL 48,227,"OVERLAY-PLEASE WAIT",1
1760 LOCATE 20,161.666667,10,95
1770 SCALE -3,2,0,3
1780 CSIZE 5,.5 @ LINE TYPE 1
1790 FOR I=1 TO NDATA1 @ PLOT LDt(I),LDP(I) @ LABEL "o" @ NEXT I @ GOTO 2170
1800 REM ------------------------------------------------------------------
1810 REM
1820 REM
1830 REM
1840 REM  SUBROUTINE FOR IDENTIFICATION OF THE THEORETICAL PRESSURE RESPONSES
1850 REM ------------------------------------------------------------------
1860 IF TC=1 THEN CDS=1.E70
1870 IF TC=2 THEN CDS=1.E50
1880 IF TC=3 THEN CDS=1.E40
1890 IF TC=4 THEN CDS=1.E30
1900 IF TC=5 THEN CDS=1.E20
1910 IF TC=6 THEN CDS=1.E15
1920 IF TC=7 THEN CDS=10000000000
1930 IF TC=8 THEN CDS=100000000
1940 IF TC=9 THEN CDS=1000000
1950 IF TC=10 THEN CDS=10000
1960 IF TC=11 THEN CDS=1000
1970 IF TC=12 THEN CDS=100
1980 IF TC=13 THEN CDS=10
1990 IF TC=14 THEN CDS=1
2000 IF TC=15 THEN CDS=.1
2010 IF TC=16 THEN CDS=.05
2020 IF TC=17 THEN CDS=.01
2030 IF TC=18 THEN CDS=.005
2040 IF TC=19 THEN CDS=.001
2050 IF TC=20 THEN CDS=.0005
2060 IF CDS)= 1000 THEN D$="DAMAGED WELL"
2070 IF CDS<1000 AND CDS)= 10 THEN D$="NON DAMAGED WELL"
2080 IF CDS<10 AND CDS)= .5 THEN D$="ACIDIZED WELL"
2090 IF CDS<.5 THEN D$="FRACTURED WELL"
2100 RETURN
2110 REM ------------------------------------------------------------------
2120 REM
2130 REM
2140 REM
2150 REM    PERFORM (LOG-LOG PLOT/TYPE CURVE-GHOM ) OVERLAY ON THE MONITOR
2160 REM ------------------------------------------------------------------
2170 SETTIME 0,0 @ FAST LABEL 48,227,"                    ",0
2180 INC=17/6 @ X1=20 @ X2=161.666667 @ Y1=10 @ Y2=95
2190 SETGU @ FAST LABEL 6,2,"L=",1 @ FAST LABEL 14,2,"R=",1
```

```
2200 FAST LABEL 22,2,"U=",1 @ FAST LABEL 30,2,"D=",1 @ FAST LABEL 38,2,"INC=",1
2210 FAST LABEL 52,227,"            ",0
2220 TAKE KEYBOARD @ U1,D1,L1,R1=0
2230 FAST LABEL 8,2,"###",1 ! LEFT  (159)
2240  FAST LABEL 16,2,"###",1 ! RIGHT(170)
2250  FAST LABEL 24,2,"###",1 ! UP   (163)
2260  FAST LABEL 32,2,"###",1 ! DOWN (164)
2270 FAST LABEL 42,2,"######",1
2280 SEG=INC*.6/17 @ FAST LABEL 42,2,VAL$ (SEG),1
2290 A=NUM (KEY$ ) @ IF NOT A THEN 2290
2300 IF A=159 THEN GOSUB 2420 @ GOSUB 2480 @ GOSUB 2500 @ GOTO 2290
2310 IF A=170 THEN GOSUB 2430 @ GOSUB 2490 @ GOSUB 2510 @ GOTO 2290
2320 IF A=163 THEN GOSUB 2440 @ GOSUB 2460 @ GOSUB 2520 @ GOTO 2290
2330 IF A=164 THEN GOSUB 2450 @ GOSUB 2470 @ GOSUB 2530 @ GOTO 2290
2340 IF A=154 THEN 2350 ELSE 2360
2350 GOSUB 440 @ GLOAD "GHOM" @ GOSUB 440 @ GOSUB 2370 @ GOSUB 450 @ GOTO 2540
2360 GOTO 2290
2370 GRAPHALL @ LOCATE X1,X2,Y1,Y2 @ LINE TYPE 5 @ SCALE -3,2,0,3 @ FRAME
2380 LINE TYPE 3 @ GRID .1,.1,-3,0,10,10
2390 MOVE LDt(1),LDP(1) @ CSIZE 3,.3
2400 FOR I=1 TO NDATA1 @ PLOT LDt(I),LDP(I) @ LABEL "o" @ NEXT I @ RETURN
2410 GOTO 2290
2420 L1=L1+1 @ FAST LABEL 8,2,VAL$ (L1),1 @ WAIT 50 @ RETURN
2430 R1=R1+1 @ FAST LABEL 16,2,VAL$ (R1),1 @ WAIT 50 @ RETURN
2440 U1=U1+1 @ FAST LABEL 24,2,VAL$ (U1),1 @ WAIT 50 @ RETURN
2450 D1=D1+1 @ FAST LABEL 32,2,VAL$ (D1),1 @ WAIT 50 @ RETURN
2460 Y1=Y1+INC @ Y2=Y2+INC @ RETURN
2470 Y1=Y1-INC @ Y2=Y2-INC @ RETURN
2480 X1=X1-INC @ X2=X2-INC @ RETURN
2490 X1=X1+INC @ X2=X2+INC @ RETURN
2500 TDM0=TDM0-INC*.6/17 @ TDM1=TDM1-INC*.6/17 @ TDM2=TDM2-INC*.6/17 @ RETURN
2510 TDM0=TDM0+INC*.6/17 @ TDM1=TDM1+INC*.6/17 @ TDM2=TDM2+INC*.6/17 @ RETURN
2520 PDM1=PDM1+INC*.6/17 @ PDM2=PDM2+INC*.6/17 @ PDM3=PDM3+INC*.6/17 @ RETURN
2530 PDM1=PDM1-INC*.6/17 @ PDM2=PDM2-INC*.6/17 @ PDM3=PDM3-INC*.6/17 @ RETURN
2540 TAKE KEYBOARD @ FAST LABEL 52,227,"MATCH <Y>/<N>",1
2550 ZZ=NUM (KEY$ ) @ IF NOT ZZ THEN 2550
2560 IF ZZ=89 OR ZZ=121 THEN 2750
2570 IF ZZ=78 OR ZZ=110 THEN 2590 ELSE GOSUB 2600
2580 GOTO 2550
2590 FAST LABEL 52,227,"            ",0 @ GOSUB 2610 @ GOTO 2190
2600 FOR I=1 TO 10 @ BEEP I,50 @ NEXT I @ RETURN
2610 TAKE KEYBOARD @ FAST LABEL 52,227,"INC=",1 @ FAST LABEL 57,227,VAL$ (SEG),1
2620 ZZ=NUM (KEY$ ) @ IF NOT ZZ THEN 2620
2630 IF ZZ=154 THEN GRAPHALL @ RETURN
2640 IF ZZ=47 THEN INC=INC/2 @ SEG=INC*.6/17 @ GOTO 2670
2650 IF ZZ=42 THEN INC=INC*2 @ SEG=INC*.6/17 @ GOTO 2670
2660 GOTO 2620
2670 FAST LABEL 57,227,"      ",0 @ FAST LABEL 57,227,VAL$ (SEG),1 @ WAIT 100
2680 GOTO 2620
2690 REM ------------------------------------------------------------------
2700 REM
2710 REM
2720 REM
2730 REM       IDENTIFICATION OF THE PRESSURE AND TIME AXES MATCH POINTS
2740 REM ------------------------------------------------------------------
2750 TAKE KEYBOARD @ FAST LABEL 52,227,"            ",0
```

```
2760 FAST LABEL 54,200,"PD AXIS MATCH",1
2770 FAST LABEL 54,210,"LOG(10)   = 1",1
2780 FAST LABEL 54,220,"LOG(100)  = 2",1
2790 FAST LABEL 54,230,"LOG(1000) = 3",1
2800 AA=NUM (KEY$ ) @ IF NOT AA THEN 2800
2810 IF AA=49 THEN DPN=1 @ GOTO 2850
2820 IF AA=50 THEN DPN=2 @ GOTO 2850
2830 IF AA=51 THEN DPN=3 @ GOTO 2850
2840 GOSUB INCORRECT  @ GOTO 2800
2850 FAST LABEL 54,200,"TD/CD X MATCH",1
2860 FAST LABEL 54,210,"LOG (1)  =  0",1
2870 FAST LABEL 54,220,"LOG(10)  =  1",1
2880 FAST LABEL 54,230,"LOG(100) =  2",1
2890 AA=NUM (KEY$ ) @ IF NOT AA THEN 2890
2900 IF AA=48 THEN DTN=0 @ GOTO 2940
2910 IF AA=49 THEN DTN=1 @ GOTO 2940
2920 IF AA=50 THEN DTN=2 @ GOTO 2940
2930 GOSUB INCORRECT  @ GOTO 2890
2940 FAST LABEL 54,200,"            ",0
2950 FAST LABEL 54,210,"            ",0
2960 FAST LABEL 54,220,"            ",0
2970 FAST LABEL 54,230,"            ",0
2980 REM ------------------------------------------------------------------------
2990 REM
3000 REM
3010 REM
3020 REM         PERFORM CHARACTERIZATION ANALYSIS OF THE FORMATION
3030 REM ------------------------------------------------------------------------
3040 IF DPN=1 THEN PDmatch=PDM1
3050 IF DPN=2 THEN PDmatch=PDM2
3060 IF DPN=3 THEN PDmatch=PDM3
3070 IF DTN=0 THEN TDmatch=TDM0
3080 IF DTN=1 THEN TDmatch=TDM1
3090 IF DTN=2 THEN TDmatch=TDM2
3100 FAST LABEL 52,227,"TC NO = ",1 @ CSIZE 5,.5
3110 SET6U @ MOVE 208,2 @ INPUT TC@ FAST LABEL 52,227,"            ",0
3120 GOSUB 1860
3130 SETTIME 0,0 @ FAST LABEL 52,227,"PLEASE WAIT ",1
3140 GOTO 3280
3150 MATCH1:
3160 TDmatch=10^TDmatch @ PDmatch=10^PDmatch @ DPN=10^DPN @ DTN=10^DTN
3170 PRESSUREmatch=PDmatch/DPN @ TIMEmatch=DTN/TDmatch
3180 Kh=141.2*qo*Bo*Vo*PRESSUREmatch
3190 WBC=.000295*Kh*TIMEmatch/Vo
3200 WBCD=.8936*WBC/(O*Ct*h*rw*rw) @ S=.5*LOG (CDS/WBCD)
3210 PST=LGT (PDmatch) @ TST=LGT (TDmatch) @ LDP=LGT (DPN) @ LDT=LGT (DTN)
3220 FAST LABEL 52,160,"TC NO=########",1 @ FAST LABEL 58,160,VAL$ (TC),1
3230 FAST LABEL 52,170,"PD-MA=########",1 @ FAST LABEL 58,170,VAL$ (PST),1
3240 FAST LABEL 52,180,"TD-MA=########",1 @ FAST LABEL 58,180,VAL$ (TST),1
3250 FAST LABEL 52,190," P-MA=########",1 @ FAST LABEL 58,190,VAL$ (LDP),1
3260 FAST LABEL 52,200," T-MA=########",1 @ FAST LABEL 58,200,VAL$ (LDT),1
3270 RETURN
3280 GOSUB MATCH1  @ GPLOTMATCHV=TIME
3290 SETTIME 0,0 @ FAST LABEL 52,227,"           ",0
3300 REM ------------------------------------------------------------------------
3310 REM
```

```
3320 REM
3330 REM
3340 REM           DIRECT FINAL OUTPUT TO THE PRINTER PORT
3350 REM ------------------------------------------------------------------
3360 TAKE KEYBOARD @ FAST LABEL 52,227,"TRUE TC NO Y/N",1
3370 AA=NUM (KEY$ ) @ IF NOT AA THEN 3370
3380 IF AA=89 OR AA=121 THEN GOTO 3440
3390 IF AA=78 OR AA=110 THEN 3400 ELSE 3430
3400 FAST LABEL 52,227,"              ",0
3410 FAST LABEL 52,227,"TC NO =  ",1 @ SETGU @ CSIZE 5,.5 @ MOVE 208,2
3420 INPUT TC@ GOSUB 1860 @ GOSUB 460 @ GOTO 3440
3430 GOSUB INCORRECT  @ GOTO 3370
3440 FAST LABEL 52,227,"              ",0
3450 FAST LABEL 52,160,"TC NO=########",1 @ FAST LABEL 58,160,VAL$ (TC),1
3460 ON TIMER# 1,20000000 GOTO 300 @ AA=NUM (KEY$ )
3470 IF AA=89 OR AA=121 THEN 3520
3480 IF AA=78 OR AA=110 THEN 3530
3490 FAST LABEL 52,227,"HARD COPY  Y/N",1 @ WAIT 300
3500 FAST LABEL 52,227,"HRAD COPY  Y/N",0 @ WAIT 300
3510 GOTO 3460
3520 SETTIME 0,0 @ DUMP GRAPHICS 0,0,0,1 @ FPLOTP=TIME
3530 K=Kh/h @ CDE2S=CDS
3540 FAST LABEL 50,160,"CDES=##############",1 @ FAST LABEL 55,160,VAL$ (CDE2S),1
3550 FAST LABEL 50,170,"K-MD=##############",1 @ FAST LABEL 55,170,VAL$ (K),1
3560 FAST LABEL 50,180,"H-FT=##############",1 @ FAST LABEL 55,180,VAL$ (h),1
3570 FAST LABEL 50,190,"WBSC=##############",1 @ FAST LABEL 55,190,VAL$ (WBC),1
3580 FAST LABEL 50,200,"WBCD=##############",1 @ FAST LABEL 55,200,VAL$ (WBCD),1
3590 FAST LABEL 50,210,"SKIN=##############",1 @ FAST LABEL 55,210,VAL$ (S),1
3600 PRINT @ PRINT @ PRINT USING 3610 ; CDS
3610 IMAGE 10X,"CURVE MATCH CDE2S          = ",2Z.2DE
3620 PRINT USING 3630 ; PRESSUREmatch
3630 IMAGE 10X,"PRESSUREmatch              = ",2Z.4D
3640 PRINT USING 3650 ; TIMEmatch
3650 IMAGE 10X,"TIMEmatch                  = ",2Z.4D
3660 PRINT USING 3670 ; Kh
3670 IMAGE 10X,"PERMEABILITY THICKNESS     = ",5D.D,5X,"MD-FT"
3680 PRINT USING 3690 ; K
3690 IMAGE 10X,"PERMEABILITY               = ",5D.D,5X,"MD"
3700 PRINT USING 3710 ; WBC
3710 IMAGE 10X,"WELL BORE STORAGE COEFF.   = ",Z.5D,5X,"BBL/PSI"
3720 PRINT USING 3730 ; WBCD
3730 IMAGE 10X,"DIMENSIONLESS WBS (CD)     = ",4Z.2D,5X
3740 PRINT USING 3750 ; S
3750 IMAGE 10X,"SKIN FACTOR (WRT TIMEmatch) = ",S3Z.D
3760 PRINT @ PRINT "         POSSIBLE WELL CONDITION    :   ";D$
3770 DATIME=(DV1T+DP1T)/60 @ PLTIME=(GPLOTV+GPLOTMATCHV+GPLOTP+FPLOTP)/60
3780 PRINT @ PRINT
3790 PRINT USING 3800 ; DATIME
3800 IMAGE 10X,"   DATA ANALYSIS I/O (VDU+PRINTER)= ",3Z.2D,5X,"MIN"
3810 PRINT USING 3820 ; PLTIME
3820 IMAGE 10X,"   PLOTTING ROUTINES (VDU+PRINTER)= ",3Z.2D,5X,"MIN"
3830 END
3840 REM ------------------------------------------------------------------
 99320
```

# APPENDIX E

## TOPAZ WELL TESTING NETWORK

